



SAPIENZA
UNIVERSITÀ DI ROMA

Faculty of Pharmacy and Medicine

PhD Thesis in Pharmaceutical Sciences

XXXIII cycle

**Development of novel inhibitors targeting the tumour-
related carbonic anhydrase isoforms and of small molecule
ligands targeting the human tyrosinase and tyrosinase
related protein 1**

PhD student

Giulia Rotondi

Tutor

Prof. Daniela Secci

Table of contents

Section I.....	6
Development of novel inhibitors targeting the tumour-related carbonic anhydrase isoforms IX and XII	6
1. Introduction to the human carbonic anhydrases	7
1.1. Structural features and functions of human carbonic anhydrases.....	7
1.2. Carbonic anhydrase IX and XII: the tumour-related isoforms	10
1.3. Carbonic anhydrases: activators and inhibitors	14
1.4. The aim of the project.....	20
2. Design, synthesis and biological activity of selective carbonic anhydrase inhibitors based on 2-(benzylsulfinyl)benzoic acid scaffold.....	22
2.1. Design of novel inhibitors based on 2-(benzylsulfinyl)benzoic acid scaffold.....	22
2.2. Chemistry	23
2.3. Results and discussion	24
2.4. Conclusions.....	27
2.5. Experimental section.....	27
2.5.1. General	27
2.5.2. Synthesis and characterization data of derivatives 1-15	28
2.5.3. Enzyme inhibition assays	38
3. Novel insights on saccharin- and acesulfame-based carbonic anhydrase inhibitors: design, synthesis, modelling investigations and biological activity evaluation	41
3.1. Design of novel inhibitors based on the saccharin and acesulfame scaffold.....	41
3.2. Chemistry	45
3.3. Results and discussion	49
3.3.1. Inhibitory activity of saccharin-based derivatives	49

3.3.2. Inhibitory activity of acesulfame-based derivatives.....	57
3.3.3. Modelling studies	59
3.4. Conclusions.....	63
3.5. Experimental section.....	63
3.5.1. General	63
3.5.2. Synthesis and characterization data of saccharin-based derivatives	65
3.5.3. Synthesis and characterization data of acesulfame-based derivatives	84
3.5.4. Enzyme inhibition assays	94
3.5.5. Molecular modelling studies	95
Section II.	98
Development of novel ligands targeting human tyrosinase and tyrosinase related protein 1	98
1. Introduction to human tyrosinase and tyrosinase related proteins	99
1.1. Structural features and functions of human tyrosinase and tyrosinase related proteins	99
1.2. Tyrosinase and tyrosinase related protein 1: activators and inhibitors	103
1.3. Tyrosinase and tyrosinase related protein 1: melanoma specific antigens	107
1.4. The aim of the project.....	109
2. Development of small molecule ligands from DNA encoded chemical libraries.....	111
2.1. Design of small molecule ligands from DNA encoded chemical libraries.....	111
2.2. Chemistry.....	113
2.3. Biological evaluation	115
2.4. Results and discussion	116
2.5. Conclusions.....	117
2.6. Experimental section.....	118
2.6.1 General	118
2.6.1. Synthesis and characterization data.....	118

2.6.3. Biological evaluation.....	124
3. Development of multimeric ligands of Thiamidol™.....	125
3.1. Design of multimeric ligands of Thiamidol™.....	125
3.2. Chemistry.....	130
3.3. Biological evaluation.....	136
3.4. Results and discussion.....	136
3.5. Conclusions.....	139
3.6. Experimental section.....	139
3.6.1. General.....	139
3.6.2. Synthesis and characterization data.....	140
3.6.3. Biological evaluation.....	152
Bibliography.....	154
List of publications.....	177

During my PhD studies in the field of medicinal chemistry, I dealt with two different targets thus, this Thesis consists of two Sections.

The first one is focused on my main project conducted in the Research Group of Professor Daniela Secci: the development of novel and selective inhibitors targeting the tumour-related carbonic anhydrases isoforms IX and XII.

The second one is focused on the project performed during my stay abroad in the Research group of Professor Dario Neri at the Eidgenössische Technische Hochschule Zürich (ETH Zurich): the development of small molecule ligands targeting the human tyrosinase and tyrosinase-related protein 1.

Section I.

Development of novel inhibitors targeting the tumour-related carbonic anhydrase isoforms IX and XII

1. Introduction to the human carbonic anhydrases

1.1. Structural features and functions of human carbonic anhydrases

The carbonic anhydrases (CAs, EC 4.2.1.1) are a superfamily of metalloenzymes that catalyse the reversible hydration of carbon dioxide (CO₂) into bicarbonate (HCO₃⁻) and protons (H⁺) (eq. 1) [1].



This reaction is too slow in most tissues and organisms at physiological pH [2] and since CO₂, HCO₃⁻ and H⁺ are involved in several important physiological processes related to metabolism (photosynthesis, carboxylation reaction, etc.), pH regulation, secretion of electrolytes, etc. throughout the tree of life [3–5], eight distinct genetic families, α -, β -, γ -, δ -, η -, ζ , θ and ι have been identified [6–13]. These CA families possess a similar active site containing a central divalent ion M(II) coordinated to three conserved amino acid residues and to a hydroxide nucleophilic species. The metal ions are Zn(II) [5], Cd(II) in ζ -CAs [14], Fe(II) in γ -CAs, at least in anaerobic conditions [15,16], Co(II) in the δ class [7] and Mn(II) in ι [13]. The apoenzymes are devoid of CA catalytic activity [5,17,18].

The human CAs (hCAs), belonging to the α -family, are involved in several functions such as respiration and transport of CO₂/HCO₃⁻, pH and CO₂ homeostasis, electrolyte secretion in tissues and organs, biosynthetic reactions, bone resorption and calcification [5,19].

Fifteen human isoforms (hCA I–XIV) have been identified to date and the analysis of their crystal structures revealed high structural and sequence similarity for the catalytic domains [20–22]. It is cone shaped, composed of a 10-stranded β sheet with seven α helices located at the surface and divided into a half half hydrophobic and half half hydrophilic that lead to a “bipolar” active site. This unique architecture is related to the diverse chemical nature of the CO₂ and HCO₃⁻ and H⁺: the hydrophobic part serves as a trap for the CO₂ and the hydrophilic part enables the binding of the hydrophilic components, HCO₃⁻ and H⁺, and their release from the active site. The Zn(II) metal ion, located at the bottom of this large cavity (approximately 12 Å wide and 13 Å deep), is coordinated to three conserved histidine (His) residues (His94, His96 and His119 in hCA II active site taken as representative of hCA isoforms) and to a H₂O or hydroxide ion that determines the inactive and active form of the enzyme, respectively. The H₂O/hydroxide ion is involved in hydrogen bonds with other two molecule of H₂O, the first,

called deep-H₂O, located in the hydrophobic part, and the second H₂O located at the entrance of the active site, and with the hydroxyl moiety of the conserved threonine residue (Thr199). This residue is bound in turn to the carboxylate moiety of a conserved glutamic acid residue (Glu106). This pair of amino acids, called gate-keeper residues, trigger the entire process increasing the nucleophilicity of the hydroxide ion and orienting the CO₂ in a favourable position for the nucleophilic attack (**Figure 1.1**) [5,23–27].

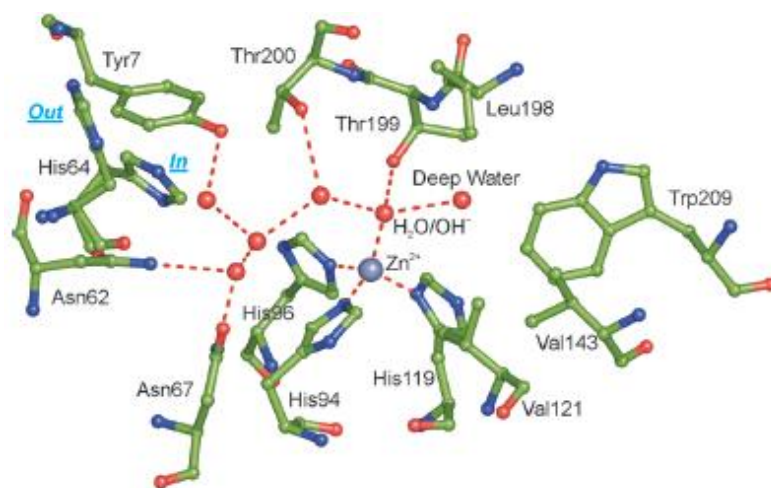
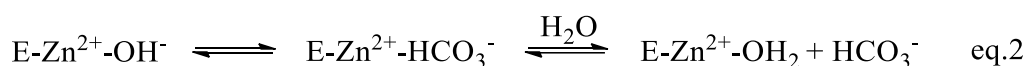


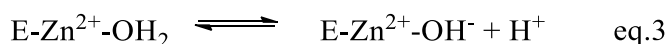
Figure 1.1. The active site of hCA II, taken as representative hCA isoform, describing the network of interactions in the active site. The H₂O molecules are indicated as red spheres and the side chain of the His64 is represented in the “in” and “out” conformation [26].

The hydration of CO₂ in HCO₃⁻ and H⁺ occurs in a two-step ping pong catalytic mechanism. The first step in the hydration reaction involves the nucleophilic attack of the Zn²⁺-OH⁻ on CO₂, bound in the hydrophobic pocket, leading to the formation of the HCO₃⁻ coordinated to the Zn²⁺ metal ion. This bond is rather weak so HCO₃⁻ is replaced by an incoming H₂O molecule yielding the acidic and inactive form of the enzyme, E-Zn²⁺-OH₂ (eq. 2).



The second and rate-limiting step involves the restoration of the active form proceeding through a proton transfer reaction from the active site to the buffer, assisted by an ordered H₂O molecule network and by a proton donor/acceptor, the conserved histidine residue (His64), located at the rim of the active site [5,27–29]. Interestingly, His64 has been found in an “in” conformation, pointing inside the active site, and an “out” conformation, pointing outside the active site,

suggesting that it is able to accept the proton from the H₂O molecule network then turn and release it into the environment, thus restoring the active form of the enzyme, E-Zn²⁺-OH⁻ (eq. 3) [29,30]. Compounds able to interact with this residue have been shown to act as activators (see **1.3.**). Conversely, the absence or the substitution of this proton transfer residue, as in hCA III, impairs the activity of about 500-fold [31,32].



This unique ping-pong mechanism (eq.2 and eq.3) yields some of these isoforms among the most efficient enzymes known in nature, possessing k_{cat}/K_M values close to the limit of the diffusion-controlled processes [33].

Though sharing a conserved active site architecture, these isozymes differ from each other for their cellular localization, tissue and organ distribution, oligomeric arrangement and kinetic properties [23]. Five of these isoforms are cytosolic (hCA I-III, hCA VII and hCA XIII), two are mitochondrial (CA VA and VB), four are membrane bound (hCA IV, hCA IX, hCA XII, hCA XIV and hCA XV) and one is secreted (hCA VI) [34]. The three isoforms VIII, X and XI, defined as CA-related proteins (CARPs), are non-catalytic due to the absence of one or more Zn-binding His residues in the active site [35]. Commonly, hCAs are monomers apart from the CA IX and CA XII that are homodimers stabilised through disulphide bond (**Figure 1.2**) [34,36].

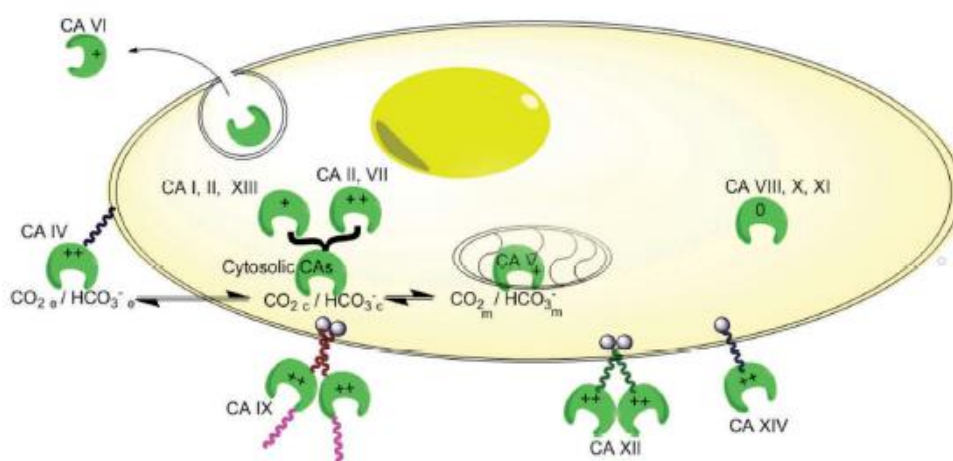


Figure 1.2. Domain composition and subcellular localization of the hCAs [37].

The most studied and investigated isoforms are the hCA I, hCA II, known as the ubiquitous ones for their huge distribution in tissues and organs [37] and the hCA IX and hCA XII, known as tumour-related isoforms for their up regulation during tumorigenesis [38,39], extensively described further in this Chapter.

The highest accumulation of hCA I and hCA II is found in erythrocytes for their role in maintaining and regulating the blood pH [40]. Though hCA I is up to 5 or 6 times more dominant, hCA II is the most efficient being defined as the “rapid” isoform [20,26]. It is located almost in every tissue including the gastrointestinal tract, lungs, bone marrow, eyes, kidney, liver, brain, salivary gland and in breast tissue, and covers several important physiological functions. Thus, its dysregulation leads to several pathological disorders such as glaucoma, edema, and epilepsy [26,41] and pathologies such as acute mountain sickness (AMS), atherosclerosis and osteoporosis [42].

The remaining isoforms are more tissue specific. hCA III is found in muscle tissue and adipocytes and it has been suggested to act as antioxidant agent because of the presence of reactive sulfhydryl groups on its surface, that are able to bind to glutathione [43,44]. hCA IV is found in the heart, brain, capillary of the eye, and erythrocytes and it is a possible drug target for several pathologies, including glaucoma, similarly to hCA II [45]. The mitochondrial isoforms, hCA VA and hCA VB, are implicated in metabolism at different stages [41,46]. hCA VI, the secreted isoform, is implicated in cariogenic disorders [47]. hCA VII is involved in neuronal excitation, determining epileptiform conditions, similarly to hCA II and XI [48]. Albeit devoid of catalytic activity, hCA VIII seems to be involved in neurodegenerative diseases and in tumours, being upregulated in colorectal and lung cancer [49]. The physio and pathological role of the other non-catalytic isoforms, hCA X and hCA XI is still under investigation. hCA XIII is distributed in the thymus, kidney, submandibular gland, small intestine, and in reproductive organs, standing for its involvement in sperm motility processes [50,51]. hCA XIV is involved in epileptogenic conditions and is localized in the apical and basal membranes of the retinal pigment epithelium suggesting specific and unique functions for the acid-base balance in the retina [49].

1.2. Carbonic anhydrase IX and XII: the tumour-related isoforms

The tumour-related isoforms hCA IX and hCA XII possess several peculiarities in their structure, localization and implication in tumorigenesis [36,38,39], thus capturing an increased interest over the last years.

hCA IX is a homodimer possessing two catalytic domains and associated to form a dimer through an intermolecular disulphide bond. Each monomer consists of four domains: a catalytic domain, which faces the extracellular environment for efficient CO₂ hydration and sharing 30-40 % of sequence identity with the other isoforms, a single-pass helical trans-membrane region, a C-terminal short intracellular tail and N-terminal proteoglycan domain (PG), which is a unique feature of hCA IX [36,52]. It has been suggested that each of these constituents could be involved in specific functions in tumorigenesis:

- the catalytic domain is involved in the pH regulation of the tumour microenvironment, thus enabling tumour growth and proliferation;
- the PG domain, located at the entrance of the active site clefts, could support the CO₂ hydration at more acidic pH (pK_a around 6.49), as the one found in solid tumours micro environment, and could foster cell adhesion and intercellular communications;
- the intracellular tail, containing several phosphorylation sites, could participate in signal transduction, contributing to the activation of a number of cancer related signalling cascades, such as the HIF-1 and the PI3/Akt kinase pathway. Interestingly, it has been shown that mutations of this tail could cause the suppression of cell adhesion and of the extracellular acidification capabilities of hCA IX [36,53,54].

The expression of hCA IX is limited to the stomach and intestine [55] but it is ectopically expressed in a large number of solid tumours including glioblastoma, colorectal, breast cancer and in the clear cell renal carcinoma (ccRCC) [56,57]. It has been related to the activation of the transcription factor HIF-1 that occurs *via* hypoxia, to peculiarities of solid tumours, and to mutations of Von Hippel Lindau (VHL) tumour suppressor, that mimics hypoxia, respectively [57–63]. hCA IX upregulation is usually related to chemotherapeutic resistance, poor prognosis, and poor clinical outcome [62,64–67].

hCA XII is a dimeric transmembrane isoform with two external catalytic domains (pK_a around 7.1) and devoid of the PG domain [68,69]. Similarly to hCA IX, hCA XII is involved in the pH regulation in solid tumours, although there are some differences [69–71]: its dependence on the HIF-1 is not completely understood as its activation in breast cancer occurs *via* the estrogen receptor (ER) pathway and the hypoxia response element (HRE) on its gene has not been identified; it is related to less aggressive tumour phenotypes; it is more distributed in normal tissues and organs and its catalytic activity is medium high [69–72]. Recent investigations showed that the silencing of the CA9 gene can increase the expression of hCA XII thus defining a potential role of cooperation: the *in vivo* knockdown of CA9 gene alone led to a tumour

regression of 40% and a consequent upregulation of hCA XII, whereas the invalidation of both led to a tumour regression of 85% [73].

The rapid proliferation of tumour tissues resulted in increased distance to the blood vessels leading to inadequate oxygen levels that activate and stabilize the hypoxia-inducible factor 1 (HIF-1) [74,75]. This protein is a heterodimer that consists of the HIF-1 α subunit, defined as oxygen sensor as its concentration depends on the concentration of oxygen and the HIF-1 β subunit, constitutively located inside the nucleus. Under normoxia, the HIF-1 α undergoes proline hydroxylation through the oxygen-dependent prolyl-4-hydroxylase domain (PHD), and thus it is recognized and tagged by the VHL tumour suppressor for ubiquitin proteasome degradation. Under hypoxia, or in case of mutations of the VHL tumour suppressor, the HIF-1 α cannot be hydroxylated, and thus it moves to the nucleus and heterodimerizes to the HIF-1 β . This leads to the formation of the active transcription factor HIF-1 that, binding to the HRE in the promoter-enhancer regions, activates the transcription of genes involved in oxygen and glucose supplies [54,57]. These genes include the glucose transporters (GLUT1 and GLUT3), glycolytic proteins, the vascular endothelial growth factor (VEGF), and specific pumps, transporters and proteins, including hCA IX and hCA XII (**Figure 1.3**) [74,76–78].

The absence of oxygen forces these cells to switch their metabolism from aerobic (glycolysis and oxidative phosphorylation of pyruvate) to anaerobic (glycolysis, lactic acid fermentation), the so-called Warburg effect [79,80], that leads to an increase of acid side products from the lactic fermentation. Interestingly, anaerobic metabolism is favoured also if adequate levels of oxygen are restored, because it is faster and because it produces fundamental precursors for the rapid replication of tumour cells (nucleotides, amino acids and lipids) [81,82]. The accumulation of acid side products in the cytoplasm leads to a decrease in the intracellular pH that is promptly balanced through a concerted interplay of pumps, transporters, and proteins. These include hCA IX and hCA XII that serve the fundamental role of setting the novel pH set points: weakly alkaline inside ($\text{pH}_i = 7.2\text{-}7.4$) and more acidic outside ($\text{pH}_e = 6.8$) [82–85]. Conversely, in normal cells it is the extracellular space that maintains a slightly more basic environment ($\text{pH}_e > 7.3$) than the intracellular environment ($\text{pH}_i = 7.2$) [82,83].

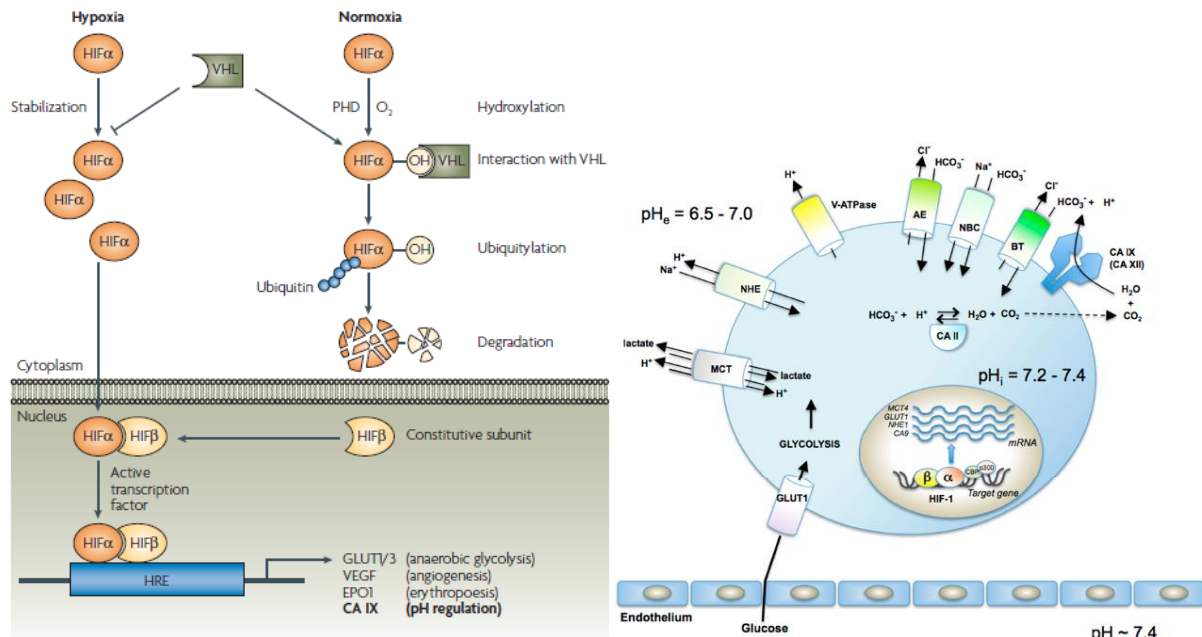


Figure 1.3. Mechanism of hypoxia-induced gene expression mediated by the HIF-1 transcription factor [54] and the related transcribed proteins including hCA IX and hCA XII [78].

Particularly, although they have a significant anaerobic metabolism, a lot of tumours produce a large amount of CO_2 [86,87]. Its prompt removal is fundamental for the regulation of pH and for eliminating a potential detrimental product from a poorly perfused but metabolically active tissue (mismatch among metabolic demand and the capacity to remove metabolic waste products) [84].

hCA IX converts CO_2 , which is produced in the cytosol *via* hCA II, to H^+ and HCO_3^- (**Figure 1.3**) [83,84,88,89]:

- H^+ accumulation leads to a decrease of the pH_e , which favours: extracellular matrix (ECM) degradation, which results in tumour dissemination and invasion; the suppression of immune surveillance, which inhibits T-cells activation; the evasion from apoptosis [54], and the multidrug resistance. At lower pH_e the antitumor basic drugs undergo ionization and thus the penetration of these compounds is prevented in the so-called ion trapping process [83,90–92]. Furthermore, this slightly acidic pH results suitable for the hCA IX catalytic activity [36,54].
- HCO_3^- anions are recycled inside the cells through transporters, which are closely associated to hCA IX (this coupled system is defined metabolon) and upregulated by the HIF-1, for the internal titration of H^+ formed as tumour side products. This leads to the restoration of a slight alkaline pH that stimulates glycolysis (through the expression

of glycolytic enzymes) and lactate hydrogenase (LDH) activity and inhibits gluconeogenesis and apoptosis [39,86,93].

Slight variations, as small as 0.1 pH units, in the intra and extracellular pH, could be detrimental for solid tumours [94]. It has been suggested that hCA IX could fit the role of a pH-stat, continuously sensing the pH in order to keep its value constant [84,87]. Its catalytic activity responds to each single perturbation of the tumour microenvironment: at pH values above 6.8, the rate of hCA IX hydration reaction is higher than dehydration, at pH values below 6.8 its rate of dehydration reaction exceeds the rate of hydration. Thus, it has been proposed that hCA IX does not necessarily decrease pH_e and produce HCO_3^- to be transported inside, but may also play a role in raising the pH_e to sustainable acidic values for cell survival [84,89]. This equilibrium could depend on the emission of CO_2 over lactic acid, on the substrate availabilities and on the area and the stage of tumours [84,89].

1.3. Carbonic anhydrases: activators and inhibitors

As they cover so many important physiological functions and are widely distributed in diverse tissues and organs, the up- or down-regulation of hCA isoforms has been related to several pathological processes [23,37], as previously reported.

The hCA activators (hCAAs), that are emerging as potential therapeutic agents, have been proposed in the treatment of Alzheimer's disease, aging and memory consolidation [95]. They could facilitate synaptic transmission in brain cells acting or supporting the His64 during the shuttling of protons from the active site, that constitutes the rate limiting step of the entire process. This unique mechanism of action has been confirmed from the X-ray crystal structure of several compounds bound to hCA II: they are located in the same region but on the opposite side of His64, thus participating in favourable interactions between the amino acid residues and the H_2O molecules network [5,96].

Conversely, the hCA inhibitors (hCAIs) have been used in clinical practice and approved as diuretics [97], antiglaucoma [98], antiepileptic [48] and anti-obesity agents [46] and thousands of compounds targeting the tumour-related isoforms hCA IX and hCA XII are in preclinical development [72], [23].

Commonly, hCAIs are divided in four classes based on their mechanism of action plus a fifth class of compounds with an unknown mechanism of action [99].

The first class of hCAIs are the zinc binders [99] and includes sulphonamides and their bio-isosteres (sulfamides and sulfamates) [23,100], the metal complexing anions [101], the

dithiocarbamates [102], the xanthates [103], the ureates [104], and the hydroxamates [105] (zinc binding group, ZBG). They act by binding the Zn(II) metal ion preventing its bond to the H₂O/hydroxide ion in the active site. Particularly, the sulphonamides (-SO₂NH₂) [99] the most used in clinical practice (**Figure 1.4**) [27,106], bind to the Zn(II) metal ion in their deprotonated form: the -NH₂ is coordinated to the zinc and it is involved in an hydrogen bond to the Thr199. This binding is strengthened by a second hydrogen bond among the oxygen of the sulphonamide and the -NH of the Thr199 (**Figure 1.5**) [99].

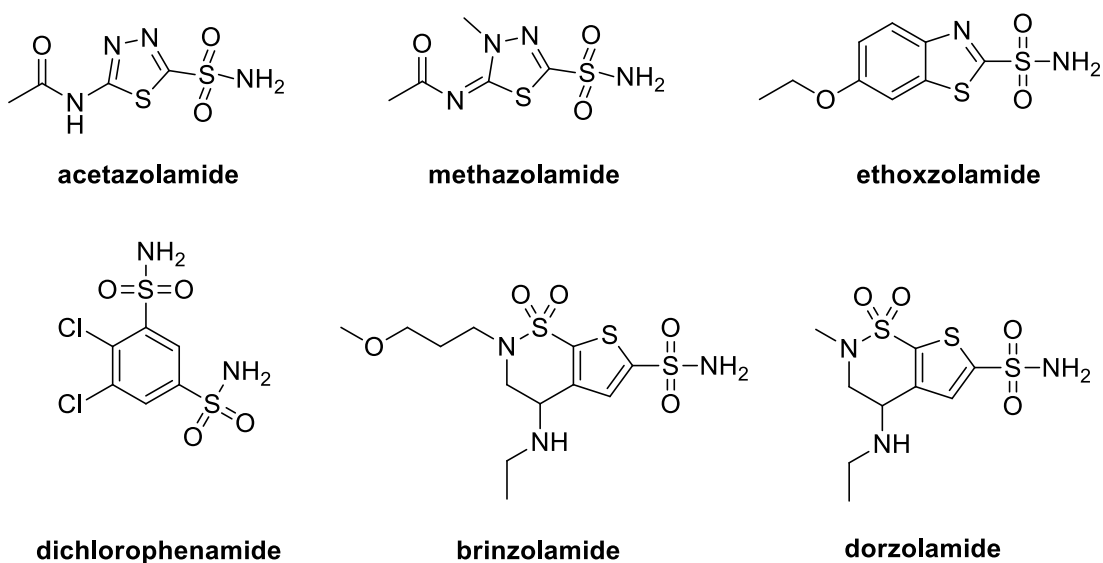


Figure 1.4. Chemical structure of some of the clinical available hCAIs bearing the primary sulphonamide [23].

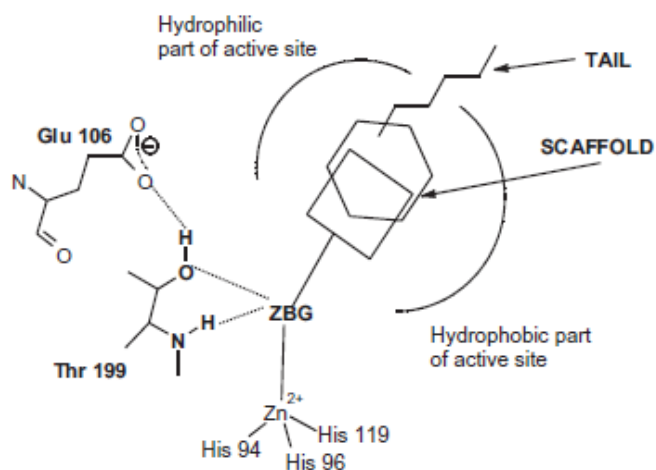


Figure 1.5. Schematic representation of the hCAIs anchoring to the central zinc ion [99].

The other classes of hCAIs include inhibitors anchoring to the zinc coordinated H₂O/hydroxide, occluding the active site and binding out of the active site [99].

Phenols, certain carboxylates and esters, the polyamines and the sulfocoumarins (hydrolysed to sulfonic acid) (anchoring group, AG) act by anchoring the H₂O/hydroxide ion avoiding the formation of the pattern of hydrogen bonds in the active site, fundamental in the initial stages of the entire process (**Figure 1.6**) [99]. The phenol and the spermine are the first inhibitors that have been reported to show this mechanism of action [107,108].

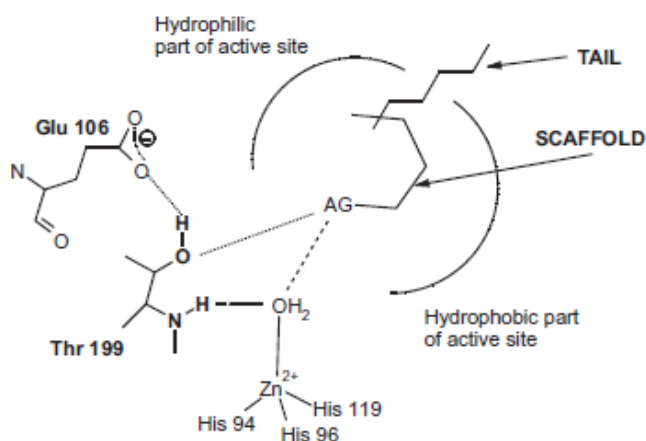


Figure 1.6. Schematic representation of hCAIs anchoring to the zinc-coordinated water/hydroxide ion [99].

Coumarins, substituted coumarins, 5- and 6-membered lactones and thiolactones or quinolines (stick group, SG) act as prodrugs activated *in situ* from the esterase activity of hCAs that release the *cis* or *trans* acid isomers [99,109,110]. Due to their steric hindrance, compounds containing these moieties occlude the active site entrance (**Figure 1.7**) [99], the most variable region among the isoforms [34].

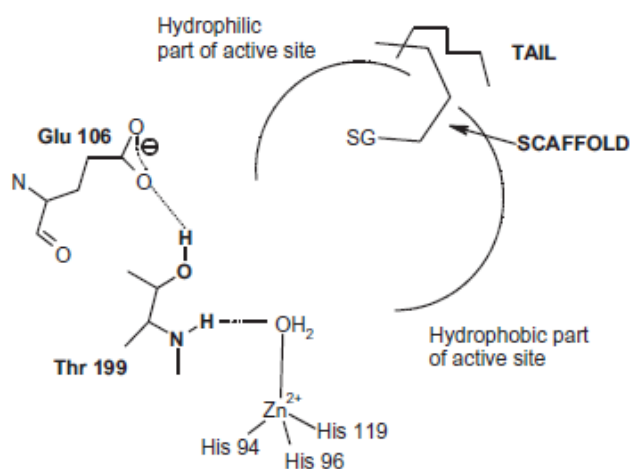


Figure 1.7. Schematic representation of hCAIs occluding the entrance of the active site [99].

Although compounds containing carboxylic acids are commonly zinc or H₂O/hydroxide ion binders, a recent investigation revealed that the 2-(benzylsulfonyl)-benzoic acid possess a unique mechanism of action since it binds out of the active site, representing the fourth mechanism of action to have been identified (**Figure 1.8**).

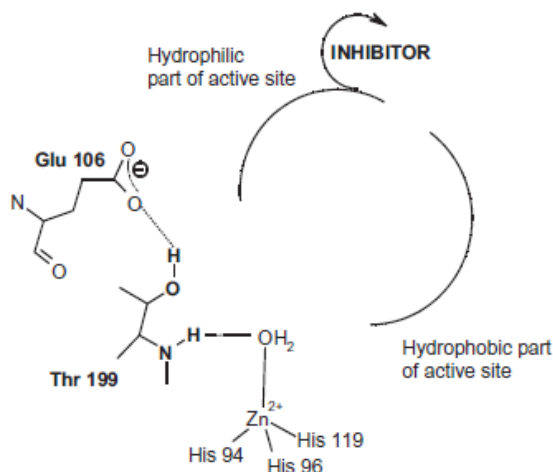


Figure 1.8. Schematic representation of the 2-(benzylsulfonyl)-benzoic acid binding out of the active site [99].

The electron density analysis, obtained from the adduct among the 2-(benzylsulfonyl)-benzoic acid and the hCA II, suggested that its carboxylate group is involved in a hydrogen bond with two H₂O molecules, one of these bound to the His64, the proton shuttle residue. This favourable pathway of interactions freezes the His64 in its “out” conformation thus preventing and inhibiting the restoration of the catalytic process. Interestingly, 2-(benzylsulfonyl)-benzoic acid possesses a significant inhibitory activity only against the hCA II and hCA IX (IC₅₀ = 0.15 μM and IC₅₀ = 1.29 μM, respectively) that could be due to the diverse amino acid residues delimiting this pocket [111] (**Figure 1.9**).

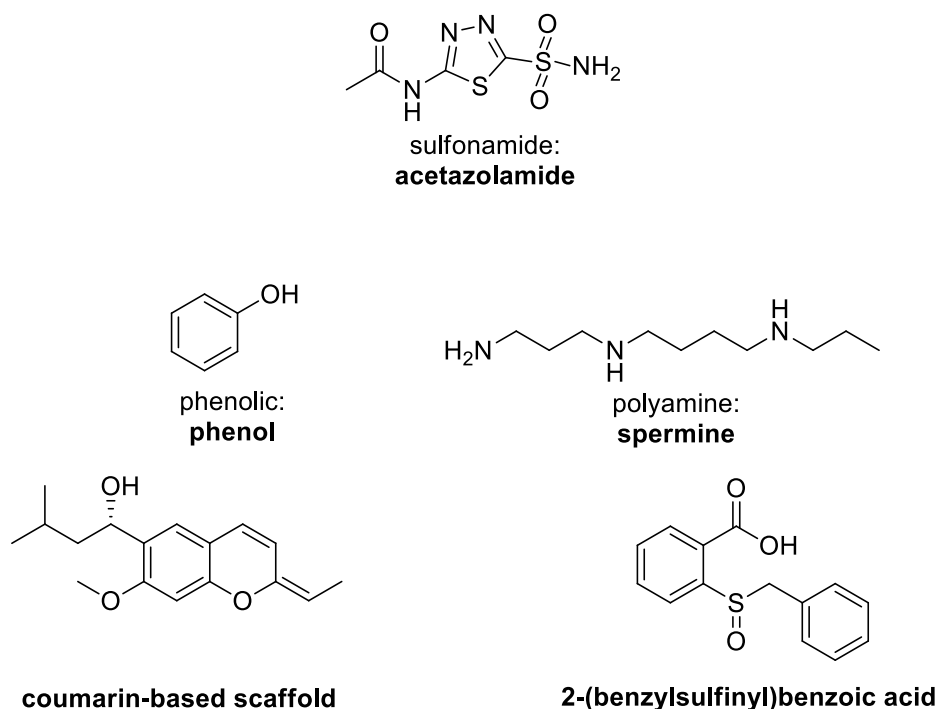


Figure 1.9. Representative inhibitors of each of the four classes of hCAIs.

These four mechanisms of action have been established and proven through kinetic enzymatic activity studies, mass spectroscopy and X-ray crystal structures, but there is still a large number of compounds that possess unknown mechanisms of action [99].

Saccharin and acesulfame derivatives, obtained from the derivatization of the secondary sulphonamide and sulfamate respectively, belong to this class and possess potent and selective hCA IX and XII inhibitory activity [57,99], though apparently devoid of a binding group able to interact in the active site, as proved by several papers in the field [112–115].

The main challenge for the development of selective hCAIs remains the high homology and similarity of the active site architecture among the fifteen isoforms [23]: the same compounds approved in clinical practice as diuretic, antiglaucoma and anticonvulsant agents are often associated with a range of side effects due to their off-target interactions [23].

Several strategies have been proposed and used to overcome this issue, such as the tail approach [18,26,62], leading to isoform selective compounds [82]. The practice consists in the insertion of a tail that, pending from the central core of the inhibitors [18,99], is able to interact with a more variable region far from the active site [34].

This approach turned out to be useful in the design of a class of ureidobenzenesulfonamides [116] including SLC-0111 [99], ((4-(4-fluorophenylureido)-benzenesulfonamide)), that successfully completed phase I clinical trials for the treatment of solid tumours overexpressing hCA IX and it has been scheduled for phase II clinical trials ($K_i = 45$ nM on hCA IX and $K_i =$

4.5 nM on hCA XII) [68,117,118]. X-ray crystal studies suggested that this isoform's selective profile is due to the active site entrance conformation, which is more occlusive for hCA I and hCA II due to the presence of bulky residues, and more affordable for hCA IX and hCA XII [117].

The other compound advancing in phase II clinical trials is E-7070 ((*N*-(3-chloro-7-indolyl)-1,4-benzenedisulfonamide)), also known as Indisulam [68,119]: its success in the treatment of solid tumours could be related to its double activity: inhibition of hCA IX and XII through the sulphonamide moiety and inhibition of cyclin-dependent kinases (CDKs) that regulate cell cycle progression [68] (**Figure 1.6**).

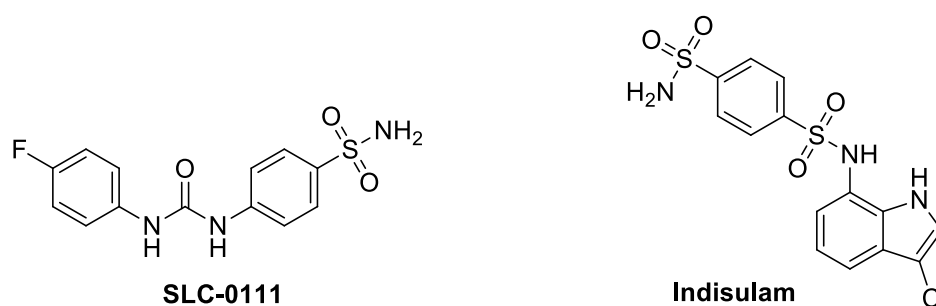


Figure 1.10. Chemical structure of SLC-0111 and Indisulam.

1.4. The aim of the project

hCA IX and hCA XII can be considered as suitable targets for the treatment of solid tumours due to their targetable extracellular domain [36,54], their limited expression in healthy tissues and their implication in tumorigenesis [38,39]. Though a large number of inhibitors have been developed to date, only two of the sulphonamide-based inhibitors, SLC-0111 and E7070/Indisulam, are currently in clinical trials [68], highlighting the urgent need of novel and selective inhibitors targeting these tumour related isoforms.

The aim of this project was the design, synthesis and SAR analysis of two libraries of compounds based on the 2-(benzylsulfinyl)benzoic acid scaffold and on the saccharin and acesulfame nucleus. The biological evaluation and the modelling studies were performed in the Research Group of Professor Claudiu T. Supuran,

These scaffolds possess peculiar features, resulting in attractive lead compounds for the development of potent and selective inhibitors:

- 2-(benzylsulfinyl)benzoic acid acts in a pocket out of the active site consisting of the highest variability in the amino acid sequence [111] ;
- saccharin is affine for hCA IX in the nanomolar range and is more than 50-fold selective over hCA II [120,121],
- acesulfame acts exclusively on hCA IX, not affecting hCA I, hCA II and hCA XII [122].

*This Chapter is part of the paper “Design, synthesis and biological activity of selective hCAs inhibitors based on 2-(benzylsulfinyl)benzoic acid scaffold” by **G. Rotondi**, P. Guglielmi, S. Carradori, D. Secci, C. De Monte, B. De Filippis, C. Maccallini, R. Amoroso, R. Cirilli, A. Akdemir, A. Angeli, C.T. Supuran published in *J. Enzyme Inhib. Med. Chem.* 34 (2019) 1400-1413 [123].*

2. Design, synthesis and biological activity of selective carbonic anhydrase inhibitors based on 2-(benzylsulfinyl)benzoic acid scaffold

2.1. Design of novel inhibitors based on 2-(benzylsulfinyl)benzoic acid scaffold

A recent investigation found that the 2-(benzylsulfinyl)benzoic acid displayed an atypical mechanism of action involving the occupancy of a pocket near the entrance of the active site through interactions that froze the His64 residue in the “out” conformation [111]. This amino acid, that can be found in two conformations called “in” and “out”, acts as a proton shuttle residue transferring a proton from the Zn-coordinated H₂O molecule to the environment, in order to reconstitute the catalytic active form of the isoform. Interfering in this process led to the blocking of or a strong reduction in enzymatic activity, thus leading to enzyme inhibition. Interestingly, this lead compound resulted as inactive against hCA I and XII (K_i hCA I/XII >10 μ M), but showed inhibitory activity in the low micromolar range towards hCA II and IX (K_i hCA II = 0.15 μ M, K_i hCA IX = 1.29 μ M).

Previous studies by our research group [123], which aimed at evaluating the impact of the substitution of the carboxylate, the benzyl moiety, and the diverse sulphur oxidation state on the activity and selectivity of the 2-(benzylsulfinyl)benzoic acid, led to the identification of 2-(benzylthio)benzamide as the first-in-class derivative. This derivative manifests nanomolar activity against hCA IX (K_i = 46 nM) but also micromolar activity against hCA II (K_i = 8.22 μ M).

Based on these findings, I attempted the insertion of unsaturated alkyl chains of increasing lengths on the 2-thiobenzamide, in order to evaluate if the presence of groups able to give hydrophobic interactions, could improve the activity, with particular attention to the selectivity against hCA IX (and presumably hCA XII), that possesses a more hydrophobic and affordable active site compared to the off-target isoforms, hCA I and hCA II. The role of the sulphur atom was also investigated, to evaluate if its oxidation to sulfinyl (sulfoxides) and sulphonyl (sulfones) derivatives could affect the inhibitory activity (**Figure 2.1**).

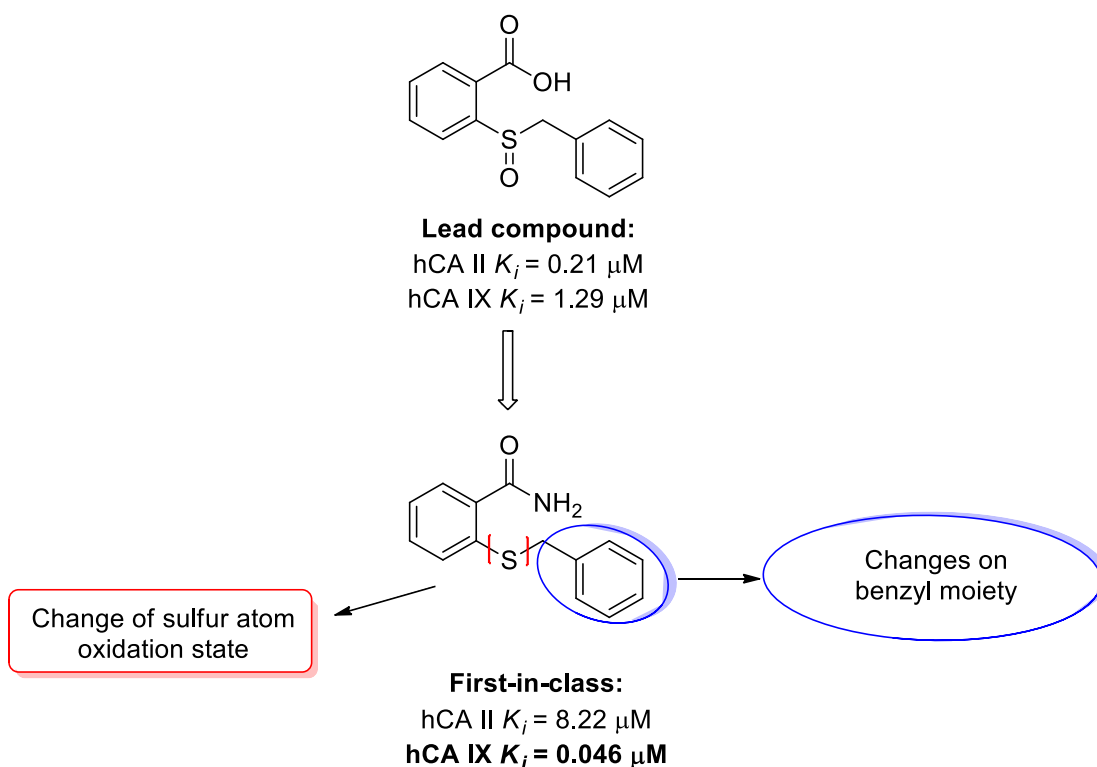


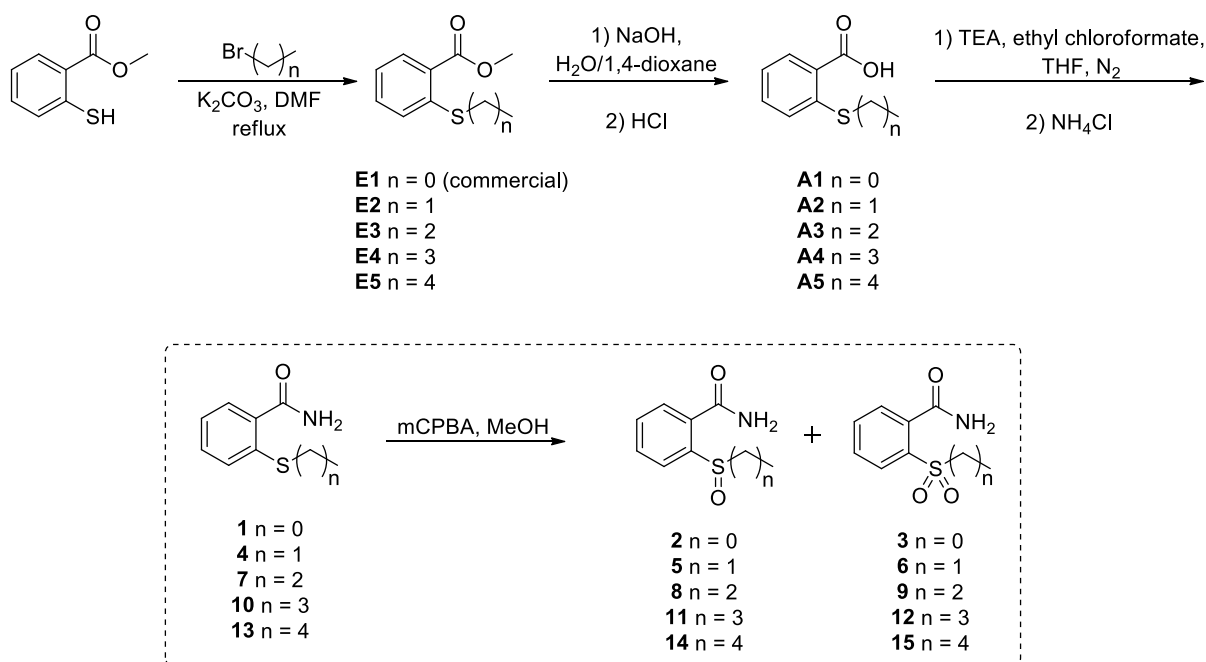
Figure 2.1. Chemical modifications on the first-in-class compound identified from a large library based on the 2-(benzylsulfinyl)benzoic acid scaffold.

2.2. Chemistry

The synthetic procedure employed to obtain derivatives **1-15** is reported in **Scheme 2.1**.

Methyl 2-mercaptobenzoate reacted in the presence of bromoalkanes of increasing length and potassium carbonate K_2CO_3 , in *N,N*-dimethylformamide (DMF) at reflux, to obtain intermediates **E2-E5** (**E1**, methyl 2-(methylthio)benzoate is commercially available). These intermediates were hydrolysed with an aqueous solution of sodium hydroxide (NaOH) 2 N added in a mixture of equal amounts of water and 1,4-dioxane (50:50, v:v). After the synthesis completion, the reactions were quenched with hydrochloric acid (HCl), yielding the intermediates **A1-A5**. The activation of the carboxylic acid group for the amide synthesis was obtained using the mixed anhydride approach [124]. In presence of an excess of triethylamine (Et_3N), ethyl chloroformate was used in tetrahydrofuran (THF) under nitrogen atmosphere (N_2). To check for the reaction with thin layer chromatography (TLC), the disappearance of the acidic intermediate was controlled until the completion of anhydride formation. Finally, ammonium chloride (NH_4Cl) was added. The presence of the triethylamine excess caused the “de-blocking” of NH_3 from NH_4Cl , giving the final products (**1, 4, 7, 10, 13**).

The so-obtained compounds (**1** and **15**) were treated in an oxidative reaction using *meta*-chloroperbenzoic acid (mCPBA). Although many routes to afford sulphur oxidation have been published [125], I chose this approach in order to obtain the two oxidation products, the sulfoxide and the sulfone, in the same reaction. In fact, by controlling the amount of oxidant added during the reaction, I was able to obtain both the species resolved chromatographically.



mCPBA = *m*-chloroperbenzoic acid

TEA = triethylamine

$n = 1-4$

Scheme 2.1. Synthetic procedure of derivatives **1-15**.

2.3. Results and discussion

The synthesized compounds were tested to evaluate their inhibitory activity against the ubiquitous off-target isoforms, hCA I and II, and the cancer-related ones, hCA IX and XII, using a stopped-flow, CO₂ hydrase assay method [126].

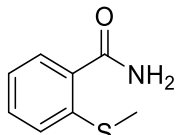
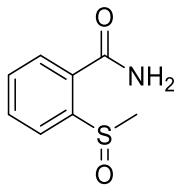
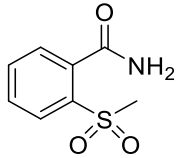
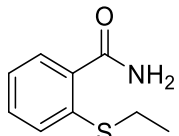
The hCA inhibition data, reported as K_i values, are summarized in **Table 2.1**.

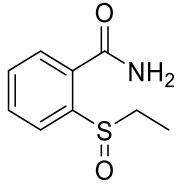
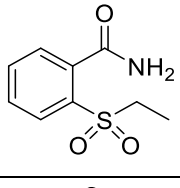
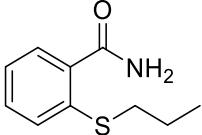
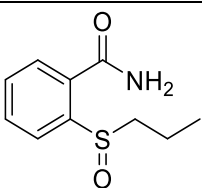
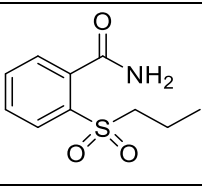
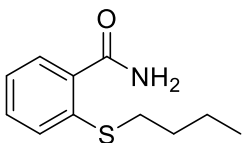
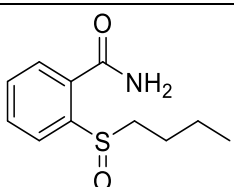
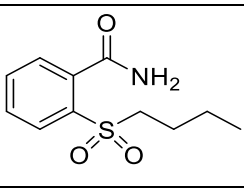
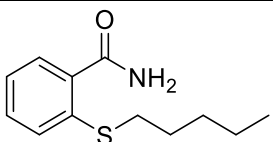
The effect and importance of the phenyl moiety were evaluated on the 2-(benzylthio)benzamide and its oxidised forms, using linear alkyl chains of increasing length (**1-15**) (from the methyl to pentyl moieties).

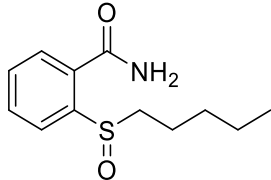
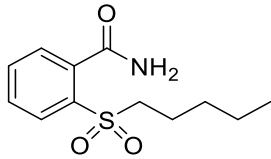
Interestingly, derivatives **1-15** exhibited their effect exclusively against hCA IX, not affecting hCA I, hCA II and hCA XII. This could be due to the hydrophobic hCA IX active site, that could favour interactions among the alkyl chains of these compounds and the hydrophobic

amino acids of its cavity. Only derivative **7**, bearing a propyl chain bound to the sulphur atom, exhibited a certain affinity against hCA II (K_i hCA II = 90.9 μ M), although this was weak. Compound **9**, the sulfone analogue of sulphide **7**, was the best inhibitor inhibiting the hCA IX with a K_i value of 2.3 μ M. Good results were found also for derivative **10** and **13**, containing the sulphur atom and bearing a butyl or pentyl chain, respectively (**10**, K_i hCA IX = 2.5 μ M; **13**, K_i hCA IX = 2.7 μ M), possibly assuming the binding pose of the benzyl group. Apart from the triad bearing the propyl chain (**7-9**) that possess a reversed trend, the compounds containing the sulfhydryl group displayed better inhibitory activity than the related sulfoxide and sulfone analogues (**Table 2.1**). A similar result was found for the 2-(benzylthio)benzamide. The reported compounds resulted less active than their lead compound, suggesting a better outcome for the benzyl group.

Table 2.1. Inhibition data of selected human CA isoforms (hCA I, II, IX and XII) with the proposed derivatives **1-15** and the standard sulphonamide inhibitor acetazolamide (**AAZ**) by a stopped flow CO₂ hydrase assay [126].

Compound	Structure	K_i (μ M)*			
		hCA I	hCA II	hCA IX	hCA XII
1		>100	>100	6.5	>100
2		>100	>100	34.5	>100
3		>100	>100	14.0	>100
4		>100	>100	16.7	>100

5		>100	>100	40.9	>100
6		>100	>100	22.7	>100
7		>100	90.9	>100	>100
8		>100	>100	38.2	>100
9		>100	>100	2.3	>100
10		>100	>100	2.5	>100
11		>100	>100	36.4	>100
12		>100	>100	13.5	>100
13		>100	>100	2.7	>100

14		>100	>100	27.3	>100
15		>100	>100	8.7	>100
AAZ		0.25	0.012	0.025	0.006

2.4. Conclusions

The chemical substitutions of the benzyl moiety of 2-(benzylthio)benzamide were explored. This compound resulted as the first-in class of a large library of compounds obtained from modifications on the 2-(benzylsulfinyl)benzoic acid scaffold, an innovative and atypical inhibitor, recently discovered.

Particularly, the chemical modifications attempted on the 2-(benzylthio)benzamide and its oxidised derivatives involved the substitution of the benzyl group using alkyl chains of increasing lengths that led to 15 derivatives tested against the off-target isoforms, hCA I and II, and the cancer-related ones, hCA IX and XII. Interestingly, these compounds appeared to be effective exclusively against hCA IX, albeit less active than their lead compound, thus suggesting that the replacement of the benzyl ring impaired the activity but increased the selectivity against hCA IX.

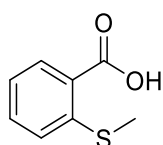
2.5. Experimental section

2.5.1. General

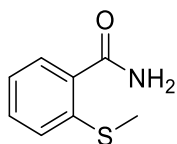
Solvents were used as supplied without further purification. If solvent mixtures are described, their ratio is expressed as *volume:volume* (*v:v*). Starting materials and other chemicals were purchased by Sigma-Aldrich (Italy) and used in the synthesis and in the biological assays without further purification. All synthesized compounds were fully characterized by analytical and spectral data. Analytical thin-layer chromatography (TLC) was carried out on Sigma-Aldrich® silica gel on TLC aluminium foils with fluorescent indicator 254 nm. Visualization was carried out under UV irradiation (254 and 365 nm). Silica for column chromatography were purchased from Sigma-Aldrich (Milan, Italy) (high purity grade, pore size 60 Å, 230-400

mesh particle size). ^1H NMR spectra were recorded on a Bruker AV400 (^1H : 400 MHz, ^{13}C : 101 MHz) using the solvents (CDCl_3 , $\text{DMSO-}d_6$ and D_2O) at room temperature. The final concentration of the samples was of ~ 5 mg/mL for ^1H -NMR acquisition and ~ 25 mg/mL for the recording of the ^{13}C -NMR ones. Chemical shifts are quoted in ppm, based on appearance rather than interpretation, and are referenced to the residual non deuterated solvent peak. Missing signals must be attributed to overlapping peaks. Chemical shifts are presented as δ units (parts per millions) using the solvent signal as the internal standard. ^1H spectra are described as reported below: δ_{H} (spectrometer frequency, solvent): chemical shift/ppm (multiplicity, J -coupling constant(s), number of protons, assignment). ^{13}C spectra are described as reported below: δ_{C} (spectrometer frequency, solvent): chemical shift/ppm (assignment). Coupling constants J are valued in Hertz (Hz) using these abbreviations to indicate the splitting: s – singlet; d – doublet; t – triplet; q – quartet; m – multiplet. If needed, it is also reported the abbreviation br – to indicate the broad shape of the specific peak. All melting points were measured on a Stuart[®] melting point apparatus SMP1 and are uncorrected (temperatures are reported in $^{\circ}\text{C}$). If given, systematic compound names are those generated by ChemBioDraw Ultra[®] 12.0 following IUPAC conventions. Silica for column chromatography were purchased from Sigma-Aldrich (Milan, Italy) (high purity grade, pore size 60 Å, 230-400 mesh particle size).

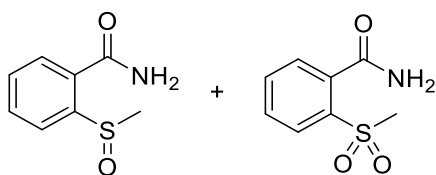
2.5.2. Synthesis and characterization data of derivatives 1-15



2-(Methylthio)benzoic acid (A1): lithium hydroxide (1.2 equiv.), dissolved in 3 mL of water, was added dropwise to a stirring solution of methyl 2-(methylthio)benzoate (1 equiv.) in H_2O :methanol (50 mL, 50:50 v:v). The reaction was stirred at 70 $^{\circ}\text{C}$ for 2 h, concentrated *in vacuo* to remove methanol and quenched with 2N HCl. The precipitate was collected by filtration and washed with *n*-hexane (2 x 10 mL) to give the title compound as a white solid (89% yield); mp 171 - 173 $^{\circ}\text{C}$. ^1H NMR (400 MHz, $\text{DMSO-}d_6$): δ 2.39 (s, 3H, CH_3), 7.19-7.22 (m, 1H, Ar), 7.35 (d, $J = 8.1$ Hz, 1H, Ar), 7.52-7.57 (m, 1H, Ar), 7.90-7.91 (m, 1H, Ar); ^{13}C NMR (101 MHz, $\text{DMSO-}d_6$): δ 15.2 (CH_3), 123.9 (Ar), 125.0 (Ar), 127.8 (Ar), 131.4 (Ar), 133.0 (Ar), 142.9 (Ar), 167.9 (COOH).



2-(Methylthio)benzamide (1): triethylamine (3 equiv.) and ethyl chloroformate (1.2 equiv.) were added to a stirring solution of 2-(methylthio)benzoic acid (1 equiv.) in 10 mL of tetrahydrofuran. After monitoring the anhydride intermediate formation with silica TLC plates, ammonium chloride (1.4 equiv.) was added. The reaction was stirred under nitrogen atmosphere for 16 h at 50 °C, concentrated *in vacuo* and the resulting suspension extracted with ethyl acetate (3 × 20 mL). The organics were reunited, dried over sodium sulphate and concentrated under reduced pressure to give a crude product purified by column chromatography on silica gel (ethyl acetate:cyclohexane, 2:1). The title compound was a white solid (70% yield); mp 145-147 °C. ¹H NMR (400 MHz, DMSO-*d*₆): δ 2.39 (s, 3H, CH₃), 7.15-7.19 (m, 1H, Ar), 7.32-7.47 (m, 3H Ar + 1H NH₂, D₂O exch.), 7.76 (br s, 1H, NH₂, D₂O exch.); ¹³C NMR (101 MHz, DMSO-*d*₆): δ 15.7 (CH₃), 124.3 (Ar), 125.8 (Ar), 128.0 (Ar), 130.7 (Ar), 135.2 (Ar), 138.6 (Ar), 169.9 (CONH₂).

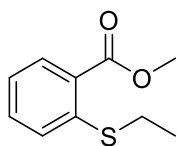


2-(Methylsulfinyl)benzamide (2) and 2-(methylsulfonyl)benzamide (3): 3-chloroperbenzoic acid (1 equiv.), dissolved in 5 mL of methanol, was added dropwise to a stirring solution of 2-(methylthio)benzamide (1) (1 equiv.) in 25 mL of methanol. After 2 h, another aliquot of 3-chloroperbenzoic acid (1 equiv. in 5 mL of methanol) was added and the reaction stirred for further 24 h. The mixture was concentrated *in vacuo* and purified by column chromatography on silica gel (ethyl acetate:cyclohexane, 5:1) to give separately the title compounds **2** and **3**.

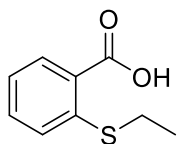
2: white solid, 34% yield, mp 175-177 °C. ¹H NMR (400 MHz, DMSO-*d*₆): δ 2.76 (s, 3H, CH₃), 7.62 (t, *J* = 7.4 Hz, 1H, Ar), 7.70 (br s, 1H, NH₂, D₂O exch.), 7.81 (t, *J* = 7.5 Hz, 1H, Ar), 7.89 (d, *J* = 7.6 Hz, 1H, Ar), 8.12 (d, *J* = 7.8 Hz, 1H, Ar), 8.26 (br s, 1H, NH₂, D₂O exch.); ¹³C NMR (101 MHz, DMSO-*d*₆): δ 45.2 (CH₃), 124.0 (Ar), 128.3 (Ar), 130.6 (Ar), 131.9 (Ar), 132.5 (Ar), 149.3 (Ar), 168.1 (CONH₂).

3: white solid, 30% yield, mp 165-167 °C. ¹H NMR (400 MHz, DMSO-*d*₆): δ 3.38 (s, 3H, CH₃), 7.56-7.58 (m, 1H, Ar), 7.65 (br s, 1H, NH₂, D₂O exch.), 7.66-7.70 (m, 1H, Ar), 7.75-7.79 (m, 1H, Ar), 7.96-7.98 (m, 1H, Ar), 8.07 (br s, 1H, NH₂, D₂O exch.); ¹³C NMR (101 MHz, DMSO-

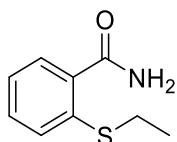
d_6): δ 45.5 (CH₃), 129.1 (Ar), 129.6 (Ar), 130.2 (Ar), 134.1 (Ar), 138.3 (Ar), 138.4 (Ar), 170.0 (CONH₂).



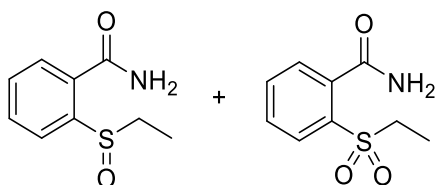
Methyl 2-(ethylthio)benzoate (E2): anhydrous potassium carbonate (1.1 equiv.) was added to a stirring solution of methyl thiosalicylate (1 equiv.) in 10 mL of *N,N*-dimethylformamide. After 1 h, ethyl bromide was added dropwise and the reaction stirred under nitrogen atmosphere at 70 °C for 5 h. The mixture was poured on ice and the resulting suspension extracted with dichloromethane (3 × 20 mL). The organics were reunited, dried over sodium sulphate and concentrated *in vacuo* to give a crude product purified by column chromatography on silica gel (cyclohexane:ethyl acetate, 7:1). The title compound was a colourless oil (90% yield). ¹H NMR (400 MHz, CDCl₃): δ 1.41 (t, *J* = 7.4 Hz, 3H, CH₃), 2.95-3.01 (m, 2H, CH₂), 3.93 (s, 3H, CH₃), 7.15-7.19 (m, 1H, Ar), 7.33 (d, *J* = 8.0 Hz, 1H, Ar), 7.44-7.48 (m, 1H, Ar), 7.97-7.99 (m, 1H, Ar); ¹³C NMR (101 MHz, CDCl₃): δ 13.2 (CH₃), 26.0 (CH₂), 52.1 (CH₃), 123.7 (Ar), 125.4 (Ar), 127.4 (Ar), 131.3 (Ar), 132.3 (Ar), 142.1 (Ar), 167.0 (C=O).



2-(Ethylthio)benzoic acid (A2): lithium hydroxide (1.2 equiv.), dissolved in 10 mL of water, was added dropwise to a stirring solution of methyl 2-(ethylthio)benzoate (E2) (1 equiv.) in H₂O/methanol (50 mL, 50:50 v:v). The reaction was stirred at 70 °C for 2 h, concentrated *in vacuo* to remove methanol and quenched with 2N HCl. The precipitate was collected by filtration and washed with *n*-hexane to give the title compound as a white solid (92% yield); mp 141-143 °C. ¹H NMR (400 MHz, DMSO-*d*₆): δ 1.43 (t, *J* = 7.4 Hz, 3H, CH₃), 2.98-3.03 (m, 2H, CH₂), 7.20-7.24 (m, 1H, Ar), 7.38 (d, *J* = 7.9 Hz, 1H, Ar), 7.50-7.54 (m, 1H, Ar), 8.15-8.18 (m, 1H, Ar), 11.46 (br s, 1H, COOH, D₂O exch.).



2-(Ethylthio)benzamide (4): triethylamine (3 equiv.) and ethyl chloroformate (1.2 equiv.) were added to a stirring solution of 2-(ethylthio)benzoic acid (**A2**) (1 equiv.) in 10 mL of tetrahydrofuran. After monitoring the anhydride intermediate formation with silica TLC plates, ammonium chloride (1.4 equiv.) was added. The reaction was stirred under nitrogen atmosphere for 16 h at 50 °C and concentrated *in vacuo*. Water (70 mL) was added and the resulting suspension extracted with ethyl acetate (3 × 20 mL). The organics were reunited, dried over sodium sulphate and concentrated under reduced pressure to give a crude product purified by column chromatography on silica gel (ethyl acetate:cyclohexane, 2:1). The title compound was a white solid (65% yield); mp 122-124 °C. ¹H NMR (400 MHz, CDCl₃): δ 1.32 (t, *J* = 7.4 Hz, 3H, CH₃), 2.95-3.00 (m, 2H, CH₂), 6.00 (br s, 1H, NH₂, D₂O exch.), 6.92 (br s, 1H, NH₂, D₂O exch.), 7.27-7.32 (m, 1H, Ar), 7.39-7.47 (m, 2H, Ar), 7.78-7.80 (m, 1H, Ar); ¹³C NMR (101 MHz, CDCl₃): δ 14.0 (CH₃), 28.7 (CH₂), 126.4 (Ar), 129.7 (Ar), 130.8 (Ar), 131.0 (Ar), 134.7 (Ar), 135.3 (Ar), 169.8 (CONH₂).

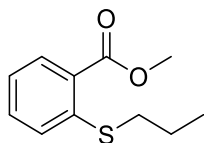


2-(Ethylsulfinyl)benzamide (5) and 2-(ethylsulfonyl)benzamide (6): 3-chloroperbenzoic acid (1 equiv.), dissolved in 5 mL of methanol, was added dropwise to a stirring solution of 2-(ethylthio)benzoic acid (**4**) (1 equiv.) in 25 mL of methanol. After 2 h, another aliquot of 3-chloroperbenzoic acid (1 equiv. in 5 mL of methanol) was added and the reaction stirred for further 24 h. The mixture was concentrated *in vacuo* and purified by column chromatography on silica gel (ethyl acetate:cyclohexane, 5:1) to give separately the title compounds **5** and **6**.

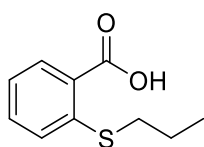
5: white solid, 48% yield, mp 155-157 °C. ¹H NMR (400 MHz, DMSO-*d*₆): δ 1.09 (t, *J* = 7.4 Hz, 3H, CH₃), 2.64-2.73 (m, 1H, CH₂), 3.13-3.22 (m, 1H, CH₂), 7.60-7.64 (m, 1H, Ar), 7.68 (br s, 1H, NH₂, D₂O exch.), 7.76-7.80 (m, 1H, Ar), 7.89-7.91 (m, 1H, Ar), 8.01-8.03 (m, 1H, Ar), 8.25 (br s, 1H, NH₂, D₂O exch.); ¹³C NMR (101 MHz, CDCl₃): δ 6.7 (CH₃), 50.0 (CH₂), 125.1 (Ar), 128.5 (Ar), 130.5 (Ar), 131.9 (Ar), 132.1 (Ar), 146.4 (Ar), 168.1 (CONH₂).

6: white solid, 29% yield, mp 141-143 °C. ¹H NMR (400 MHz, CDCl₃): δ 1.31 (t, *J* = 7.5, 3H, CH₃), 3.51-3.57 (m, 2H, CH₂), 5.98 (br s, 1H, NH₂, D₂O exch.), 6.29 (br s, 1H, NH₂, D₂O

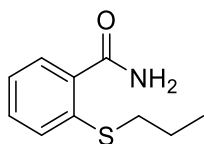
exch.), 7.60-7.64 (m, 2H, Ar), 7.68-7.72 (m, 1H, Ar), 8.02-8.04 (m, 1H, Ar); ^{13}C NMR (101 MHz, CDCl_3): δ 7.1 (CH_3), 51.1 (CH_2), 128.6 (Ar), 130.2 (Ar), 130.8 (Ar), 133.7 (Ar), 136.2 (Ar), 136.8 (Ar), 170.2 (CONH_2).



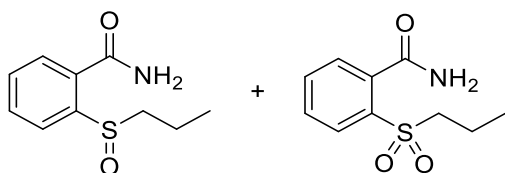
Methyl 2-(propylthio)benzoate (E3): anhydrous potassium carbonate (1.1 equiv.) was added to a stirring solution of methyl thiosalicylate (1 equiv.) in 10 mL of *N,N*-dimethylformamide. After 1 h, 1-bromopropane was added dropwise and the reaction stirred under nitrogen atmosphere at 70 °C for 5 h. The mixture was poured on ice and the resulting suspension was extracted with dichloromethane (3×20 mL). The organics were reunited, dried over sodium sulphate and concentrated *in vacuo* to give a crude product purified by column chromatography on silica gel (cyclohexane:ethyl acetate, 5:1). The title compound was a colourless oil (93% yield). ^1H NMR (400 MHz, CDCl_3): δ 1.10 (t, $J = 7.4$ Hz, 3H, CH_3), 1.75-1.81 (m, 2H, CH_2), 2.90-2.94 (m, 2H, CH_2), 3.93 (s, 3H, CH_3), 7.13-7.17 (m, 1H, Ar), 7.33 (d, $J = 8.0$ Hz, 1H, Ar), 7.42-7.47 (m, 1H, Ar), 7.95-7.98 (m, 1H, Ar); ^{13}C NMR (101 MHz, CDCl_3): δ 13.8 (CH_3), 21.7 (CH_2), 34.1 (CH_2), 52.0 (CH_3), 123.6 (Ar), 125.6 (Ar), 127.6 (Ar), 131.3 (Ar), 132.2 (Ar), 142.2 (Ar), 167.0 ($\text{C}=\text{O}$).



2-(Propylthio)benzoic acid (A3): lithium hydroxide (1.2 equiv.), dissolved in 10 mL of water, was added dropwise to a stirring solution of methyl 2-(propylthio)benzoate (**E3**) (1 equiv.) in H_2O /methanol (50 mL, 50:50 v:v). The reaction was stirred at 70 °C for 2 h, concentrated *in vacuo* to remove methanol and quenched with 2N HCl. The precipitate was collected by filtration and washed with *n*-hexane to give the title compound as a white solid (95% yield); mp 125-127 °C. ^1H NMR (400 MHz, CDCl_3): δ 1.12 (t, $J = 7.4$ Hz, 3H, CH_3), 1.76-1.85 (m, 2H, CH_2), 2.93-2.97 (m, 2H, CH_2), 7.20-7.24 (m, 1H, Ar), 7.38 (d, $J = 7.8$ Hz, 1H, Ar), 7.49-7.53 (m, 1H, Ar), 8.15-8.17 (m, 1H, Ar), 11.94 (br s, 1H, COOH , D_2O exch.).



2-(Propylthio)benzamide (7): triethylamine (3 equiv.) and ethyl chloroformate (1.2 equiv.) were added to a stirring solution of 2-(propylthio)benzoic acid (**A3**) (1 equiv.) in 10 mL of tetrahydrofuran. After monitoring the anhydride intermediate formation with silica TLC plates, ammonium chloride (1.4 equiv.) was added. The reaction was stirred under nitrogen atmosphere for 16 h at 50 °C and concentrated *in vacuo*. Water (70 mL) was added and the resulting suspension extracted with ethyl acetate (3 × 20 mL). The organics were reunited, dried over sodium sulphate and concentrated under reduced pressure to give a crude product purified by column chromatography on silica gel (ethyl acetate:cyclohexane, 1:1). The title compound was a white solid (68% yield); mp 122-124 °C. ¹H NMR (400 MHz, CDCl₃): δ 0.94 (t, *J* = 7.3 Hz, 3H, CH₃), 1.54-1.63 (m, 2H, CH₂), 2.83 (t, *J* = 7.3 Hz, 2H, CH₂), 6.47 (br s, 1H, NH₂, D₂O exch.), 6.98 (br s, 1H, NH₂, D₂O exch.), 7.17-7.21 (m, 1H, Ar), 7.29-7.33 (m, 1H, Ar), 7.36 (d, *J* = 7.2 Hz, 1H, Ar), 7.69 (d, *J* = 7.6 Hz, 1H, Ar); ¹³C NMR (101 MHz, CDCl₃): δ 13.5 (CH₃), 22.3 (CH₂), 36.7 (CH₂), 126.3 (Ar), 129.7 (Ar), 130.8 (Ar), 131.1 (Ar), 135.0 (Ar), 135.1 (Ar), 170.2 (CONH₂).

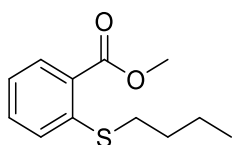


2-(propylsulfinyl)benzamide (8) and 2-(propylsulfonyl)benzamide (9): a solution of 3-chloroperbenzoic acid (1 equiv.), dissolved in 5 mL of methanol, was added dropwise to a stirring solution of 2-(propylthio)benzamide (**7**) (1 equiv.) in 25 mL of methanol. After 2 h, another aliquot of 3-chloroperbenzoic acid (1 equiv. in 5 mL of methanol) was added and the reaction was stirred for further 24 h. The mixture was concentrated *in vacuo* and purified by column chromatography on silica gel (ethyl acetate:cyclohexane, 3:1) to give separately the title compounds **8** and **9**.

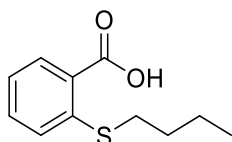
8: white solid, 35% yield, mp 162-164 °C. ¹H NMR (400 MHz, DMSO-*d*₆): δ 0.97 (t, *J* = 7.4 Hz, 3H, CH₃), 1.51-1.63 (m, 1H, CH₂), 1.72-1.84 (m, 1H, CH₂), 2.53-2.60 (m, 1H, CH₂), 3.11-3.18 (m, 1H, CH₂), 7.59-7.63 (m, 1H, Ar), 7.68 (br s, 1H, NH₂, D₂O exch.), 7.76-7.80 (m, 1H, Ar), 7.89-7.91 (m, 1H, Ar), 8.04-8.07 (m, 1H, Ar), 8.25 (br s, 1H, NH₂, D₂O exch.); ¹³C NMR

(101 MHz, DMSO-*d*₆): δ 13.3 (CH₃), 16.5 (CH₂), 59.3 (CH₂), 124.7 (Ar), 128.4 (Ar), 130.4 (Ar), 132.0 (Ar), 132.2 (Ar), 147.3 (Ar), 168.1 (CONH₂).

9: white solid, 40% yield, mp 122-124 °C. ¹H NMR (400 MHz, CDCl₃): δ 1.04 (t, *J* = 7.4 Hz, 3H, CH₃), 1.76-1.81 (m, 2H, CH₂), 3.47-3.51 (m, 2H, CH₂), 5.96 (br s, 1H, NH₂, D₂O exch.), 6.28 (br s, 1H, NH₂, D₂O exch.), 7.60-7.64 (m, 2H, Ar), 7.67-7.71 (m, 1H, Ar), 8.02-8.05 (m, 1H, Ar); ¹³C NMR (101 MHz, CDCl₃): δ 13.0 (CH₃), 16.2 (CH₂), 58.4 (CH₂), 128.6 (Ar), 130.2 (Ar), 130.5 (Ar), 133.7 (Ar), 136.7 (Ar), 136.9 (Ar), 170.2 (CONH₂).

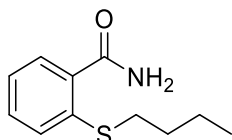


Methyl 2-(butylthio)benzoate (E4): anhydrous potassium carbonate (1.1 equiv.) was added to a stirring solution of methyl thiosalicylate (1 equiv.) in 5 mL of *N,N*-dimethylformamide. After 1 h, 1-bromobutane was added dropwise and the reaction stirred under nitrogen atmosphere at 70 °C for 5 h. The mixture was poured on ice and the resulting suspension extracted with dichloromethane (3 × 20 mL). The organics were reunited, dried over sodium sulphate and concentrated *in vacuo* to give a crude product purified by column chromatography on silica gel (cyclohexane:ethyl acetate, 6:1). The title compound was a colourless oil (89% yield). ¹H NMR (400 MHz, CDCl₃): δ 0.96 (t, *J* = 7.3 Hz, 3H, CH₃), 1.47-1.56 (m, 2H, CH₂), 1.69-1.76 (m, 2H, CH₂), 2.91-2.95 (m, 2H, CH₂), 3.92 (s, 3H, CH₃), 7.12-7.16 (m, 1H, Ar), 7.32 (d, *J* = 7.8 Hz, 1H, Ar), 7.41-7.46 (m, 1H, Ar), 7.95-7.97 (m, 1H, Ar); ¹³C NMR (101 MHz, CDCl₃): δ 13.7 (CH₃), 22.3 (CH₂), 30.2 (CH₂), 31.7 (CH₂), 52.0 (CH₃), 123.6 (Ar), 125.5 (Ar), 127.5 (Ar), 131.3 (Ar), 132.2 (Ar), 142.3 (Ar), 166.9 (C=O).

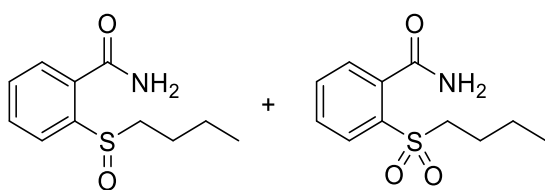


2-(Butylthio)benzoic acid (A4): lithium hydroxide (1.2 equiv.), dissolved in 10 mL of water, was added dropwise to a stirring solution of methyl 2-(butylthio)benzoate (**E4**) (1 equiv.) in H₂O/methanol (50 mL, 50:50 *v:v*). The reaction was stirred at 70 °C for 2 h, concentrated *in vacuo* to remove methanol and quenched with 2N HCl. The precipitate was collected by filtration and washed with *n*-hexane (2 x 10 mL) to give the title compound as a white solid (83% yield); mp 100-102 °C. ¹H NMR (400 MHz, CDCl₃): δ 0.99 (t, *J* = 7.3 Hz, 3H, CH₃), 1.50-1.59 (m, 2H, CH₂), 1.72-1.80 (m, 2H, CH₂), 2.95-2.98 (m, 2H, CH₂), 7.21 (t, *J* = 7.5 Hz,

1H, Ar), 7.37 (d, $J = 8.1$ Hz, 1H, Ar), 7.49-7.53 (m, 1H, Ar), 8.14-8.17 (m, 1H, Ar), 10.39 (br s, 1H, COOH, D₂O exch.); ¹³C NMR (101 MHz, CDCl₃): δ 13.7 (CH₃), 22.3 (CH₂), 30.2 (CH₂), 31.9 (CH₂), 123.8 (Ar), 125.7 (Ar), 126.3 (Ar), 132.6 (Ar), 133.1 (Ar), 143.3 (Ar), 171.6 (C=O).



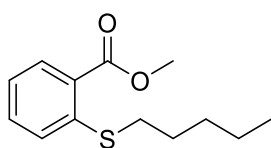
2-(Butylthio)benzamide (10): triethylamine (3 equiv.) and ethyl chloroformate (1.2 equiv.) were added to a stirring solution of 2-(butylthio)benzoic acid (**A4**) (1 equiv.) in 10 mL of tetrahydrofuran. After monitoring the anhydride intermediate formation with silica TLC plates, ammonium chloride (1.4 equiv.) was added. The reaction was stirred under nitrogen atmosphere for 16 h at 50 °C and concentrated *in vacuo*. Water (70 mL) was added and the resulting suspension extracted with ethyl acetate (3 × 30 mL). The organics were reunited, dried over sodium sulphate and concentrated under reduced pressure to give a crude product purified by column chromatography on silica gel (ethyl acetate:cyclohexane, 1:1). The title compound was a white solid (68% yield); mp 100-102 °C. ¹H NMR (400 MHz, CDCl₃): δ 0.92 (t, $J = 7.3$ Hz, 3H, CH₃), 1.41-1.50 (m, 2H, CH₂), 1.59-1.57 (m, 2H, CH₂), 2.93 (t, $J = 7.3$ Hz, 2H, CH₂), 6.58 (br s, 1H, NH₂, D₂O exch.), 7.06 (br s, 1H, NH₂, D₂O exch.), 7.25-7.27 (m, 1H, Ar), 7.37-7.45 (m, 2H, Ar), 7.75-7.78 (m, 1H, Ar); ¹³C NMR (101 MHz, CDCl₃): δ 13.6 (CH₃), 22.0 (CH₂), 30.9 (CH₂), 34.4 (CH₂), 126.2 (Ar), 129.7 (Ar), 130.6 (Ar), 131.1 (Ar), 134.9 (Ar), 135.3 (Ar), 170.2 (CONH₂).



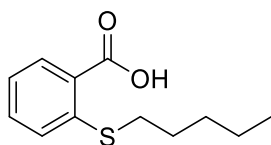
2-(Butylsulfinyl)benzamide (11) and 2-(butylsulfonyl)benzamide (12): a solution of 3-chloroperbenzoic acid (1 equiv.), dissolved in 5 mL of methanol, was added dropwise to a stirring solution of 2-(propylthio)benzamide (**10**) (1 equiv.) in 25 mL of methanol. After 2 h, another aliquot of 3-chloroperbenzoic acid (1 equiv. in 5 mL of methanol) was added and the reaction stirred for further 24 h. The mixture was concentrated *in vacuo* and purified by column chromatography on silica gel (ethyl acetate:cyclohexane, 3:1) to give separately the title compounds **11** and **12**.

11: white solid, 44% yield, mp 130-132 °C. ^1H NMR (400 MHz, DMSO- d_6): δ 0.88 (t, $J = 7.3$ Hz, 3H, CH₃), 1.33-1.43 (m, 2H, CH₂), 1.44-1.55 (m, 1H, CH₂), 1.72-1.79 (m, 1H, CH₂), 2.55-2.61 (m, 1H, CH₂), 3.15-3.22 (m, 1H, CH₂), 7.59-7.63 (m, 1H, Ar), 7.68 (br s, 1H, NH₂, D₂O exch.), 7.76-7.80 (m, 1H, Ar), 7.88-7.90 (m, 1H, Ar), 8.04-8.06 (m, 1H, Ar), 8.25 (br s, 1H, NH₂, D₂O exch.).

12: white solid, 40% yield, mp 129-131 °C. ^1H NMR (400 MHz, CDCl₃): δ 0.92 (t, $J = 7.3$ Hz, 3H, CH₃), 1.40-1.49 (m, 2H, CH₂), 1.69-1.77 (m, 2H, CH₂), 3.49-3.53 (m, 2H, CH₂), 5.93 (br s, 1H, NH₂, D₂O exch.), 6.26 (br s, 1H, NH₂, D₂O exch.), 7.60-7.64 (m, 2H, Ar), 7.67-7.71 (m, 1H, Ar), 8.03-8.05 (m, 1H, Ar).

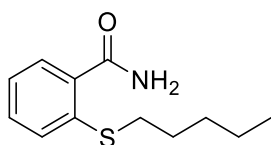


Methyl 2-(pentylthio)benzoate (E5): anhydrous potassium carbonate (1.1 equiv.) was added to a stirring solution of methyl thiosalicylate (1 equiv.) in 5 mL of *N,N*-dimethylformamide. After 1 h, 1-bromopentane was added dropwise and the reaction stirred under nitrogen atmosphere at 70 °C for 5 h. The mixture was poured on ice and the resulting suspension extracted with dichloromethane (3 × 20 mL). The organics were reunited, dried over sodium sulphate and concentrated *in vacuo* to give a crude product purified by column chromatography on silica gel (cyclohexane:ethyl acetate, 7:1). The title compound was a colourless oil (85% yield). ^1H NMR (400 MHz, DMSO- d_6): δ 0.86 (t, $J = 7.2$ Hz, 3H, CH₃), 1.27-1.33 (m, 2H, CH₂), 1.35-1.43 (m, 2H, CH₂), 1.56-1.64 (m, 2H, CH₂), 2.92 (t, $J = 7.4$ Hz, 2H, CH₂), 3.82 (s, 3H, CH₃), 7.20-7.24 (m, 1H, Ar), 7.42 (d, $J = 7.8$ Hz, 1H, Ar), 7.51-7.56 (m, 1H, Ar), 7.84-7.86 (m, 1H, Ar); ^{13}C NMR (101 MHz, DMSO- d_6): δ 14.3 (CH₃), 22.2 (CH₂), 28.0 (CH₂), 31.1 (CH₂), 31.4 (CH₂), 52.5 (CH₃), 124.4 (Ar), 126.4 (Ar), 128.0 (Ar), 131.1 (Ar), 133.0 (Ar), 141.3 (Ar), 166.6 (C=O).

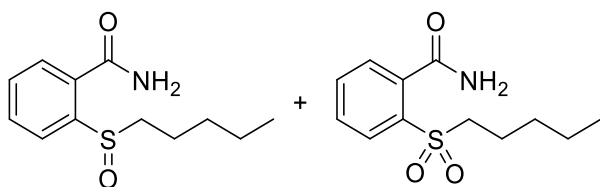


2-(Pentylthio)benzoic acid (A5): lithium hydroxide (1.2 equiv.), dissolved in 10 mL of water, was added dropwise to a stirring solution of methyl 2-(butylthio)benzoate (**E5**) (1 equiv.) in H₂O/methanol (70 mL, 50:50 v:v). The reaction was stirred at 70 °C for 2 h, concentrated *in vacuo* to remove methanol and quenched with 2N HCl. The precipitate was collected by

filtration and washed with *n*-hexane (2 x 10 mL) to give the title compound as a white solid (85% yield); mp 104-107 °C. ¹H NMR (400 MHz, CDCl₃): δ 0.94 (t, *J* = 7.2 Hz, 3H, CH₃), 1.35-1.44 (m, 2H, CH₂), 1.47-1.54 (m, 2H, CH₂), 1.74-1.81 (m, 2H, CH₂), 2.94-2.98 (m, 2H, CH₂), 7.21 (t, *J* = 7.5 Hz, 1H, Ar), 7.37 (d, *J* = 8.1 Hz, 1H, Ar), 7.49-7.53 (m, 1H, Ar), 8.14-8.17 (m, 1H, Ar), 9.58 (br s, 1H, COOH, D₂O exch.); ¹³C NMR (101 MHz, CDCl₃): δ 13.9 (CH₃), 22.3 (CH₂), 27.9 (CH₂), 31.4 (CH₂), 32.2 (CH₂), 123.8 (Ar), 125.7 (Ar), 126.3 (Ar), 132.6 (Ar), 133.1 (Ar), 142.2 (Ar), 171.6 (COOH).



2-(Pentylthio)benzamide (13): triethylamine (3 equiv.) and ethyl chloroformate (1.2 equiv.) were added to a stirring solution of 2-(pentylthio)benzoic acid (**A5**) (1 equiv.) in 10 mL of tetrahydrofuran. After monitoring the anhydride intermediate formation with silica TLC plates, ammonium chloride (1.4 equiv.) was added. The reaction was stirred under nitrogen atmosphere for 16 h at 50 °C and concentrated *in vacuo*. Water (70 mL) was added and the resulting suspension extracted with ethyl acetate (3 × 30 mL). The organics were reunited, dried over sodium sulphate and concentrated under reduced pressure to give a crude product purified by column chromatography on silica gel (*n*-hexane:ethyl acetate, 3:1). The title compound was a white solid (60% yield); mp 95-97 °C. ¹H NMR (400 MHz, CDCl₃): δ 0.91 (t, *J* = 7.2 Hz, 3H, CH₃), 1.27-1.37 (m, 2H, CH₂), 1.39-1.46 (m, 2H, CH₂), 1.62-1.70 (m, 2H, CH₂), 2.94 (t, *J* = 7.4 Hz, 2H, CH₂), 5.87 (br s, 1H, NH₂, D₂O exch.), 6.95 (br s, 1H, NH₂, D₂O exch.), 7.27-7.31 (m, 1H, Ar), 7.39-7.47 (m, 2H, Ar), 7.79-7.81 (m, 1H, Ar); ¹³C NMR (101 MHz, CDCl₃): δ 13.9 (CH₃), 22.2 (CH₂), 28.6 (CH₂), 31.0 (CH₂), 34.8 (CH₂), 126.3 (Ar), 129.8 (Ar), 130.8 (Ar), 131.0 (Ar), 135.1 (Ar), 135.2 (Ar), 169.7 (CONH₂).



2-(pentylsulfinyl)benzamide (14) and 2-(pentylsulfonyl)benzamide (15): 3-chloroperbenzoic acid (1 equiv.), dissolved in 5 mL of methanol, was added dropwise to a stirring solution of 2-(propylthio)benzamide (**13**) (1 equiv.) in 25 mL of methanol. After 2 h, another aliquot of 3-chloroperbenzoic acid (1 equiv. in 5 mL of methanol) was added and the

reaction was stirred for further 24 h. The mixture was concentrated *in vacuo* and purified by column chromatography on silica gel (cyclohexane:ethyl acetate, 1:1) to give separately the title compounds **14** and **15**.

14: white solid, 39% yield, mp 126-128 °C. ¹H NMR (400 MHz, DMSO-*d*₆): δ 0.88 (t, *J* = 8 Hz, 3H, CH₃), 1.26-1.41 (m, 4H, 2 x CH₂), 1.50-1.56 (m, 1H, CH₂), 1.74-1.79 (m, 1H, CH₂), 2.53-2.60 (m, 1H, CH₂), 3.14-3.21 (m, 1H, CH₂), 7.59-7.63 (m, 1H, Ar), 7.69 (br s, 1H, NH₂, D₂O exch.), 7.76-7.80 (m, 1H, CH₂), 7.88-7.90 (m, 1H, Ar), 8.04-8.06 (m, 1H, Ar), 8.25 (br s, 1H, NH₂, D₂O exch.).

15: white solid, 37% yield, mp 95-97 °C. ¹H NMR (400 MHz, CDCl₃): δ 0.89 (t, *J* = 7.1 Hz, 3H, CH₃), 1.28-1.43 (m, 2H, CH₂), 1.61-1.63 (m, 2H, CH₂), 1.72-1.80 (m, 2H, CH₂), 3.48-3.52 (m, 2H, CH₂), 5.91 (br s, 1H, NH₂, D₂O exch.), 6.24 (br s, 1H, NH₂, D₂O exch.), 7.61-7.64 (m, 2H, Ar), 7.68-7.72 (m, 1H, Ar), 8.04-8.07 (m, 1H, Ar); ¹³C NMR (101 MHz, CDCl₃): δ 13.7 (CH₃), 22.0 (CH₂), 22.1 (CH₂), 30.3 (CH₂), 56.7 (CH₂), 128.6 (Ar), 130.2 (Ar), 130.5 (Ar), 133.6 (Ar), 136.7 (Ar), 136.9 (Ar), 170.2 (CONH₂).

2.5.3. Enzyme inhibition assays

An Applied Photophysics stopped-flow instrument was used for assaying the CA catalysed CO₂ hydration activity [126]. Phenol red (0.2 mM) was used as an indicator, working at the absorbance maximum of 557 nm, with 20 mM Hepes (pH 7.5, for α-CAs) as buffer and 20 mM NaClO₄ (for maintaining constant the ionic strength), following the initial rates of the CA-catalysed CO₂ hydration reaction for a period of 10-100 s. The CO₂ concentrations ranged from 1.7 to 17 mM for the determination of the kinetic parameters and inhibition constants. In particular, CO₂ was bubbled in distilled deionized water for 30 min till saturation. A CO₂ kit (Sigma, Milan, Italy) was used to measure the concentration in serially diluted solutions from the saturated one at the same temperature. For each inhibitor at least six traces of the initial 5-10% of the reaction were used for determining the initial velocity. The uncatalyzed rates were determined in the same manner and subtracted from the total observed rates. Stock solutions of the inhibitor (1 μM) were prepared in distilled-deionized water and dilutions up to 0.1 nM were conducted thereafter with the assay buffer procedure. Inhibitor and enzyme solutions were preincubated together for 15 min at room temperature prior to the assay buffer, to allow for the formation of the E-I complex or to allow for active site mediated hydrolysis of the inhibitor. The inhibition constants were obtained by non-linear least-squares methods using PRISM 3 and the Cheng-Prusoff equation [127], and represented the average from at least three different

determinations. All recombinant CA isoforms were obtained in-house as previously reported [128,129].

*This Chapter refers to the paper “Novel insights on saccharin- and acesulfame-based carbonic anhydrase inhibitors: design, synthesis, modelling investigations and biological activity” by P. Guglielmi, **G. Rotondi**, D. Secci, A. Angeli, P. Chimenti, A. Nocentini, A. Bonardi, P. Gratteri, S. Carradori, C. T. Supuran published in J. Enzyme Inhib. Med. Chem. 35 (2020) 1891-1905 [130].*

3. Novel insights on saccharin- and acesulfame-based carbonic anhydrase inhibitors: design, synthesis, modelling investigations and biological activity evaluation

3.1. Design of novel inhibitors based on the saccharin and acesulfame scaffold

In the past few years many compounds devoid of the primary sulphonamide group attribute have been discovered and evaluated as effective hCAs inhibitors [26,99,131,132]

As previously described, among the scaffolds frequently used for the development of non-classical inhibitors of hCAs, saccharin and acesulfame have gained great importance. Particularly, since the discovery of its inhibitory activity against hCAs, saccharin has caught the attention as a valuable hit compound for the design of novel molecules acting towards hCAs [121]. Several research groups, including ours, have developed numerous hCAs inhibitors based on this promising scaffold [133–137].

The approaches that have been used to modify this nucleus are based on the derivatization of the benzene moiety to retain the cyclic sulphonamide secondary group, or on its derivatization to obtain *N*-substituted saccharins. Our research group has mostly focused on the second procedure synthesizing a large library of *N*-alkyl, *N*-benzyl or *N*-benzoyl methylene derivatives [112,114,138].

As part of the research group's efforts to develop novel inhibitors of carbonic anhydrase, I report a large library of derivatives aimed at further explore the saccharin scaffold, taking advantage of a variety of design strategies.

The first strategy I used (**Figure 3.1**) relied on the replacement of the saccharin nitrogen with an unsaturated and branched alkyl chain, benzyl or benzoyl methylene moieties, as already proposed by our research group in the past years. These substituents could represent a corollary for the robust structure-activity relationships already published [112,114,138].

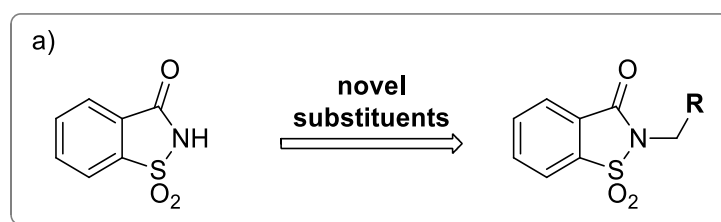


Figure 3.1. The first design strategy proposed for the saccharin scaffold.

The second strategy I used (**Figure 3.2**) was based on the removal of the methylene bridge included in the benzyl substituted derivatives. I tried to evaluate, on one side, the effects resulting from the loss of conformational freedom and, on the other, the consequences of the direct binding of the sulphonamide nitrogen atom to the phenyl ring. The removal of the methylene linker affected the electronic distribution, due to the onset of conjugation between the electron pair of nitrogen with the π -electrons of the phenyl ring, previously prevented by the presence of the CH₂ group.

Furthermore, the synthesis of the saccharin derivatives, consisting of a multistep approach, was studied *ad hoc* to obtain potential inhibitors for hCAs in each step (**Figure 3.2, ii and iii**). The acid intermediates **ii** possess two functional groups suitable for anchoring the zinc ion or the relative anchored water in the catalytic active site (-SO₂NH- and COOH, respectively); moreover, they reflect the structure of the opened saccharins, reported by Ivanova *et al*, that exhibited improved selectivity than their parent closed analogues against the tumour-related isoforms of hCA [137]. These acid derivatives were obtained through the hydrolysis of the ester precursors (**Figure 3.2, ii**) that could themselves be potential inhibitors of the hCAs since they retain the secondary sulphonamide group. Moreover, considering the esterase activity of hCAs [139], these molecules, if not active as esters, could undergo the enzyme-mediated hydrolysis in the active site, acting as putative prodrugs of the acid analogues. The derivatives belonging to the sub-groups **ii** and **iii** can also be considered the isosteres of the series of compounds partly presented in the second Chapter of this Section [123]. These inhibitors, even if devoid of a ZBG, resulted selectively active against hCA IX in the μ M range, suggesting that the replacement of -CH₂ by -NH could improve the activity against hCAs.

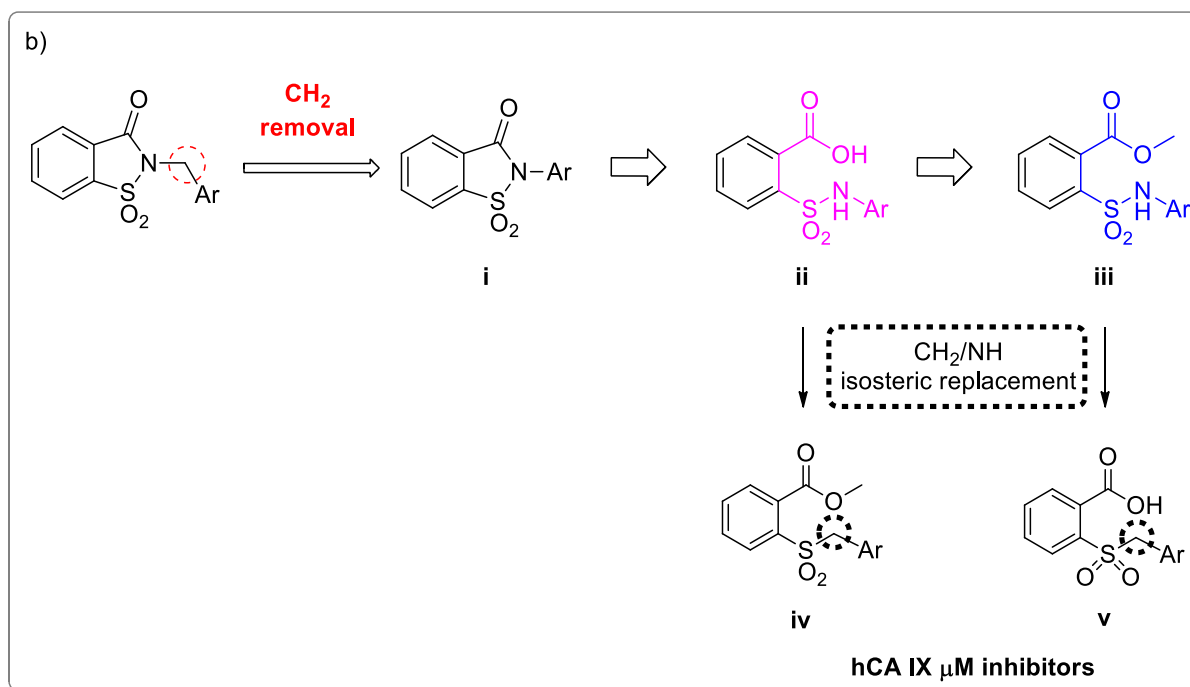


Figure 3.2. The second design strategy proposed for the saccharin scaffold: design and retrosynthetic approach.

The third design strategy I used was inspired by the findings of our recent paper [115] regarding a series of saccharin/isoxazole and saccharin/isooxazoline derivatives (**Figure 3.3**) [115]. These compounds, characterized by an isoxazole or isooxazoline linker that disconnected the methylene moiety from the phenyl ring, resulted in a strong affinity for hCA IX and hCA XII and selectivity over hCA I and hCA II (**Figure 3.3, A**). Thus, based on these promising results, I proposed the replacement of the isoxazole “linker” with the triazole one, that resulted advantageous for some hCAs inhibitors (**Figure 3.3, B**) [140–143]. The triazole ring is an aromatic five-membered heterocyclic ring, similarly to the isoxazole one, although it contains only the nitrogen heteroatom instead of the oxygen/nitrogen ones of the isoxazole core. Moreover, just as the isoxazole, it can establish stacking interactions in the lipophilic side of the active site, and it is easy to insert through the “click” reaction azide-alkyne cycloaddition. For some of these derivatives, I also evaluated the hydrolytic ring opening and/or the introduction of an additional methylene group between the N1 of the triazole and the phenyl ring bound to it. The ring opening can lead to the same improvements discussed above, and the insertion of the methylene group could increase the “flexibility” of the tail, interrupting the electronic conjugation (**Figure 3.3**).

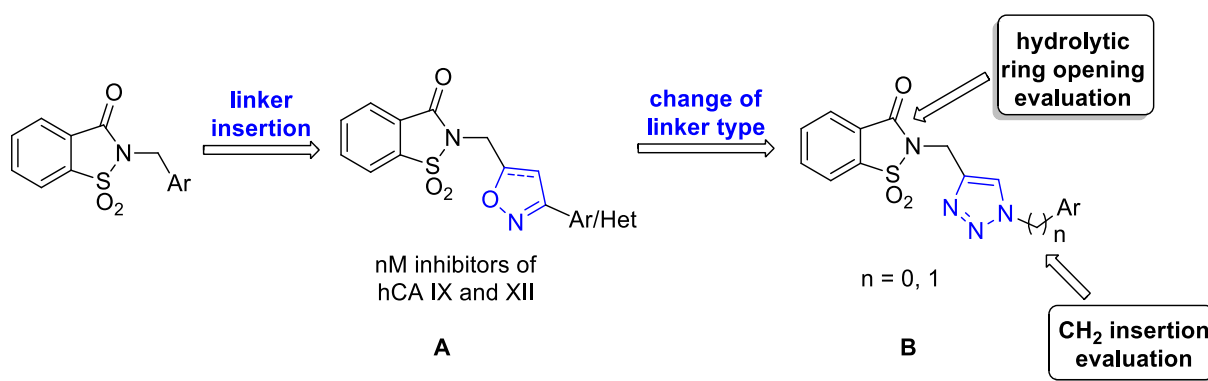


Figure 3.3. The third design strategy proposed for the saccharin scaffold.

Similar to saccharin, the other artificial sweetener potassium acesulfame (Ace K) is a valid scaffold used in the development of hCA inhibitors. It has been largely explored both for its capability to inhibit carbonic anhydrase as such [122], and after oxygen/nitrogen derivatization with different substituents (i.e. (un)saturated alkyl chains, (un)substituted benzyl or benzoyl methylene moieties [113,114]. Ace K bearing benzoyl moieties exhibited good inhibitory activity against hCA IX and XII, although some of them retained residual activity against the “off-targets” hCA I/II. Taking advantage of the substitution approaches proposed for the saccharin-based compounds, I translated the first and the third design strategies on the acesulfame scaffold (**Figure 3.4**, a and b). Adjusting the synthesis conditions, I chose to preferentially address the propargylation and then the triazole assembling, either at the oxygen or the nitrogen of the acesulfame core to achieve *N*- and *O*-substituted analogues, respectively (**Figure 3.4**, b). I then attempted the insertion of an additional methylene group, disconnecting the phenyl group from the N1 of the triazole ring. Interestingly, since some of the reported compounds differ only for their nucleus (saccharin or acesulfame), it was also possible to evaluate the effects on the activity and selectivity of the molecules retaining the same tail but not the main core.

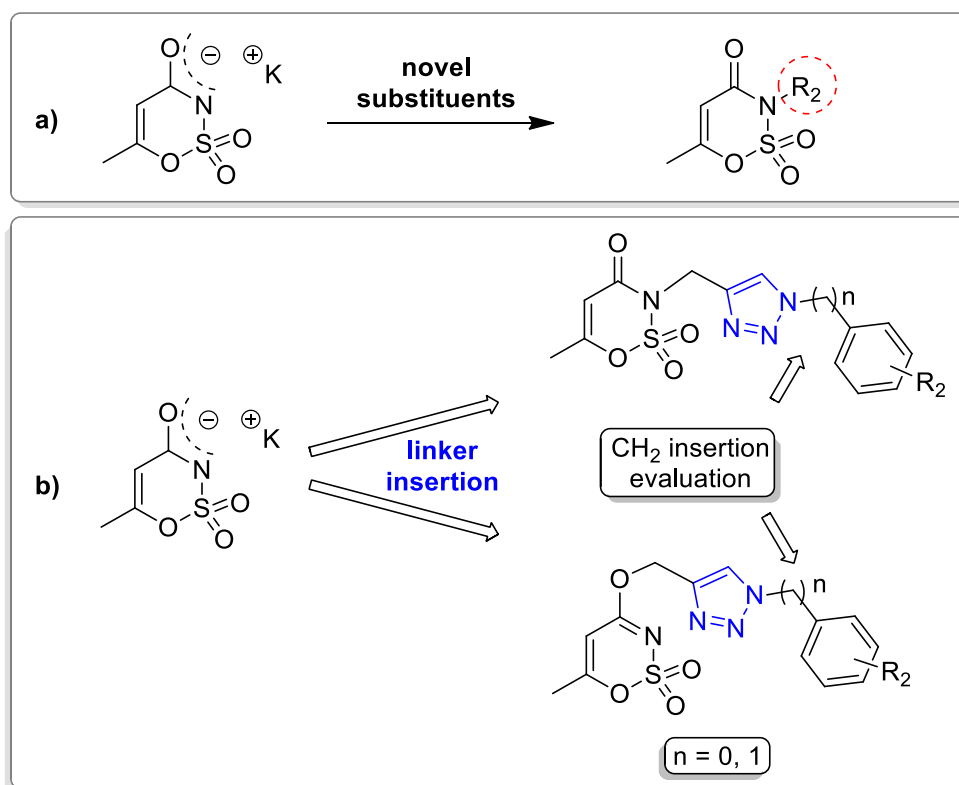
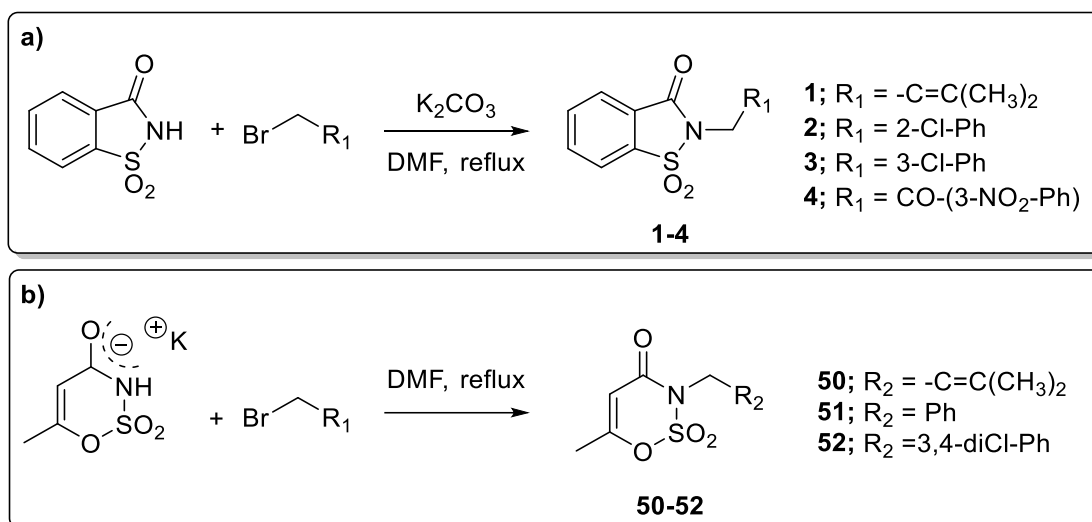


Figure 3.4. The first and third strategy translated on the acesulfame scaffold.

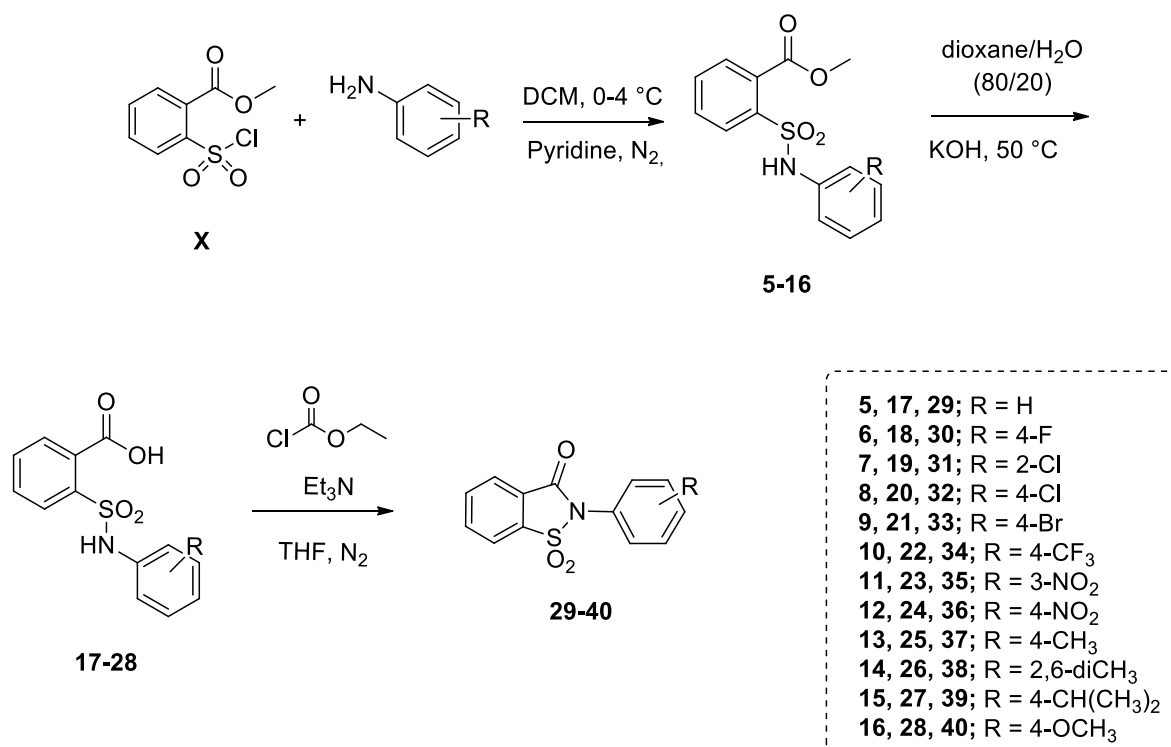
3.2. Chemistry

The derivatives **1-4** and **50-52** were synthesized according to our previously published protocols [114], consisting in the nucleophilic substitution reaction between saccharin or potassium acesulfame with the proper electrophile at 80 °C for 24-48 h, as appropriate (**Scheme 3.1**, a and b). These reactions were performed in DMF, in the presence of freshly ground anhydrous potassium carbonate (K_2CO_3) for saccharin derivatives (**Scheme 3.1**, a); Ace K did not require the adding of further base to activate the nucleophile site, being employed as potassium salt (**Scheme 3.1**, b).



Scheme 3.1. Synthetic procedure for derivatives **1-4** and **50-52**.

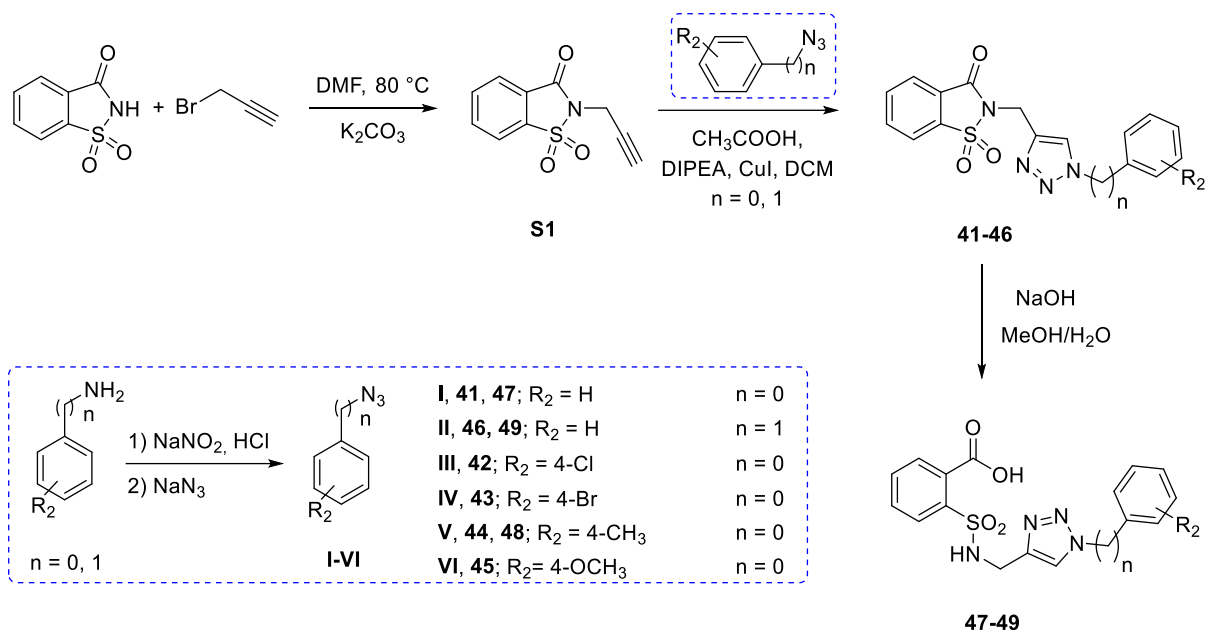
Derivatives **29-40** were synthesized using the multistep procedure reported in **Scheme 3.2**; selecting this synthetic pathway I was able to obtain also the derivatives **5-28**, that are the synthetic precursors and the opened analogues of the compounds **29-40**. The first step, leading to the ester intermediates **5-16**, involved the reaction between the methyl 2-(chlorosulfonyl)benzoate (**Scheme 3.2, X**) and the proper aniline in dichloromethane (DCM) at 0 °C, in presence of pyridine that functioned both as base and catalyst. For this purpose, the first attempt involved one single addition of the aniline to the solution of methyl 2-(chlorosulfonyl)benzoate and pyridine. Since the yield was not satisfying, I attempted different methods and the best one resulted in the portioned addition of the methyl 2-(chlorosulfonyl)benzoate to the solution of aniline and pyridine over a period of 45 minutes. The ester derivatives (**5-16**) were hydrolysed to the corresponding acids (**17-28**) employing potassium hydroxide before dissolved in a mixture of water:1,4-dioxane in the ratio 80:20 (v:v). The isothiazolone ring closure was achieved taking advantage of the mixed anhydride method, used to activate carboxylic acid group [144]. The synthesis was performed in THF using ethyl chloroformate as activating agent in the presence of triethylamine, affording the saccharin-based compounds **29-40**.



Scheme 3.2. Synthetic procedure for derivatives **5-16**, **17-28** and **29-40**.

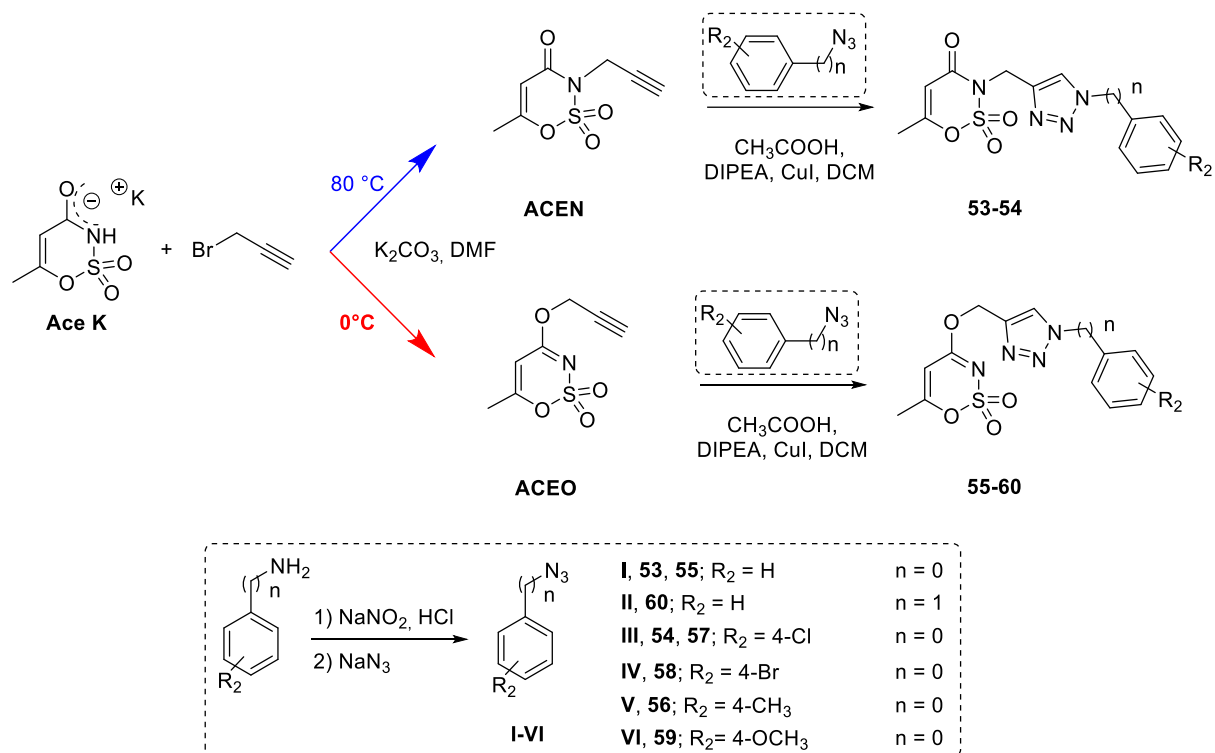
For the synthesis of the molecules **41-46** (and the opened analogues **47-49**) I also exploited a multistep approach (**Scheme 3.3**). I first performed the preparation of the intermediates, consisting of propargylated saccharin and the proper phenyl or benzyl azide, that then reacted in the final “click” reaction giving the final compounds in good yield.

The propargylated saccharin (**Scheme 3.3**, **S1**) was synthesized accordingly to our published procedure that involves the nucleophilic substitution between the saccharin and the propargyl bromide in DMF, at 80 °C for 48 h in the presence of potassium carbonate [112]. The azide intermediates were synthesized through the nucleophilic aromatic substitution between the diazonium salt of the suitable aniline or benzylamine, prepared *in situ* and the sodium azide. Then, the so obtained intermediates, have been “clicked” in the final reaction in the presence of a catalytic amount of copper iodide, *N,N*-diisopropylethylamine (DIPEA) and acetic acid [145]. Compounds **47-49** were attained through the hydrolysis of their closed analogues using NaOH dissolved in a mixture of MeOH:H₂O in the ratio 50:50 (*v:v*).



Scheme 3.3. Synthetic procedure for derivatives **41-49**.

The synthesis of the acesulfame derivatives bearing the triazole “linker” moiety was performed in a similar manner (**Scheme 3.4**). By finely regulating the synthetic conditions of the Ace K propargylation step, I specifically addressed the derivatization on the nitrogen or oxygen to obtain *N*- (**53-54**) or *O*-substituted (**55-60**) acesulfame analogues, respectively. Particularly, I observed that the *N*-propargylated derivative resulted as the main product when conducting the synthesis at 80 °C (**Scheme 3.4, ACEN**); conversely, performing the reaction at lower temperature (0 °C), I attained the *O*-propargylated one as the primary product (**Scheme 3.4, ACEO**). These intermediates reacted along with the phenyl/benzyl azides, seen before in the final “click” reaction, using the same conditions adopted for saccharin derivatives. All the compounds were characterized by a melting point, TLC parameters, ¹H and ¹³C NMR. Their purity was evaluated through HPLC analysis, employing two different methods: the first used for acesulfame derivatives (**50-60**), closed saccharins (**1-4, 29-46**) and opened saccharins containing methyl ester group (**5-16**); the second used for opened saccharin derivatives with a carboxylic acid group (**17-28, 47-49**). The compounds were analysed using isocratic elution with a binary mobile phase composed by water and acetonitrile (added of 0.1 % with trifluoroacetic acid for the acidic derivatives) and were $\geq 96\%$ HPLC pure (See Experimental section).



Scheme 3.4. Synthetic procedure for derivatives **53-60**.

3.3. Results and discussion

The synthesized compounds were tested to evaluate their inhibitory activity against the ubiquitous off-target isoforms, hCA I and II, and the cancer-related ones, hCA IX and XII, using a stopped-flow, CO₂ hydrase assay method [126]. Their CA inhibition data, reported as K_i values, are summarized in **Table 3.1** and **Table 3.2**. The inhibitory activity of the compounds **1-60** resulted strictly influenced by the substituent group/linker bound to the saccharin and acesulfame cores. Generally, these derivatives resulted less effective than the previously reported compounds [112–114,138], although some of them retained nanomolar activity and selectivity against hCA IX and hCA XII.

3.3.1. Inhibitory activity of saccharin-based derivatives

The inhibitory activity data of saccharin derivatives are reported in **Table 3.1**. Compound **1**, endowed with the unsaturated/branched prenyl group (3-methylbut-2-en-1-yl) bound at the nitrogen atom of the saccharin core, exhibited exclusive inhibitory activity against the tumour related isoforms hCA IX and XII (K_i hCA I/II > 1000 μ M). The two isoforms were inhibited in the nanomolar range, with a slight preference for the isoform XII (K_i hCA IX = 390 nM; K_i hCA XII = 230 nM). The derivatives **2** and **3**, endowed with 2- and 3-chlorobenzyl group

respectively, and **4**, bearing the 3-nitrobenzoyl methylene moiety, were ineffective against the off-targets hCA I and II. Compound **4** did not exhibit activity against hCA IX, too (K_i hCA IX > 1000 μ M), while it inhibited hCA XII in the high nanomolar range (K_i hCA XII = 410 nM). Interestingly, the removal of the carbonyl group, turning from benzoyl methylene moiety to the benzyl one (**2** and **3**), improved the activity against hCA IX. Compound **2**, bearing the chloro atom in the *meta* position of the phenyl ring, was three times more potent than the *ortho*-chloro analogue **3** (**2**, K_i hCA IX = 100 nM; **3**, K_i hCA IX = 300 nM); an opposite inhibitory profile was observed against hCA XII, since **3** displayed better activity than **2** (**2**, K_i hCA XII = 220 nM; **3**, K_i hCA XII = 1300 nM).

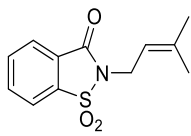
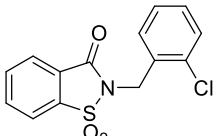
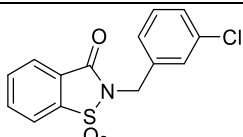
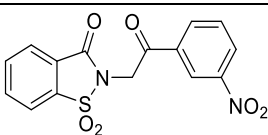
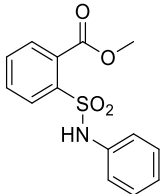
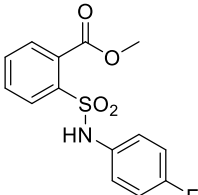
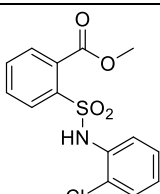
With the aim of investigating the importance of the methylene “linker” included in the benzyl group for the inhibitory profile of such compounds, I attempted the removal of this moiety, leading to a series of compounds in the opened (**5-28**) as well as in the closed (**29-40**) form. Thus, three different “sub-series” were evaluated. The first (**5-16**) is based on the opened saccharin core containing the methyl ester group instead of the carboxylic acid one that is present in the second sub-group (**17-28**). On the carbon atom neighbouring the one bearing the ester/carboxylic acid functional groups, these derivatives possess a secondary sulphonamide, whose nitrogen atom binds to a (un)substituted phenyl rings. The third sub-group includes closed saccharin derivatives substituted at the nitrogen with the same (un)substituted phenyl groups of the opened analogues (**29-40**). These compounds were less effective than their “counterpart” containing the methylene bridge. Regarding the derivatives in the opened form, only compound **9**, bearing the 4-bromophenyl ring, exhibited a weak affinity for hCA IX, although this was in the micromolar range (K_i hCA XII = 6.7 μ M). The other methyl ester opened saccharins were almost or completely ineffective against the tested isoforms (see **Table 3.1**). Compounds **17-28**, bearing the carboxylic acid group instead of the methyl ester one, exhibited an inhibitory profile similar to that observed for compounds **5-16**. Compound **24**, containing the *p*-nitrophenyl group bound at the nitrogen of sulphonamides, displayed an effective inhibition towards hCA IX (K_i hCA IX = 240 nM), retaining a residual activity against hCA II, although this was in the high micromolar range (K_i hCA II = 66.9 μ M). The ring closure, leading to the derivatives **29-40**, was unproductive because of the absence of inhibitory activity against all the hCA isoforms evaluated. Regardless of the chemical properties of the nitrogen substituents, no activity better than 443 μ M (**36**) was observed against hCA IX; furthermore, all these compounds were inactive against hCA I and XII and only compound **31** exhibited an extremely weak activity against hCA II (**31**, K_i hCA II = 477.8 μ M). Overall, considering these results, it is certain that the methylene linker, removed to obtain compounds **5-40**, is

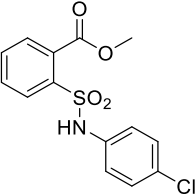
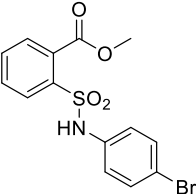
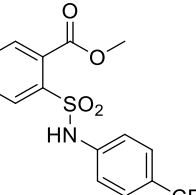
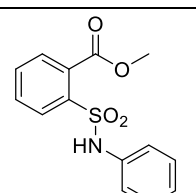
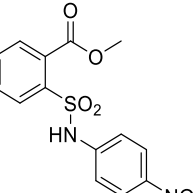
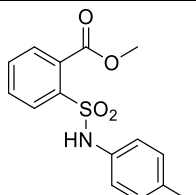
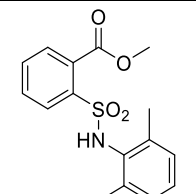
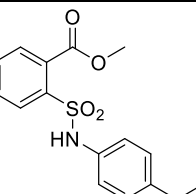
fundamental for the activity. The reason of this structural requirement could be related to the degrees of freedom that this linker confers to the phenyl moiety, giving it the opportunity to “search” for points of interactions inside the active site. Moreover, it cannot be excluded that in compounds **5-40** the presence of a direct bond between the nitrogen and the phenyl ring may change the electronic distribution, negatively affecting the placement inside the active site, also making the secondary sulphonamide of the opened forms (**5-28**) ineffective in rising the activity.

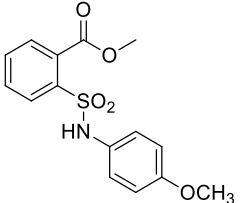
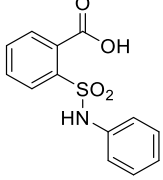
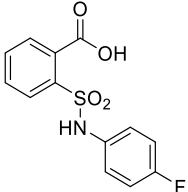
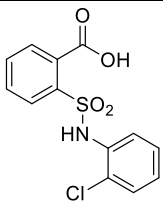
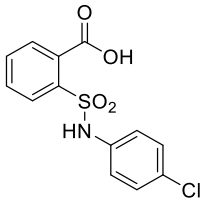
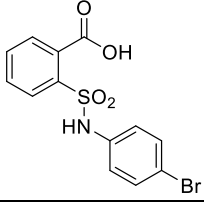
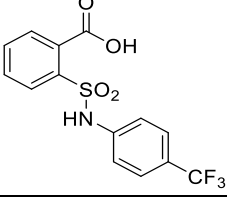
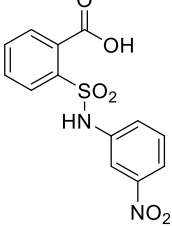
Based on these observations, and considering the promising results gained by the insertion of the isoxazole/isooxazoline heterocyclic linker in our previous paper [115], I tried to evaluate the effects deriving from the insertion of a triazole core between the methylene group and the phenyl ring, substituting the isoxazole one (**41-49**). This replacement did not elicit the desired results, because most of these analogues were devoid of inhibitory activity against the evaluated isoforms. Compound **41**, the simplest one of these group of derivatives, did not exhibit inhibition towards all the tested isoforms (K_i hCA I/II/IX/XII > 1000 μ M). The introduction of substituents, placed at the *para* position of the phenyl ring bound to the triazole N1, only slightly affected the activity against hCA II and IX, whereas it did not ameliorate the affinity towards hCA XII (see **Table 3.1**). The only change that dramatically improved the inhibitory activity was the insertion of a second methylene group that “disconnected” the triazole N1 from the phenyl ring bound to it. For compound **46**, that is the analogue of **41** containing that methylene moiety, the increment of inhibitory activity was remarkable, turning from an absence of affinity against the tumour related isoforms (K_i hCA IX/XII > 1000 μ M) to a micromolar inhibitory activity against the two target isoforms (K_i hCA IX = 20.9 μ M; K_i hCA XII = 7.4 μ M). A comparable effect, coming from the addition of the methylene group, was observed for **47** and **49**, that are the hydrolytically obtained opened analogues of **41** and **46**, respectively. Compound **47**, devoid of the “extra” methylene group, was ineffective against the tested isoforms (as also the compound **48**, which differs from the former for a *p*-methyl substitution on the phenyl ring); conversely, derivative **49**, endowed with the additional methylene group, exhibited low micromolar inhibitory activity exclusively against the two cancer related isoforms, even better than its closed analogue **46** (**46**, K_i hCA IX = 20.9 μ M; K_i hCA IX = 7.4 μ M; **49**, K_i hCA IX = 1.9 μ M; K_i hCA IX = 4.5 μ M). Therefore, the presence of the triazole ring instead of the isoxazole/isooxazoline ones did not positively affect the inhibitory activity. Particularly, I observed that similarly to the results detected for saccharins **5-40**, the presence of the methylene group between the N1 of the triazole ring and the phenyl group improved the activity (see the

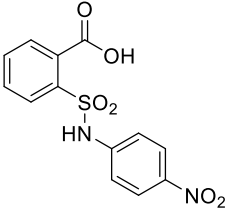
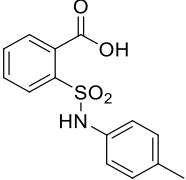
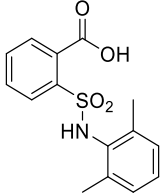
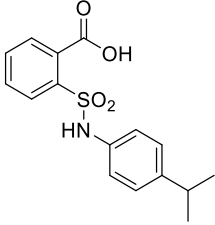
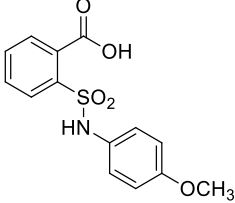
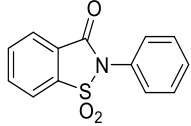
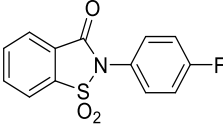
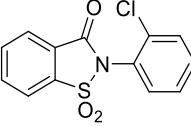
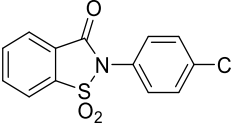
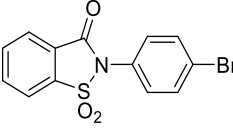
couples **41/46** and **47/49**), and the hydrolytic ring opening seemed to increase the inhibitory activity against the tumour related isoforms hCA IX and XII.

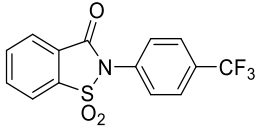
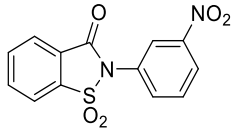
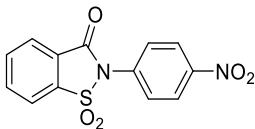
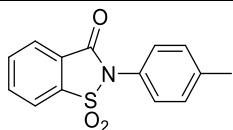
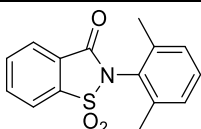
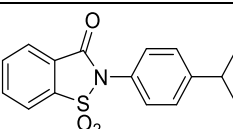
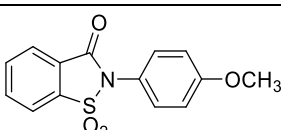
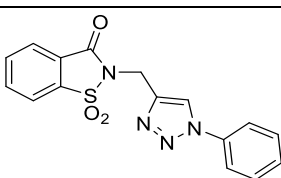
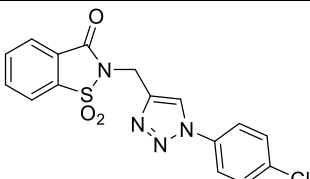
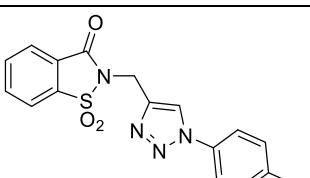
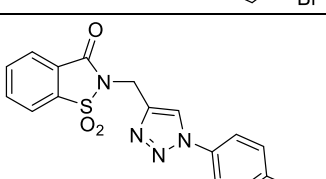
Table 3.1. Inhibition data of selected human CA isoforms (hCA I, II, IX and XII) with the proposed saccharin-based derivatives **1-49** and the standard sulphonamide inhibitor acetazolamide (**AAZ**) by a stopped flow CO₂ hydrase assay [126].

	Structure	K _i (μM)			
		hCA I	hCA II	hCA IX	hCA XII
1		>1000	>1000	0.39	0.23
2		>1000	>1000	0.30	0.22
3		>1000	>1000	0.10	1.3
4		>1000	>1000	>1000	0.41
5		>1000	>1000	59.6	>1000
6		>1000	>1000	261.8	>1000
7		>1000	>1000	427.5	>1000

8		>1000	>1000	955.3	>1000
9		>1000	688.7	6.7	>1000
10		>1000	>1000	562.6	>1000
11		>1000	>1000	>1000	>1000
12		>1000	>1000	62.8	>1000
13		>1000	>1000	68.2	>1000
14		>1000	>1000	39.7	>1000
15		>1000	>1000	57.6	>1000

16		>1000	>1000	93.3	>1000
17		>1000	>1000	46.5	>1000
18		>1000	>1000	45.8	>1000
19		>1000	>1000	>1000	>1000
20		>1000	>1000	>1000	>1000
21		>1000	>1000	72.8	>1000
22		>1000	>1000	84.8	>1000
23		>1000	>1000	>1000	>1000

24		>1000	66.9	0.24	>1000
25		>1000	>1000	>1000	>1000
26		>1000	>1000	>1000	>1000
27		>1000	>1000	>1000	>1000
28		>1000	>1000	>1000	>1000
29		>1000	>1000	>1000	>1000
30		>1000	>1000	>1000	>1000
31		>1000	477.8	640.0	>1000
32		>1000	>1000	>1000	>1000
33		>1000	>1000	869.1	>1000

34		>1000	>1000	>1000	>1000
35		>1000	>1000	>1000	>1000
36		>1000	>1000	443.5	>1000
37		>1000	>1000	>1000	>1000
38		>1000	>1000	>1000	>1000
39		>1000	>1000	>1000	>1000
40		>1000	>1000	>1000	>1000
41		>1000	>1000	>1000	>1000
42		>1000	80.8	758.6	>1000
43		>1000	76.4	537.6	>1000
44		>1000	>1000	669.6	>1000

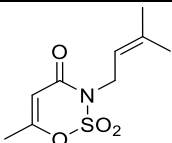
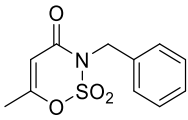
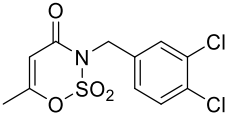
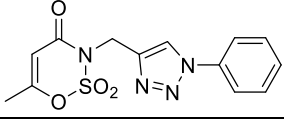
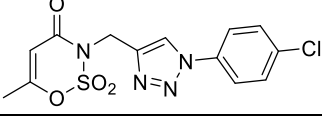
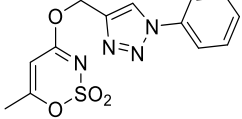
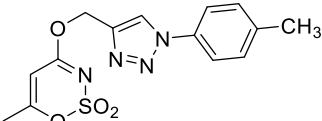
45		>1000	>1000	666.1	>1000
46		>100	>100	20.9	7.4
47		>1000	>1000	926.9	>1000
48		>1000	>1000	>1000	>1000
49		>100	>100	1.9	4.5
AAZ		0.25	0.012	0.025	0.006

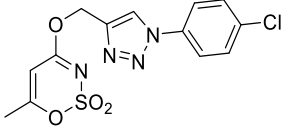
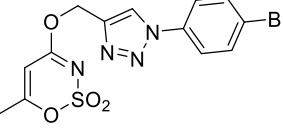
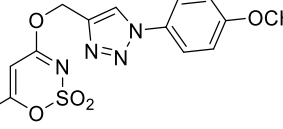
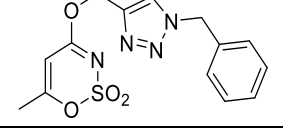
3.3.2. Inhibitory activity of acesulfame-based derivatives

The inhibitory activity data of acesulfame-based derivatives are reported in **Table 3.2**. Compounds **50-52** are acesulfame derivatives substituted at the nitrogen atom with (un)substituted benzyl groups (**51** and **52**) or with the prenyl one (**50**). These molecules exhibited selectivity against hCA IX and XII, missing affinity towards the *off-target* isoforms (**50-52**, K_i hCA I/II > 1000 μ M). Among the three derivatives, **50** exhibited the best inhibition profile against hCA IX and XII (K_i hCA IX = 330 nM; K_i hCA XII = 240 nM). Compound **51**, bearing the unsubstituted benzyl group, efficiently inhibited the isoform XII (K_i hCA XII = 270 nM), and in a lesser extent the isoform IX (K_i hCA IX = 2.7 μ M). Conversely, **52**, containing the 3,4-dichloro benzyl group, exhibited preference for hCA IX, that was inhibited in the nanomolar range (K_i hCA IX = 2.7 μ M), instead of hCA XII, that was affected only at the micromolar range (K_i hCA XII = 2.0 μ M). To evaluate the effects of the insertion of the triazole linker on the acesulfame scaffolds, compounds **53-54** (*N*-substituted) and **55-60** (*O*-substituted) were synthesized and assessed against the hCA isoforms seen before. These molecules were devoid of appreciable activity against these enzymes, as previously observed for saccharin analogues. Indeed, the position of the substituents on the acesulfame core (*O*- or *N*-substituted)

and the groups bound to the phenyl ring (see Table 3.2) did not contribute to a satisfactory inhibitory activity. As already observed for saccharin derivatives, the insertion of an additional methylene group between the phenyl ring and the triazole N1 led to the onset of low micromolar activity against hCA IX for compound **60**, the only active compound of this series (K_i hCA IX = 1.1 μ M). Thus, the data obtained from the acesulfame derivatives confirm those observed for saccharins, namely that the insertion of an additional methylene group between the triazole N1 and the phenyl ring, positively affected their inhibitory activity.

Table 3.2. Inhibition data of selected human CA isoforms (hCA I, II, IX and XII) with the proposed acesulfame-based derivatives **50-60** and the standard sulphonamide inhibitor acetazolamide (AAZ) by a stopped flow CO₂ hydrase assay [126].

	Structure	K_i (μ M)			
		hCA I	hCA II	hCA IX	hCA XII
50		>1000	>1000	0.33	0.24
51		>1000	>1000	2.7	0.27
52		>1000	>1000	0.47	2.0
53		>1000	>1000	>1000	>1000
54		>1000	>1000	>1000	>1000
55		>1000	>1000	>1000	>1000
56		>1000	>1000	>1000	>1000

57		>1000	>1000	>1000	>1000
58		>1000	>1000	>1000	>1000
59		>1000	>1000	>1000	>1000
60		>100	>100	1.1	>100
AAZ		0.25	0.012	0.025	0.006

^aMean from 3 different assay, by a stopped flow technique (errors were in the range of \pm 5-10% of the reported values).

3.3.3. Modelling studies

A subset of CAIs, namely compounds **2**, **46**, **49** and **51**, endowed with the best hCA IX and XII inhibitory profiles, was selected to study the interaction mechanism driving the inhibition profiles reported in **Tables 3.1 and 3.2**. A computational protocol, consisting of joint docking procedure and MD simulations, was used to investigate the compounds binding mode within hCAs IX and XII (Experimental Section), considering the derivatives as hCAIs anchoring to zinc-bound water molecule, based on a number of considerations: i) zinc-binder CAI chemotypes, such as primary sulphonamides, sulfamates and sulfamides, mono- and dithiocarbamates, or hydroxamates, mainly act in the deprotonated form, as anions, directly coordinating the Zn(II) ion from the enzyme active site [118]; ii) saccharin **1-4**, **29-46** and acesulfame **50-60** derivatives bearing a tertiary sulphonamide moiety cannot interact with the targets in the deprotonated form; iii) although the deprotonation of the secondary sulphonamide group of hydrolysed saccharin derivatives **5-28** and **47-49** is possible, its internal position in the molecules does not allow it to coordinate the Zn ion, due to the steric hindrance of the groups surrounding the negatively charged sulphonamide; iv) crystallographic evidence has shown that deprotonated sulfonate moieties, that possess similar features as the SO₂ group of the reported saccharin and acesulfame compounds, drive CA inhibition, by anchoring to the zinc-bound water molecule/hydroxide ion (not by coordination to the zinc ion) [118]. This led us to consider the nucleophile mediated anchoring mechanism for derivatives **2**, **46** and **51** in our *in silico*

studies. Likewise, crystallographic evidence has shown that carboxylic acids such as **49**, except for few cases, act as CAIs anchoring to the zinc-bound nucleophile [118].

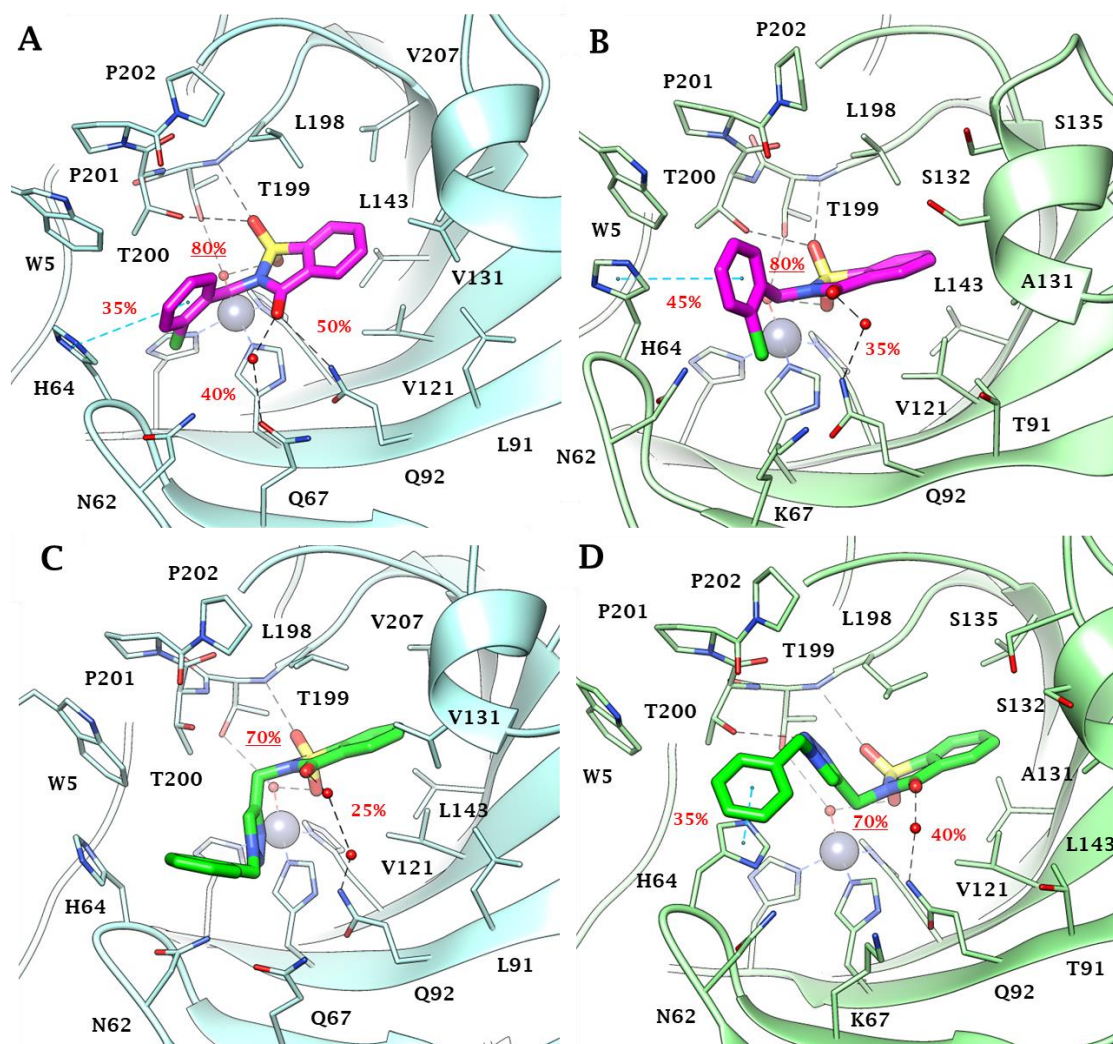


Figure 3.5. Predicted binding mode of compounds **2** and **46** into (A, C) hCA IX and (B, D) hCA XII active site. H-bonds and π - π stackings are represented as black and blue dashed lines, respectively. Dashed bonds occupancy over the MD simulation is indicated as percentage, among which underlined is the occupancy of the anchorage to the zinc-bound water. Water molecules are shown as red spheres. Amino acids are labelled with one letter symbols: A, Ala; H, His; K, Lys; L, Leu; N, Asn; P, Pro; Q, Gln; S, Ser; T, Thr; V, Val; W, Trp.

Thus, dockings were performed including the Zn-bound water molecule in the target and the reliability of poses for derivatives **2**, **46**, **49** and **51** within CA IX and XII active sites (**Figures 3.5** and **3.6**) assessed with MD simulations. The MD trajectories showed the stability of the anchorage to the zinc-bound water molecule that persists for >70-80% of the simulation time; moreover, the ligands maintained constant hydrophobic contacts with different portions of the active sites. In both hCA IX and XII saccharin derivatives **2** and **46** were H-bond anchored by

one S=O group to the metal-coordinated water that was, in turn, H-bonded to side chain hydroxyl group of Thr199 (**Figures 3.5 and 3.6**). The other S=O group of both ligands accepted one H-bond by Thr199 backbone NH, but just derivative **2** also engaged in hydrogen bonding with the side chain hydroxyl group of Thr200 (O \cdots H-O Tyr200). Of note, this H-bonds network persisted for most MD simulations mainly contributing to the pose stability. Moreover, the C=O group of the ligands engaged direct or water bridged H-bonds with Gln67 and Gln92 that fluctuated over the MD computations. The N-benzyl group of derivative **2** accommodated in the pocket lined by Trp5, His64 and Asn62 forming Van der Waals contacts and π - π interactions with the aromatic residues. This cleft was only partially occupied by the 1-benzyl-1,2,3-triazol-4-yl *N*-pendant of derivative **46** over the MD course making the docking poses less stable, and thereby providing a plausible explanation of the worst hCA IX and XII inhibitory profile of **46** compared to **2** (**Figures 3.5 and 3.6**). The interaction mode of **2** and **46** within both hCA IX and XII c explain the lower up to absent hCAs inhibition observed for the *N*-phenyl saccharin derivatives **29-40** and 1-phenyl-1,2,3-triazole **41-45**.

The lack of a methylene spacer between the heterocycle and the aromatic pendant (as in **29-40**) or between the triazole and the outer aromatic ring (as in **41-45**) hampered a suitable ligand/target complementarity interaction and stable accommodation of the pendant in the pocket formed by Trp5, His64 and Asn62 (**Figure 3.7**, Experimental Section).

Both in the CA IX and XII active sites, the hydrolysed saccharin **49** anchored to the zinc-bound water molecule by the carboxylate group, that also engages one H-bond with Thr199 backbone NH (**Figure 3.6A-B**). Its negatively charged sulphonamide group SO₂NH⁻ took part in a network of H-bonds involving multiple residues of the binding cavity: Gln92 by a fluctuating water-bridged H-bond (N-H \cdots (H)OH \cdots Gln92) and Tyr200 (N-H \cdots O-Thr200). In hCA IX, the hydroxyl side chain of Thr200 was also in H-bond contact with the ligand triazole N3 atom, and π - π contacts were formed by the indole moiety of Trp5 and the outer phenyl ring of **49**. In contrast, the placing of the 1-benzyl-1,2,3-triazol-4-yl *N*-pendant within the pocket formed by Trp5, His64 and Asn62 in hCA XII was less stable over the MD course comparing to the hCA IX, as well as the water bridged H-bond formed by the triazole NH and Asn62 and the π - π interactions (**Figure 3.6B**). Again, the absence of a methylene spacer between the sulphonamide and the aromatic *N*-pendant, as in the methyl esters **5-16** and carboxylic acids **17-28**, translated into lower hCA IX and XII inhibition activity of these derivatives when compared to **49**. The drop of efficacy resulted lower than that observed with saccharin analogues most likely because of the greater conformational flexibility and adaptation

capability within the active site of the hydrolysed ligands than cyclized compounds. Surprisingly, instead of a total loss of hCA XII inhibition activity observed for **5-28**, their medium micromolar profile against hCA IX was likely to be related to the hydrophobic features of the hCA IX active site and to the larger size of its cleft able to host the benzoate group if the triazole ring brought both a phenyl and benzyl moiety. As already observed for **47** and **48** the absence of the methylene spacer between the triazole and the outer aromatic ring, produced a whole loss of action against CAs.

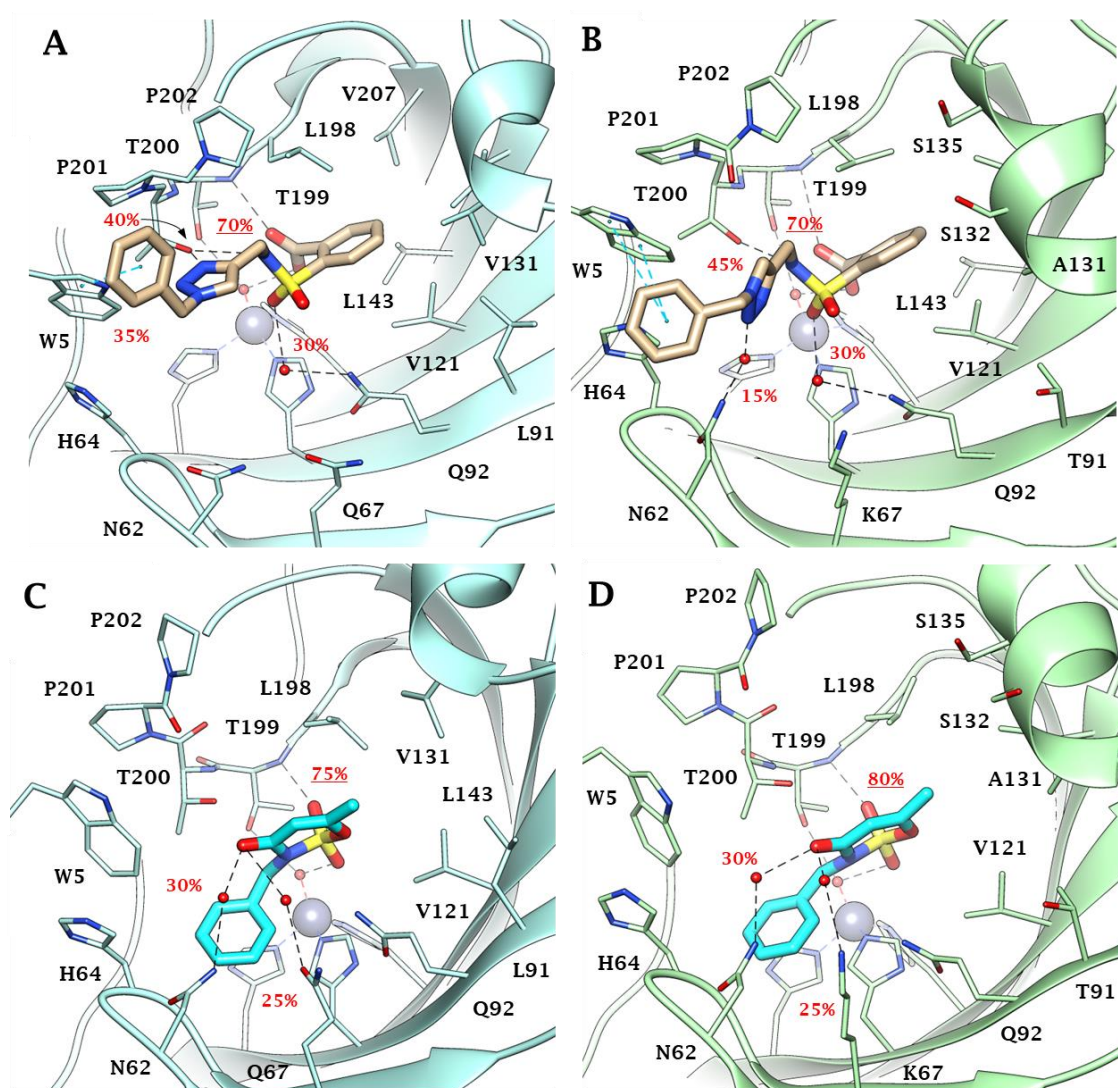


Figure 3.6. Predicted binding mode of compounds **49** and **51** into (A, C) hCA IX and (B, D) hCA XII active site. H-bonds and π - π stackings are represented as black and blue dashed lines, respectively. Dashed bonds occupancy over the MD simulation is indicated as percentage, among which underlined is the occupancy of the anchorage to the zinc-bound water. Water molecules are shown as red spheres. Amino acids are labelled with one letter symbols: A, Ala; H, His; K, Lys; L, Leu; N, Asn; P, Pro; Q, Gln; S, Ser; T, Thr; V, Val; W, Trp.

Likewise, in both hCA IX and XII, acesulfame **51** anchored to the zinc-bound water molecule through the sulfimide S=O (**Figures 3.6C-D**) and the anchorage was strengthened by another H-bond occurring between the other S=O group and Thr199 backbone NH. The carbonyl group of **51** was involved in a network of water-bridged H-bond with Asn62, Asn/Lys67 (CA IX/XII) and Gln92. Interestingly, the *N*-benzyl moiety stably accommodated (>65% MD) within the pocket formed by Trp5, Tyr7, His64, Asn62 and His96 engaging Van der Waals contacts. On the basis of the depicted binding mode, a 1-phenyl-1,2,3-triazol-4-yl *N*- or *O*-pendant dropped the inhibitory action of acesulfame derivatives **53-59** because of steric hindrance reasons in hCA IX and XII active sites. Consistently to the inhibition profile in **Tables 3.1** and **3.2**, the binding mode predicted for **2**, **46**, **49** and **51** in hCA IX and XII was likely not allowed in the narrower and hindered active site of hCA I and II (**Figure 3.8**, Experimental Section), wherein the used computational protocol was not able to find reliable solutions.

3.4. Conclusions

The design, synthesis, and biological activity of novel saccharin- and acesulfame-based compounds were described. The different approaches attempted for the development of these inhibitors underlined the importance of flexibility for the correct distribution of the molecular fragments inside the hCA IX and XII active site. The removal of the methylene group in the *N*-benzyl saccharins to obtain the *N*-phenyl analogues elicited detrimental effects, with the only exception of the opened-saccharin derivative **24**. For the triazole bearing derivatives, the insertion of a second methylene group separating the triazole moiety from the outer phenyl ring improved the activity. Docking and MD studies described the most probable binding mode of compounds (**2**, **46**, **49**, **51**) based on the anchoring to zinc-bound water, also confirming and explaining the correlation between inhibitory activity and the ability to occupy sites in order to establish interactions that influence the binding affinity.

3.5. Experimental section

3.5.1. General

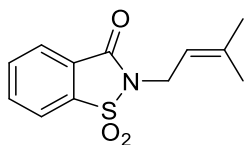
Unless otherwise specified, the reactions reported in this paper were performed under nitrogen atmosphere in washed and oven-dried glassware at room temperature. The solvents (anhydrous or not) and the reagents used in the chemical and biological experimental protocols were used as supplied. If solvent mixtures are described, their ratio is expressed as *volume:volume* (v:v).

The melting points of each compound were measured on a Stuart[®] melting point apparatus SMP1 and the related temperature values reported in °C (uncorrected). Proton (¹H) and Carbon (¹³C) nuclear magnetic resonance spectra were recorded at 400 and 101 MHz respectively, on a Bruker spectrometer using the solvents (CDCl₃, DMSO-*d*₆, CD₃OD and CD₃CN) at room temperature. The final concentration of the samples was of ~5 mg/mL for ¹H-NMR acquisition and ~25 mg/mL for the recording of the ¹³C-NMR ones.

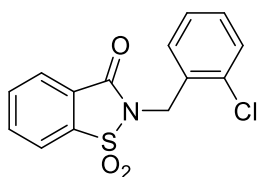
Chemical shifts are presented as δ units (parts per millions) using the solvent signal as the internal standard. ¹H spectra are described as reported below: δ_{H} (spectrometer frequency, solvent): chemical shift/ppm (multiplicity, *J*-coupling constant(s), number of protons, assignment). ¹³C spectra are described as reported below: δ_{C} (spectrometer frequency, solvent): chemical shift/ppm (assignment). Coupling constants *J* are valued in Hertz (Hz) using these abbreviations to indicate the splitting: s – singlet; d – doublet; t – triplet; q – quartet; m – multiplet. If needed, it is also reported the abbreviation br – to indicate the broad shape of the specific peak.

Silica for column chromatography were purchased from Sigma-Aldrich (Milan, Italy) (high purity grade, pore size 60 Å, 230-400 mesh particle size). Reactions and purifications were checked by TLC performed on 0.2 mm thick silica gel-aluminium backed plates (60 F254, Merck) and their visualization performed under ultra-violet irradiation (254 and 365 nm). If given, systematic compound names were generated by ChemBioDraw Ultra 12.0 in accordance with the IUPAC nomenclature. The HPLC analyses performed for purity evaluation were accomplished employing the Shimadzu *Prominence-i* LC-2030C 3D system endowed with autosampler, binary pump, column oven and a photodiode array detector (PDA). The separation has been obtained through the use of the column Kinetex Biphenyl, 5 μm , 100 Å (Phenomenex, Bologna, Italy) at a constant flow of 1.0 mL min⁻¹, employing an isocratic elution. For the acesulfame derivatives (**50-60**), closed saccharins (**1-4**, **29-46**) as well as the opened ones containing the ester functional group (**5-16**), were employed the two eluents water (solvent A) and acetonitrile (solvent B) mixed in the constant ratio of 50:50 (*v:v*). For the opened saccharins containing the carboxylic acid group (**17-28**, **47-49**) the two solvents were added with 0.1% of trifluoroacetic acid (TFA) maintaining the ratio 50:50 (*v:v*); all the runs have been completed in 10 minutes. All the analyte solutions were prepared in acetonitrile (acetonitrile plus 0.1% of TFA for acidic derivatives) at the concentration between 0.5-2 mg mL⁻¹, and 5 μL were directly injected for the HPLC analysis. All compounds reported were $\geq 96\%$ HPLC pure. The solvents used in the HPLC analysis were acetonitrile, purchased from Carlo Erba Reagents and mQ water 18 M Ω cm, obtained from Millipore's Direct-Q3 system.

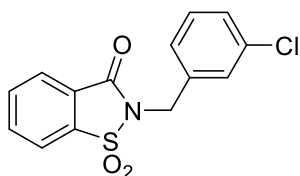
3.5.2. Synthesis and characterization data of saccharin-based derivatives



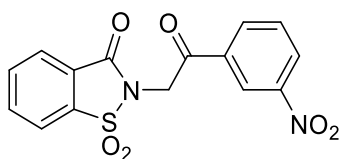
2-(3-methylbut-2-en-1-yl)benzo[*d*]isothiazol-3(2*H*)-one 1,1-dioxide (1): anhydrous potassium carbonate (1 equiv.) was added to a stirring solution of saccharin (1 equiv.) in *N,N*-dimethylformamide. After 15 min, 3,3-dimethylallyl bromide (1 equiv.) was added and the suspension stirred under nitrogen atmosphere for 24 h at 0 °C. Once the reaction completion the mixture was poured on ice. The resulting suspension was filtered and the collected solid washed with chloroform giving the title compound as an oil (57% yield); ¹H NMR (300 MHz, CDCl₃): δ 1.71 (s, 3H, CH₃), 1.80 (s, 3H, CH₃), 4.33 (d, *J* = 7.2 Hz, 2H, CH₂), 5.32-5.37 (m, 1H, CH=), 7.74-7.89 (m, 3H, Ar), 7.97-8.00 (m, 1H, Ar). ¹³C NMR (76 MHz, CDCl₃): δ 17.9 (CH₃), 25.8 (CH₃), 37.1 (CH₂), 116.9 (Ar), 120.9 (CH=), 125.1 (Ar), 127.5 (Ar), 134.2 (Ar), 134.6 (C=), 137.8 (Ar), 138.9 (Ar), 158.7 (C=O).



2-(2-chlorobenzyl)benzo[*d*]isothiazol-3(2*H*)-one 1,1-dioxide (2): anhydrous potassium carbonate (1 equiv.) was added to a stirring solution of saccharin (1 equiv.) in *N,N*-dimethylformamide. After 15 min, 1-(bromomethyl)-2-chlorobenzene (1 equiv.) was added and the suspension stirred under nitrogen atmosphere for 8 h at 80 °C. Once the reaction completion the mixture was poured on ice. The resulting suspension was filtered and the collected solid washed with *n*-hexane, to afford the title compound as a yellow solid (65% yield); mp 143-145°C; ¹H NMR (300 MHz, CDCl₃): δ 5.11 (s, 2H, CH₂), 7.28 (s, 2H, Ar), 7.44 (d, *J* = 2.4 Hz, 2H, Ar), 7.87-7.96 (m, 3H, Ar), 8.12 (d, *J* = 4.8 Hz, 1H, Ar). ¹³C NMR (76 MHz, CDCl₃): δ 40.2 (CH₂), 121.1 (Ar), 125.4 (Ar), 127.2 (2 × Ar), 129.2 (Ar), 129.4 (Ar), 129.7 (Ar), 131.9 (Ar), 133.3 (Ar), 134.4 (Ar), 135.0 (Ar), 137.9 (Ar), 158.9 (C=O).



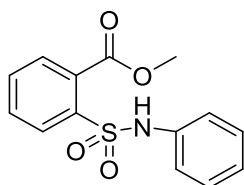
2-(3-chlorobenzyl)benzo[d]isothiazol-3(2H)-one 1,1-dioxide (3): anhydrous potassium carbonate (1 equiv.) was added to a stirring solution of saccharin (1 equiv.) in *N,N*-dimethylformamide. After 15 min, 1-(bromomethyl)-3-chlorobenzene (1 equiv.) was added and the suspension stirred under nitrogen atmosphere for 12 h at 80 °C. Once the reaction completion the mixture was poured on ice. The resulting suspension was filtered and the collected solid washed with *n*-hexane, to afford the title compound as a yellow solid (57% yield); mp 78-80 °C; ¹H NMR (300 MHz, CDCl₃): δ 4.85 (s, 2H, CH₂), 7.24-7.26 (m, 2H, Ar), 7.35-7.38 (m, 1H, Ar), 7.47 (s, 1H, Ar), 7.75-7.84 (m, 2H, Ar), 7.88-7.91 (m, 1H, Ar), 7.99-8.02 (m, 1H, Ar). ¹³C NMR (76 MHz, CDCl₃): δ 41.9 (CH₂), 121.1 (Ar), 125.3 (Ar), 126.8 (Ar), 127.0 (Ar), 128.5 (Ar), 128.7 (Ar), 130.0 (Ar), 134.5 (Ar), 134.5 (Ar), 135.0 (Ar), 136.6 (Ar), 137.5 (Ar), 158.9 (C=O).



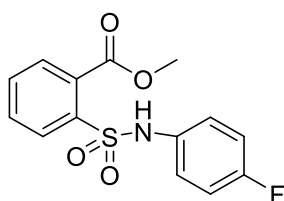
2-(2-(3-nitrophenyl)-2-oxoethyl)benzo[d]isothiazol-3(2H)-one 1,1-dioxide (4): anhydrous potassium carbonate (1 equiv.) was added to a stirring solution of saccharin (1 equiv.) in *N,N*-dimethylformamide. After 15 min, 2-bromo-3'-nitroacetophenone (1 equiv.) was added and the suspension stirred under nitrogen atmosphere for 24 h at 80 °C. Once the reaction completion the mixture was poured on ice. The resulting suspension was filtered and the collected solid washed with *n*-hexane to afford the title compound as a yellow solid (65% yield); mp 190-191 °C; ¹H NMR (300 MHz, CDCl₃): δ 5.19 (s, 2H, CH₂), 7.77 (t, *J* = 7.8 Hz, 1H, Ar), 7.89-8.01 (m, 3H, Ar), 8.12-8.14 (m, 1H, Ar), 8.33-8.36 (m, 1H, Ar), 8.50-8.53 (m, 1H, Ar), 8.85 (t, *J* = 1.5 Hz, 1H, Ar). ¹³C NMR (76 MHz, CDCl₃): δ 44.5 (CH₂), 121.3 (Ar), 123.1 (Ar), 123.7 (Ar), 125.6 (Ar), 127.5 (Ar), 128.5 (Ar), 130.4 (Ar), 133.7 (Ar), 134.6 (Ar), 135.2 (Ar), 135.2 (Ar), 137.6 (Ar), 148.5 (C=O), 187.3 (C=O).

General synthesis and characterization data of derivatives 5-16

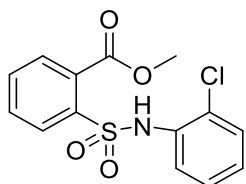
To a stirring solution of the proper aniline (1.0 equiv.) in dichloromethane at 0 °C, pyridine was added (1.2 equiv.). After 20 min, methyl 2-(chlorosulfonyl)benzoate (1 equiv.) was added portion wise and the reaction stirred under nitrogen atmosphere for 2 h. Once the synthesis completion the mixture was extracted with dichloromethane (3 × 20 mL) and HCl. The organic layers were reunited, dried over sodium sulphate and concentrated *in vacuo*. Purification through column chromatography on silica gel, using the proper solvents, gave compounds 5-16 as white or yellow solids.



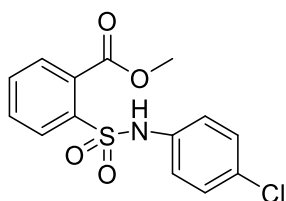
Methyl 2-(N-phenylsulfamoyl)benzoate (5): white solid, mp 70-72 °C; ¹H NMR (400 MHz, CDCl₃): δ 4.07 (s, 3H, OCH₃), 7.11-7.15 (m, 1H, Ar), 7.17-7.19 (m, 2H, Ar), 7.22-7.26 (m, 2H, Ar), 7.45-7.51 (m, 1H, Ar), 7.57-7.61 (m, 1H, Ar), 7.82-7.83 (m, 1H, Ar), 7.84-7.85 (m, 1H, Ar), 8.04 (br s, 1H, SO₂NH, D₂O exch.). ¹³C NMR (101 MHz, CDCl₃): δ 53.6 (OCH₃), 122.9 (2 × Ar), 125.8 (Ar), 129.2 (2 × Ar), 130.4 (Ar), 130.5 (Ar), 130.6 (Ar), 131.5 (Ar), 132.6 (Ar), 136.6 (Ar), 138.0 (Ar), 168.3 (C=O).



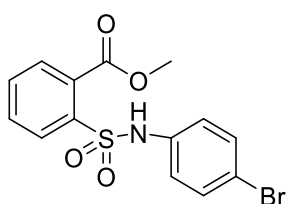
Methyl 2-(N-(4-fluorophenyl)sulfamoyl)benzoate (6): white solid, mp 102-104 °C; ¹H NMR (400 MHz, CDCl₃): δ 4.07 (s, 3H, OCH₃), 6.90-6.94 (m, 2H, Ar), 7.12-7.15 (m, 2H, Ar), 7.48-7.52 (m, 1H, Ar), 7.59-7.63 (m, 1H, Ar), 7.77-7.79 (m, 1H, Ar), 7.84-7.86 (m, 1H, Ar), 8.02 (br s, 1H, SO₂NH, D₂O exch.). ¹³C NMR (101 MHz, CDCl₃): δ 53.6 (OCH₃), 116.0 (d, ²J_{C-F} = 22.2 Hz, 2 × Ar), 125.4 (d, ³J_{C-F} = 8.4 Hz, 2 × Ar), 130.5 (Ar), 130.6 (Ar), 130.6 (Ar), 131.5 (Ar), 132.5 (d, ⁴J_{C-F} = 3.03 Hz, Ar), 132.7 (Ar), 137.7 (Ar), 160.9 (d, ¹J_{C-F} = 245.5 Hz, C-F), 168.4 (C=O).



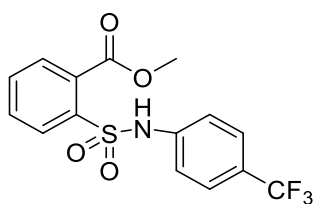
Methyl 2-(N-(2-chlorophenyl)sulfamoyl)benzoate (7): white solid, mp 90-92 °C; ^1H NMR (400 MHz, CDCl_3): δ 4.07 (s, 3H, OCH_3), 7.06-7.10 (m, 1H, Ar), 7.25-7.29 (m, 2H, Ar), 7.53-7.58 (m, 1H, Ar), 7.62-7.66 (m, 1H, Ar), 7.74-7.76 (m, 1H, Ar), 7.87-7.91 (m, 2H, Ar), 8.51 (br s, 1H, SO_2NH , D_2O exch.). ^{13}C NMR (101 MHz, CDCl_3): δ 53.5 (OCH_3), 124.3 (Ar), 126.1 (Ar), 126.2 (Ar), 127.7 (Ar), 129.5 (2 x Ar), 130.6 (Ar), 131.0 (Ar), 131.6 (Ar), 132.9 (Ar), 133.8 (Ar), 138.9 (Ar), 167.5 ($\text{C}=\text{O}$).



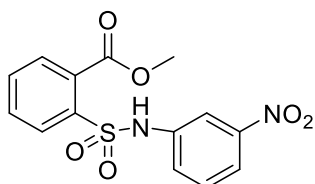
Methyl 2-(N-(4-chlorophenyl)sulfamoyl)benzoate (8): white solid, mp 108-112 °C; ^1H NMR (400 MHz, CDCl_3): δ 4.07 (s, 3H, OCH_3), 7.11-7.14 (m, 2H, Ar), 7.19-7.22 (m, 2H, Ar), 7.50-7.54 (m, 1H, Ar), 7.59-7.63 (m, 1H, Ar), 7.82-7.86 (m, 2H, Ar), 8.09 (br s, 1H, SO_2NH , D_2O exch.). ^{13}C NMR (101 MHz, CDCl_3): δ 53.6 (OCH_3), 124.2 (2 x Ar), 129.3 (2 x Ar), 130.5 (Ar), 130.5 (Ar), 130.7 (Ar), 131.5 (Ar), 131.6 (Ar), 132.8 (Ar), 135.2 (Ar), 137.8 (Ar), 168.4 ($\text{C}=\text{O}$).



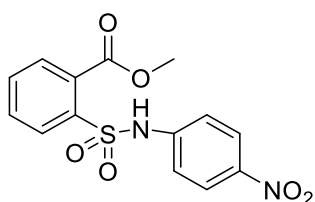
Methyl 2-(N-(4-bromophenyl)sulfamoyl)benzoate (9): white solid, mp 116-118 °C; ^1H NMR (400 MHz, CDCl_3): δ 4.08 (s, 3H, OCH_3), 7.36-7.39 (m, 2H, Ar), 7.57-7.67 (m, 2H, Ar), 7.87-7.90 (m, 1H, Ar), 7.97-7.99 (m, 1H, Ar), 8.12-8.15 (m, 2H, Ar), 8.59 (br s, 1H, SO_2NH , D_2O exch.). ^{13}C NMR (101 MHz, CDCl_3): δ 53.6 (OCH_3), 119.2 (Ar), 124.4 (2 x Ar), 130.4 (Ar), 130.5 (Ar), 130.7 (Ar), 131.7 (Ar), 132.3 (2 x Ar), 132.8 (Ar), 135.8 (Ar), 137.7 (Ar), 168.4 ($\text{C}=\text{O}$).



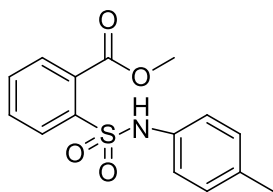
Methyl 2-(N-(4-(trifluoromethyl)phenyl)sulfamoyl)benzoate (10): white solid, mp 92-96 °C; ^1H NMR (400 MHz, CDCl_3): δ 4.08 (s, 3H, OCH_3), 7.32 (d, $J = 8.4$ Hz, 2H, Ar), 7.50 (d, $J = 8.5$ Hz, 2H, Ar), 7.53-7.57 (m, 1H, Ar), 7.60-7.65 (m, 1H, Ar), 7.85-7.88 (m, 1H, Ar), 7.90-7.93 (m, 1H, Ar), 8.35 (br s, 1H, SO_2NH , D_2O exch.). ^{13}C NMR (101 MHz, $\text{DMSO}-d_6$): δ 53.7 (OCH_3), 121.6 (2 x Ar), 123.9 (d, $^1J_{\text{C-F}} = 271.9$ Hz, CF_3), 126.5 (q, $^3J_{\text{C-F}} = 3.8$ Hz, 2 x Ar), 127.4 (d, $^2J_{\text{C-F}} = 32.8$ Hz, Ar), 130.4 (Ar), 130.4 (Ar), 130.9 (Ar), 131.8 (Ar), 133.0 (Ar), 137.8 (Ar), 140.0 (Ar), 168.3 (C=O).



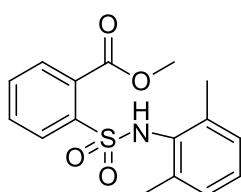
Methyl 2-(N-(3-nitrophenyl)sulfamoyl)benzoate (11): yellow solid, mp 168-170 °C; ^1H NMR (400 MHz, CDCl_3): δ 4.09 (s, 3H, OCH_3), 7.45 (t, $J = 8.1$ Hz, 1H, Ar), 7.53-7.67 (m, 3H, Ar), 7.63-7.67 (m, 1H, Ar), 7.88-7.91 (m, 1H, Ar), 7.96-7.99 (m, 1H, Ar), 8.01-8.02 (m, 1H, Ar), 8.50 (br s, 1H, SO_2NH , D_2O exch.). ^{13}C NMR (101 MHz, CDCl_3): δ 53.8 (OCH_3), 116.8 (Ar), 120.3 (Ar), 128.1 (Ar), 130.1 (Ar), 130.3 (Ar), 130.4 (Ar), 131.2 (Ar), 131.9 (Ar), 133.2 (Ar), 137.6 (Ar), 138.2 (Ar), 148.7 (Ar), 168.3 (C=O).



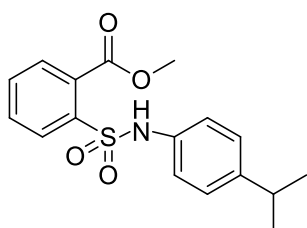
Methyl 2-(N-(4-nitrophenyl)sulfamoyl)benzoate (12): yellow solid, mp 170-174 °C; ^1H NMR (400 MHz, CDCl_3): δ 4.08 (s, 3H, CH_3), 7.35-7.39 (m, 2H, Ar), 7.56-7.61 (m, 1H, Ar), 7.63-7.67 (m, 1H, Ar), 7.87-7.89 (m, 1H, Ar), 7.97-7.99 (m, 1H, Ar), 8.11-8.15 (m, 2H, Ar), 8.60 (br s, 1H, SO_2NH , D_2O exch.). ^{13}C NMR (101 MHz, CDCl_3): δ 53.8 (OCH_3), 120.7 (2 x Ar), 125.1 (2 x Ar), 130.3 (Ar), 130.3 (Ar), 131.2 (Ar), 131.9 (Ar), 133.3 (Ar), 137.7 (Ar), 142.9 (Ar), 144.7 (Ar), 168.3 (C=O).



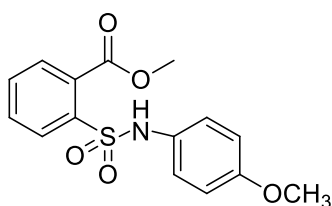
Methyl 2-(*N*-(*p*-tolyl)sulfamoyl)benzoate (13): white solid, mp 78-82 °C; ^1H NMR (400 MHz, CDCl_3): δ 2.27 (s, 3H, CH_3), 4.07 (s, 3H, OCH_3), 7.01-7.07 (m, 4H, Ar), 7.47-7.51 (m, 1H, Ar), 7.57-7.61 (m, 1H, Ar), 7.80-7.85 (m, 2H, Ar), 7.94 (br s, 1H, SO_2NH , D_2O exch.). ^{13}C NMR (101 MHz, CDCl_3): δ 20.9 (CH_3), 53.5 (OCH_3), 123.3 (2 x Ar), 129.7 (2 x Ar), 130.5 (Ar), 130.5 (Ar), 130.5 (Ar), 131.4 (Ar), 132.5 (Ar), 133.9 (Ar), 135.8 (Ar), 138.1 (Ar), 168.4 ($\text{C}=\text{O}$).



Methyl 2-(*N*-(2,6-dimethylphenyl)sulfamoyl)benzoate (14): white solid, mp 170-174 °C; ^1H NMR (400 MHz, CDCl_3): δ 2.14 (s, 6H, 2 x CH_3), 4.08 (s, 3H, OCH_3), 7.03-7.12 (m, 3H, Ar), 7.57-7.61 (m, 1H, Ar), 7.64-7.68 (m, 1H, Ar), 7.77 (br s, 1H, SO_2NH , D_2O exch.), 7.87-7.91 (m, 2H, Ar). ^{13}C NMR (101 MHz, CDCl_3): δ 18.8 (2 x CH_3), 53.5 (OCH_3), 127.6 (Ar), 128.6 (2 x Ar), 128.8 (Ar), 130.2 (Ar), 130.5 (Ar), 131.9 (Ar), 132.2 (Ar), 133.4 (Ar), 137.7 (2 x Ar), 141.6 (Ar), 168.6 ($\text{C}=\text{O}$).



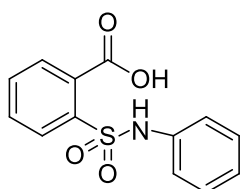
Methyl 2-(*N*-(4-isopropylphenyl)sulfamoyl)benzoate (15): white solid, mp 58-62 °C; ^1H NMR (400 MHz, CDCl_3): δ 1.19 (d, $J = 6.9$ Hz, 6H, 2 x CH_3), 2.80-2.87 (m, 1H, CH), 4.07 (s, 3H, OCH_3), 7.06-7.10 (m, 4H, Ar), 7.48-7.52 (m, 1H, Ar), 7.57-7.61 (m, 1H, Ar), 7.82-7.85 (m, 2H, Ar), 7.96 (br s, 1H, SO_2NH , D_2O exch.). ^{13}C NMR (101 MHz, CDCl_3): δ 23.9 (2 x CH_3), 35.5 (CH), 53.5 (OCH_3), 123.2 (2 x Ar), 127.1 (2 x Ar), 130.4 (Ar), 130.5 (Ar), 130.6 (Ar), 131.4 (Ar), 132.5 (Ar), 134.1 (Ar), 138.3 (Ar), 146.7 (Ar), 168.4 ($\text{C}=\text{O}$).



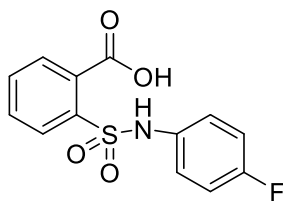
Methyl 2-(N-(4-methoxyphenyl)sulfamoyl)benzoate (16): white solid, mp 108-112 °C; ^1H NMR (400 MHz, CDCl_3): δ 3.76 (s, 3H, OCH_3), 4.07 (s, 3H, OCH_3), 6.73-6.77 (m, 2H, Ar), 7.04-7.08 (m, 2H, Ar), 7.48-7.50 (m, 1H, Ar), 7.57-7.61 (m, 1H, Ar), 7.75-7.77 (m, 1H, Ar), 7.83-7.86 (m, 2H, 1H Ar + SO_2NH , D_2O exch.). ^{13}C NMR (101 MHz, CDCl_3): δ 53.6 (OCH_3), 55.4 (OCH_3), 114.3 (2 x Ar), 125.7 (2 x Ar), 129.2 (Ar), 130.5 (Ar), 130.5 (Ar), 130.6 (Ar), 131.4 (Ar), 132.5 (Ar), 138.1 (Ar), 158.1 (Ar), 168.4 (C=O).

General synthesis and characterization of derivatives 17-28

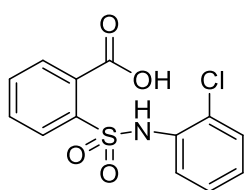
To a stirring solution of the proper ester derivative (1 equiv.) in dioxane (8 mL) 2 mL of aqueous KOH (2.2 equiv.) were added dropwise. The reaction was stirred at 50 °C for 48-72 h until completion of the synthesis; then the organic solvent was evaporated *in vacuo*. The basic solution, containing the potassium salt of the acidic derivative, was extracted at first with dichloromethane (3 x 20 mL) and then acidified with HCl 4N. The resulting suspension was filtered and the collected solid washed with *n*-hexane to afford the title compounds as white or yellow solids.



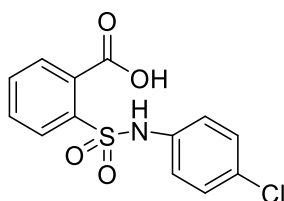
2-(N-phenylsulfamoyl)benzoic acid (17): white solid, mp 160-162 °C; ^1H NMR (400 MHz, $\text{DMSO}-d_6$): δ 7.03 (t, $J = 7.3$ Hz, 1H, Ar), 7.10 (d, $J = 7.6$ Hz, 2H, Ar), 7.23 (t, $J = 7.9$ Hz, 2H, Ar), 7.58-7.64 (m, 1H, Ar), 7.67 (d, $J = 3.9$ Hz, 2H, Ar), 7.79 (d, $J = 7.7$ Hz, 1H, Ar), 9.94 (br s, 1H, SO_2NH , D_2O exch.), 13.65 (br s, 1H, COOH , D_2O exch.). ^{13}C NMR (101 MHz, $\text{DMSO}-d_6$): δ 120.7 (2 x Ar), 124.7 (Ar), 128.9 (Ar), 129.6 (2 x Ar), 129.6 (Ar), 131.0 (Ar), 133.4 (Ar), 134.2 (Ar), 137.0 (Ar), 137.8 (Ar), 169.0 (COOH).



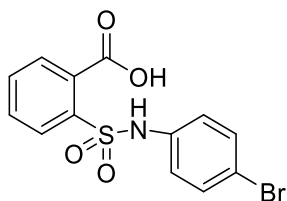
2-(N-(4-fluorophenyl)sulfamoyl)benzoic acid (18): white solid, mp 127-129 °C; ^1H NMR (400 MHz, DMSO- d_6): δ 7.06-7.13 (m, 4H, Ar), 7.55-7.62 (m, 1H, Ar), 7.64-7.69 (m, 2H, Ar), 7.73-7.75 (m, 1H, Ar), 10.04 (br s, 1H, SO₂NH, D₂O exch.), 13.72 (br s, 1H, COOH, D₂O exch.). ^{13}C NMR (101 MHz, DMSO- d_6): δ 116.3 (d, $^2J_{\text{C-F}} = 22.7$ Hz, 2 \times Ar), 123.6 (d, $^3J_{\text{C-F}} = 8.28$ Hz, 2 \times Ar), 128.9 (Ar), 129.7 (Ar), 130.8 (Ar), 133.4 (Ar), 134.1 (d, $^4J_{\text{C-F}} = 2.2$ Hz, Ar), 134.6 (Ar), 136.7 (Ar), 159.6 (d, $^1J_{\text{C-F}} = 241.1$, C-F), 169.0 (COOH).



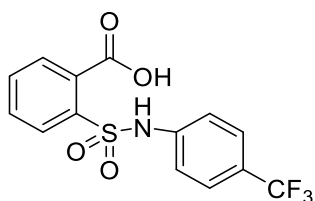
2-(N-(2-chlorophenyl)sulfamoyl)benzoic acid (19): white solid, mp 158-160 °C; ^1H NMR (400 MHz, DMSO- d_6): δ 7.13-7.17 (m, 1H, Ar), 7.25-7.29 (m, 1H, Ar), 7.36-7.42 (m, 2H, Ar), 7.59-7.63 (m, 1H, Ar), 7.69-7.73 (m, 1H, Ar), 7.78-7.82 (m, 2H, Ar), 10.16 (br s, 1H, SO₂NH, D₂O exch.). ^{13}C NMR (101 MHz, DMSO- d_6): δ 125.4 (Ar), 127.1 (Ar), 127.5 (Ar), 128.3 (Ar), 128.6 (Ar), 130.3 (Ar), 130.8 (Ar), 130.9 (Ar), 130.9 (Ar), 133.6 (Ar), 134.6 (Ar), 138.0 (Ar), 169.1 (COOH).



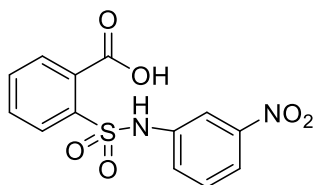
2-(N-(4-chlorophenyl)sulfamoyl)benzoic acid (20): white solid, mp 156-158 °C; ^1H NMR (400 MHz, DMSO- d_6): δ 7.10-7.13 (m, 2H, Ar), 7.28-7.32 (m, 2H, Ar), 7.60-7.64 (m, 1H, Ar), 7.65-7.69 (m, 2H, Ar), 7.80 (d, $J = 7.9$ Hz, 1H, Ar), 10.13 (br s, 1H, SO₂NH, D₂O exch.), 13.64 (br s, 1H, COOH, D₂O exch.). ^{13}C NMR (101 MHz, DMSO- d_6): δ 122.3 (2 \times Ar), 128.8 (Ar), 128.9 (Ar), 129.5 (2 \times Ar), 129.6 (Ar), 131.0 (Ar), 133.6 (Ar), 134.3 (Ar), 136.7 (Ar), 136.8 (Ar), 168.9 (COOH).



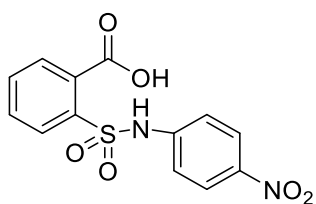
2-(N-(4-bromophenyl)sulfamoyl)benzoic acid (21): white solid, mp 134-136 °C; ^1H NMR (400 MHz, DMSO- d_6): δ 7.03-7.06 (m, 2H, Ar), 7.39-7.42 (m, 2H, Ar), 7.45-7.48 (m, 1H, Ar), 7.57-7.61 (m, 1H, Ar), 7.65-7.69 (m, 2H, Ar), 11.61 (br s, 1H, SO₂NH, D₂O exch.). ^{13}C NMR (101 MHz, DMSO- d_6): δ 116.5 (Ar), 123.0 (2 × Ar), 127.7 (Ar), 129.2 (Ar), 130.0 (Ar), 131.9 (2 × Ar), 132.8 (Ar), 136.0 (Ar), 137.3 (Ar), 137.6 (Ar), 168.7 (COOH).



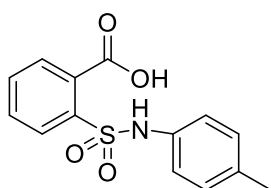
2-(N-(4-(trifluoromethyl)phenyl)sulfamoyl)benzoic acid (22): white solid, mp 232-236 °C; ^1H NMR (400 MHz, DMSO- d_6): δ 7.29 (d, J = 8.4 Hz, 2H, Ar), 7.34-7.38 (m, 1H, Ar), 7.51-7.57 (m, 3H, Ar), 7.61-7.63 (m, 1H, Ar), 7.72-7.74 (m, 1H, Ar). ^{13}C NMR (101 MHz, DMSO- d_6): δ 121.5 (2 x Ar), 124.4 (Ar), 124.7 (d, $^1J_{\text{C-F}}$ = 271.4 Hz, CF₃), 126.7 (2 x Ar), 127.4 (Ar), 128.7 (Ar), 131.4 (Ar), 133.0 (Ar), 136.5 (Ar), 140.3 (Ar), 143.2 (Ar), 169.7 (COOH).



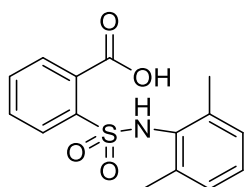
2-(N-(3-nitrophenyl)sulfamoyl)benzoic acid (23): yellow solid, mp 170-172 °C; ^1H NMR (400 MHz, DMSO- d_6): δ 7.51-7.57 (m, 2H, Ar), 7.63-7.72 (m, 3H, Ar), 7.86-7.90 (m, 2H, Ar), 7.97-7.98 (m, 1H, Ar), 10.69 (br s, 1H, SO₂NH, D₂O exch.), 13.63 (br s, 1H, COOH, D₂O exch.). ^{13}C NMR (101 MHz, DMSO- d_6): δ 114.4 (Ar), 119.0 (Ar), 126.0 (Ar), 129.0 (Ar), 129.6 (Ar), 131.1 (Ar), 131.2 (Ar), 133.9 (Ar), 134.4 (Ar), 136.4 (Ar), 139.2 (Ar), 148.6 (Ar), 168.7 (COOH).



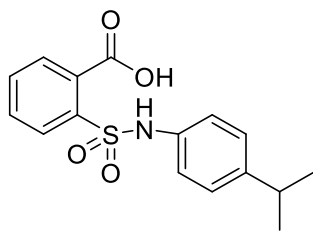
2-(N-(4-nitrophenyl)sulfamoyl)benzoic acid (24): yellow solid, mp 102-106 °C; ^1H NMR (400 MHz, DMSO- d_6): δ 7.30 (d, J = 9.2 Hz, 2H, Ar), 7.61-7.70 (m, 3H, Ar), 7.91 (d, J = 7.7 Hz, 1H, Ar), 8.13 (d, J = 9.2 Hz, 2H, Ar). ^{13}C NMR (101 MHz, DMSO- d_6): δ 118.9 (2 x Ar), 125.7 (2 x Ar), 128.7 (Ar), 130.1 (Ar), 130.9 (Ar), 133.8 (Ar), 135.1 (Ar), 136.6 (Ar), 143.0 (Ar), 144.9 (Ar), 168.6 (COOH).



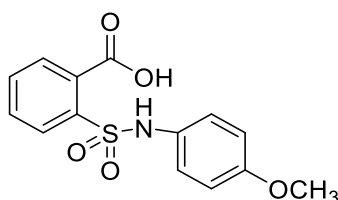
2-(N-(*p*-tolyl)sulfamoyl)benzoic acid (25): white solid, mp 160-162 °C; ^1H NMR (400 MHz, DMSO- d_6): δ 2.18 (s, 3H, CH₃), 6.98-7.04 (m, 4H, Ar), 7.57-7.62 (m, 1H, Ar), 7.63-7.68 (m, 2H, Ar), 7.75 (d, J = 7.6 Hz, 1H, Ar), 9.70 (s, 1H, SO₂NH, D₂O exch.), 13.64 (br s, 1H, COOH, D₂O exch.). ^{13}C NMR (101 MHz, DMSO- d_6): δ 20.8 (CH₃), 121.3 (2 x Ar), 128.95 (Ar), 129.6 (Ar), 130.01 (2 x Ar), 130.9 (Ar), 133.3 (Ar), 134.1 (Ar), 134.1 (Ar), 135.1 (Ar), 137.1 (Ar), 169.1 (COOH).



2-(N-(2,6-dimethylphenyl)sulfamoyl)benzoic acid (26): white solid, mp 176-178 °C; ^1H NMR (400 MHz, DMSO- d_6): δ 2.00 (s, 6H, 2 x CH₃), 7.01-7.03 (m, 2H, Ar), 7.06-7.09 (m, 1H, Ar), 7.63-7.67 (m, 2H, Ar), 7.71-7.79 (m, 2H, Ar), 8.66 (s, 1H, SO₂NH, D₂O exch.), 13.79 (br s, 1H, COOH, D₂O exch.). ^{13}C NMR (101, MHz, CDCl₃): δ 18.9 (2 x CH₃), 127.8 (Ar), 128.5 (Ar), 128.7 (2 x Ar), 130.01 (Ar), 131.5 (Ar), 132.8 (Ar), 133.2 (Ar), 134.1 (Ar), 138.2 (2 x Ar), 140.1 (Ar), 169.5 (COOH).



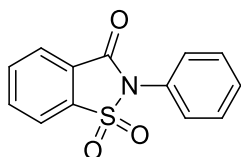
2-(N-(4-isopropylphenyl)sulfamoyl)benzoic acid (27): white solid, mp 80-84 °C; ^1H NMR (400 MHz, $\text{DMSO-}d_6$): δ 1.12 (d, $J = 6.9$ Hz, 6H, $2 \times \text{CH}_3$), 2.74-2.81 (m, 1H, CH), 7.01 (d, $J = 8.5$ Hz, 2H, Ar), 7.10 (d, $J = 8.5$ Hz, 2H, Ar), 7.54-7.58 (m, 1H, Ar), 7.62-7.69 (m, 2H, Ar), 7.76 (d, $J = 7.8$ Hz, 1H, Ar), 10.13 (br s, 1H, SO_2NH , D_2O exch.). ^{13}C NMR (101 MHz, $\text{DMSO-}d_6$): δ 24.2 ($2 \times \text{CH}_3$), 33.2 (CH), 121.2 ($2 \times \text{Ar}$), 127.3 ($2 \times \text{Ar}$), 128.7 (Ar), 129.8 (Ar), 130.6 (Ar), 133.2 (Ar), 135.0 (Ar), 135.6 (Ar), 137.2 (Ar), 144.9 (Ar), 169.2 (COOH).



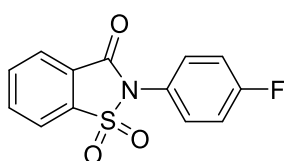
2-(N-(4-methoxyphenyl)sulfamoyl)benzoic acid (28): white solid, mp 152-156 °C; ^1H NMR (400 MHz, $\text{DMSO-}d_6$): δ 3.67 (s, 3H, CH_3), 6.80 (d, $J = 9.0$ Hz, 2H, Ar), 7.01 (d, $J = 9$ Hz, 2H, Ar), 7.56-7.62 (m, 1H, Ar), 7.64-7.72 (m, 3H, Ar), 9.46 (br s, 1H, SO_2NH , D_2O exch.), 13.68 (br s, 1H, COOH, D_2O exch.). ^{13}C NMR (101 MHz, $\text{DMSO-}d_6$): δ 55.6 (CH_3), 114.7 ($2 \times \text{Ar}$), 124.1 ($2 \times \text{Ar}$), 129.1 (Ar), 129.7 (Ar), 130.2 (Ar), 130.9 (Ar), 133.3 (Ar), 133.9 (Ar), 137.1 (Ar), 157.2 (Ar), 169.2 (COOH).

General synthesis and characterization of derivatives 29-40

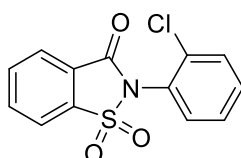
Triethylamine (3 equiv.) and ethyl chloroformate (1.2 equiv.) were added to a stirring solution of the proper acid derivative (1.0 equiv.) in tetrahydrofuran and stirred under nitrogen atmosphere for 1 h at room temperature. Once the reaction completion, the mixture was extracted with ethyl acetate (3×20 mL) and 2N HCl. The organics were reunited, dried over sodium sulphate and concentrated *in vacuo*. Purification through column chromatography on silica gel, using the proper mixtures of solvents, gave compounds 29-40 as white or yellow solids.



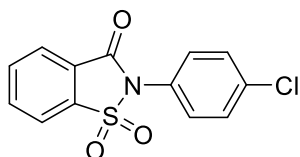
2-phenylbenzo[*d*]isothiazol-3(2*H*)-one 1,1-dioxide (29): white solid, mp 188-190 °C; ¹H NMR (400 MHz, CDCl₃): δ 7.54-7.61 (m, 5H, Ar), 7.89-7.98 (m, 2H, Ar), 8.02-8.04 (m, 1H, Ar), 8.18-8.20 (m, 1H, Ar). ¹³C NMR (101 MHz, CDCl₃): δ 121.3 (Ar), 125.7 (Ar), 127.2 (Ar), 128.7 (Ar), 128.8 (2 × Ar), 129.9 (2 × Ar), 130.1 (Ar), 134.5 (Ar), 135.1 (Ar), 137.6 (Ar), 158.4 (C=O).



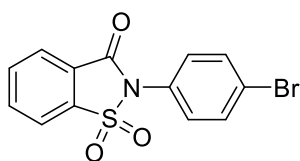
2-(4-fluorophenyl)benzo[*d*]isothiazol-3(2*H*)-one 1,1-dioxide (30): white solid, mp 163-165 °C; ¹H NMR (400 MHz, CDCl₃): δ 7.25-7.31 (m, 2H, Ar), 7.53-7.58 (m, 2H, Ar), 7.91-7.95 (m, 1H, Ar), 7.96-8.00 (m, 1H, Ar), 8.03-8.05 (m, 1H, Ar), 8.19-8.21 (m, 1H, Ar). ¹³C NMR (101 MHz, CDCl₃): δ 117.1 (d, ²*J*_{C-F} = 23.1 Hz, 2 × Ar), 121.3 (Ar), 124.4 (d, ⁴*J*_{C-F} = 23.1 Hz, Ar), 125.7 (Ar), 127.1 (Ar), 131.0 (d, ³*J*_{C-F} = 9.1 Hz, 2 × Ar), 134.6 (Ar), 135.2 (Ar), 137.6 (Ar), 131.5 (Ar), 132.5 (d, *J* = 3.03 Hz, 1 × Ar), 132.7 (Ar), 137.7 (Ar), 158.4 (C=O), 163.5 (d, ¹*J*_{C-F} = 250.9, C-F).



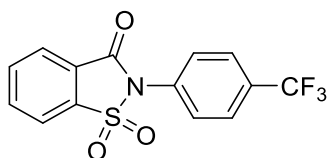
2-(2-chlorophenyl)benzo[*d*]isothiazol-3(2*H*)-one 1,1-dioxide (31): white solid, mp 208-210 °C; ¹H NMR (400 MHz, CDCl₃): δ 7.46-7.50 (m, 1H, Ar), 7.52-7.57 (m, 1H, Ar), 7.62-7.67 (m, 2H, Ar), 7.91-7.99 (m, 2H, Ar), 8.03-8.05 (m, 1H, Ar), 8.20-8.22 (m, 1H, Ar). ¹³C NMR (101 MHz, CDCl₃): δ 121.4 (Ar), 125.9 (Ar), 126.2 (Ar), 126.9 (Ar), 128.1 (Ar), 131.1 (Ar), 132.0 (Ar), 132.0 (Ar), 134.5 (Ar), 135.2 (Ar), 135.3 (Ar), 138.1 (Ar), 157.5 (C=O).



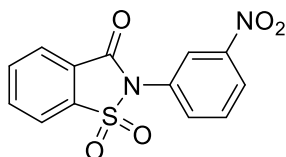
2-(4-chlorophenyl)benzo[*d*]isothiazol-3(2*H*)-one 1,1-dioxide (32): white solid, mp 156-158 °C; ¹H NMR (400 MHz, CDCl₃): δ 7.50-7.57 (m, 4H, Ar), 7.91-7.95 (m, 1H, Ar), 7.95-7.99 (m, 1H, Ar), 8.0.3 (d, *J* = 7.3 Hz, 1H, Ar), 8.19 (d, *J* = 7.8 Hz, 1H, Ar). ¹³C NMR (101 MHz, CDCl₃): δ 121.3 (Ar), 125.7 (Ar), 127.0 (Ar), 127.3 (Ar), 129.9 (2 × Ar), 130.2 (2 × Ar), 134.6 (Ar), 135.3 (Ar), 136.3 (Ar), 137.5 (Ar), 158.2 (C=O).



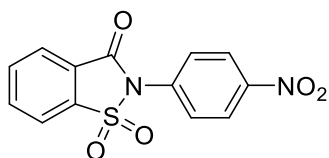
2-(4-bromophenyl)benzo[*d*]isothiazol-3(2*H*)-one 1,1-dioxide (33): white solid, mp 141-143 °C; ¹H NMR (400 MHz, CDCl₃): δ 7.43-7.47 (m, 2H, Ar), 7.69-7.72 (m, 2H, Ar), 7.90-7.98 (m, 2H, Ar), 8.01-8.03 (m, 1H, Ar), 8.18 (d, *J* = 7.4 Hz, 1H, Ar). ¹³C NMR (101 MHz, CDCl₃): δ 121.3 (2 x Ar), 124.4 (Ar), 125.8 (Ar), 127.0 (Ar), 127.8 (Ar), 130.1 (2 × Ar), 133.2 (2 × Ar), 134.6 (Ar), 135.3, (Ar), 137.5 (Ar), 158.2 (C=O).



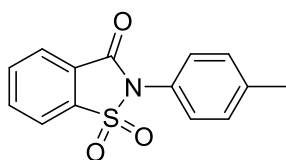
2-(4-(trifluoromethyl)phenyl)benzo[*d*]isothiazol-3(2*H*)-one 1,1-dioxide (34): white solid, mp 158-160 °C; ¹H NMR (400 MHz, CDCl₃): δ 7.75 (d, *J* = 8.4 Hz, 2H, Ar), 7.85 (d, *J* = 8.4 Hz, 2H, Ar), 7.92-8.01 (m, 2H, Ar), 8.03-8.06 (m, 1H, Ar), 8.20-8.22 (m, 1H, Ar). ¹³C NMR (101 MHz, DMSO-*d*₆): δ 121.3 (Ar), 123.6 (d, ¹*J*_{C-F} = 272.6 Hz, CF₃), 125.9 (Ar), 126.9 (Ar), 127.0 (q, ³*J*_{C-F} = 3.7 Hz, 2 x Ar), 128.4 (2 × Ar), 131.9 (m, Ar), 132.5 (Ar), 134.7 (Ar), 135.4 (Ar), 137.5 (Ar), 158.1 (C=O).



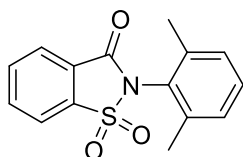
2-(3-nitrophenyl)benzo[d]isothiazol-3(2H)-one 1,1-dioxide (35): yellow solid, mp 136-138 °C; ¹H NMR (400 MHz, CDCl₃): δ 7.78 (t, *J* = 8.2 Hz, 1H, Ar), 7.94-7.98 (m, 2H, Ar), 7.99-8.03 (m, 1H, Ar), 8.04-8.06 (m, 1H, Ar), 8.22 (d, *J* = 7.2 Hz, 1H, Ar) 8.40-8.43 (m, 1H, Ar), 8.49 (t, *J* = 2.0 Hz, 1H, Ar). ¹³C NMR (101 MHz, CDCl₃): δ 121.4 (Ar), 123.6 (Ar), 124.6 (Ar), 126.0 (Ar), 126.7 (Ar), 130.4 (Ar), 130.8 (Ar), 134.0 (Ar), 134.9 (Ar), 135.6 (Ar), 137.4 (Ar), 149.0 (Ar), 158.1 (C=O).



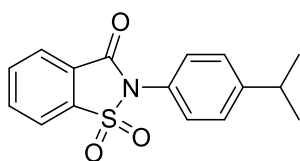
2-(4-nitrophenyl)benzo[d]isothiazol-3(2H)-one 1,1-dioxide (36): yellow solid, mp 232-234 °C; ¹H NMR (400 MHz, CDCl₃): δ 7.92 (d, *J* = 9.0 Hz, 2H, Ar), 8.09 (t, *J* = 7.2 Hz, 1H, Ar), 8.15 (t, *J* = 7.1 Hz, 1H, Ar), 8.24 (d, *J* = 7.5 Hz, 1H, Ar), 8.44-8.50 (m, 3H, Ar). ¹³C NMR (101 MHz, CDCl₃): δ 121.4 (Ar), 125.1 (2 × Ar), 126.0 (Ar), 126.7 (Ar), 128.0 (2 × Ar), 134.9 (Ar), 135.3 (Ar), 135.7 (Ar), 137.3 (Ar), 147.9 (Ar), 157.9 (C=O).



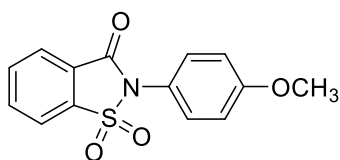
2-(p-tolyl)benzo[d]isothiazol-3(2H)-one 1,1-dioxide (37): white solid, mp 172-174 °C; ¹H NMR (400 MHz, CDCl₃): δ 2.46 (s, 3H, CH₃), 7.38 (d, *J* = 8.3 Hz, 2H, Ar), 7.43-7.45 (m, 2H, Ar), 7.88-7.96 (m, 2H, Ar), 8.01-8.03 (m, 1H, Ar), 8.16-8.18 (m, *J* = 8 Hz, 1H, Ar). ¹³C NMR (101 MHz, CDCl₃): δ 21.4 (CH₃), 121.3 (Ar), 125.6 (Ar), 125.8 (Ar), 127.3 (Ar), 128.7 (2 × Ar), 130.6 (2 × Ar), 134.4 (Ar), 135.03 (Ar), 137.7 (Ar), 140.5 (Ar), 158.5 (C=O).



2-(2,6-dimethylphenyl)benzo[*d*]isothiazol-3(2*H*)-one 1,1-dioxide (38): white solid, mp 224-228 °C; ¹H NMR (400 MHz, CDCl₃): δ 2.36 (s, 6H, 2 x CH₃), 7.24 (d, *J* = 7.6 Hz, 2H, Ar), 7.32-7.36 (m, 1H, Ar), 7.90-7.98 (m, 2H, Ar), 8.02-8.04 (m, 1H, Ar), 8.19-8.21 (m, 1H, Ar). ¹³C NMR (101 MHz, CDCl₃): δ 18.5 (2 x CH₃), 121.2 (Ar), 125.7 (Ar), 126.3 (Ar), 127.0 (Ar), 129.2 (2 x Ar), 130.6 (Ar), 134.4 (Ar), 135.1 (Ar), 138.4 (Ar), 139.9 (Ar), 158.2 (C=O).

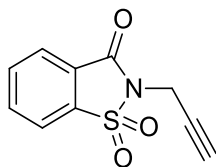


2-(4-isopropylphenyl)benzo[*d*]isothiazol-3(2*H*)-one 1,1-dioxide (39): white solid, mp 138-140 °C; ¹H NMR (400 MHz, CDCl₃): δ 1.32 (d, *J* = 6.9 Hz, 6H, 2 x CH₃), 2.96-3.07 (m, 1H, CH), 7.42-7.48 (m, 4H, Ar), 7.88-7.96 (m, 2H, Ar), 8.02 (d, *J* = 7.2 Hz, 1H, Ar), 8.17-8.19 (m, 1H, Ar). ¹³C NMR (101 MHz, CDCl₃): δ 23.8 (2 x CH₃), 34.0 (CH), 121.3 (Ar), 125.6 (Ar), 126.0 (Ar), 127.3 (Ar), 128.1 (2 x Ar), 128.7 (2 x Ar), 134.4 (Ar), 135.03 (Ar), 137.7 (Ar), 151.2 (Ar), 158.5 (C=O).



2-(4-methoxyphenyl)benzo[*d*]isothiazol-3(2*H*)-one 1,1-dioxide (40): white solid, mp 192-196 °C; ¹H NMR (400 MHz, CDCl₃): δ 3.89 (s, 3H, OCH₃), 7.06-7.10 (m, 2H, Ar), 7.44-7.48 (m, 2H, Ar), 7.88-7.97 (m, 2H, Ar), 8.01-8.03 (m, 1H, Ar), 8.17-8.19 (m, 1H, Ar). ¹³C NMR (101 MHz, CDCl₃): δ 55.6 (CH₃), 115.3 (2 x Ar), 120.5 (Ar), 121.3 (Ar), 125.6 (Ar), 127.3 (Ar), 130.5 (2 x Ar), 134.4 (Ar), 135.01 (Ar), 137.7 (Ar), 158.7 (Ar), 161.01 (C=O).

Synthesis and characterization data of intermediates S1 and I-VI

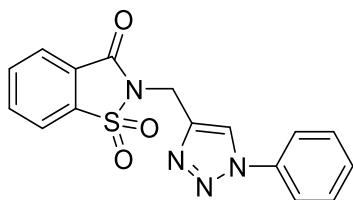


2-(prop-2-yn-1-yl)benzo[*d*]isothiazol-3(2*H*)-one 1,1-dioxide (S1): for the synthesis and characterization data of the compound S1, see ref. [112].

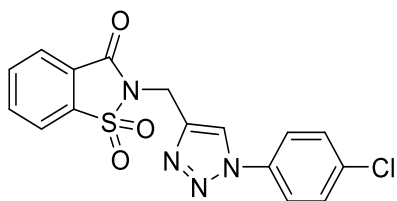
NaNO₂ (1.2 equiv.) was slowly added to a solution of the proper aniline (1.0 equiv.) in a 4M HCl aqueous solution at 0 °C. After 30 min NaN₃ (1.5 equiv.) was added portion-wise and the resulting mixture stirred at room temperature for 1 h. The mixture was then extracted with ethyl acetate (3 × 20 mL). The organic layers were reunited, dried over sodium sulphate and concentrated *in vacuo*. The residual crude product was used directly without further purification. For the characterization data of **azides I-VI**, see references [140,146,147]

Synthesis and characterization data of derivatives 41-46

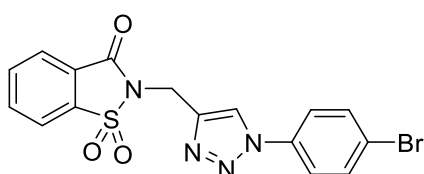
Propargylated saccharin (1.0 equiv.) and the proper benzyl azide (1.05 equiv.) were added to a stirring solution of CuI (0.02 equiv.), DIPEA (0.04 equiv.) and CH₃COOH (0.04 equiv.) in dichloromethane and stirred at room temperature until the alkyne disappeared. The mixture was then extracted with dichloromethane (3 × 20 mL) and H₂O. The organics were reunited, dried over sodium sulphate and concentrated *in vacuo*. Purification through column chromatography on silica gel, using the proper solvents mixtures, gave compounds **STR1-STR6** as white solids.



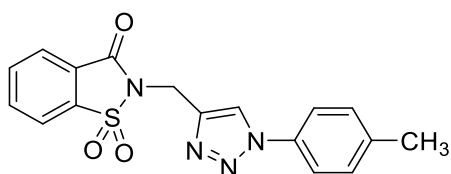
2-((1-phenyl-1*H*-1,2,3-triazol-4-yl)methyl)benzo[*d*]isothiazol-3(2*H*)-one 1,1-dioxide (41): white solid, 134-136 °C; ¹H NMR (400 MHz, CDCl₃): δ 5.18 (s, 2H, CH₂), 7.41-7.45 (m, 1H, Ar), 7.49-7.52 (m, 2H, Ar), 7.71-7.73 (m, 2H, Ar), 7.84-7.93 (m, 2H, Ar), 7.96 (d, *J* = 7.2 Hz, 1H, Ar), 8.08-8.10 (m, 1H, Ar), 8.13 (s, 1H, Ar-triazole). ¹³C NMR (101 MHz, CDCl₃): δ 34.0 (CH₂), 120.7 (2 x Ar), 121.1 (Ar), 121.7 (Ar-triazole), 125.4 (Ar), 127.1 (Ar), 128.9 (Ar), 129.7 (2 x Ar), 134.5 (Ar), 135.1 (Ar), 136.9 (Ar-triazole), 137.7 (Ar), 142.5 (Ar) 158.6 (C=O).



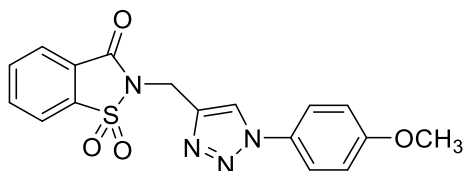
2-((1-(4-chlorophenyl)-1H-1,2,3-triazol-4-yl)methyl)benzo[d]isothiazol-3(2H)-one 1,1-dioxide (42): white solid, 196-198 °C; ¹H NMR (400 MHz, CDCl₃): δ 5.19 (s, 2H, CH₂), 7.50 (d, *J* = 8.8 Hz, 2H, Ar), 7.69 (d, *J* = 8.8 Hz, 2H, Ar), 7.86-7.94 (m, 2H, Ar), 7.98 (d, *J* = 7.3 Hz, 1H, Ar), 8.11-8.12 (m, 2H, Ar-triazole + Ar). ¹³C NMR (101 MHz, CDCl₃): δ 34.9 (CH₂), 121.1 (Ar), 121.6 (Ar-triazole), 121.8 (2 x Ar), 125.4 (Ar), 127.1 (Ar), 129.9 (2 x Ar), 134.4 (Ar), 134.7 (Ar), 135.1 (Ar), 135.4 (Ar-triazole), 137.7 (Ar), 142.8 (Ar), 158.6 (C=O).



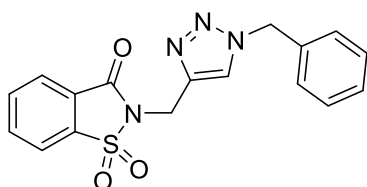
2-((1-(4-bromophenyl)-1H-1,2,3-triazol-4-yl)methyl)benzo[d]isothiazol-3(2H)-one 1,1-dioxide (43): white solid, 184-188 °C; ¹H NMR (400 MHz, DMSO-*d*₆): δ 5.10 (s, 2H, CH₂), 7.77-7.81 (m, 2H, Ar), 7.86-7.90 (m, 2H, Ar), 8.01-8.05 (m, 1H, Ar), 8.06-8.10 (m, 2H, Ar), 8.15-8.17 (m, 1H, Ar), 8.88 (s, 1H, Ar-triazole). ¹³C NMR (101 MHz, DMSO-*d*₆): δ 33.9 (CH₂), 121.9 (Ar-triazole), 122.1 (Ar), 122.4 (2 x Ar), 122.7 (Ar), 125.7 (Ar), 126.8 (Ar), 133.3 (2 x Ar), 135.8 (Ar), 136.1 (Ar-triazole), 136.4 (Ar), 137.3 (Ar), 143.2 (Ar), 158.8 (C=O).



2-((1-(*p*-tolyl)-1H-1,2,3-triazol-4-yl)methyl)benzo[d]isothiazol-3(2H)-one 1,1-dioxide (44): white solid, 172-174 °C; ¹H NMR (400 MHz, CDCl₃): δ 2.32 (s, 3H, CH₃), 5.08 (s, 2H, CH₂), 7.20 (d, *J* = 8.6 Hz, 2H, Ar), 7.50 (d, *J* = 8.5 Hz, 2H, Ar), 7.74-7.88 (m, 3H, Ar), 7.99-8.01 (m, 2H, Ar-triazole + Ar). ¹³C NMR (101 MHz, CDCl₃): δ 21.1 (CH₃), 34.1 (CH₂), 120.6 (2 x Ar), 121.1 (Ar), 121.6 (Ar-triazole), 125.4 (Ar), 127.2 (Ar), 130.2 (2 x Ar), 134.5 (Ar), 134.6 (Ar-triazole), 135.1 (Ar), 137.7 (Ar), 139.0 (Ar), 142.4 (Ar), 158.6 (C=O).



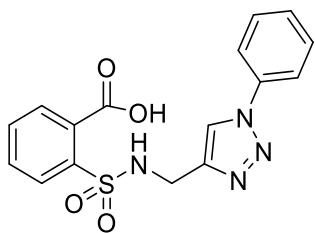
2-((1-(4-methoxyphenyl)-1H-1,2,3-triazol-4-yl)methyl)benzo[d]isothiazol-3(2H)-one 1,1-dioxide (45): white solid, 174-176 °C; ¹H NMR (400 MHz, CDCl₃): δ 3.86 (s, 3H, OCH₃), 5.17 (s, 2H, CH₂), 6.98-7.02 (m, 2H, Ar), 7.59-7.63 (m, 2H, Ar), 7.84-7.88 (m, 1H, Ar), 7.88-7.92 (m, 2H, Ar), 7.96 (d, *J* = 7.2 Hz, 1H, Ar), 8.04 (s, 1H, Ar-triazole). ¹³C NMR (101 MHz, CDCl₃): δ 34.1 (OCH₃), 55.6 (CH₂), 114.7 (2 x Ar), 121.1 (Ar), 121.8 (Ar-triazole), 122.3 (2 x Ar), 125.4 (Ar), 127.2 (Ar), 130.3 (Ar-triazole), 134.5 (Ar), 135.1 (Ar), 137.7 (Ar), 142.4 (Ar), 158.6 (Ar), 159.9 (C=O).



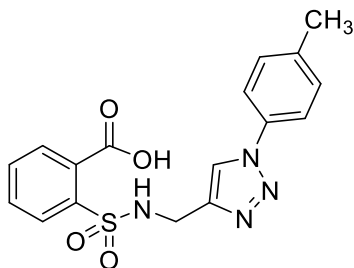
2-((1-benzyl-1H-1,2,3-triazol-4-yl)methyl)benzo[d]isothiazol-3(2H)-one 1,1-dioxide (46): white solid, 130-132 °C; ¹H NMR (400 MHz, DMSO-*d*₆): δ 4.99 (s, 2H, CH₂), 5.16 (s, 2H, CH₂), 7.28-7.38 (m, 5H, Ar), 7.99-8.03 (m, 1H, Ar), 8.04-8.08 (m, 1H, Ar), 8.13 (m, 1H, Ar), 8.20 (s, 1H, Ar-triazole), 8.32 (d, *J* = 7.5 Hz, 1H, Ar). ¹³C NMR (101 MHz, DMSO-*d*₆): δ 34.0 (CH₂), 53.3 (CH₂), 122.1 (Ar), 124.7 (Ar), 125.7 (Ar), 126.7 (Ar-triazole), 128.3 (2 x Ar), 128.6 (Ar), 129.2 (2 x Ar), 135.8 (Ar), 136.4 (Ar), 136.4 (Ar-triazole), 137.3 (Ar), 141.9 (Ar), 158.7 (C=O).

General synthesis and characterization data of derivatives 47-49

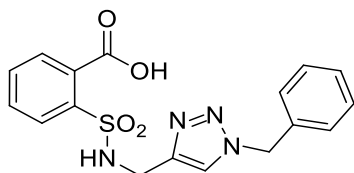
To a stirring solution of the proper saccharin derivative (1 equiv.) in tetrahydrofuran (10 mL) at room temperature 10 mL of aqueous 2N NaOH (5.0 equiv.) were added dropwise. After 2 h the organic solvent was evaporated and the basic solution, containing the acid derivative as sodium salt, acidified with 4N HCl. The resulting suspension was filtered and the collected solid washed with *n*-hexane to afford the title compounds as a white solid.



2-(N-((1-phenyl-1H-1,2,3-triazol-4-yl)methyl)sulfamoyl)benzoic acid (47): white solid, 162-166 °C; ^1H NMR (400 MHz, DMSO- d_6): δ 4.29 (d, $J = 3.7$ Hz, 2H, CH₂), 7.49 (t, $J = 7.4$ Hz, 1H, Ar), 7.57-7.71 (m, 5H, Ar), 7.76-7.78 (m, 3H, 2 x Ar + SO₂NH, D₂O exch.), 7.88-7.91 (m, 1H, Ar), 8.48 (s, 1H, Ar-triazole), 13.71 (br s, 1H, COOH, D₂O exch.). ^{13}C NMR (101 MHz, DMSO- d_6): δ 38.6 (CH₂), 120.5 (2 x Ar), 122.0 (Ar-triazole), 128.9 (Ar), 129.1 (Ar), 129.5 (Ar), 130.4 (2 x Ar), 131.1 (Ar), 133.0 (Ar), 133.4 (Ar-triazole), 136.9 (Ar-), 138.1 (Ar), 144.8 (Ar), 169.4 (COOH).



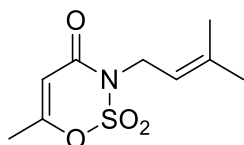
2-(N-((1-(p-tolyl)-1H-1,2,3-triazol-4-yl)methyl)sulfamoyl)benzoic acid (48): white solid, 182-186 °C; ^1H NMR (400 MHz, DMSO- d_6): δ 2.37 (s, 3H, CH₃), 4.27 (d, $J = 5.5$ Hz, 2H, CH₂), 7.38 (t, $J = 8.3$ Hz, 2H, Ar), 7.60-7.69 (m, 5H, Ar), 7.73-7.77 (br s, 1H, SO₂NH, D₂O exch.), 7.83-7.90 (m, 1H, Ar), 8.41 (s, 1H, Ar-triazole), 13.70 (br s, 1H, COOH, D₂O exch.). ^{13}C NMR (101 MHz, DMSO- d_6): δ 21.0 (CH₃), 38.6 (CH₂), 120.4 (2 x Ar), 121.9 (Ar-triazole), 129.0 (Ar), 129.5 (Ar), 130.7 (2 x Ar), 131.1 (Ar), 132.9 (Ar), 133.4 (Ar-triazole), 134.7 (Ar), 138.1 (Ar), 138.8 (Ar), 144.6 (Ar), 169.4 (COOH).



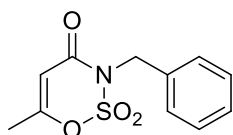
2-(N-((1-benzyl-1H-1,2,3-triazol-4-yl)methyl)sulfamoyl)benzoic acid (49): white solid, 144-146 °C; ^1H NMR (400 MHz, DMSO- d_6): δ 4.15 (s, 2H, CH₂), 5.49 (s, 2H, CH₂), 7.23-7.25 (m, 2H, Ar), 7.31-7.40 (m, 3H, Ar), 7.54-7.59 (m, 1H, Ar), 7.64 (d, $J = 4.1$ Hz, 2H, Ar), 7.82 (d, $J = 7.8$ Hz, 1H, Ar), 7.85 (s, 1H, Ar triazole). ^{13}C NMR (101 MHz, DMSO- d_6): 38.7 (CH₂), 53.1

(CH₂), 123.7 (Ar-triazole), 128.4 (2 x Ar), 128.7 (Ar), 128.7 (Ar), 129.2 (2 x Ar), 129.7 (Ar), 130.7 (Ar), 132.9 (Ar), 134.3 (Ar), 136.4 (Ar), 138.0 (Ar-triazole), 144.2 (Ar), 169.4 (COOH).

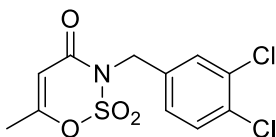
3.5.3. Synthesis and characterization data of acesulfame-based derivatives



6-methyl-3-(3-methylbut-2-en-1-yl)-1,2,3-oxathiazin-4(3H)-one 2,2-dioxide (50): 3,3-dimethylallyl bromide (1 equiv.) was added to a stirring solution of acesulfame K (1 equiv.) in *N,N*-dimethylformamide and the reaction stirred under nitrogen atmosphere at 0° C for 48 h. The mixture was poured on ice and the resulting aqueous phase/emulsion extracted with dichloromethane (3 × 20 mL). The organic layers were reunited, dried over sodium sulphate, and concentrated *in vacuo*. Purification through column chromatography on silica gel (*n*-hexane:ethyl acetate, 2:1) gave the title compound as a yellow oil (70% yield); ¹H NMR (300 MHz, CDCl₃): δ 1.70 (s, 3H, CH₃), 1.73 (s, 3H, CH₃), 2.17 (s, 3H, CH₃) 4.40 (d, *J* = 6.9 Hz, 2H, CH₂), 5.24 (t, *J* = 1.2 Hz, 1H, CH=), 5.76 (d, *J* = 1.2 Hz, 1H, CH=). ¹³C NMR (76 MHz, CDCl₃): δ 17.8 (CH₃), 19.6 (CH₃), 25.7 (CH₃), 41.0 (CH₂), 104.4 (CH=, acesulfame), 117.1 (CH=C), 139.0 (C=CH), 160.0 (C=O), 161.6 (COSO₂).

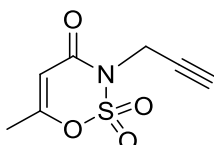


3-benzyl-6-methyl-1,2,3-oxathiazin-4(3H)-one 2,2-dioxide (51): benzyl bromide (1 equiv.) was added to a stirring solution of acesulfame K (1 equiv.) in *N,N*-dimethylformamide and the reaction stirred under nitrogen atmosphere at 0 °C for 48 h. The mixture was poured on ice and the resulting aqueous phase/emulsion extracted with dichloromethane (3 × 20 mL). The organic layers were reunited, dried over sodium sulphate and concentrated *in vacuo*. Purification through column chromatography on silica gel (*n*-hexane:ethyl acetate, 2:1) gave the title compound as a colourless oil (75% yield); ¹H NMR (300 MHz, CDCl₃): δ 2.23 (d, *J* = 0.3 Hz, 3H, CH₃), 5.37 (s, 2H, CH₂), 5.81 (d, *J* = 0.6 Hz, 1H, CH=), 7.42 (s, 5H, Ar). ¹³C NMR (101, MHz, CDCl₃): δ 20.5 (CH₃), 70.7 (CH₂), 95.7 (CH=, acesulfame), 128.8 (2 x Ar), 128.9 (2 x Ar), 129.2 (Ar), 133.5 (Ar), 168.8 (C=O), 169.1 (COSO₂).

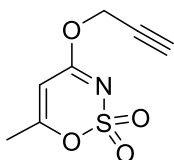


3-(3,4-dichlorobenzyl)-6-methyl-1,2,3-oxathiazin-4(3H)-one 2,2-dioxide (52): 3,4-dichlorobenzyl bromide (1 equiv.) was added to a stirring solution of acesulfame K (1 equiv.) in *N,N*-dimethylformamide and the reaction stirred under nitrogen atmosphere at 0 °C for 48 h. The mixture was poured on ice and the resulting aqueous phase/emulsion extracted with dichloromethane (3 × 20 mL). The organic layers were reunited, dried over sodium sulphate and concentrated *in vacuo*. Purification through column chromatography on silica gel (*n*-hexane:ethyl acetate, 2:1) gave the title compound as a white solid (75% yield); 93-94 °C; ¹H NMR (400 MHz, CDCl₃): δ 2.22 (s, 3H, CH₃), 4.92 (s, 2H, CH₂), 5.84 (d, *J* = 1.2 Hz, 1H, CH=), 7.24-7.27 (m, 1H, Ar), 7.41 (d, *J* = 8.4 Hz, 1H, Ar), 7.51 (d, *J* = 2.4 Hz, 1H, Ar). ¹³C NMR (101 MHz, CDCl₃): δ 19.8 (CH₃), 45.0 (CH₂), 104.5 (CH=, acesulfame), 128.2 (2 x Ar), 130.7 (Ar), 130.8 (Ar), 132.8 (Ar), 134.8 (Ar), 160.0 (C=O), 162.1 (COSO₂).

General synthesis and characterization data of intermediates ACEN, ACEO and I-IV



6-methyl-3-(prop-2-yn-1-yl)-1,2,3-oxathiazin-4(3H)-one 2,2-dioxide (ACEN): propargyl bromide (1.1 equiv.) was added to a stirring solution of potassium acesulfame (1.0 equiv.) in *N,N*-dimethylformamide and stirred under nitrogen atmosphere for 24 h at 80 °C. Upon completion the mixture was poured on ice and extracted with dichloromethane (3 × 20 mL). The organic layers were reunited, dried over sodium sulphate and concentrated *in vacuo*. Purification through column chromatography on silica gel (petroleum ether:ethyl acetate, 5:1) afforded the title compound as a yellow oil (51% yield). ¹H NMR (400 MHz, CDCl₃): δ 2.18 (d, *J* = 1.0 Hz, 3H, CH₃), 2.31 (t, *J* = 2.5 Hz, 1H, CH=), 4.53 (d, *J* = 2.5 Hz, 2H, CH₂), 5.79 (d, *J* = 1.0 Hz, 1H, CH≡). ¹³C NMR (101, MHz, CDCl₃): δ 19.8 (CH₃), 31.6 (CH₂), 73.6 (CH≡), 75.9 (C≡), 104.3 (CH=C), 159.3 (CO), 162.2 (COSO₂).

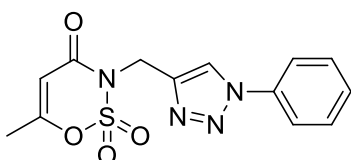


6-methyl-4-(prop-2-yn-1-yloxy)-1,2,3-oxathiazine 2,2-dioxide (ACEO): propargyl bromide (1.1 equiv.) was added to a stirring solution of potassium acesulfame (1.0 equiv.) in *N,N*-dimethylformamide and stirred under nitrogen atmosphere for 24 h at room temperature. Once the completion the mixture was poured on ice and extracted with dichloromethane (3 × 20 mL). The organic layers were reunited, dried over sodium sulphate and concentrated *in vacuo*. Purification through column chromatography on silica gel (petroleum ether:ethyl acetate, 4:1) gave the title compound as a yellow oil (40% yield). For the characterization data see reference [113].

NaNO₂ (1.2 equiv.) was slowly added to a solution of the proper aniline (1.0 equiv.) in a 4M HCl aqueous solution at 0 °C. After 30 min NaN₃ (1.5 equiv.) was added portion-wise and the resulting mixture stirred at room temperature for 1 h. The mixture was then extracted with ethyl acetate (3 × 20 mL). The organic layers were reunited, dried over sodium sulphate and concentrated *in vacuo*. The residual crude product was used directly without further purification. For the characterization data of azides I-VI, see references [140,146,147].

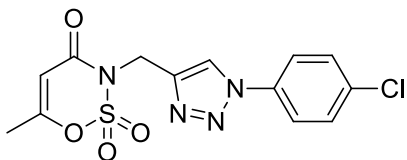
General synthesis and characterization data of derivatives 53-60

Propargylated acesulfame (1.0 equiv) and the proper benzyl azide (1.05 equiv) were added to a stirring solution of CuI (0.02 equiv), DIPEA (0.04 equiv) and CH₃COOH (0.04 equiv) in dichloromethane and stirred at room temperature until the alkyne disappeared. The mixture was extracted with dichloromethane (3 × 20 mL) and H₂O. The organics were reunited, dried over sodium sulphate and concentrated *in vacuo*. Purification through column chromatography on silica gel, using the proper solvents, gave compounds 53-60 as white solids.

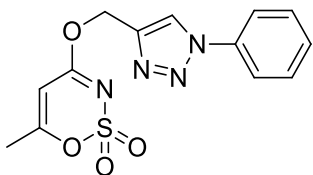


6-methyl-3-((1-phenyl-1H-1,2,3-triazol-4-yl)methyl)-1,2,3-oxathiazin-4(3H)-one 2,2-dioxide (53): white solid, 140-142 °C; ¹H NMR (400 MHz, CDCl₃): δ 2.15 (s, 3H, CH₃), 5.15 (s, 2H, CH₂), 5.78 (s, 1H, CH=), 7.34-7.38 (m, 1H, Ar), 7.44 (t, *J* = 7.7 Hz, 2H, Ar), 7.64 (d, *J*

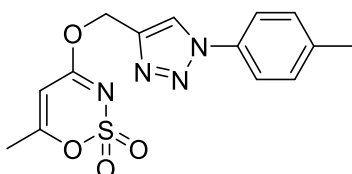
= 7.7 Hz, 2H, Ar), 7.97 (s, 1H, Ar-triazole). ^{13}C NMR (101 MHz, CDCl_3): δ 19.8 (CH_3), 37.8 (CH_2), 104.4 ($\text{CH}=\text{, acesulfame}$), 120.7 (2 x Ar), 121.8 (Ar-triazole), 128.9 (Ar), 129.8 (2 x Ar), 136.9 (Ar-triazole), 142.5 (Ar), 160.0 ($\text{C}=\text{O}$), 162.3 (COSO_2).



3-((1-(4-chlorophenyl)-1H-1,2,3-triazol-4-yl)methyl)-6-methyl-1,2,3-oxathiazin-4(3H)-one 2,2-dioxide (54): white solid, 154-158 °C; ^1H NMR (400 MHz, CDCl_3): δ 2.16 (d, $J = 0.9$ Hz, 3H, CH_3), 5.14 (s, 2H, CH_2), 5.78 (d, $J = 0.9$ Hz, 1H, $\text{CH}=\text{, Ar}$), 7.40-7.43 (m, 2H, Ar), 7.58-7.62 (m, 2H, Ar), 7.96 (s, 1H, Ar-triazole). ^{13}C NMR (101 MHz, CDCl_3): δ 19.8 (CH_3), 37.8 (CH_2), 104.4 ($\text{CH}=\text{, acesulfame}$), 121.7 (Ar-triazole), 121.8 (2 x Ar), 129.9 (2 x Ar), 134.7 (Ar), 135.3 (Ar-triazole), 142.7 (Ar), 160.0 ($\text{C}=\text{O}$), 162.3 (COSO_2).

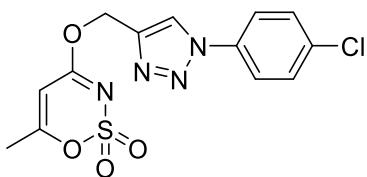


6-methyl-4-((1-phenyl-1H-1,2,3-triazol-4-yl)methoxy)-1,2,3-oxathiazine 2,2-dioxide (55): white solid, 118-120 °C; ^1H NMR (400 MHz, CDCl_3): δ 2.24 (d, $J = 0.7$ Hz, 3H, CH_3), 5.60 (s, 2H, CH_2), 5.81 (d, $J = 0.9$ Hz, 1H, $\text{CH}=\text{, Ar}$), 7.46-7.50 (m, 1H, Ar), 7.54-7.57 (m, 2H, Ar), 7.73-7.76 (m, 2H, Ar), 8.21 (s, 1H, Ar-triazole). ^{13}C NMR (101 MHz, CDCl_3): δ 20.6 (CH_3), 61.3 (CH_2), 95.5 ($\text{CH}=\text{, acesulfame}$), 120.7 (2 x Ar), 123.3 (Ar-triazole), 129.2 (Ar), 129.9 (2 x Ar), 136.7 (Ar), 141.3 (Ar-triazole), 168.9 ($\text{C}=\text{N}$), 169.2 (COSO_2).

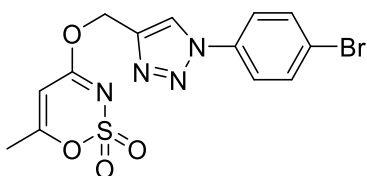


6-methyl-4-((1-(p-tolyl)-1H-1,2,3-triazol-4-yl)methoxy)-1,2,3-oxathiazine 2,2-dioxide (56): white solid, 144-148 °C; ^1H NMR (400 MHz, CDCl_3): δ 2.24 (d, $J = 0.7$ Hz, 3H, CH_3), 2.44 (s, 3H, CH_3), 5.59 (s, 2H, CH_2), 5.81 (d, $J = 0.7$ Hz, 1H, $\text{CH}=\text{, Ar}$), 7.34 (d, $J = 8.0$ Hz, 2H, Ar), 7.61 (d, $J = 8.4$ Hz, 2H, Ar), 8.16 (s, 1H, Ar-triazole). ^{13}C NMR (101 MHz, CDCl_3): δ 20.6 (CH_3),

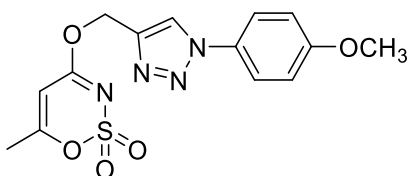
21.3 (CH₃), 61.4 (CH₂), 95.5 (CH=, acesulfame), 120.6 (2 x Ar), 123.2 (Ar-triazole), 130.4 (2 x Ar), 134.4 (Ar), 139.4 (Ar), 141.1 (Ar-triazole), 168.9 (C=N), 169.2 (COSO₂).



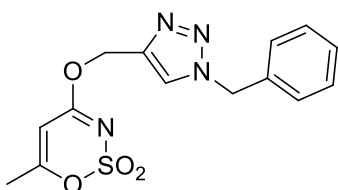
4-((1-(4-chlorophenyl)-1H-1,2,3-triazol-4-yl)methoxy)-6-methyl-1,2,3-oxathiazine 2,2-dioxide (57): white solid, 152-154 °C; ¹H NMR (400 MHz, CDCl₃): δ 2.24 (s, 3H, CH₃), 5.60 (s, 2H, CH₂), 5.81 (s, 1H, CH=), 7.52-7.55 (m, 2H, Ar), 7.69-7.72 (m, 2H, Ar), 8.20 (s, 1H, Ar-triazole). ¹³C NMR (101 MHz, CDCl₃): δ 20.6 (CH₃), 61.2 (CH₂), 95.5 (CH=, acesulfame), 121.9 (2 x Ar), 123.2 (Ar-triazole), 130.1 (2 x Ar), 135.0 (2 x Ar), 135.1 (Ar), 141.5 (Ar-triazole), 168.8 (C=N), 169.3 (COSO₂).



4-((1-(4-bromophenyl)-1H-1,2,3-triazol-4-yl)methoxy)-6-methyl-1,2,3-oxathiazine 2,2-dioxide (58): white solid, 168-170 °C; ¹H NMR (400 MHz, CDCl₃): δ 2.25 (d, *J* = 0.7 Hz, 3H, CH₃), 5.60 (s, 2H, CH₂), 5.81 (d, *J* = 0.8 Hz, 1H, CH=), 7.63-7.66 (m, 2H, Ar), 7.68-7.71 (m, 2H, Ar), 8.20 (s, 1H, Ar-triazole). ¹³C NMR (101 MHz, CDCl₃): δ 20.6 (CH₃), 61.2 (CH₂), 95.5 (CH=, acesulfame), 122.1 (2 x Ar), 123.0 (Ar-triazole), 123.2 (Ar), 133.1 (2 x Ar), 135.6 (Ar), 141.6 (Ar-triazole), 168.8 (C=N), 169.3 (COSO₂).

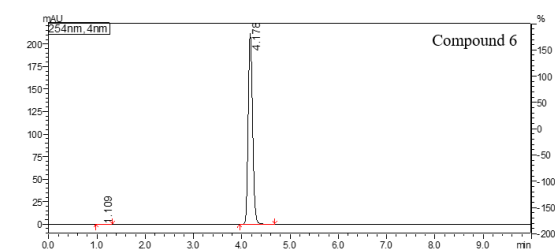
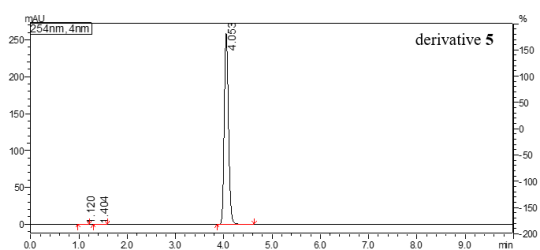
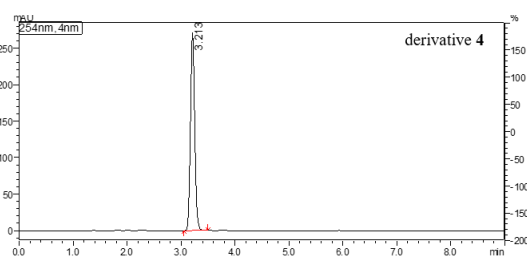
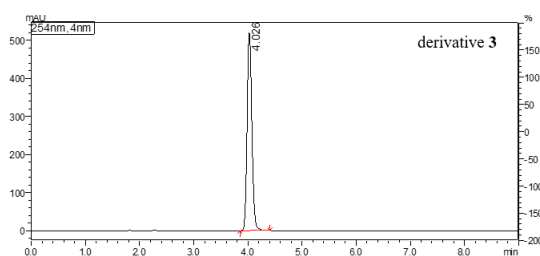
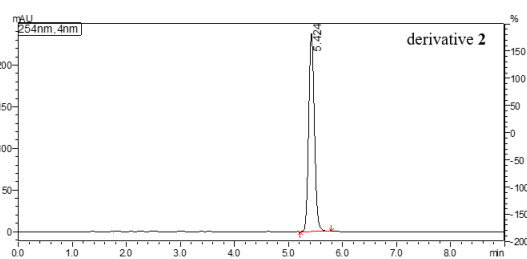
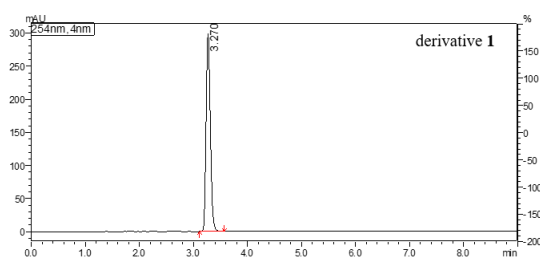


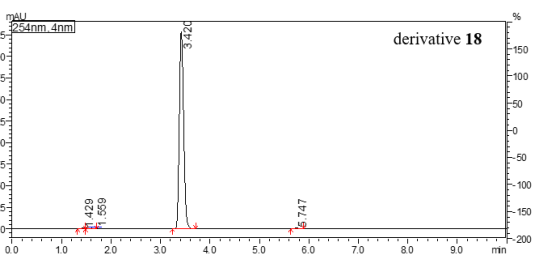
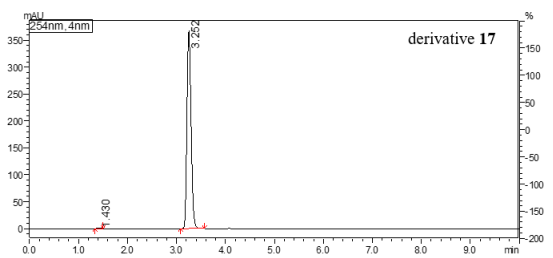
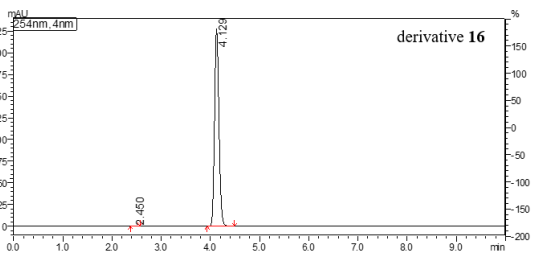
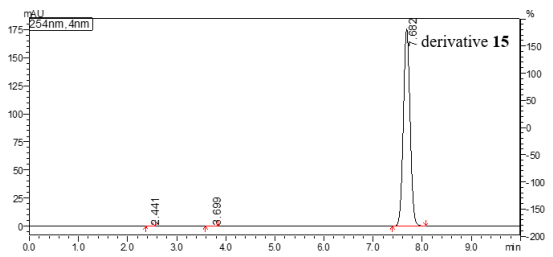
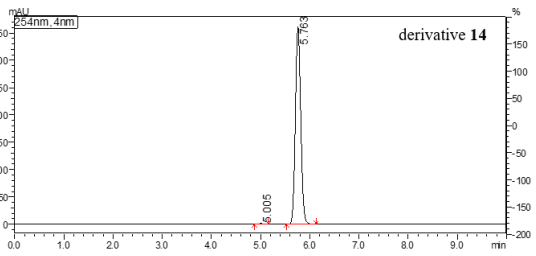
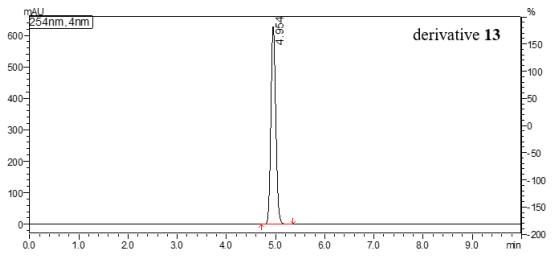
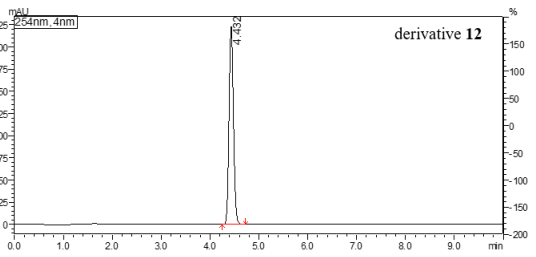
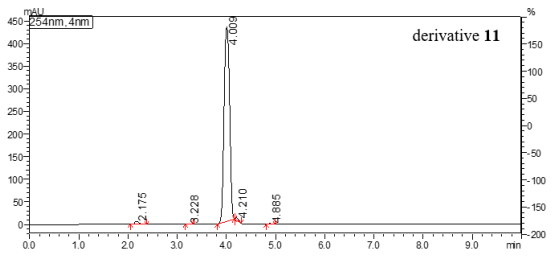
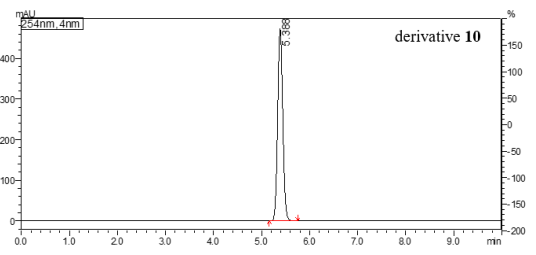
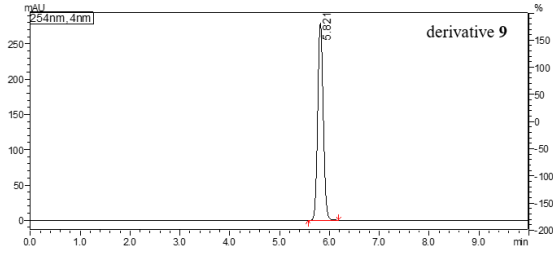
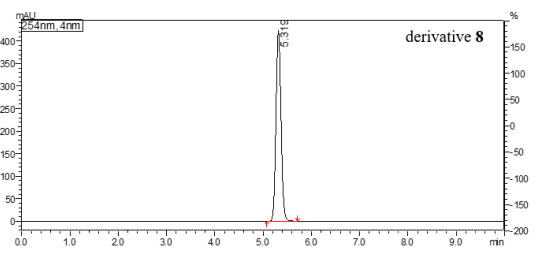
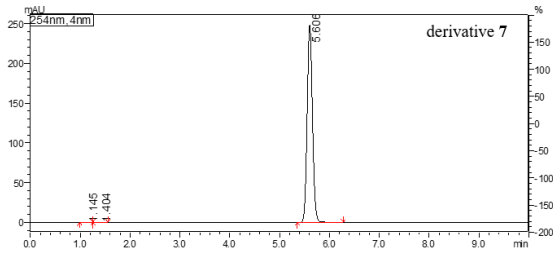
4-((1-(4-methoxyphenyl)-1H-1,2,3-triazol-4-yl)methoxy)-6-methyl-1,2,3-oxathiazine 2,2-dioxide (59): white solid, 138-140 °C; ¹H NMR (400 MHz, CDCl₃): δ 2.24 (d, *J* = 0.7 Hz, 3H, OCH₃), 3.88 (s, 3H, CH₃), 5.85 (s, 2H, CH₂), 5.81 (d, *J* = 0.8 Hz, 1H, CH=), 7.03-7.05 (m, 2H, Ar), 7.62-7.65 (m, 2H, Ar), 8.12 (s, 1H, Ar-triazole). ¹³C NMR (101, MHz, CDCl₃): δ 20.6 (CH₃), 55.7 (CH₃), 61.4 (CH₂), 95.5 (CH=, acesulfame), 114.9 (2 x Ar), 122.4 (2 x Ar), 123.4 (Ar-triazole), 130.1 (Ar), 135.6 (Ar), 141.0 (Ar-triazole), 168.9 (C=N), 169.2 (COSO₂).

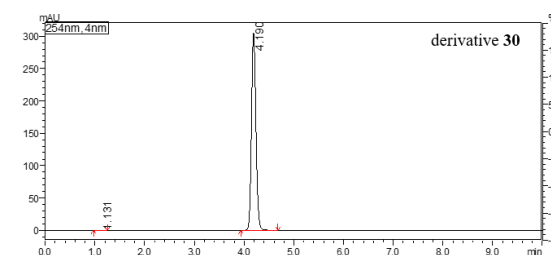
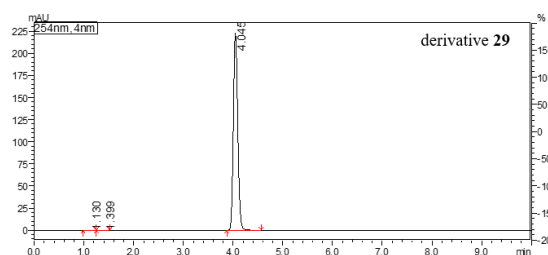
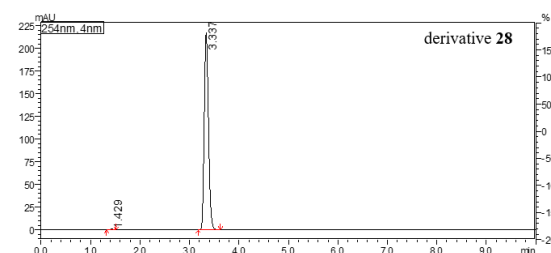
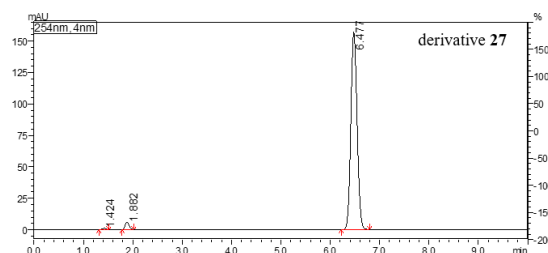
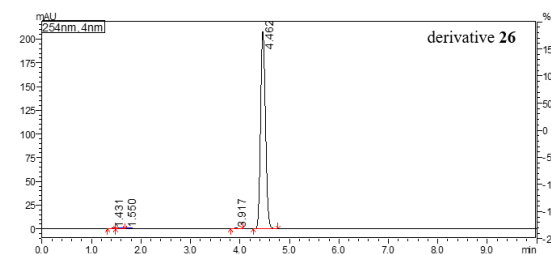
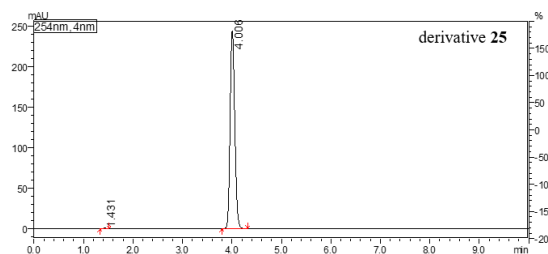
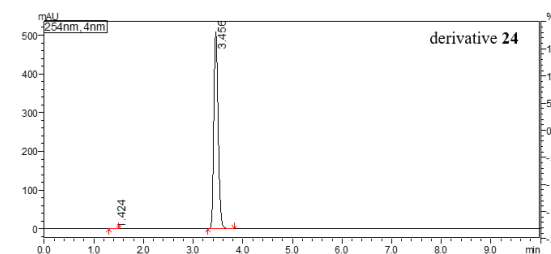
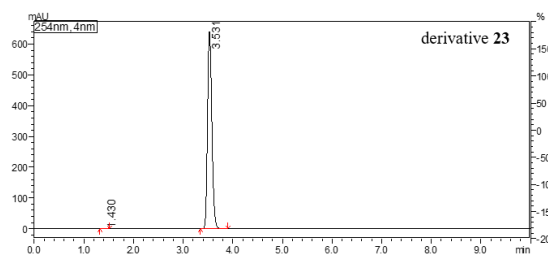
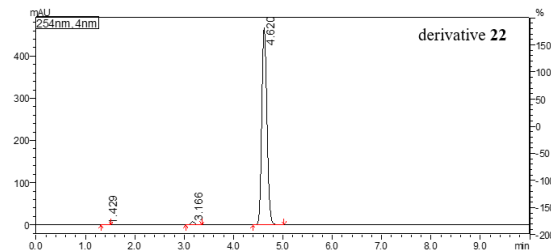
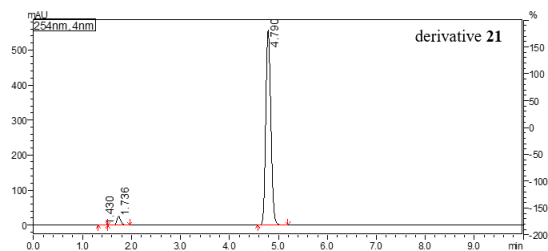
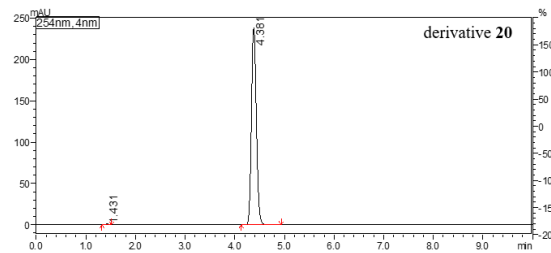
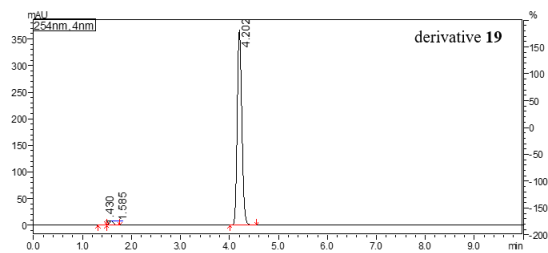


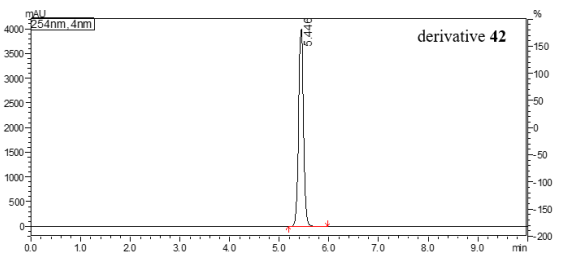
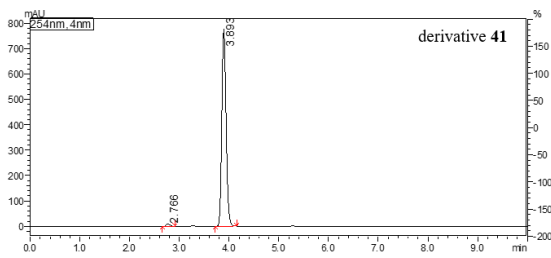
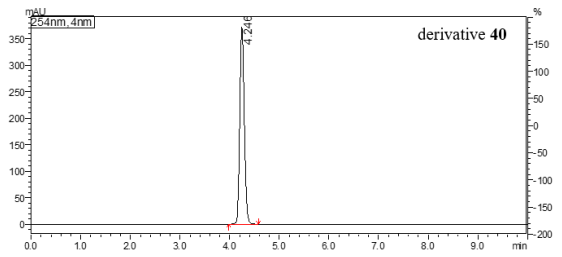
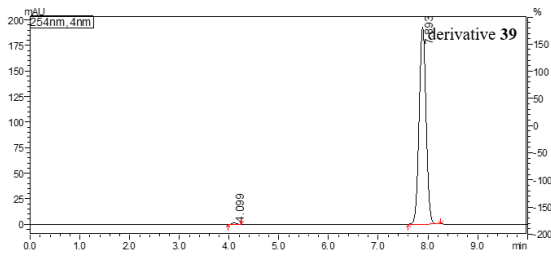
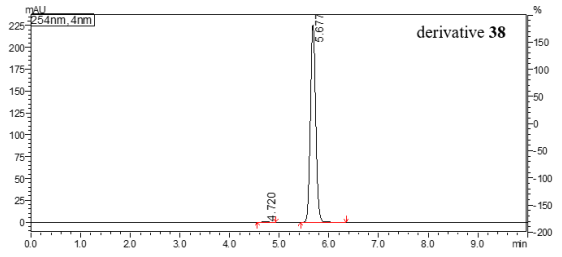
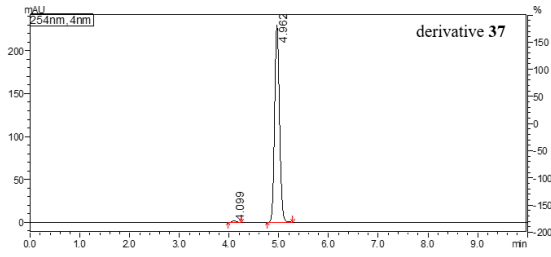
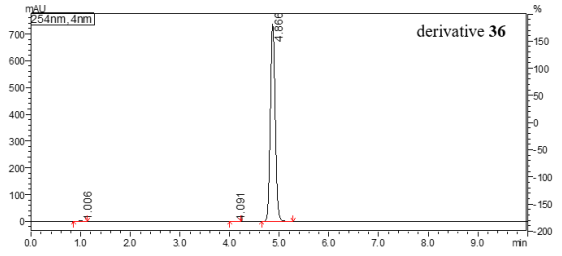
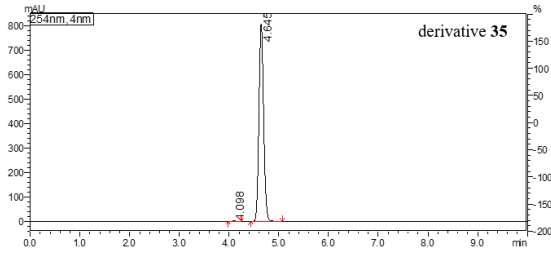
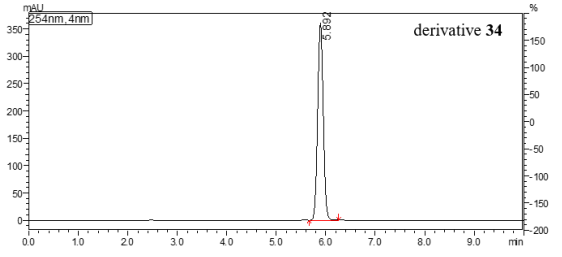
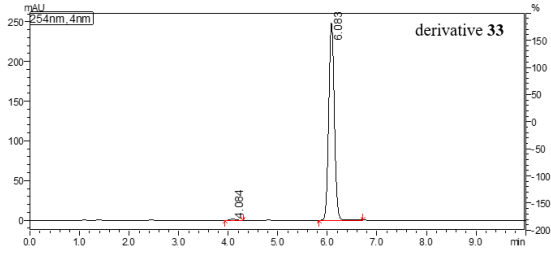
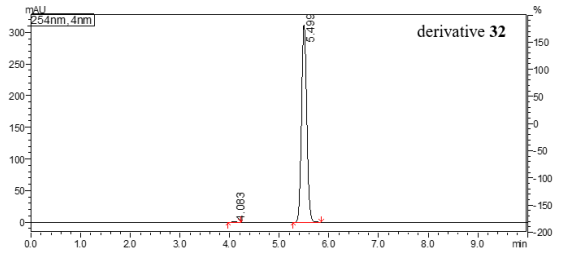
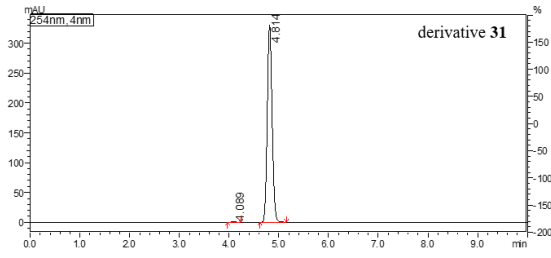
4-((1-benzyl-1H-1,2,3-triazol-4-yl)methoxy)-6-methyl-1,2,3-oxathiazine 2,2-dioxide (60): white solid, 142-144 °C; ^1H NMR (400 MHz, CDCl_3): δ 2.13 (s, 3H, CH_3), 5.39 (s, 2H, CH_2), 5.47 (s, 2H, CH_2), 5.68 (s, 1H, $\text{CH}=\text{}$), 7.21-7.23 (m, 2H, Ar), 7.28-7.35 (m, 3H, Ar), 7.59 (s, 1H, Ar-triazole). ^{13}C NMR (101 MHz, CDCl_3): δ 20.6 (CH_3), 54.4 (CH_3), 61.4 (CH_2), 95.5 ($\text{CH}=\text{}$, acesulfame), 124.8 (Ar-triazole), 128.2 (2 x Ar), 129.0 (Ar), 129.3 (2 x Ar), 134.1 (Ar), 140.9 (Ar-triazole), 168.8 ($\text{C}=\text{N}$), 169.1 (COSO_2).

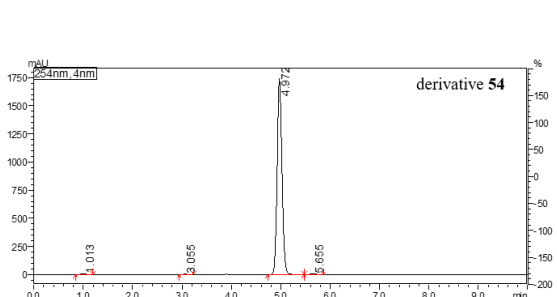
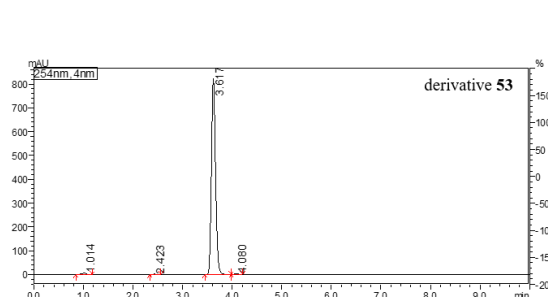
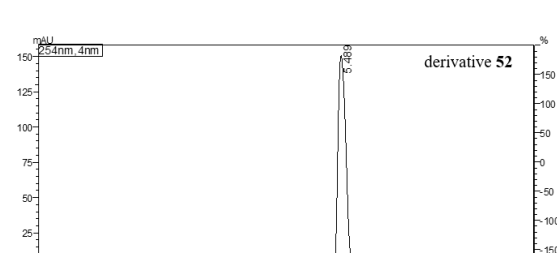
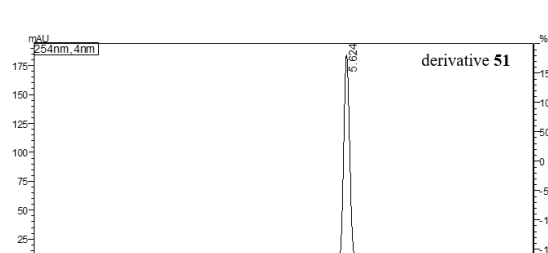
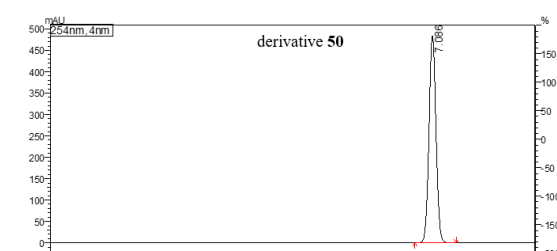
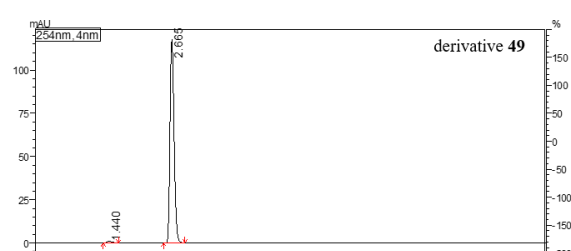
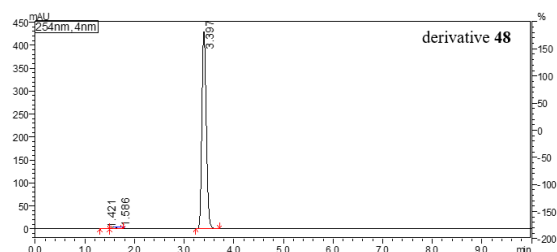
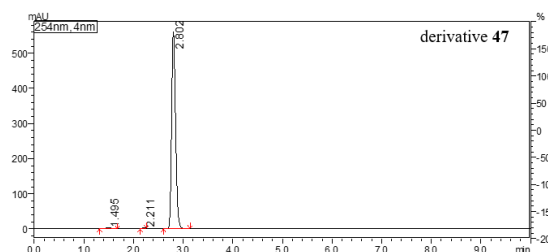
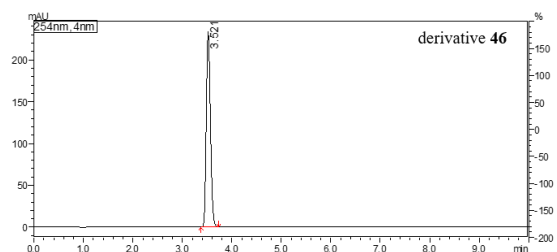
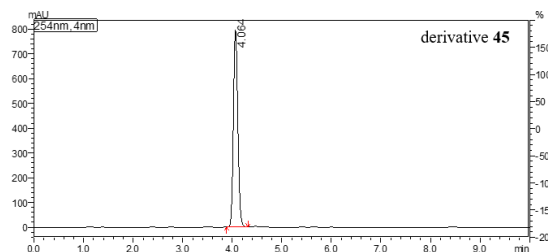
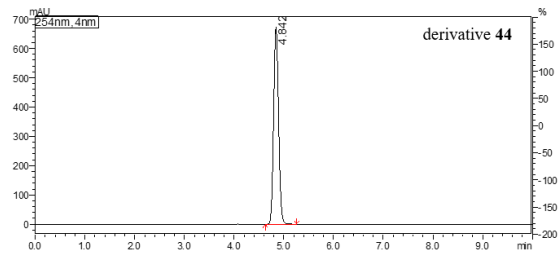
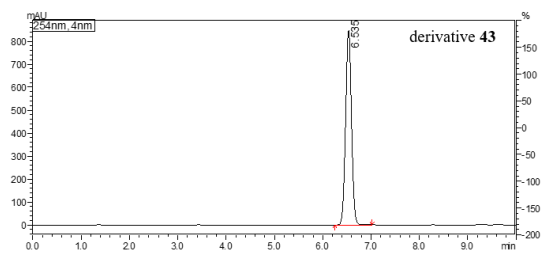
HPLC analysis of the derivatives 1-60

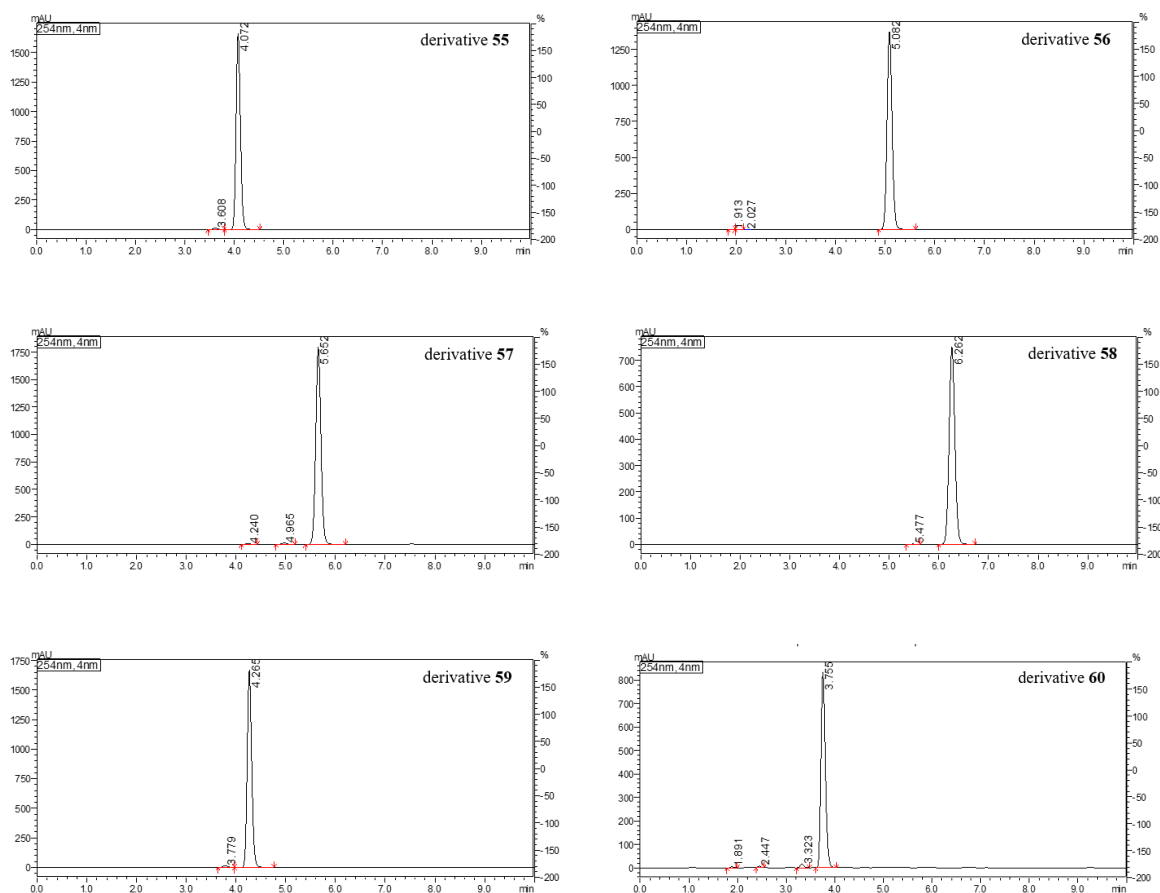












3.5.4. Enzyme inhibition assays

An Applied Photophysics stopped-flow instrument was used for assaying the CA-catalysed CO₂ hydration activity [126]. Phenol red, at a concentration of 0.2 mM, was used as an indicator, working at the maximum absorbance of 557 nm with 20 mM HEPES, 4-(2-hydroxyethyl)-1-piperazineethanesulfonic acid, (pH 7.5 for α -CAs) as buffer and 20 mM Na₂SO₄ (for maintaining constant the ionic strength, but without inhibiting the enzyme). The initial rates of the CA-catalysed CO₂ hydration reaction were followed for a period of 10–100 s. The CO₂ concentrations ranged from 1.7 to 17 mM for the determination of the kinetic parameters and inhibition constants. For each inhibitor, at least six traces of the initial 5–10% of the reaction were used for determining the initial velocity. The uncatalyzed rates were determined in the same manner and subtracted from the total observed ones. Stock solutions of each inhibitor (0.1 mM) were prepared in distilled–deionized water and dilutions up to 0.01 mM were done thereafter with distilled–deionized water. Inhibitor and enzyme solutions were preincubated together for 15 min at room temperature prior to assay to allow for the formation of the E–I complex. The inhibition constants were obtained by nonlinear least-squares methods using the Cheng-Prusoff equation and represent the mean from at least three different determinations.

Errors were in the range of $\pm 5\text{--}10\%$ of the reported K_I values. Human CA isoforms were recombinant enzymes obtained in-house as reported earlier [148–150]. The enzyme concentrations in the assay system were as follows: hCA I, 13.2 nM; hCA II, 8.4 nM; hCA IX, 7.9 nM; hCA XII, 15.2 nM.

3.5.5. Molecular modelling studies

The crystal structures of hCA IX (pdb 5DVX) [80] and hCA XII (pdb 1JCZ) [22] were prepared using the Protein Preparation Wizard tool implemented in Maestro - Schrödinger suite, assigning bond orders, adding hydrogens, deleting water molecules, and optimizing H-bonding networks [151]. Energy minimization protocol with a root mean square deviation (RMSD) value of 0.30 was applied using an Optimized Potentials for Liquid Simulation (OPLS3e) force field. 3D ligand structures were prepared by Maestro [151a] and evaluated for their ionization states at $\text{pH } 7.4 \pm 0.5$ with Epik [151b]. OPLS3e force field in Macromodel [151e] was used for energy minimization for a maximum number of 2500 conjugate gradient iteration and setting a convergence criterion of $0.05 \text{ kcal mol}^{-1} \text{ \AA}^{-1}$. The centroid of the zinc-bound water molecule was selected as grid center and Glide used with default settings. Ligands were docked with the standard precision mode (SP) of Glide [151e] and the best 5 poses of each molecule retained as output. The best pose for each compound to CA IX and CA XII, evaluated in terms of anchorage, hydrogen bond interactions and hydrophobic contacts, was submitted to a MD simulation using Desmond and the OPL3e force field. Specifically, the system was solvated in an orthorhombic box using TIP4PEW water molecules, extended 15 Å away from any protein atom. It was neutralized adding chlorine and sodium ions. The simulation protocol included a starting relaxation step followed by a final production phase of 100 ns. In particular, the relaxation step comprised the following: (a) a stage of 100 ps at 10 K retaining the harmonic restraints on the solute heavy atoms (force constant of $50.0 \text{ kcal mol}^{-1} \text{ \AA}^{-2}$) using the NPT ensemble with Brownian dynamics; (b) a stage of 12 ps at 10 K with harmonic restraints on the solute heavy atoms (force constant of $50.0 \text{ kcal mol}^{-1} \text{ \AA}^{-2}$), using the NVT ensemble and Berendsen thermostat; (c) a stage of 12 ps at 10 K and 1 atm, retaining the harmonic restraints and using the NPT ensemble and Berendsen thermostat and barostat; (f) a stage of 12 ps at 300 K and 1 atm, retaining the harmonic restraints and using the NPT ensemble and Berendsen thermostat and barostat; (g) a final 24 ps stage at 300 K and 1 atm without harmonic restraints, using the NPT Berendsen thermostat and barostat. The final production phase of MD was run using a canonical NPT Berendsen ensemble at temperature 300 K. During the MD simulation,

a time step of 2 fs was used while constraining the bond lengths of hydrogen atoms with the M-SHAKE algorithm. The atomic coordinates of the system were saved every 100 ps along the MD trajectory. Protein and ligand RMSD values, ligand torsions evolution and occupancy of intermolecular hydrogen bonds and hydrophobic contacts were computed along the production phase of the MD simulation with the Simulation Interaction Diagram tools implemented in Maestro.

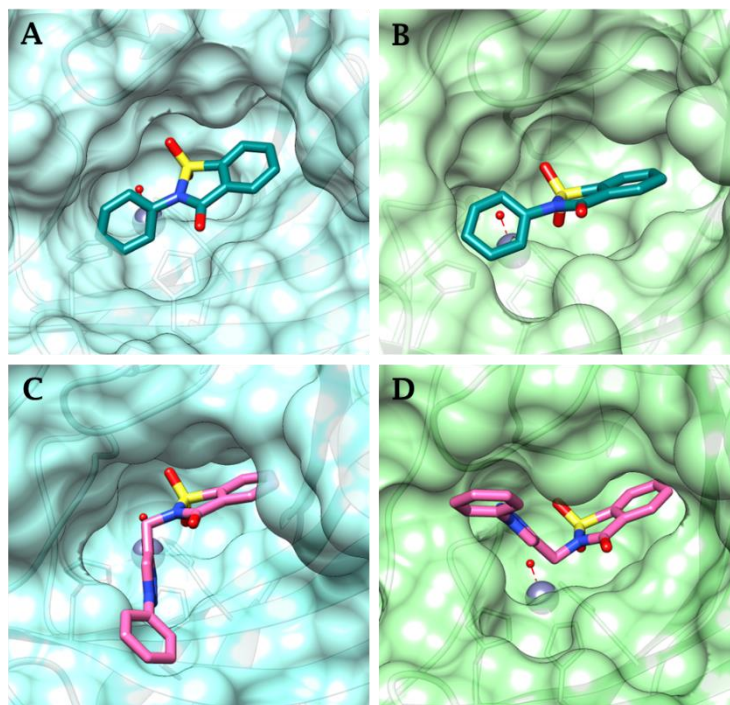


Figure 3.7. Replacement of the benzyl moiety of **2** and **46** with a phenyl ring (to give **29** and **41**, respectively) within the ligand/target complexes found by docking. Compound **29** in the active site of A) hCA IX and B) hCA XII; compound **41** in the active site of C) CA IX and D) CA XII. All graphical representations point out significant protein-ligand clashes.

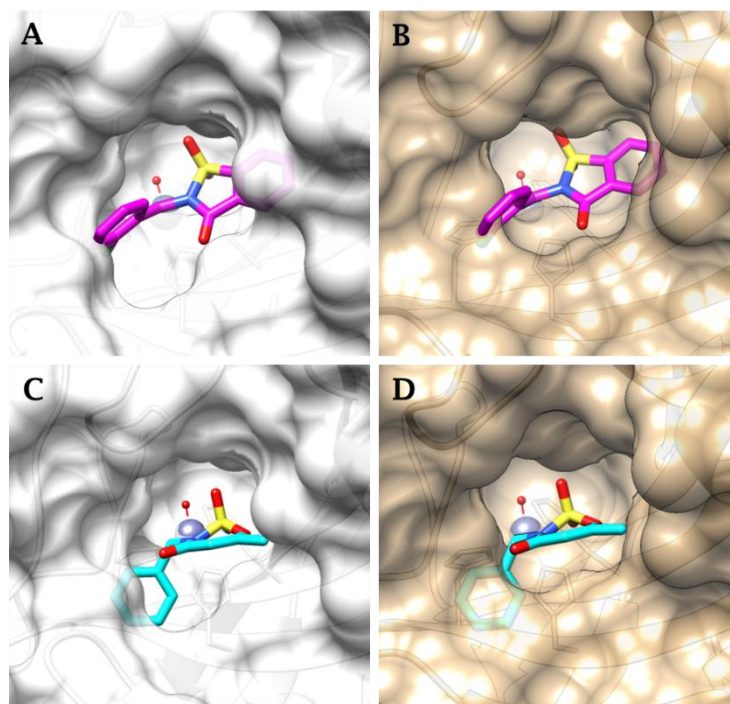


Figure 3.8. Representation of the hCA IX predicted binding mode of **2** and **51** in hCA I and hCA II after isoforms overlay. (A) **2**-CA I, (B) **2**-CA II, (C) **51**-CA I and (D) **51**-CA II. All graphical representations point out significant protein-ligand clashes.

Section II.

Development of novel ligands targeting human tyrosinase and tyrosinase related protein 1

1. Introduction to human tyrosinase and tyrosinase related proteins

1.1. Structural features and functions of human tyrosinase and tyrosinase related proteins

Tyrosinases (TYRs) are type three copper proteins [152], largely spread in the biosphere [153,154], possessing monooxygenase and oxidase activity that leads to the formation of *o*-quinone derivatives from the corresponding monophenols and *o*-diphenols derivatives (**Figure 1.1**) [155].

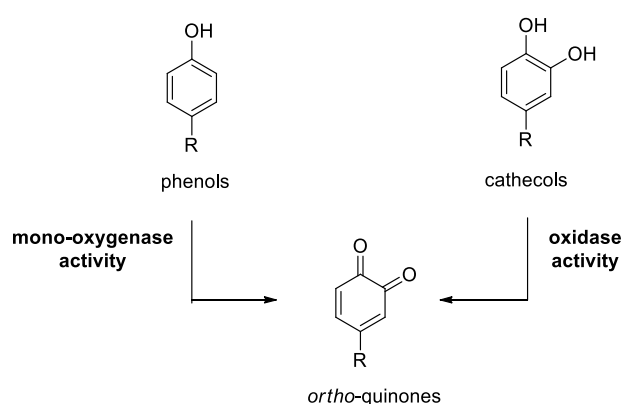


Figure 1.1. Schematic representation of the monooxygenase and oxidase activity of TYR.

These enzymes are involved in the rate limiting step of melanin biosynthesis, called melanogenesis, catalysing the conversion of L-tyrosine (monophenol) to L-dopaquinone [156], the precursor of melanin pigments [157].

In humans, melanogenesis is related to the function of the TYR protein family that includes Tyrosinase related proteins 1 and 2 (TYRP1 and TYRP2), as well as human TYR (hTYR) [153]. These melanogenic proteins are located in melanosomes, organelles contained in the melanocytes found in the skin and hair [152,156]. These proteins are codified by three separate genes, 40% of amino acid sequence identity and 70% of amino acid homology [158].

They are single transmembrane proteins containing metals in their active sites and sharing the same structural features: *N*-terminal signal peptide, a single transmembrane α -helix, a small flexible C-terminal cytoplasmatic domain and a large intra melanosome domain. The transmembrane domain is responsible for the anchoring to the melanosome membrane. The intra-melanosome domain contains a cysteine (Cys)-rich subdomain (unique in mammalian TYR and TYRPs) and a catalytic TYR subdomain containing the binuclear metal binding sites

[152,159] bound to O₂, forming a peroxide bridge [160,161], and coordinating two sets of conserved histidine residues (**Figure 1.2**) [152,159].

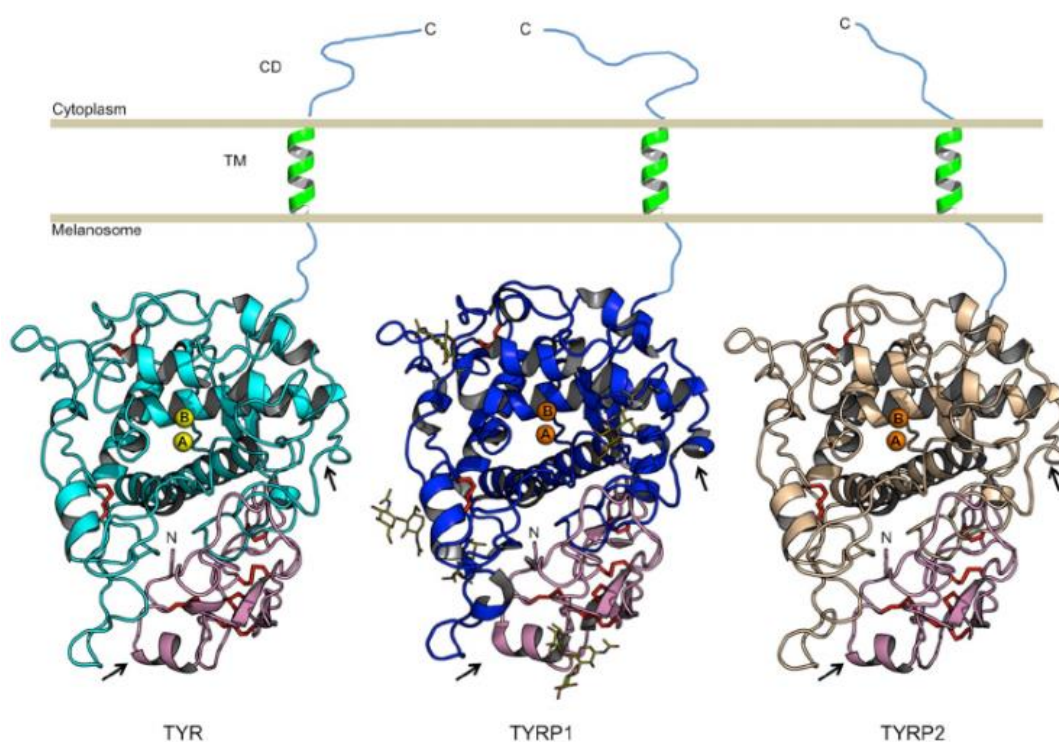


Figure 1.2. Structures of the human melogenic proteins hTYR, TYRP1 and TYRP2 based on the crystal structural model of TYRP1. Copper and zinc ions (A and B) are represented as yellow and orange spheres[152].

The type of ions differs among these three proteins as it consists of copper atoms for hTYR [162] and zinc atoms for TYRPs [163,164]. This is the reason of the distinct catalytic functions of the three enzymes in melanogenesis [153]: the redox properties of the two copper ions, usually identified as CuA and CuB in hTYR [165], contribute to its oxidation reactions (monooxygenase and oxidase activity), whereas the redox lacking properties of the two zinc ions in TYRP2 contributes to its isomerization reaction [159]. TYRP2 gene is related to the dopachrome tautomerase, a protein involved in the conversion of dopachrome to 5,6-dihydroxyindole-2-carboxylic acid (DHICA) [166,167]. It has been suggested that TYRP1 could be involved in melanogenesis oxidation reactions, although recent studies [153,168] and the identification of its crystal structure have refuted this hypothesis [169]. Thus, its mechanism of action remains under debate, although the consequences of mutations in TYRP1 gene suggest a significant role of this protein in melanogenesis [153,169,170]. Interestingly, TYRP1 binds typical hTYR substrates through a quite similar ligand coordination pattern, suggesting a certain conservation of the active site [152].

hTYR is the only melogenic protein possessing an established mechanism of action *in vivo* [171] and though Lai *et al* succeeded in the recombinant production of the intra-melanosome hTYR [172], its crystal structure has not been identified [152]. Its unique catalytic mechanism has been briefly described, focusing on its monooxygenase and oxidase activity, which leads to formation of L-DOPA [156], disproving the common claim that L-DOPA is synthesised as an oxidative intermediate of L-Tyrosine [156]. hTYR is found in four diverse oxidation states that determine its monooxygenase and oxidase activities, that arise from the binding of O₂ to the Cu atoms located in the active site [153]:

- the *met*-state: represents the resting and stable form of hTYR that enables the oxidation of catechols to *o*-quinone; the hydroxyl ion is bound to two Cu(II) ions;
- the *deoxy*-state: enables the binding of O₂ restoring the active form; the copper ions are reduced to Cu(I);
- the *oxy*-state: represents the active form of hTYR, that enables the oxidation of monophenols through its monooxygenase activity and catechols to *o*-quinone through its oxidase activity; O₂ is held in place in a peroxy form by two Cu(II) ions
- the *deact*-state: the copper atoms are reduced to Cu⁰, represents the inactive form of hTYR; the copper atoms are reduced to Cu⁰ (**Figure 1.3**) [154,156,173,174].

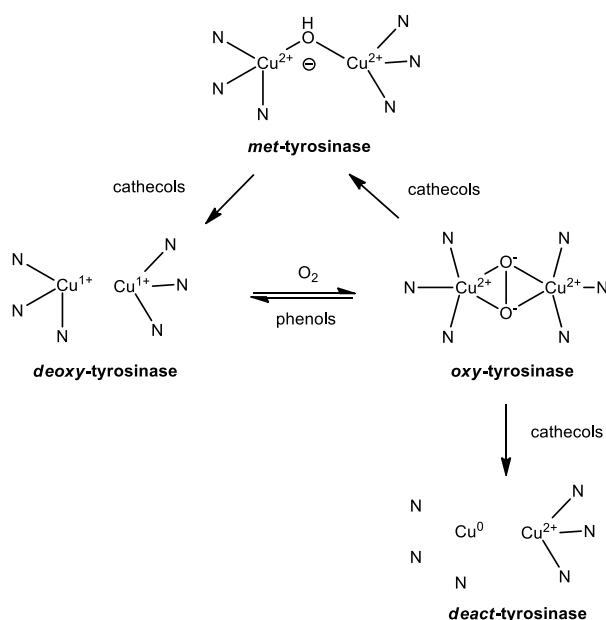


Figure 1.3. Schematic representation of the four oxidation states of hTYR.

The oxidation of L-Tyrosine to L-dopaquinone, i.e. the first step of melanogenesis, occurs in the *oxy*-state of hTYR. It has been suggested that the oxygen of the phenol binds to Cu followed

by the electrophilic monooxygenation of the ring. This leads to a structure that, binding both the Cu(I), undergoes a homolytic dissociation yielding the L-dopaquinone and the *deoxy*-form of the enzyme that, after binding the O₂, restores the *oxy*-form (**Figure 1.4**).

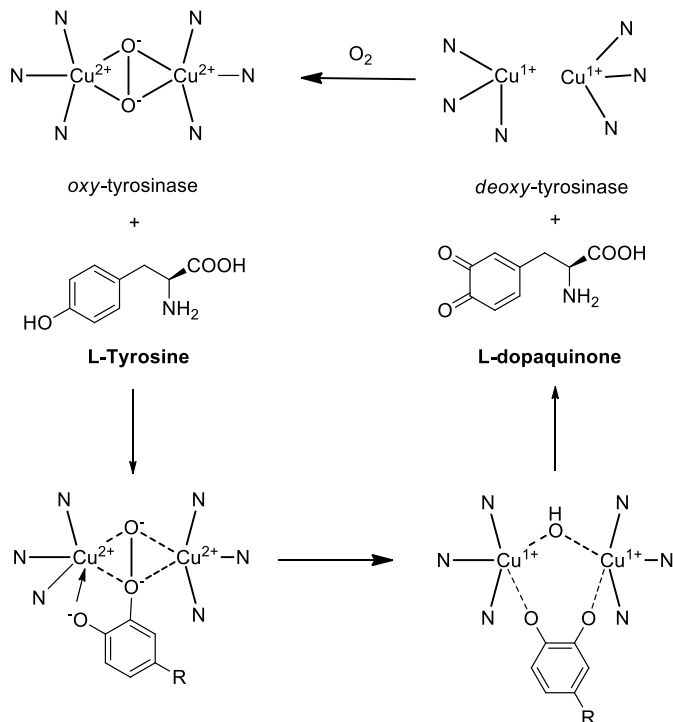


Figure 1.4. Schematic representation of the mechanism of hTYR monooxygenase activity.

The described mechanism represents the monooxygenase activity through which hTYR catalyses the conversion of L-Tyrosine to L-dopaquinone [156]. It does not include the formation of L-DOPA intermediate, as sometimes reported in literature [175,176], that occurs through a non-enzymatic mechanism [156]: proceeding in the synthesis of melanin pigments, as soon as L-dopaquinone is produced, it undergoes the intramolecular addition of the amino group yielding cyclodopa (leucodopachrome). The redox exchange among cyclodopa and dopaquinone leads to the formation of dopachrome and L-DOPA. Thus, L-DOPA is formed in this step during melanogenesis (**Figure 1.5**). It is then oxidized to L-dopaquinone by the *oxy*-form (oxidase activity) or the *met*-form of the enzyme [156].

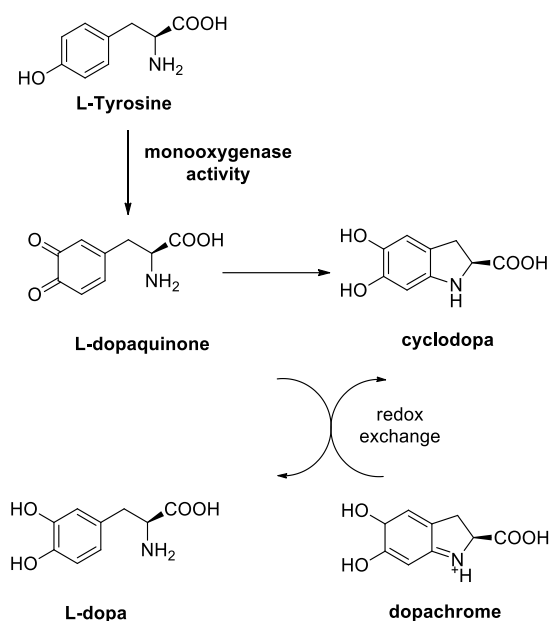


Figure 1.5. Synthesis of L-DOPA through a non-catalytic reaction during melanogenesis.

Dopachrome, formed in the same step of L-DOPA, is then converted to either 5,6-dihydroxyindole (DHI) through a spontaneous decarboxylation [159] or to DHICA in presence of TYRP1 [157]. The ratio DHI/DHICA depends on the amount of TYRP2 in melanosomes [177] and since DHI seems to be more unstable than DHICA, it has been suggested that this enzyme could protect melanocytes from the cytotoxic effects of DHI [159].

These dihydroxy indoles are oxidized to form eumelanin, the black-brown pigment. However, if cysteine is present in the environment, dopaquinone rapidly reacts to cysteine to give 5-Scysteinyl-dopas that are oxidized to give benzothiazine intermediates producing pheomelanin, the yellow-red soluble pigments [157,178].

The amount of melanin formed is proportional to dopaquinone production, that is in turn proportional to hTYR and TYRPs activities [178]. Thus, this enzymatic and not enzymatic process, results in the synthesis of eumelanin and pheomelanin [157,178].

1.2. Tyrosinase and tyrosinase related protein 1: activators and inhibitors

Since hTYR and TYRPs are involved in the rate-limiting step of melanogenesis, they have been recognized as therapeutic targets for the treatment of pigmentation related disorders [179,180]. The melanogenesis activators, being skin pigmentation agents, could be used for the treatment of vitiligo, characterised by the loss of the melanocyte functions. Some of these stimulators target the catalytic activity of hTYR, others can induce an increase and activation of TYRPs.

Most of these agents are still in the early phase of drug discovery, as they are often related to poor activity and severe side effects [181].

Always because of their role as skin pigmentation agents, melanogenesis inhibitors, are used for the treatment of melasma, actinic and senile lentigines and disorders related to an over production of melanin synthesis [180]. Even if a huge number of inhibitors have been identified to date[182], only a small amount of them have reached clinical application because of [183,184]:

- their safety concerns [183,185];
- their poor activity on hTYR [183–186].

Many hTYR inhibitors such as hydroquinone, arbutin, kojic acid, azelaic acid, L-ascorbic acid and ellagic acid, used for topical applications in clinical practice, are associated with several problems. Hydroquinone is mutagenic to mammalian cells and can cause several side effects. Arbutin, a prodrug of hydroquinone, is unstable and it can release hydroquinone, catabolized to benzene metabolites known to possess potential toxicity for bone marrow. Kojic acid is supposed to be carcinogenic and unstable during storage. L-Ascorbic acid is sensitive to heat thus it degrades easily and ellagic acid is insoluble and poorly bioavailable (**Figure 1.6**) [187].

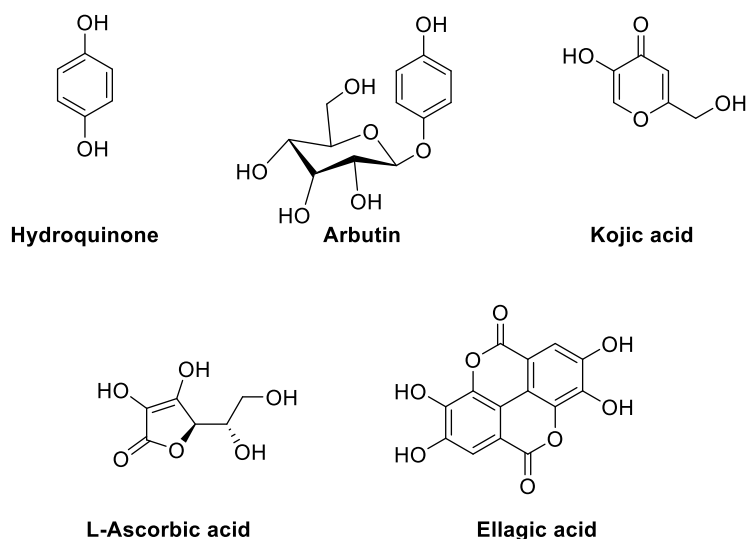


Figure 1.6. Structures of TYR inhibitors.

Since the recombinant production of intra-melanosome hTYR has become available only in recent years[172], the *in vitro* assays to determine the IC₅₀ of potential hTYR inhibitors have usually been performed on mushroom Tyrosinase from *Agaricus bisporus* (mTYR) [182,188,189], even though there are several differences among mTYR and hTYR, which share only 23% of their identity [190]. Thus, a lot of mTYR inhibitors become around 10-fold less

potent or even inactive against hTYR [186]. Precisely, Kojic acid exhibits 10-fold higher activity on mTYR (IC_{50} of 53.70 μM) than hTYR (IC_{50} of 571.17 μM) and other inhibitors such as phenylthiourea, L-mimosine, cinnamic acid, benzoic acid, and aesculetin exhibits significant differences in the inhibitory activities on mTYR and hTYR. Aesculetin, another potent mTYR inhibitor, possesses no detectable inhibitory activity against hTYR [190]. Compounds possessing a promising inhibitory activity on hTYR are found to be the β and γ derivatives of thujaplicins possessing the IC_{50} values of 8.98 and 1.15 μM , respectively [191]; linderanolide B and subamolide A able to reduce the 50% of hTYR activity at a dose of 1 μM after 48 h of treatment [192] and 4-butyl resorcinol possessing an IC_{50} of 21 μM and a complete inhibition at 100 μM and its derivatives (**Figure 1.7**) [185]. Particularly, topical products containing 4-butyl resorcinol resulted efficacious on age spots, melasma and facial hyperpigmentation [193].

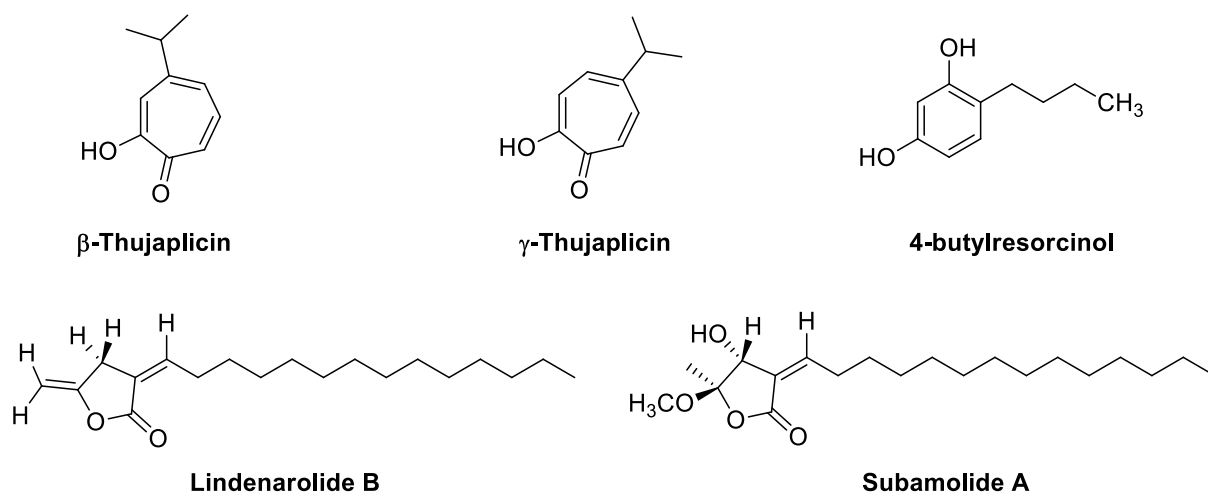
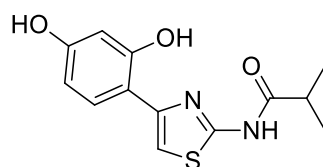


Figure 1.7. Structures of hTYR inhibitors.

Recently, Mann *et al* conducted a screening of 50 thousand compounds on a recombinant hTYR, constructed from human embryonic kidney (HEK-293) [194], identifying thiazolyl resorcinol as the most promising class (resorcinol is a redundant scaffold in TYR inhibitors, e.g., 4-butylresorcinol) [183,195]. After a lead optimization, aimed at increasing the physical-chemical properties, they identified Thiamidol™ or isobutylamido thiazolyl resorcinol (IC_{50} = 1.1 μM , K_i = 0.25 μM for competitive inhibition) as the most potent derivative (**Figure 1.8**) [183,184].



Thiamidol™

Figure 1.8. Structure of the novel hit compound Thiamidol™.

The modelling studies of Thiamidol™ revealed that one of the hydroxyl group of the aromatic ring interacts with the di-copper centre, the second one forms hydrogen bonds with the side chain of S380, that seems to be involved in the monophenolase activity of hTYR. The thiazolyl ring is held in place through hydrophobic interactions in the nonpolar pocket, formed by the side chains of amino acids (**Figure 1.9**) [183]. Similar docking results have also been obtained using the X-ray structure of TYRP1 [183], suggesting a certain homology among these proteins (in TYRP1 Ser380 corresponds to Ser394) [164].

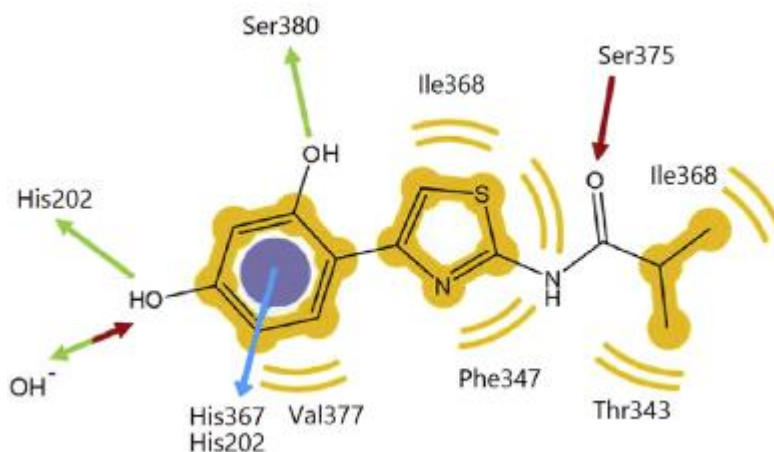


Figure 1.9. Schematic representation of the interactions of Thiamidol in the hTYR active site [183].

Conversely, Thiamidol™ has resulted to be a poor inhibitor of mTYR ($IC_{50} = 108 \mu M$), as also proved by the docking studies, since S380 is not present in the TYR from lower species and the amino acids of the nonpolar pocket differ from each other [169,183].

Interestingly, when comparing the inhibitory profile of some traditional hTYR inhibitors as hydroquinone, arbutin and kojic acid to Thiamidol™ on hTYR, the same authors found that the novel identified compound is the most potent [179,183]. Thus, it has been selected for clinical studies, where it has demonstrated a strong pigmentation reduction [183] and it has been approved as a topic product for the treatment of hyperpigmentation related disorders [196,197].

1.3. Tyrosinase and tyrosinase related protein 1: melanoma specific antigens

Being involved in the rate limiting step of melanogenesis, hTYR is an established target for the treatment of melanin disorders [179,180]. Although the research of novel compounds is challenging for the reasons previously reported, recent findings suggest that the large scale of hTYR [172] and the solved structure of TYRP1 [164], could support the design and development of novel inhibitors.

hTYR has been emerging as a potential target for melanoma, because its expression increases during tumorigenesis [177] and its localization is almost confined to the surface of melanoma lesions [198,199], as proved by several studies based on immunostaining [200] and fluorescent imaging [201] of the enzyme in the tumour site and on the tissue specific conversion of prodrugs[202]. Moreover, primary and secondary metastatic melanoma lesions are related to changes in tyrosinase-mediated pigmentation [203,204]. Several studies also reported successful results in treating melanoma based on the activation of a T-lymphocyte-mediated response, using hTYR as tumour associated antigen [205,206].

Similarly to hTYR, TYRP1 is also largely detectable and stable in melanoma progression [170,207,208]: TA99, a murine IgG2a anti-TYRP1 mAb, succeeded in localizing TYRP1 in subcutaneous melanoma xenograft [209] and *in vivo* [210] and a recent study succeeded in evaluating the efficient antitumor activity of a recombinant IgG1 mAb targeting TYRP1 [211]. Particularly noteworthy are the results obtained from the Protein Atlas that suggest that the expression of hTYR and TYRP1 is confined to the surface of melanoma lesions being poorly detectable in a limited set of healthy tissues, such as skin, eyes and hairs (**Figure 1.10**, antigens stained in black).

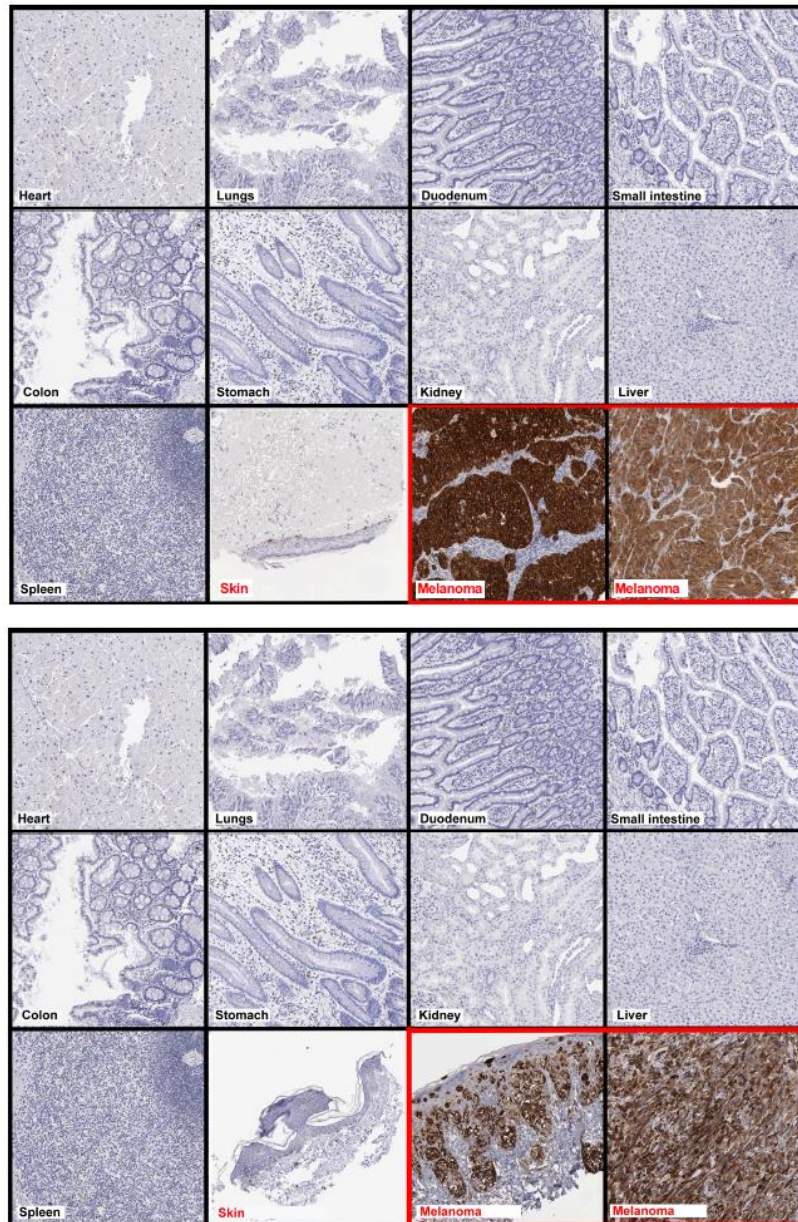


Figure 1.10. Selective expression of hTYR (on the top) and TYRP1 (on the bottom) in melanoma (red outline).

1.4. The aim of the project

hTYR and TYRP1 can be considered melanoma specific antigens due their limited confinement and upregulation on the surface of melanoma lesions [177] and as such are ideal targets for tumour targeting applications. Particularly, small molecule ligands could serve as suitable vehicles of chemical moieties for the selective targeting of hTYR and TYRP1, not affecting other tissues [212,213]: their use in drug delivery has been emerging over the last decades for their deeper tissue penetration, faster pharmacokinetics, and lower immunogenicity [214,215]. Thus, the aim of this project was to develop and evaluated small molecule ligands specific to hTYR and TYRP1 and suitable for the tumour targeting applications. The project was conduct using previously collected data elaborated from the DNA encoded chemical libraries (DELs, particularly GB-DEL [216]), novel technologies aimed at the *de novo* lead compounds identification [217], and the multivalent approach applied to an alkyne derivative of Thiamidol™, a novel identified inhibitor of hTYR, approved for the treatment of irregular pigmentation of the skin [183,184,196,197].

*These two Chapters are part of the paper “Discovery, affinity maturation and multimerization of small molecule ligands against human Tyrosinase and Tyrosinase related protein 1” by M. Catalano, G. Bassi, G. **Rotondi**, L. Khettabi, M. Dichiara, P. Murer, J. Scheuermann, M. Soler-Lopez, D. Neri. Submitted and accepted by RSC Medicinal Chemistry.*

2. Development of small molecule ligands from DNA encoded chemical libraries

DELs technologies are large collections of organic molecules covalently linked to DNA fragments, serving as carrier for the ligand identity [218], aimed at *in vitro* screening and selection of novel ligands [219]. They can be distinguished as:

- single strand (SS) libraries: compounds are attached to one DNA fragment, sometimes through a central scaffold;
- dual strand (DS) libraries: compounds are coupled to the extremity of the complementary strands of the DNA [219].

The development of DNA encoded chemical libraries usually occurs using split and pool synthesis [217]. Briefly, the first step consists in the coupling of a first set of building blocks (BBs) to short encoding DNA fragments. The so-obtained products are thus pooled and split in vessels, the second BBs added and reacted (one BB for each vessel) and then encoded to the proper DNA tag. These synthetic and encoding steps are repeated based on the number of BBs used in the library. Then, the last encoding step is pooled to yield the DNA encoded chemical library [214]. These technologies involve the creation of libraries containing millions of compounds [217] that are usually screened through affinity capture procedures on a target protein of interest, immobilized on a solid support [220,221]: molecules able to interact with the target protein are retained on the solid support, amplified through PCR of DNA barcodes and then decoded using high-throughput DNA sequencing [219]. The data from the library selections can be represented and evaluated on suitable plots, called fingerprints, that report the relative enrichment for each member able to interact with the protein of interest. Then, the best identified combinations are synthesized and validated as suitable ligands for the protein of interest (hit validation) to confirm the results of the libraries [219].

2.1. Design of small molecule ligands from DNA encoded chemical libraries

The data for the design of these novel compounds were elaborated from GB-DEL, recently developed in the Research Group of Prof. Dario Neri [216].

Briefly, this library was constructed using a derivative of the glutamic acid bearing two sets of building blocks (BBs), amines and carboxylic acids or alkynes, respectively. It contains 366'600 encoded compounds [216].

The description and the results of the selections, obtained after screening the GB-DEL on biotinylated hTYR and TYRP1, previously coated on streptavidin magnetic beads, are shown on the bi- and tri-dimensional plots (**Figure 2.1** and **Figure 2.2**).

Figure 2.1 and **Figure 2.2** indicate that the best combination is the combination of **A26** and **B389** because these BBs, besides describing persistent and continuous lines, form an enriched cross or combination, that in DEL technology stands for the preferential binding to the proteins. Interestingly, these BBs were simultaneously selected on both hTYR and TYRP1, revealing comparable and reproducible fingerprints and suggesting a certain conservation of their active sites.

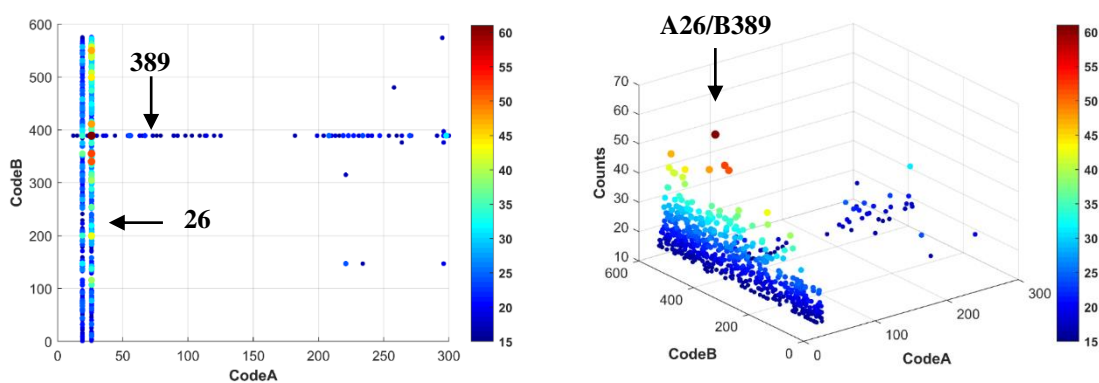


Figure 2.1. Results from the selections performed on hTYR.

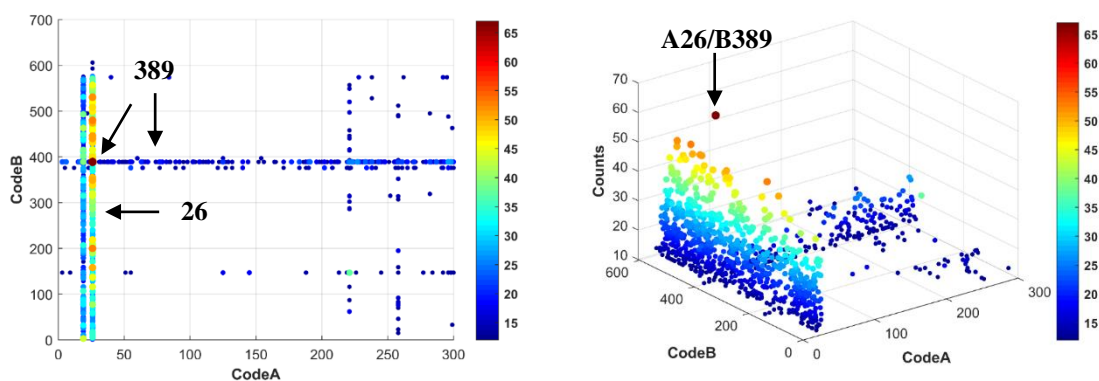


Figure 2.2. Results from the selections on TYRP1.

Thus, based on these promising results, the glutamic acid based-compounds bearing the **A26** and **B389** (**Figure 2.3**), in the L and D isomeric form, were synthesized and then evaluated as inhibitors and binders of hTYR and TYRP1, using pure preparations of these proteins. The inhibitory profile was determined through the determination of the IC_{50} that requires the compound as it is avoiding structural modifications and the binding profile through the

determination of the dissociation constant (K_d) that could require modifications on the scaffold, suitable for the insertion of fluorescein moieties (e.g., fluorescein isothiocyanate, fluorescein-5-maleimide) [222,223].

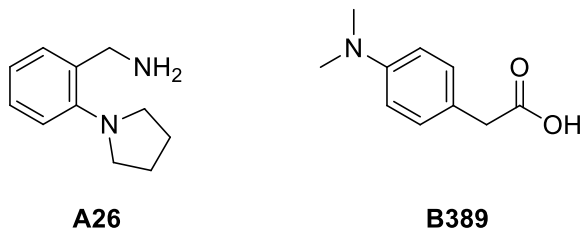
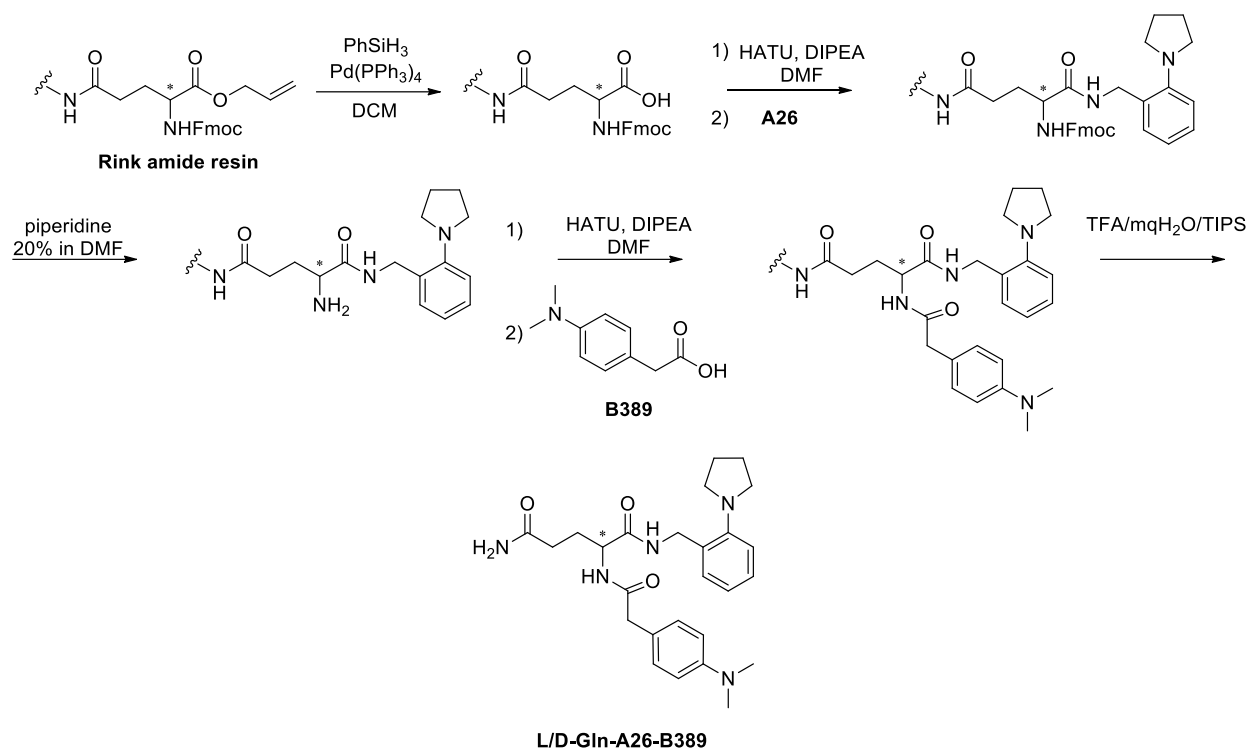


Figure 2.3. Chemical structures of **A26** and **B389** identified after selections on hTYR and TYRP1.

2.2. Chemistry

Compounds **L/D-Gln-A26-B389** were synthesized employing standard solid phase synthesis (SPPS) starting from the commercially available Rink amide resin.

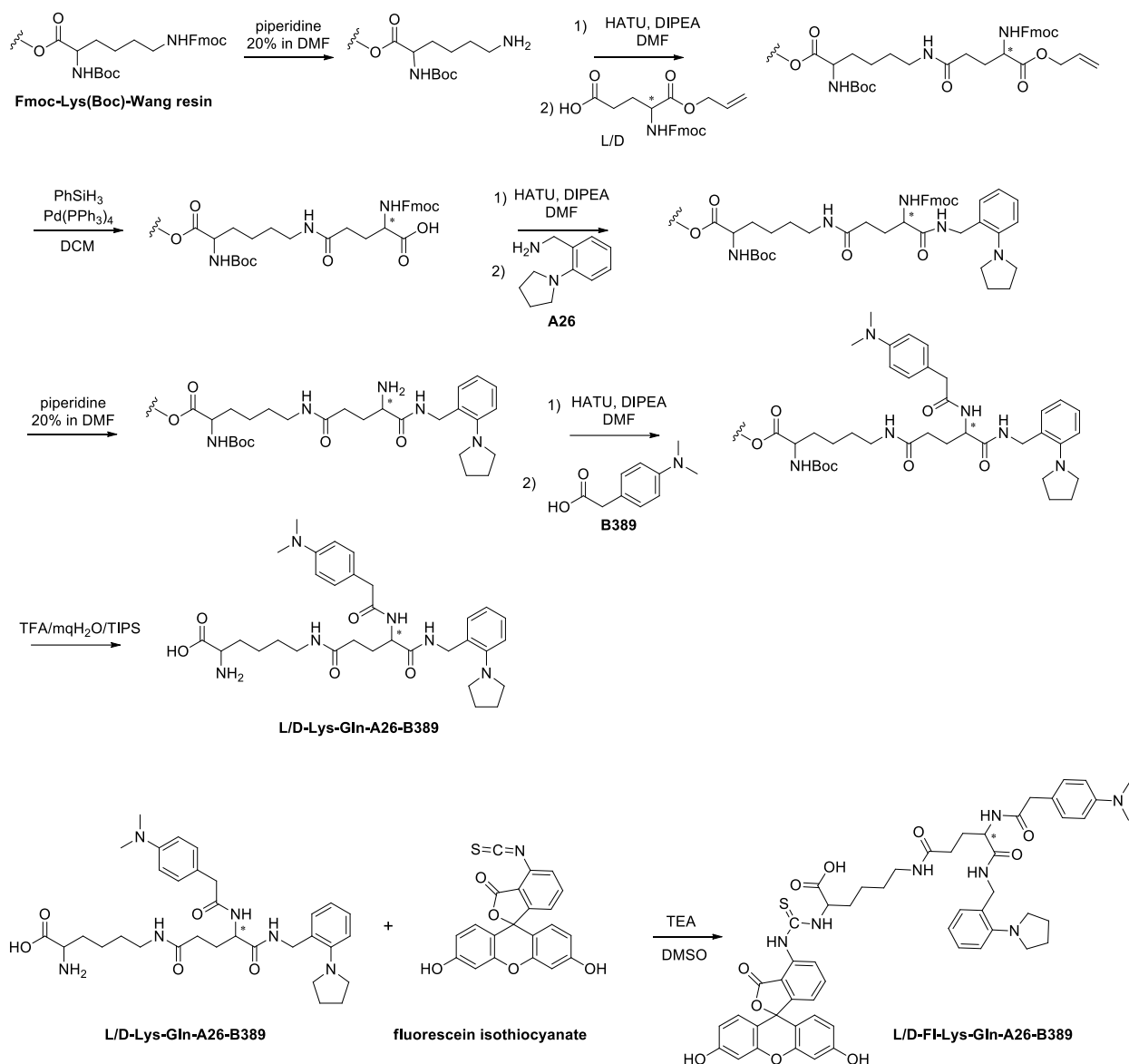
Briefly, the Rink amide resin was coupled to Fmoc-L-glutamic acid 5-allyl ester or Fmoc-D-glutamic acid 5-allyl ester in presence of HATU and DIPEA. After the *O*-allyl deprotection using Pd(PPh₃)₄ and PhSiH₃, the resin was coupled to the proper amine, **A26**, and, after the Fmoc deprotection, to the 2-(4-(dimethylamino)phenyl)acetic, **B389** (**Scheme 2.1**). The resulting compounds were cleaved from the resin and purified over a reverse phase high-performance liquid chromatography (RP-HPLC).



Scheme 2.1. Synthetic procedure of compounds **L/D-Gln-A26-B389**.

Compounds **L/D-Lys-Gln-A26-B389** were synthesized employing standard solid phase synthesis (SPPS), starting from the commercially available FmocLys(Boc)-Wang resin that was selected since it contains the suitable amino group for the coupling to the fluorescein isothiocyanate (FITC).

Briefly, FmocLys(Boc)-Wang resin, pre-treated with a 20% solution of piperidine in DMF to remove the Fmoc group, was coupled to Fmoc-L-glutamic acid 5-allyl ester or Fmoc-D-glutamic acid 5-allyl ester in presence of HATU and DIPEA. After the *O*-allyl deprotection using Pd(PPh₃)₄ and PhSiH₃, the resin was coupled to the (2-(pyrrolidin-1-yl)phenyl)methanamine (**A26**) and, after the Fmoc deprotection, to the 2-(4-(dimethylamino)phenyl)acetic (**B389**) (**Scheme 2.2**). The resulting compounds were cleaved from the resin and purified over RP-HPLC. Then, they were labelled incorporating fluorescein isothiocyanate (FITC).



Scheme 2.2. Synthetic procedure of compounds **L/D-FI-Lys-Gln-A26-B389**.

2.3. Biological evaluation

Compounds **L/D-Gln-A26-B389** were evaluated as hTYR inhibitors. The enzymatic assay used was based on the L-DOPA oxidase activity of hTYR that involves the rapid capture and derivatization of the unstable L-dopaquinone with the suitable substrate. Precisely, in case of partial or total inhibition of the protein, L-DOPA, used as hTYR substrate, leads to the formation of L-dopaquinone that, as it reacts to MBTH which is used as colorimetric compound, yields a UV-visible product measurable at 490-510 nm. The intensity of the colour is a measure of the inhibitory profile of the tested compounds [224,225]. The results, given as a function of time and optical density (OD) are reported in **Figure 2.4**.

The fluorescein compounds **L/D-FI-Lys-Gln-A26-B389** were evaluated as TYRP1 binders in FP. The compounds, at a fixed concentration, were titrated and incubated using increasing concentration of TYRP1 to determine their binding profile, through the increase of the fluorescence anisotropy (FA). The results, given as functions of protein concentration and FA, are reported in **Figure 2.5**.

2.4. Results and discussion

Based on the results obtained from GB-DEL [216], **L/D-Gln-A26-B389** and **L/D-FI-Lys-Gln-A26-B389** were synthesized in SPPS and their inhibitory activity and binding profile was determined through the enzymatic assay and FP.

Briefly, to determine if a compound is able to inhibit the enzyme at an established concentration, its line slope, reported on a suitable plot, should be evaluated: a flat line indicates that no activity is detectable and that the tested compound is inhibiting the enzyme at that concentration.

Thus, the typical plot that an inhibitor should possess is reported: the line slopes of the 4-butyl-resorcinol [185] at a concentration of 100 μM and 500 μM result flats because the enzyme is completely inhibited. However, with a decrease in concentration the slope increases, showing the biggest slope in the absence of 4-butyl-resorcinol. Subsequently, plotting the slopes to the 4-butyl-resorcinol concentration, the IC_{50} was determined (**Figure 2.3**).

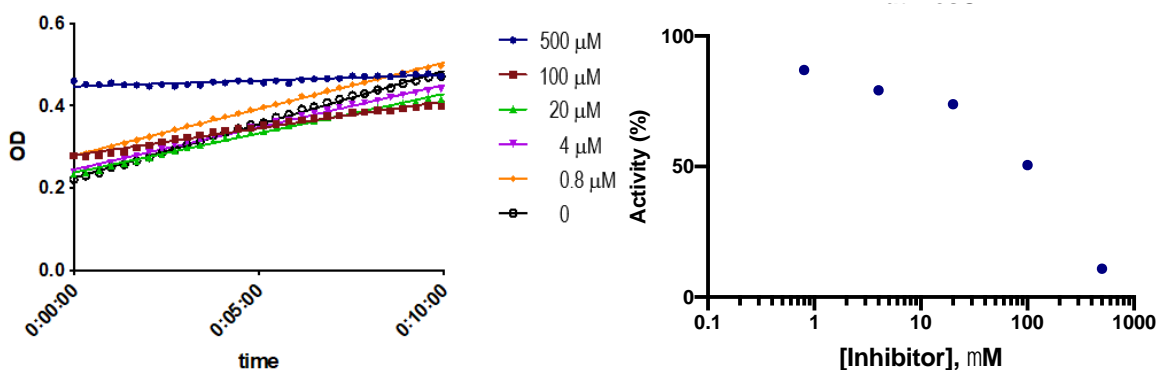


Figure 2.3. Inhibitory profile and IC_{50} of 4-butyl-resorcinol on hTYR.

Before determining the IC_{50} value of a compound, it is good practice to discriminate inhibitors in the single digit μM IC_{50} range. Thus, the first enzymatic assay was performed using the concentration of 50 μM at $\text{pH} = 6.8$ for the hit compounds. As shown by the plots (**Figure 2.4**),

none of the tested compounds possessed a significant inhibition in these conditions, apart from the 4-butyl-resorcinol, used as positive control.

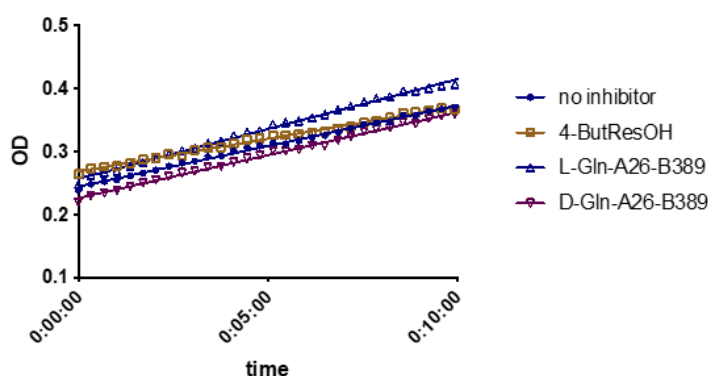


Figure 2.4. Inhibitory profile of compounds L/D-Gln-A26-B389 on hTYR.

The typical plot of a binder should produce a sigmoidal curve that starts from the baseline for free ligand and rises to a plateau (highest polarisation value) that corresponds to the complete binding of the ligand to the protein [222]. As shown in the FP plot (**Figure 2.5**), the selected compounds do not saturate TYRP1, even at higher concentration of the protein, suggesting that they could result in a micromolar binding.

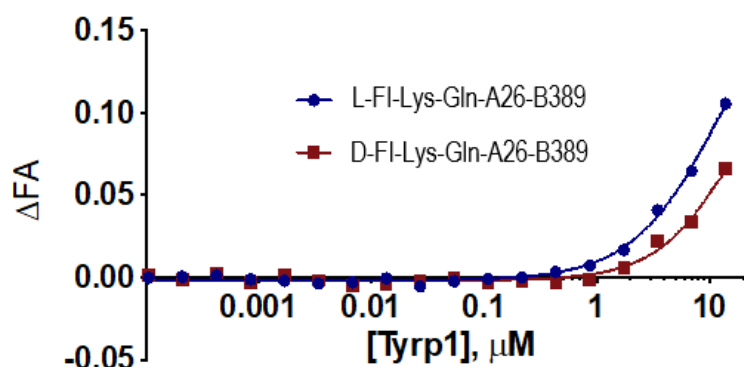


Figure 2.5. Binding profile of the L/D-FI-Lys-Gln-A26-B389 on TYRP1.

2.5. Conclusions

The synthesis and *in vitro* biological assays of the novel hit compounds from the GB-DEL, were reported. Surprisingly, regardless of the promising and consistent results obtained from the selections performed on hTYR and TYRP1 [216], these compounds were proven to act in the micromolar range.

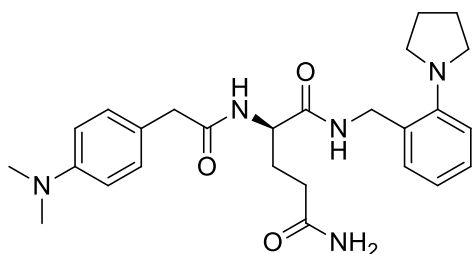
2.6. Experimental section

2.6.1 General

High-Resolution Mass Spectrometry (HRMS) spectra and analytical Reversed-Phase Ultra Performance Liquid Chromatography (UPLC) were recorded on a Waters Xevo G2-XS QTOF coupled to a Waters Acquity UPLC H-Class System with PDA UV detector, using a ACQUITY UPLC BEH C18 Column, 130 Å, 1.7 µm, 2.1 mm × 50 mm at a flow rate of 0.6 ml/min with linear gradients of solvents A and B (A = Millipore water with 0.1% FA, B = MeCN with 0.1% FA). Preparative re-versed-phase high-pressure liquid chromatography (RP-HPLC) were performed on a Waters Alliance HT RP-HPLC with PDA UV detector, using a Synergi 4µm, Polar-RP 80Å 10 × 150 mm C18 column at a flow rate of 4 ml/min with linear gradients of solvents A and B (A = Millipore water with 0.1% TFA, B = MeCN with 0.1% TFA). Proton (¹H) nuclear magnetic resonance (NMR) spectra were recorded on a Bruker AV400 (400 MHz). Carbon (¹³C) NMR spectra were recorded on a Bruker AV400 (100 MHz) spectrometer. Shifts are given in ppm using residual solvent as the internal standard. Coupling constants (*J*) are reported in Hz with the following abbreviations used to indicate splitting: s = singlet, d = doublet, t = triplet, dd = doublet of doublets.

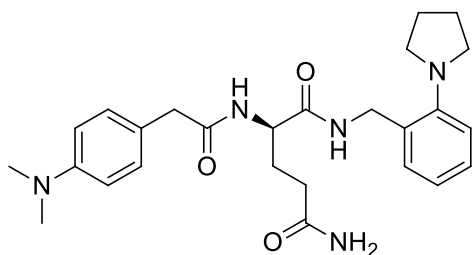
All compounds and chemical reagents were obtained from Sigma-Aldrich, TCI Europe, Enamine or ABCR, and used without further purification. Peptide grade *N,N*-dimethylformamide (DMF) for solid phase synthesis was bought from ABCR. H-Rink amide ChemMatrix® resin was purchased from Sigma Aldrich (Cat. Nr 727768-5G). Fmoc-Lys(Boc)-Wang resin, 200-400mesh was purchased from Bachem (Cat. Nr. 4003241.0005). 495142-1g).

2.6.1. Synthesis and characterization data



(S)-2-(2-(4-(dimethylamino)phenyl)acetamido)-N1-(2-(pyrrolidin-1-yl)benzyl)pentanediamide (L-Gln-A26-B389): commercially available Rink amide resin (0.02048 g, 0.1 mmol) was swollen in *N,N*-dimethylformamide (20 mL) for 2 h in a syringe

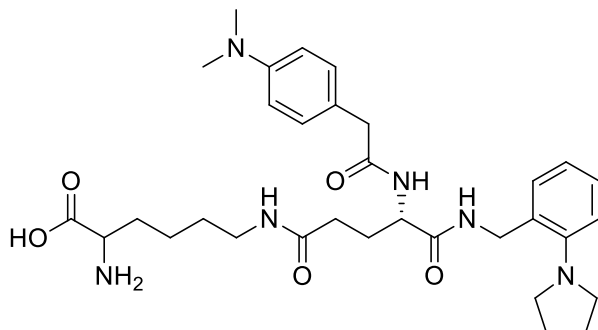
provided with a filter pad. A solution of Fmoc-L-glutamic acid 5-allyl ester (4.0 equiv., 0.4 mmol), DIPEA (4.0 equiv., 0.4 mmol) and HATU (4.0 equiv., 0.4 mmol) in *N,N*-dimethylformamide (4 mL) was added to the syringe, allowed to react for 16 h and washed with *N,N*-dimethylformamide ($5 \times 4 \text{ mL} \times 1 \text{ min}$). The O-allyl deprotection was performed using palladium-tetrakis(triphenylphosphine) ($\text{Pd}(\text{PPh}_3)_4$, 0.25 equiv., 0.025 mmol) and phenylsilane (PhSiH_3 , 24 equiv., 2.4 mmol) in dichloromethane (4 mL) for 2 h. After washing with dichloromethane ($5 \times 4 \text{ mL} \times 1 \text{ min}$) and *N,N*-dimethylformamide ($5 \times 4 \text{ mL} \times 1 \text{ min}$), a solution of (2-(pyrrolidin-1-yl)phenyl)methanamine (4 equiv., 0.4 mmol), DIPEA (8 equiv., 0.8 mmol) and HATU (4.0 equiv., 0.4 mmol) in *N,N*-dimethylformamide (4 mL) was added to the syringe and allowed to react for 16 h and washed with *N,N*-dimethylformamide ($5 \times 4 \text{ mL} \times 1 \text{ min}$). The Fmoc group was removed using a solution of 20% piperidine in *N,N*-dimethylformamide for 20 min and then washed with *N,N*-dimethylformamide ($5 \times 4 \text{ mL} \times 1 \text{ min}$). The coupling to the 2-(4-(dimethylamino)phenyl)acetic (4 equiv., 0.4 mmol) was performed using the same conditions reported before. After washing with *N,N*-dimethylformamide ($5 \times 4 \text{ mL} \times 1 \text{ min}$) the resin was cleaved using a solution of TFA:TIPS:mqH₂O (95:2.5:2.5, v:v) for 1 h at room temperature. The so-obtained solution was collected in a round-bottom flask, dried under vacuum and purified over a RP HPLC (Synergi RP Polar, 5% MeCN in 0.1% aq. TFA to 80% over 14 min). After lyophilization the final compound was collected as a white solid; ¹H-NMR (400 MHz, DMSO-*d*₆) δ 1.75-1.88 (m, 1H), 1.88-1.93 (m, 4H), 1.93-1.99 (m, 1H), 2.12 (dd, $J = 8.1, 6.2, 3.4 \text{ Hz}$, 2H), 2.88-2.91 (m, 6H), 3.11 (td, $J = 8.8, 2.6 \text{ Hz}$, 4H), 3.39 (s, 2H), 4.27-4.30 (m, 1H), 4.31 (d, $J = 5.7 \text{ Hz}$, 2H), 6.69 (dd, $J = 9.2, 2.4 \text{ Hz}$, 2H), 6.80 (s, 1H), 6.89 (t, $J = 7.4 \text{ Hz}$, 1H), 6.98 (d, $J = 8.0 \text{ Hz}$, 1H), 7.12 (d, $J = 8.7 \text{ Hz}$, 2H), 7.14-7.22 (m, 2H), 7.31 (s, 1H), 8.12 (d, $J = 8.0 \text{ Hz}$, 1H), 8.25 (t, $J = 5.6 \text{ Hz}$, 1H). ¹³C-NMR (101, MHz, DMSO-*d*₆) δ 24.9 (2 \times CH₂), 28.5 (CH₂), 32.0 (CH₂), 39.8 (2 \times CH₃), 40.8 (CH₂), 41.7 (CH₂), 51.5 (2 \times CH₂), 52.9 (CH), 112.9 (2 \times Ar), 116.8 (Ar), 120.8 (Ar), 124.3 (Ar), 127.7 (Ar), 128.7 (Ar), 129.8 (Ar), 130.0 (2 \times Ar), 148.6 (Ar), 149.6 (Ar), 171.3 (CONH₂), 171.9 (CONH), 174.1 (CONH). HRMS (ES) calculated for [M+H]⁺(m/z): 466.2813, found 466.2308.



(R)-2-(2-(4-(dimethylamino)phenyl)acetamido)-N1-(2-(pyrrolidin-1-yl)benzyl)pentanediamide (D-Gln-A26-B389): commercially available Rink amide resin (0.02048 g, 0.1 mmol) was swollen in *N,N*-dimethylformamide (20 mL) for 2 h in a syringe provided with a filter pad. A solution of Fmoc-D-glutamic acid 5-allyl ester (4.0 equiv., 0.4 mmol), DIPEA (4.0 equiv., 0.4 mmol) and HATU (4.0 equiv., 0.4 mmol) in *N,N*-dimethylformamide (4 mL) was added to the syringe, allowed to react for 16 h and washed with *N,N*-dimethylformamide ($5 \times 4 \text{ mL} \times 1 \text{ min}$). The *O*-allyl deprotection was performed using palladium-tetrakis(triphenylphosphine) ($\text{Pd}(\text{PPh}_3)_4$, 0.25 equiv., 0.025 mmol) and phenylsilane (PhSiH_3 , 24 equiv., 2.4 mmol) in dichloromethane (4 mL) for 2 h. After washing with dichloromethane ($5 \times 4 \text{ mL} \times 1 \text{ min}$) and *N,N*-dimethylformamide ($5 \times 4 \text{ mL} \times 1 \text{ min}$), a solution of (2-(pyrrolidin-1-yl)phenyl)methanamine (4 equiv., 0.4 mmol), DIPEA (8 equiv., 0.8 mmol) and HATU (4.0 equiv., 0.4 mmol) in *N,N*-dimethylformamide (4 mL) was added to the syringe and allowed to react for 16 h and washed with *N,N*-dimethylformamide ($5 \times 4 \text{ mL} \times 1 \text{ min}$). The Fmoc group was removed using a solution of 20% piperidine in *N,N*-dimethylformamide for 20 min and then washed with *N,N*-dimethylformamide ($5 \times 4 \text{ mL} \times 1 \text{ min}$). Thus, the coupling to the 2-(4-(dimethylamino)phenyl)acetic (4 equiv., 0.4 mmol) was performed using the same conditions reported before. After washing with *N,N*-dimethylformamide ($5 \times 4 \text{ mL} \times 1 \text{ min}$) the resin was cleaved using a solution of TFA:TIPS:mqH₂O (95:2.5:2.5, v:v) for 1 h at room temperature. The so-obtained solution was collected in a round-bottom flask, dried under vacuum and purified over a RP HPLC (Synergi RP Polar, 5% MeCN in 0.1% aq. TFA to 80% over 14 min). After lyophilization the final compound was collected as a white solid; ¹H NMR (400 MHz, DMSO-d₆) δ 1.76-1.84 (m, 1H, CH₂), 1.89-1.92 (m, 4H, 2 \times CH₂), 1.94-1.99 (m, 1H, CH₂), 2.10-2.15 (m, 2H, CH₂), 2.90 (s, 6H, 2 \times CH₃), 3.08-3.14 (m, 4H, 2 \times CH₂), 3.39 (s, 2H, CH₂), 4.27-4.29 (m, 1H, CH), 4.31 (d, $J = 5.7 \text{ Hz}$, 2H, CH₂), 6.68-6.71 (m, 2H, Ar), 6.80 (s, 1H, CONH₂), 6.87-6.91 (m, 1H, Ar), 6.97-6.99 (m, 1H, Ar), 7.12 (d, $J = 8.7 \text{ Hz}$, 2H, Ar), 7.15-7.20 (m, 2H, Ar), 7.31 (s, 1H, CONH₂), 8.12 (d, $J = 8.0 \text{ Hz}$, 1H, CONH), 8.25 (t, $J = 5.6 \text{ Hz}$, 1H, CONH); ¹³C NMR (101, MHz, DMSO-d₆) δ 24.9 (2 \times CH₂), 28.55 (CH₂), 32.00 (CH₂), 39.8 (2 \times CH₃), 40.8 (CH₂), 41.7 (CH₂), 51.55 (2 \times CH₂), 52.9 (CH), 112.9 (2 \times Ar),

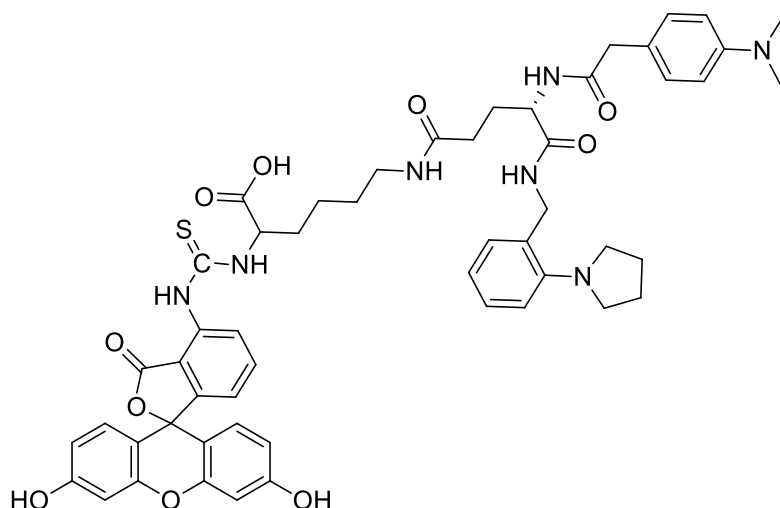
116.8 (Ar), 120.85 (Ar), 124.3 (Ar), 127.70 (Ar), 128.7 (Ar), 129.8 (Ar), 130.0 (2 × Ar), 148.6 (Ar), 149.6 (Ar), 171.3 (CONH₂), 171.9 (CONH), 174.1 (CONH).

HRMS (ES) calculated for [M+H]⁺ (*m/z*): 466.2813, found 466.2308.



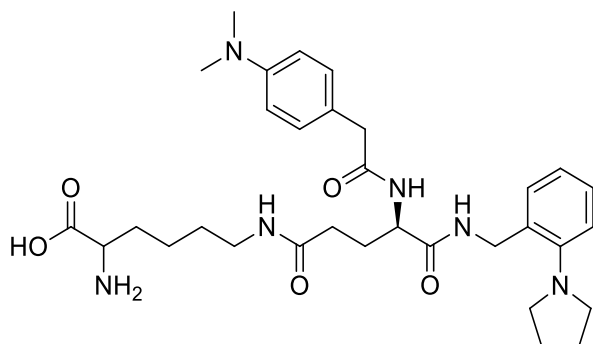
2-amino-6-(((S)-4-(2-(4-(dimethylamino)phenyl)acetamido)-5-oxo-5-((2-(pyrrolidin-1-yl)benzyl)amino)pentanamido)hexanoic acid (Lys-L-Gln-A26-B389): commercially available Fmoc-Lys(Boc)-Wang resin (0.25 mmol) was swollen in *N,N*-dimethylformamide (10 mL) for 2 h inside a syringe provided with a filter pad. The Fmoc group was removed using a solution of 20% piperidine in *N,N*-dimethylformamide for 20 min and after washing the resin with *N,N*-dimethylformamide (5 × 10 mL × 1 min), a solution of Fmoc-L-glutamic acid 5-allyl ester (4.0 equiv., 1 mmol), DIPEA (8.0 equiv., 2 mmol) and HATU (4.0 equiv., 1 mmol) in *N,N*-dimethylformamide (10 mL) was added to the syringe, allowed to react for 16 h and washed with *N,N*-dimethylformamide (5 × 10 mL × 1 min). The *O*-allyl deprotection was performed using palladium-tetrakis(triphenylphosphine) (Pd(PPh₃)₄, 0.25 equiv., 0.0625 mmol) and phenylsilane (PhSiH₃, 24 equiv., 6 mmol) in dichloromethane (20 mL) for 2 h. After washing with dichloromethane (5 × 10 mL × 1 min) and *N,N*-dimethylformamide (5 × 10 mL × 1 min) a solution of the (2-(pyrrolidin-1-yl)phenyl)methanamine (4 equiv., 1 mmol), DIPEA (8 equiv., 2 mmol) and HATU (4.0 equiv., 2 mmol) in *N,N*-dimethylformamide (10 mL) was added to the syringe and allowed to react for 16 h. After washing with *N,N*-dimethylformamide (5 × 10 mL × 1 min) the Fmoc group was removed and the coupling to the 2-(4-(dimethylamino)phenyl)acetic acid (4 equiv., 1.0 mmol) was performed using the same conditions reported before. After washing with *N,N*-dimethylformamide (5 × 10 mL × 1 min) the resin was cleaved using a solution of TFA:TIPS:mqH₂O (95:2.5:2.5, v:v) for 1 h at room temperature. The so-obtained solution was collected in a round-bottom flask, dried under vacuum and purified over a RP-HPLC (Synergi RP Polar, 5% MeCN in 0.1% aq. TFA to 100% over 14 min). After lyophilization the final compound was collected as a white solid.

HRMS (ES) calculated for [M+H]⁺ (*m/z*): 595.3603, found 595.3643.



FI-Lys-L-Gln-A26-B389: to a solution of **Lys-L-Gln-A26-B389** (2.8 mg, 1 equiv.) in dimethyl sulfoxide (100 μ L) was added DIPEA (20 μ L) and a solution of commercially available fluorescein isothiocyanate (3.7 mg, 2.0 equiv.) in dimethyl sulfoxide (100 μ L). After stirring for 30 min in the dark, the reaction was diluted with a solution of DMSO:mqH₂O (1:1 v:v,) and purified over a RP HPLC (Synergi RP Polar, 5% MeCN in 0.1% aq. TFA to 100% over 14 min). The fractions containing the product, identified by mass spectrometry, were collected and then lyophilized to give the title compound as a yellow powder.

HRMS (ES) calculated for [M+H]⁺ (*m/z*): 984.3961, found 984.3460.

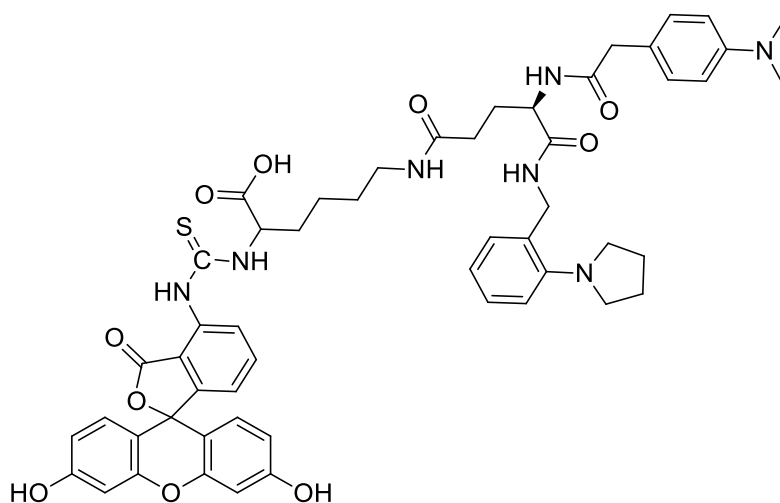


2-amino-6-((R)-4-(2-(4-(dimethylamino)phenyl)acetamido)-5-oxo-5-((2-(pyrrolidin-1-yl)benzyl)amino)pentanamido)hexanoic acid (Lys-D-Gln-A26-B389):

commercially available Fmoc-LysBoc-Wang resin (0.25 mmol) was swollen in *N,N*-dimethylformamide (10 mL) for 2 h inside a syringe provided with a filter pad. The Fmoc group was removed using a solution of 20% piperidine in *N,N*-dimethylformamide for 20 min and after washing the resin with *N,N*-dimethylformamide (5 \times 10 mL \times 1 min), a solution of Fmoc-D-glutamic acid 5-allyl ester (4.0 equiv., 1 mmol), DIPEA (8.0 equiv., 2 mmol) and HATU (4.0 equiv., 1 mmol) in *N,N*-dimethylformamide (10 mL) was prepared, added to the syringe,

allowed to react for 16 h and washed with *N,N*-dimethylformamide ($5 \times 10 \text{ mL} \times 1 \text{ min}$). The *O*-allyl deprotection was performed using palladium-tetrakis(triphenylphosphine) ($\text{Pd}(\text{PPh}_3)_4$) (0.25 equiv., 0.0625 mmol) and phenylsilane (PhSiH_3) (24 equiv., 6 mmol) in dichloromethane (20 ml) for 2 h. After washing with dichloromethane ($5 \times 10 \text{ mL} \times 1 \text{ min}$) and *N,N*-dimethylformamide ($5 \times 10 \text{ mL} \times 1 \text{ min}$) a solution of the (2-(pyrrolidin-1-yl)phenyl)methanamine (4 equiv., 1 mmol), DIPEA (8 equiv., 2 mmol) and HATU (4.0 equiv., 2 mmol) in *N,N*-dimethylformamide (10 mL) was added to the syringe and allowed to react for 16 h. After washing with *N,N*-dimethylformamide ($5 \times 10 \text{ mL} \times 1 \text{ min}$) the Fmoc group was removed and the coupling to the 2-(4-(dimethylamino)phenyl)acetic (4 equiv., 1.0 mmol) performed using the same conditions reported before. After washing with *N,N*-dimethylformamide ($5 \times 10 \text{ mL} \times 1 \text{ min}$) the resin was cleaved using a solution of TFA:TIPS:mqH₂O (95:2.5:2.5, v:v) for 1 h at room temperature. The so-obtained solution was collected in a round-bottom flask, dried under vacuum and purified over a reversed-phase HPLC (Synergi RP Polar, 5% MeCN in 0.1% aq. TFA to 100% over 14 min). After lyophilization the final compound was collected as a white solid.

HRMS (ES) calculated for $[\text{M}+\text{H}]^+$ (m/z): 595.3603, found 595.3448.



FI-Lys-D-Gln-A26-B389: to a solution of **Lys-D-Gln-A26-B389** (3.3 mg, 1 equiv.) in dimethyl sulfoxide (100 μL) was added DIPEA (20 μL) and a solution of commercially available fluorescein isothiocyanate (4.3 mg, 2.0 equiv.) in dimethyl sulfoxide (100 μL).

After stirring for 30 min in the dark, the reaction was diluted with a solution of DMSO:mqH₂O (1:1 v:v) and purified over a reversed-phase HPLC (Synergi RP Polar, 5% MeCN in 0.1% aq. TFA to 100% over 14 min). The fractions containing the product identified by mass spectrometry, collected and then lyophilized to give the title compound as a yellow powder.

HRMS (ES) calculated for $[M+H]^+$ (m/z): 984.3961, found 984.3598.

2.6.3. Biological evaluation

Enzymatic assay

The enzymatic activity of Tyrosinase was measured at 25 °C following already described procedures using L-DOPA as substrate [224,225]. In 384-well microtiter clear plates (Greiner non-binding), a mixture of 1 mM L-DOPA, 4 mM MBTH, 200 nM human Tyrosinase and the inhibitor was prepared (final volume 30 μ L in PBS 1% DMSO, pH=6.8). The increase of the absorption at 490-510 nm, due to the formation of the L-dopaquinone-MBTH complex, was recorded using a Spectra Max Paradigm multimode plate reader (Molecular Devices) over 10 minutes. Experiments were performed in duplicates and the values were fitted using Graphpad Prism software. The obtained OD values were plotted as a function of time. Linear regression of the plotted points was performed. IC_{50} values were calculated fitting the obtained slope as function of the inhibitor concentration.

Fluorescence polarization

The dilution series were done in a non-binding black 384-well microplate (Greiner Bio On.). In a final volume of 30 μ L, 50 nM of the fluorescein-conjugated ligand was incubated with a 1:1 dilution series of TYRP1 in PBS pH 7.4 The fluorescence anisotropy was measured on a Spectra Max Paradigm multimode plate reader (Molecular Devices). Experiments were performed in triplicate and the anisotropy values fitted using Graphpad Prism software.

3. Development of multimeric ligands of Thiamidol™

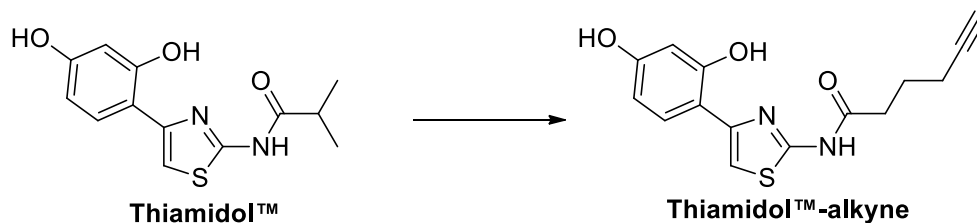
The multivalent approach is a useful and promising tool to improve tumour targeting: it is based on multiple molecular recognition events that could occur among a multimeric ligand and the related protein and on the binding to transmembrane proteins [226], as hTYR and TYRP1.

Particularly, multivalent ligands can bind to the proteins with improved potency possessing multiple copies of the pharmacophore or binder [227], thus leading to an increase in the total binding and a longer residence time in the tumour lesions compared to their monovalent counterpart, as proved from several investigations [228–233].

3.1. Design of multimeric ligands of Thiamidol™

The design of multimeric ligands involved the use of a binder, able to interact with hTYR and TYRP1, and attached to multimeric structures of different valence.

The pharmacophore selected for the conjugation was Thiamidol™, recently identified as novel and potent inhibitor of hTYR and TYRP1 [183] and approved for the treatment of hyperpigmentation related disorders [196,197]. Thiamidol™ was modified by inserting an hexynoic moiety in place of the isobutyl one on the amino group to enable further derivatizations based on a Cu-catalysed alkyne-azide cycloaddition (**Figure 3.1**). The choice of modifying this position was due to previous modelling studies that demonstrated that both the hydroxyl groups and the thiazolyl ring must be intact for an efficient inhibition of hTYR [183,184]. Despite this modification, the alkyne derivative still retains a proper IC₅₀ value, even if this was slightly worse than its parent compound (**Figure 1.18**). These values were in accordance with previous measurements performed on a series of thiazolyl-resorcinol variants [184].



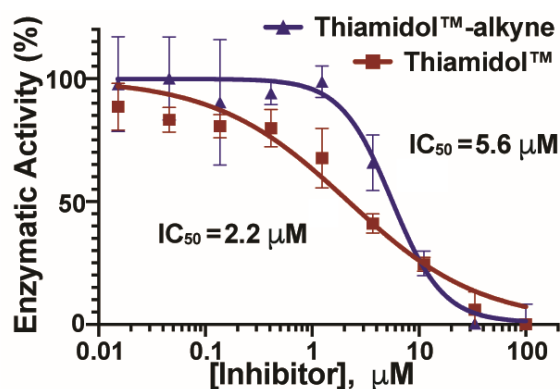


Figure 3.1. Structural modification on Thiamidol™ and relative IC_{50} of the parent and novel compounds performed on hTYR.

After the validation of the alkyne-Thiamidol™ as suitable binder, the monomeric and multimeric structures were designed and synthesised. Particularly, to improve the solubility, these structures were based on a peptidic charged structure, containing a terminal azide for the Cu-catalysed alkyne-azide cycloaddition to the Thiamidol™-alkyne.

Initially, two bivalent ligands defined, for ease, as medium and long dimers, as well as their monomer counterpart were synthesised and evaluated to assess the contribution of the multivalent approach. Then, after determining that the multimeric ligands obtained an increased binding profile, the tetramer, bearing four molecules of Thiamidol™-alkyne, was synthesised and evaluated.

The first part of the linker included the sequence cysteine (C)-caproic acid (C6)-aspartate (D)-arginine (R)-aspartate (D) instead of the sequence CDRD, initially selected [231,234,235]. The insertion of the 6-aminocaproic acid resulted fundamental in avoiding the intra molecular elimination of the CD, that occurred spontaneously during the cleavage from the resin, and in retaining the C as first amino acid, particularly convenient for its reactivity to the thiol reagents, such as the fluorescein-5 maleimide used in these studies (**Figure 3.2**).

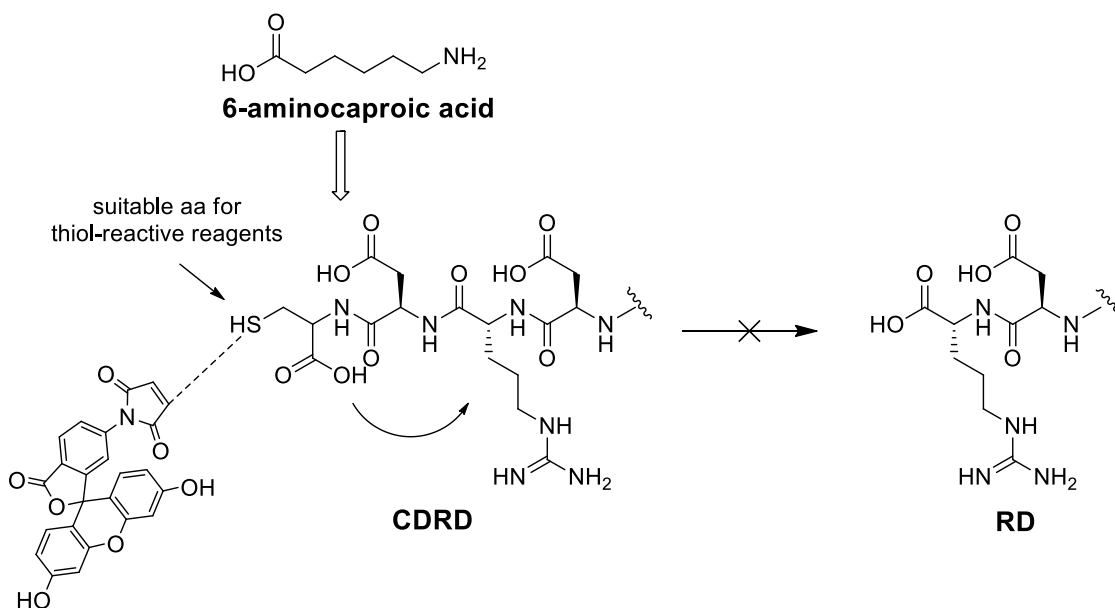
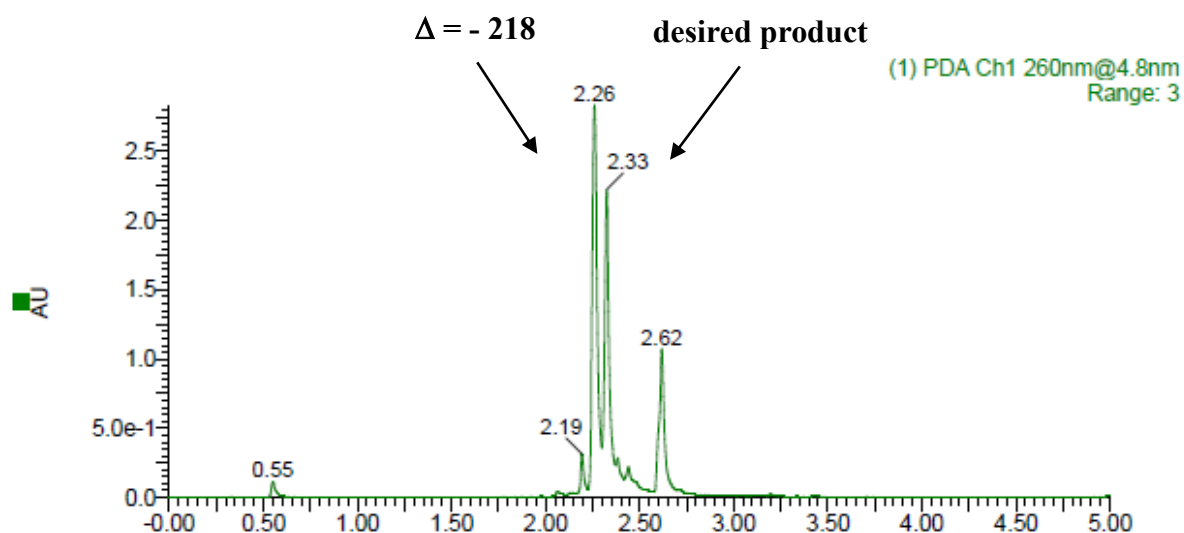


Figure 3.2. Schematic representation of the modification on the CDRD based sequence.

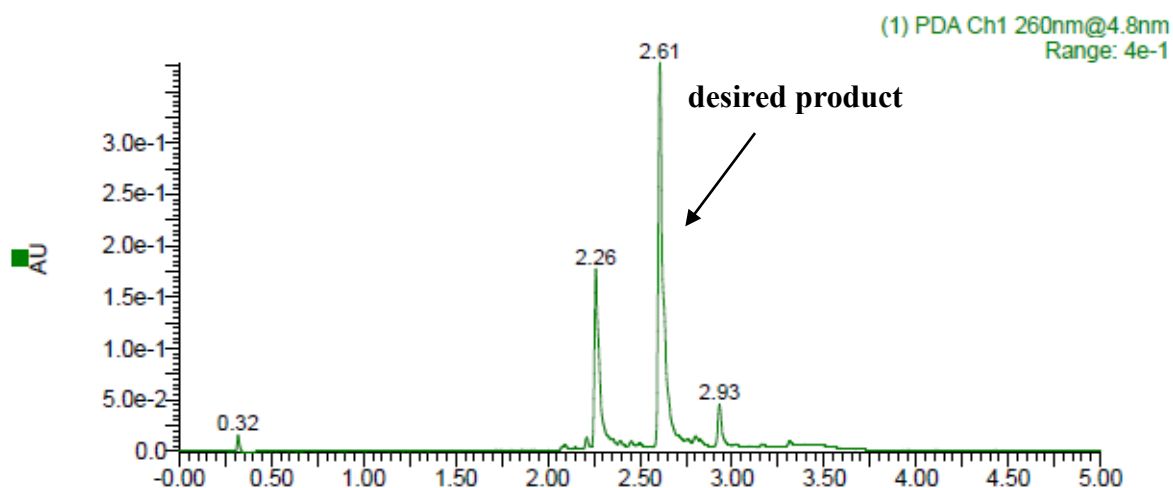
Intriguingly, from the first coupling reactions, the synthesis of CDRD resulted dirty: each chromatogram, contained at least two main peaks, the desired product and a side product that corresponded to the expected mass minus 218. After performing the click reaction on the monomer, the chromatogram revealed, as usual, two main peaks close to each other not separable over the HPLC (**Chromatogram 3.1**).



Chromatogram 3.1. Chromatogram of the CDRD-monomer after the Cu-catalysed alkyne-azide cycloaddition.

Nonetheless, the last coupling to the fluorescein-5-maleimide was performed and the chromatogram revealed that the peak, correspondent to the desired product, reacted to the

fluorescein-5-maleimide but not the other one. Since fluorescein-5-maleimide had to react to the thiol group through the Michael addition, it meant that the product, that did not react, could not contain the cysteine (**Chromatogram 3.2**). It could be suggested that the side product could be the desired product lacking the first two amino acids. Hence, the decision of adding a molecule of 6-aminocaproic acid, that dramatically improved the yield of the total synthetic procedure.



Chromatogram 3.2. Chromatogram of the FI-CDRD-monomer after fluorescein-5-maleimide reaction.

The coupling of the lysine (Lys) to this C-C6-DRD based sequence enabled the dimerization and the synthesis of the medium and long dimers, that differ for a molecule of 6-aminocaproic acid, located between the Lys and the 5-azido pentanoic acid. This was the last component of the structures that provided the Cu-catalysed alkyne-azide cycloaddition to the Thiamidol™-alkyne (**Figure 3.3**).

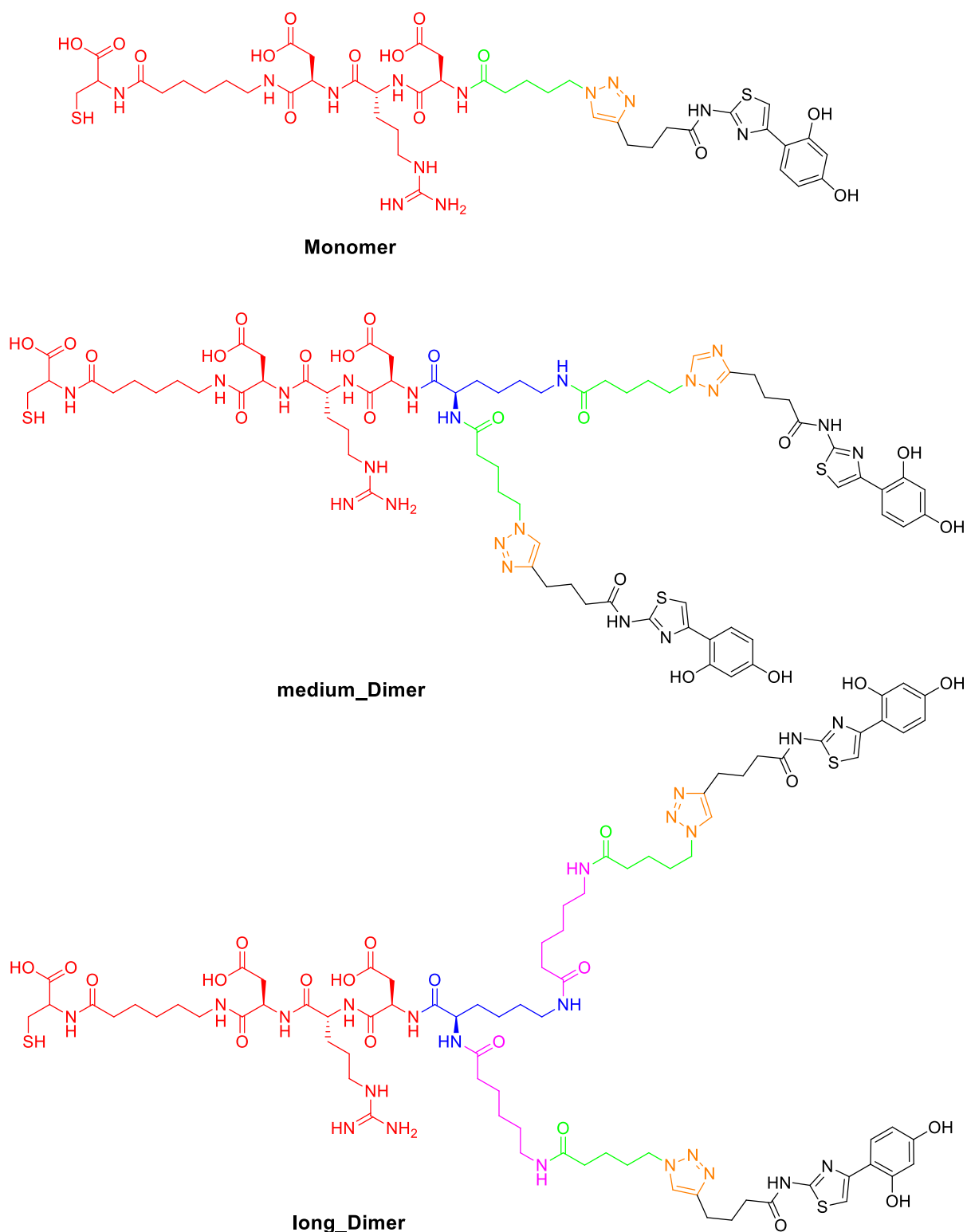


Figure 3.3. Structures of the **Monomer**, **medium_Dimer** and **long_Dimer**. Each component is outlined in diverse colours: in red is reported the common based sequence; in blue the lysine, in purple the 6-aminocaproic acid, in green the 5-azido-pentanoic acid, in orange the triazole, that constitutes the junction site between the linker and the pharmacophore and in black the alkyne.

The tetramer was synthesized using the same procedure but by reacting another molecule of Lys resulting in four sites available for the further couplings to the 6-aminocaproic acid, the 5-azido pentanoic acid, and the four molecules of Thiamidol™-alkyne (**Figure 3.4**).

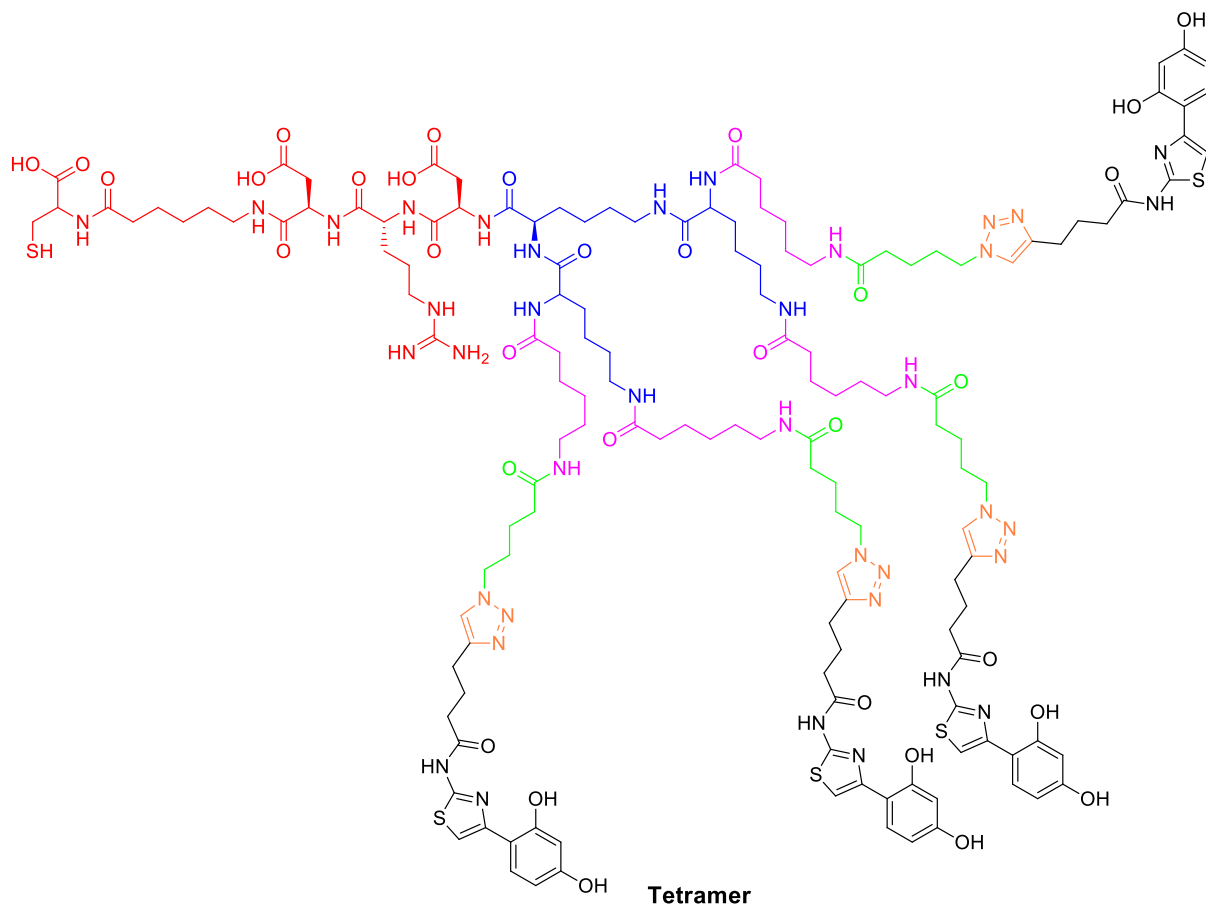


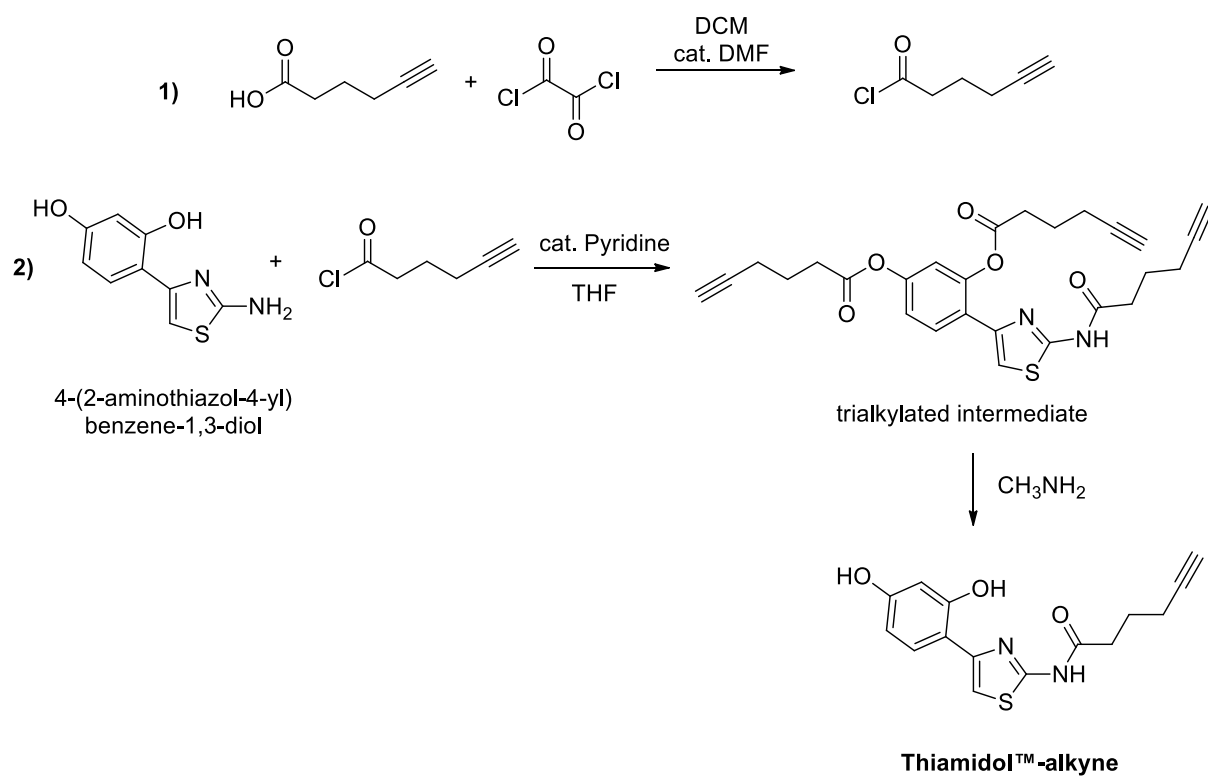
Figure 3.4. Structures of the **Tetramer**. Each component is outlined in diverse colours: in red is reported the common based sequence; in blue the lysine, in purple the 6-aminocaproic acid, in green the 5-azido-pentanoic acid, in orange the triazole, that constitutes the junction site between the linker and the pharmacophore and in black the alkyne.

3.2. Chemistry

The Thiamidol™-alkyne is not commercially available, so its synthesis was optimized into a 2-step procedure, despite the 4 steps of the published protocol [184].

The first step consisted of the activation of the 5-hexynoic acid using oxalyl chloride, followed by a nucleophilic substitution between the commercially available 4-(2-aminothiazol-4-yl)benzene-1,3-diol and the fresh chloride. Performing a selective substitution on the amino group was challenging due to the presence of the resorcinol moiety and, to overcome this issue,

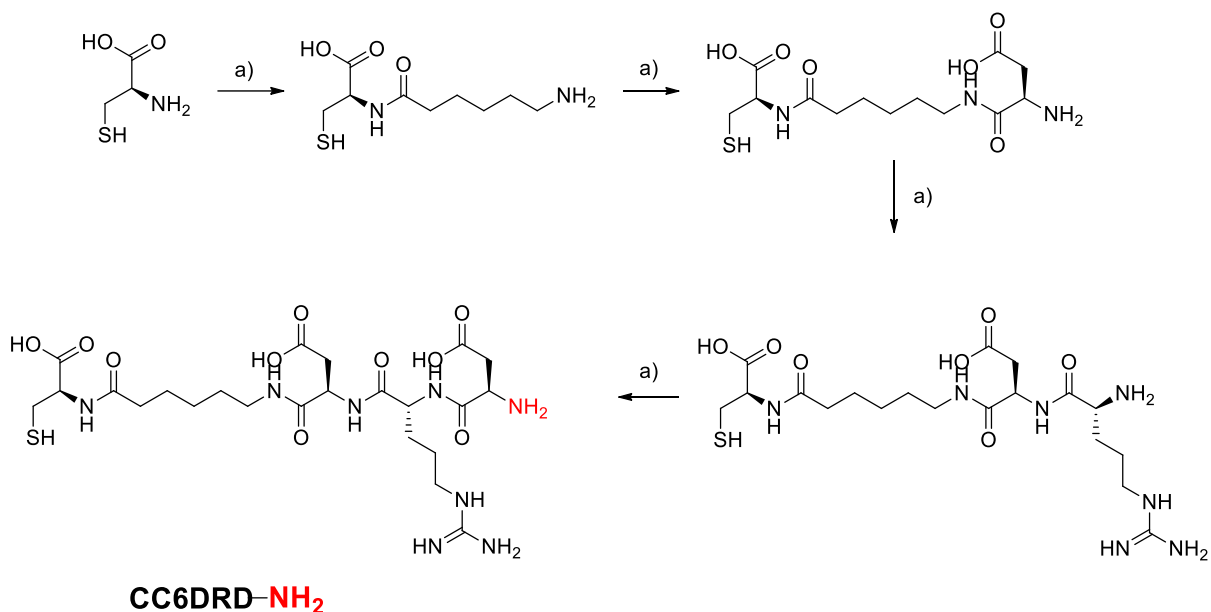
an excess of chloride equivalents was used to obtain the tri-alkylated product that was then selectively hydrolysed using methylamine solution (**Scheme 3.1**).



Scheme 3.1. Synthetic procedure of Thiamidol™-alkyne.

After obtaining the Thiamidol™-alkyne, the **Monomer**, **medium_Dimer**, **long_Dimer** and the **Tetramer** were synthesized employing standard Fmoc-based solid phase peptide synthesis (SPPS) proceeding from the successive couplings of the chosen amino acids or the proper acid to the commercially available Cysteine-Wang resin in presence of HATU and DIPEA.

Briefly, Cysteine-Wang resin, pre-treated with a 20% solution of piperidine in DMF in order to remove the Fmoc group, was coupled to **Fmoc-6-aminocaproic acid**, Fmoc-Asp(O*t*Bu)-OH, Fmoc-Arg(Pbf)-OH and Fmoc-Asp(O*t*Bu)-OH to obtain the based sequence C-C6-DRD (**Scheme 3.2**).



a) Proper NHFmoc-amino acids, HATU, DIPEA, DMF, 2h, RT - 20% piperidine DMF, 20 min, RT

Scheme 3.2. Synthetic procedure for the based sequence **CC6DRD**.

The resin was split for synthesizing each of the multimeric ligands.

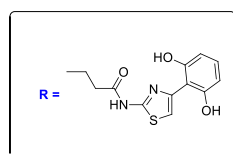
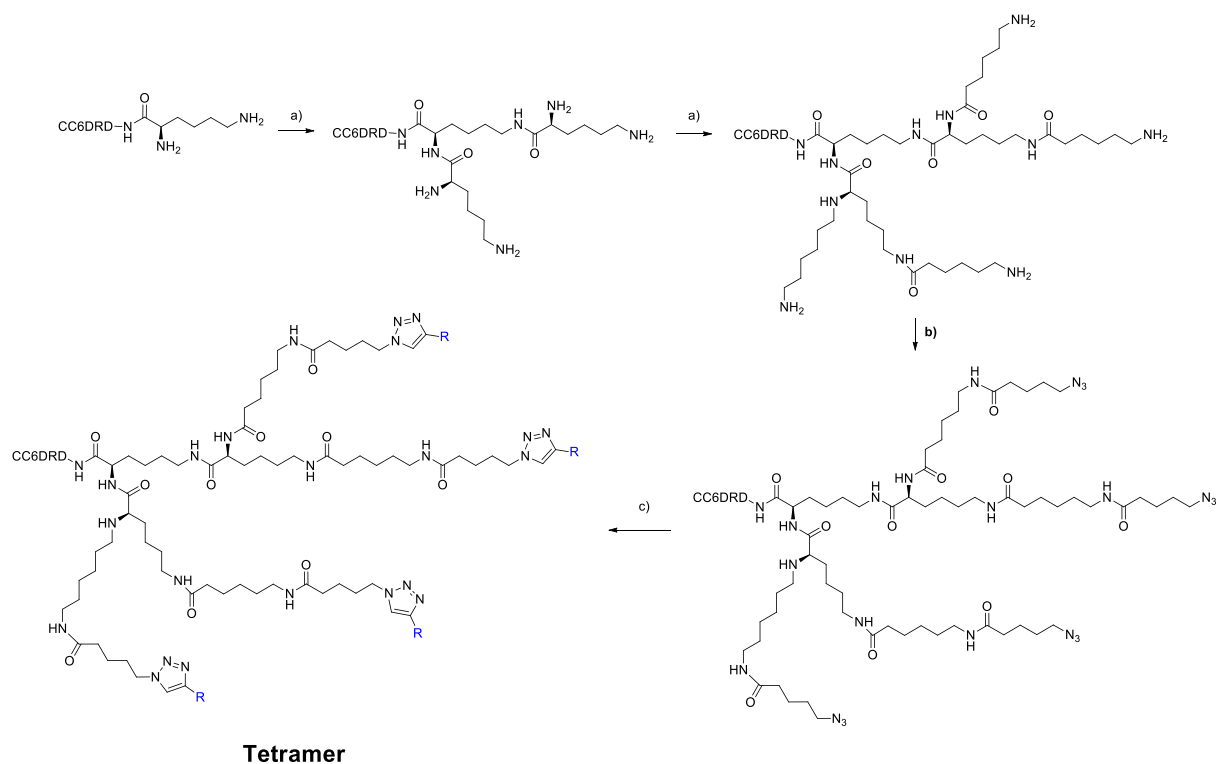
The **Monomer** was synthesized capping C-C6-DRD to the 5-azido pentanoic acid that then was clicked to the Thiamidol™-alkyne.

After coupling the C-C6-DRD to the Fmoc-Lys(Fmoc)-OH, the resin was split again.

The **medium_Dimer** was obtained capping the Lys-based peptide to the 5-azido pentanoic acid clicked to the Thiamidol™-alkyne.

The **long_Dimer** was obtained coupling and then capping the Lys-based peptide to the **Fmoc-6-aminocaproic acid** and to the 5-azido pentanoic acid clicked to the Thiamidol™-alkyne.

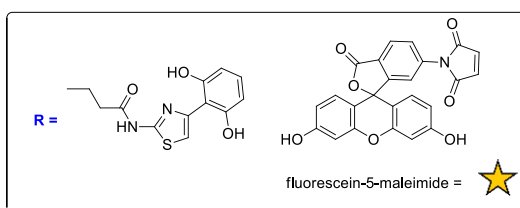
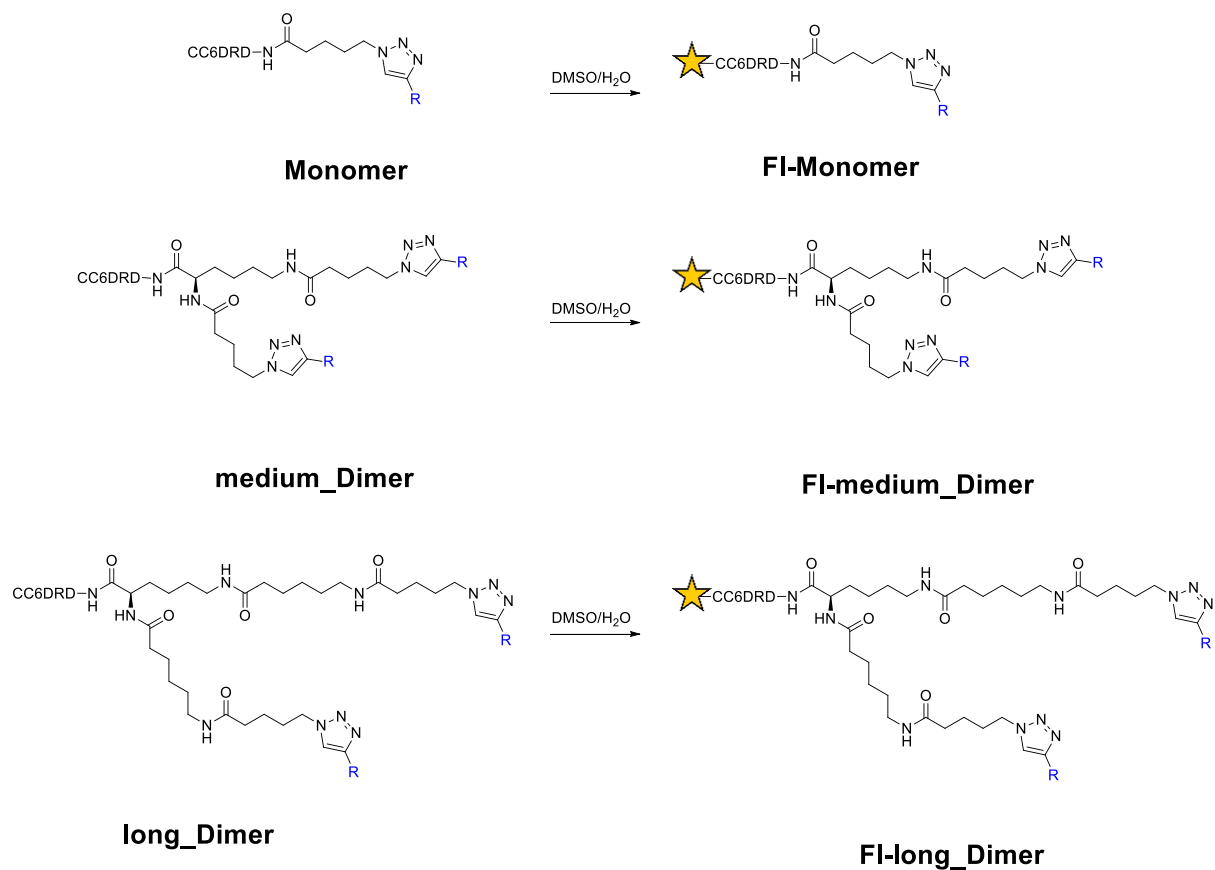
The Cu-catalyzed alkyne-azide cycloaddition was performed in presence of CuI, sodium ascorbate, DIPEA, 2,6-lutidine and the Thiamidol™-alkyne (**Scheme 3.3**)[236].



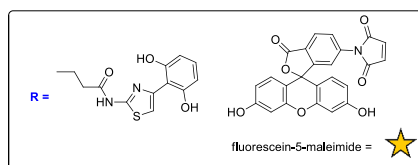
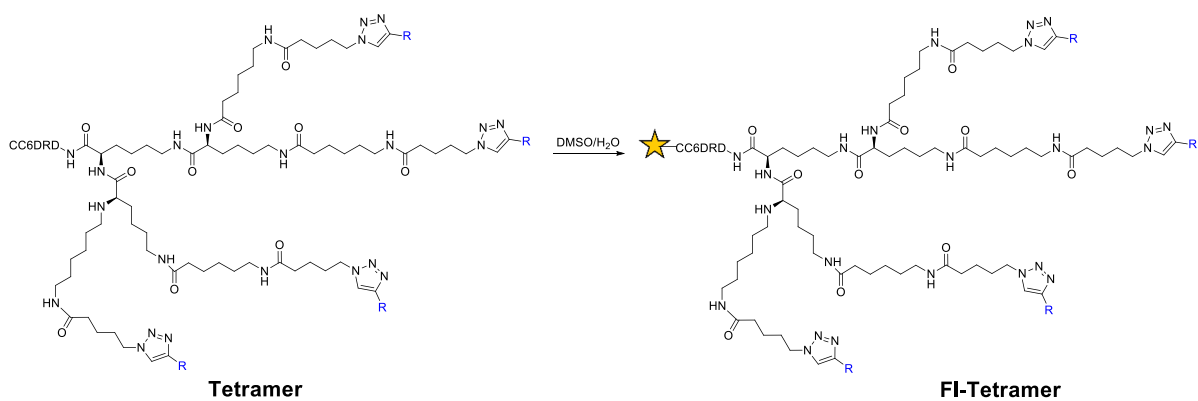
a): proper Nfmoc-amino acids, HATU, DIPEA, DMF, 2h, RT - 20% piperidine DMF, 20 min, RT
 b): 5-azido pentanoic acid, HATU, DIPEA, DMF, 2h, R
 c): alkyne, CuI, sodium ascorbate, 2,6-lutidine, DIPEA, 16h, RT

Scheme 3.4. Synthetic procedure of **Tetramer**.

After cleaving the resin and purifying the so-obtained compounds, they were labelled with fluorescein-5-maleimide yielding the final **FI-Monomer**, **FI-medium_Dimer**, **FI-long_Dimer** and **FI-Tetramer** (Scheme 3.5 and Scheme 3.6).



Scheme 3.5. Synthetic procedure of **FI-Monomer**, **FI-medium_Dimer** and **FI-long_Dimer**.



Scheme 3.6. Synthetic procedure of **FI-Tetramer**.

The same procedure was also used for the synthesis of the negative control bearing the 5-hexynoic acid in place of the **Thiamidol™-alkyne**.

3.3. Biological evaluation

FI-Monomer, **FI-medium_Dimer**, **FI-long_Dimer** and **FI-Tetramer** were evaluated as hTYR and TYRP1 binders employing a recently described Enzyme-linked immunosorbent assay (ELISA) [237], FP and Fluorescence-activated cell sorting (FACS).

The ELISA involved the use of an IgG anti FITC able to react to the fluorescein moiety of the ligands. Precisely, after coating the proteins and incubating the compounds, the IgG anti FITC was added to bind to the fluorescein moiety of the ligands, if retained on the protein. This was then, in turn, bound to the protein A-horseradish peroxidase conjugate (pA-HRP) that is able to selectively recognize the Fc-region of the IgG anti FI, through the pA and to react, through the HRP, to the 3,3',5,5'-Tetramethylbenzidine (TMB) that developed a blue coloration. The intensity of the colour is proportional to the amount of complex formed and to the concentration of ligands retained on the protein surface. After quenching the reaction, the plate was measured at 450 nm [237]. The results, given as function of ligand concentration and absorbance (Abs), are reported in **Figure 3.5**, **Figure 3.6** and **Figure 3.8** and **Figure 3.9**.

The **FI-Monomer** was evaluated as hTYR and TYRP1 binder in FP. This compound, at a fixed concentration, was titrated and incubated using increasing concentration of hTYR and TYRP1. The results, given as function of protein concentration and FA, are reported in **Figure 3.7**.

Then, the FACS analysis were set up using the B16-F10 melanoma cells as sources of the melanogenic enzymes. They were incubated with fluorescein-labelled compounds, washed to eliminate the non-binding residues and stained with an IgG anti FI labelled with Cy5-fluorophore (**Figure 3.10**).

3.4. Results and discussion

Based on the proven statement that the multimerization can enhance the affinity and the potency of a pharmacophore, **FI-Monomer**, **FI-medium_Dimer**, **FI-long_Dimer** then **FI-Tetramer** and the negative control were synthesized employing SPPS and then evaluated as binders of hTYR and TYRP in ELISA, FP and FACS.

FI-medium_Dimer and the **FI-long_Dimer** were found to be tenfold more potent than the **FI-Monomer** and the **FI-long_Dimer** was even more potent than the **FI-medium_Dimer**. Nonetheless, this plot suggested some critical issues: the use of the negative control did not

result convenient since it was found to possess a slight interaction with hTYR. Besides, though the **FI-medium_Dimer** and **FI-long_Dimer** resulted more potent than the **FI-Monomer**, suggesting that the dimerization was successful in enhancing the affinity, **FI-medium_Dimer** and **FI-long_Dimer** possessed K_d values around 10 μM (**Figure 3.5**). Similar results were obtained in the ELISA performed on TYRP1, where the use of the IgG TA99 [209,238], used as positive control, stressed the huge gap among the IgG and these ligands (**Figure 3.6**).

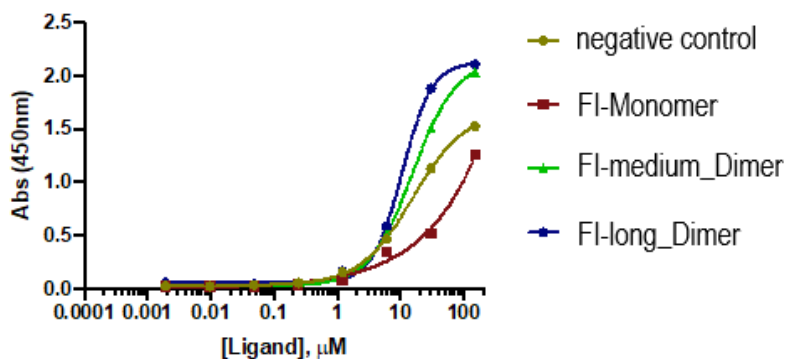


Figure 3.5. Binding profile on hTYR determined in ELISA.

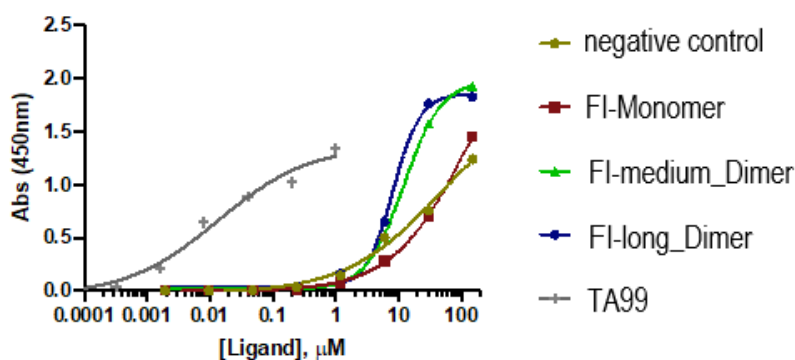


Figure 3.6. Binding affinities on TYRP1 determined in ELISA.

To further investigate this result, the FP for **FI-Monomer** was performed. The plot shows that, even at high concentration of the proteins, the compound did not saturate hTYR or TYRP1 (**Figure 3.7**).

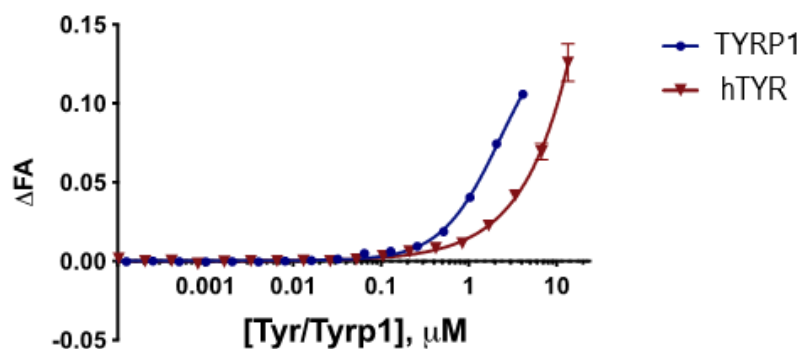


Figure 3.7. Binding affinities of **FI-Monomer** on hTYR and TYRP1 determined in FP.

The **FI-long_Dimer** obtained the best outcome, and so the evaluation of the related FI-Tetramer, bearing four molecules of **Thiamidol™-alkyne** was attempted. Effectively, the FI-Tetramer showed the strongest binding interaction with both the proteins, reaching single-digit micromolar affinity, never measured before, though this affinity was even worse than TA99 (Figure 3.8 and Figure 3.9) [209,238].

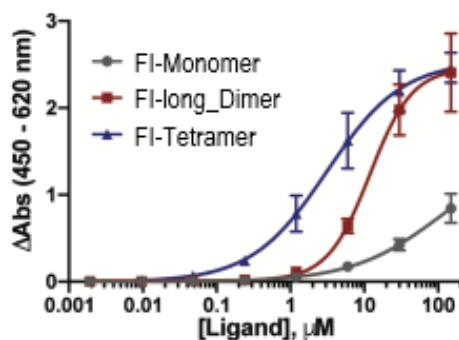


Figure 3.8. Binding affinities on hTYR determined in ELISA.

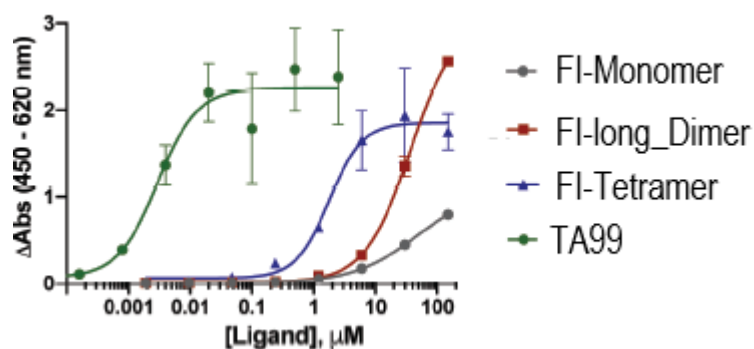


Figure 3.9. Binding affinities on TYRP1 determined in ELISA.

Subsequently, to further evaluate the ligands binding properties, **FI-Monomer**, **FI-long_Dimer** and **FI-Tetramer** were tested in FACS using B16-F10 melanoma cells as a source of hTYR and TYRP1. Similarly to the results obtained in ELISA, FI-Tetramer was found to be a better ligand on B16-F10 cells, compared to its analogue **FI-long_Dimer** and **Monomer** (3.10).

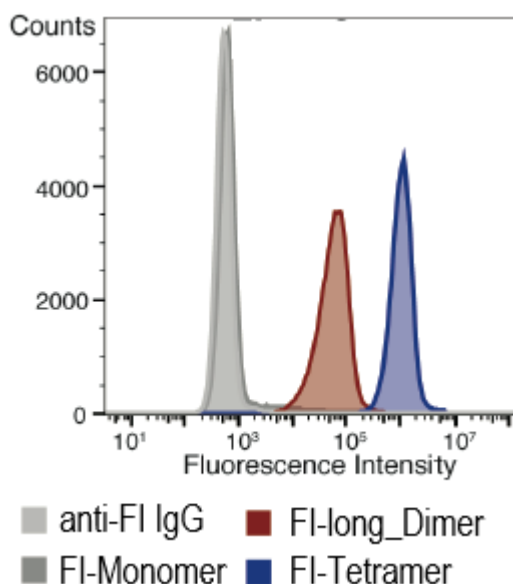


Figure 3.10. Binding properties on B16-F10 melanoma cells determined in FACS using the Cy5 dye.

3.5. Conclusions

The multimeric ligands of **Thiamidol™**, tested on hTYR and TYRP1, provided insight in the use of the multivalent approach, since the multimerization resulted in an increased binding compared to the dimeric monovalent counterpart. The **FI-Tetramer** showed the best results in terms of binding, achieving a 10-fold increase in the affinity compared to the **FI-long_Dimer** and 100-fold increase compared to the **FI-Monomer** though its binding profile has been worse than the TA99, the antibody targeting TYRP1.

3.6. Experimental section

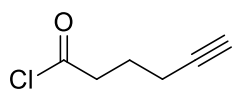
3.6.1. General

High-Resolution Mass Spectrometry (HRMS) spectra and analytical Reversed-Phase Ultra Performance Liquid Chromatography (UPLC) were recorded on a Waters Xevo G2-XS QTOF coupled to a Waters Acquity UPLC H-Class System with PDA UV detector, using a ACQUITY UPLC BEH C18 Column, 130 Å, 1.7 µm, 2.1 mm × 50 mm at a flow rate of 0.6 ml/min with linear gradients of solvents A and B (A = Millipore water with 0.1% FA, B = MeCN with 0.1%

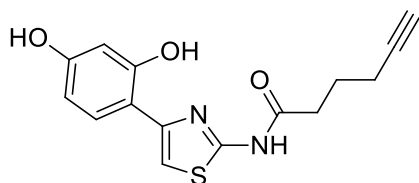
FA). Preparative re-versed-phase high-pressure liquid chromatography (RP-HPLC) were performed on a Waters Alliance HT RP-HPLC with PDA UV detector, using a Synergi 4 μ m, Polar-RP 80Å 10 \times 150 mm C18 column at a flow rate of 4 ml/min with linear gradients of solvents A and B (A = Millipore water with 0.1% TFA, B = MeCN with 0.1% TFA). Proton (^1H) nuclear magnetic resonance (NMR) spectra were recorded on a Bruker AV400 (400 MHz). Carbon (^{13}C) NMR spectra were recorded on a Bruker AV400 (100 MHz) spectrometer. Shifts are given in ppm using residual solvent as the internal standard. Coupling constants (J) are reported in Hz with the following abbreviations used to indicate splitting: s = singlet, d = doublet, t = triplet, dd = doublet of doublets.

All compounds and chemical reagents were obtained from Sigma-Aldrich, TCI Europe, Enamine or ABCR, and used without further purification. Peptide grade *N,N*-dimethylformamide (DMF) for solid phase synthesis was bought from ABCR. Fmoc-Cys(Trt)-Wang resin (100-200 mesh, 0.40-1.00 mmol/g) was purchased from Bachem (Cat. Nr. 4028211.0001). 4-(2-aminothiazol-4-yl)benzene-1,3-diol was purchased from Fluorochem (Cat. Nr. 495142-1g).

3.6.2. Synthesis and characterization data



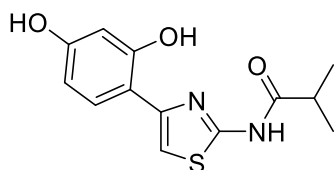
Hex-5-ynoyl chloride: To a stirring solution of 5-hexynoic acid (1.0 equiv.) in dichloromethane (0.1 M) and in presence of a catalytic amount of *N,N*-dimethylformamide, a 2.0 M solution of oxalyl chloride in dichloromethane (1.1 equiv.) was added dropwise at 0 °C. After 1 h, the reaction was completed, evaporated under vacuum and the so obtained red precipitate resuspended in a solution of tetrahydrofuran, in presence of a catalytic amount of pyridine.



***N*-(4-(2,4-dihydroxyphenyl)thiazol-2-yl)hex-5-yneamide (Thiamidol™-alkyne):** to a stirring solution of 4-(2-aminothiazol-4-yl)benzene-1,3-diol (1.0 equiv.) in tetrahydrofuran (0.1 M) the fresh solution of hex-5-ynoyl chloride (from 3.0 to 5.0 equiv. depending on the stability of the

chloride) was added drop-wise. The reaction was controlled through LC-MS analysis until the formation of a tri-functionalized derivative. After 16 h, the reaction mixture was treated with a 33 % solution of methylamine in absolute ethanol (8 M, 10 equiv.). After 2 h, the reaction was dried under vacuum, resuspended in the proper amount of CH₃CN:mqH₂O and purified over a Buchi Sepacore RP-MPLC system (2% MeCN in 0.1% aq. TFA over 10 min, 2% MeCN in 0.1% aq. TFA to 70% over 30 min). The fractions containing the product identified by mass spectrometry, were collected and then lyophilized to give the title compound as a white solid; ¹H NMR (400 MHz, DMSO-*d*₆) δ 1.76-1.83 (m, 2H, CH₂), 2.22-2.26 (m, 2H, CH₂), 2.57 (t, *J* = 7.4 Hz, 2H, CH₂), 2.84 (t, *J* = 2.6 Hz, 1H, CH), 6.29-6.32 (m, 2H, Ar), 7.41 (s, 1H, CH thiazole), 7.66 (d, *J* = 8.5 Hz, 1H, Ar), 9.49 (s, 1H, OH), 10.90 (s, 1H, OH), 12.26 (s, 1H, CONH); ¹³C NMR (101 MHz, DMSO) δ 170.6, 158.2, 156.7, 156.2, 146.3, 128.1, 110.5, 107.0, 105.1, 102.8, 83.6, 71.6, 33.6, 23.2, 17.1.

HRMS (ES) calculated for [M+H]⁺ (*m/z*): 303.0803, found 303.0596.

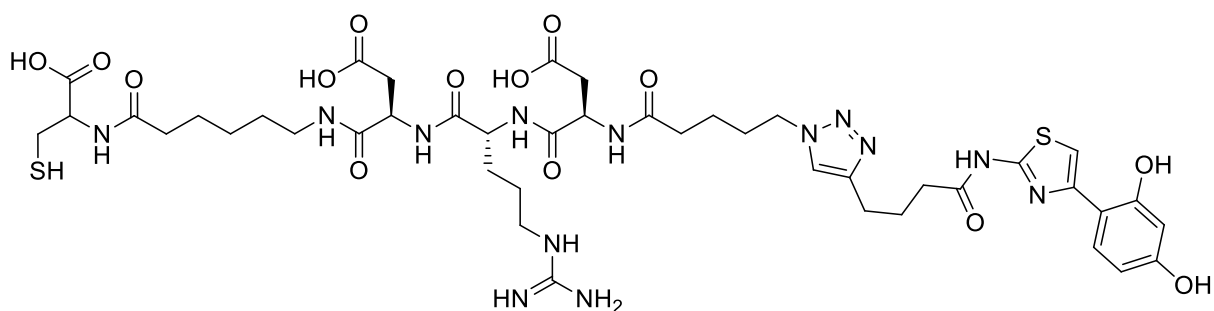


***N*-(4-(2,4-dihydroxyphenyl)thiazol-2-yl)isobutyramide (Thiamidol™)**: to a stirring solution of 4-(2-aminothiazol-4-yl)benzene-1,3-diol (1.0 equiv.) in tetrahydrofuran (0.1 M) the commercially available isobutyryl chloride (5.0 equiv.) was added drop-wise in presence of pyridine (0.1 equiv.). The reaction was controlled through LC-MS analysis until the formation of a tri-functionalized derivative. After 16 h, the reaction mixture was treated with a 33 % solution of methylamine in absolute ethanol (8 M, 10 equiv.). After 2 h, the reaction was dried under vacuum, resuspended in the proper amount of CH₃CN:mqH₂O and purified over a Purification Systems (2% MeCN in 0.1% aq. TFA over 10 min, 2% MeCN in 0.1% aq. TFA to 70% over 30 min). The fractions containing the product identified by mass spectrometry, were collected and then lyophilized to give the title compound as a white solid; ¹H NMR (400 MHz, DMSO-*d*₆) δ 1.14 (d, *J* = 6.8 Hz, 6H), 2.75 (m, *J* = 6.8 Hz, 1H), 6.37 – 6.20 (m, 2H), 7.41 (s, 1H), 7.66 (d, *J* = 8.3 Hz, 1H), 9.48 (s, 1H), 10.88 (s, 1H), 12.16 (s, 1H). NMR data are in full agreement with previously reported values [184].

General procedure on-resin

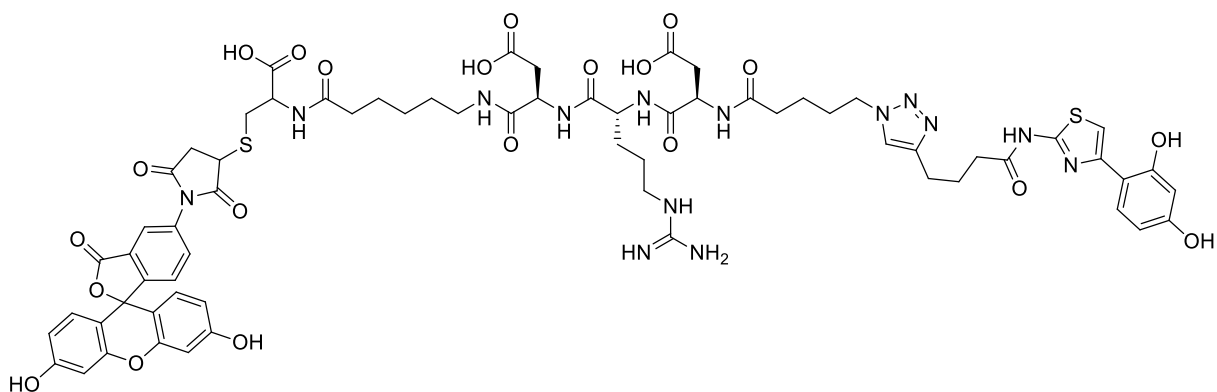
Commercially Fmoc-Cys(Trt) Wang resin (0.7 g, 0.5 mmol) was swollen in *N,N*-dimethylformamide (20 mL) for 1 h inside a syringe provided with a filter pad. The Fmoc group was removed using a solution of 20% piperidine in *N,N*-dimethylformamide for 20 min and then the resin washed with *N,N*-dimethylformamide ($5 \times 20 \text{ mL} \times 1 \text{ min}$). A solution of Fmoc-6-aminocaproic acid (4.0 equiv., 2 mmol), DIPEA (8.0 equiv., 4 mmol) and HATU (4.0 equiv., 2 mmol) in *N,N*-dimethylformamide (20 mL) was prepared, added to the syringe and allowed to react for 2 h. After washing with *N,N*-dimethylformamide ($5 \times 20 \text{ mL} \times 1 \text{ min}$) the Fmoc group was removed using a solution of 20 % piperidine in *N,N*-dimethylformamide. The peptide was extended with Fmoc-Asp(OtBu)-OH, Fmoc-Arg(Pbf)-OH and Fmoc-Asp(OtBu)-OH using the same coupling conditions (HATU/DIPEA equiv.), Fmoc deprotection (20% piperidine in DMF) and washing step as reported before.

The resin was split into different parts for the synthesis of the ThiamidolTM-derivatives and the negative control.



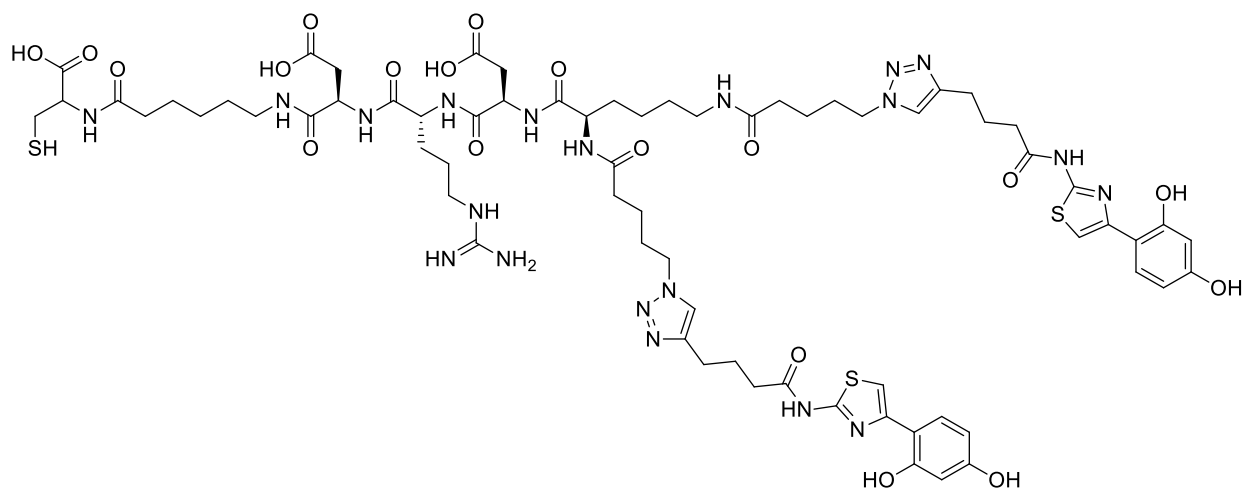
Monomer: after removing the Fmoc-group, 0.1 mmol of the obtained resin was reacted with a solution of 5-azido pentanoic acid (4 equiv., 0.4 mmol), DIPEA (8.0 equiv., 0.4 mmol) and HATU (4.0 equiv., 0.4 mmol) in *N,N*-dimethylformamide (4 mL) for 2 h. After washing with *N,N*-dimethylformamide ($5 \times 4 \text{ mL} \times 1 \text{ min}$) the Cu-catalysed alkyne-azide cycloaddition was performed. A solution of sodium ascorbate (1 equiv.), 2,6-lutidine (10 equiv.) and DIPEA (10 equiv.) in degassed mqH_2O was added to a solution of CuI (1.0 equiv.) in *N,N*-dimethylformamide. The resulting solution and the alkyne (2.0 equiv.) were added to the resin and allowed to react for 16 h. After washing with *N,N*-dimethylformamide ($5 \times 4 \text{ mL} \times 1 \text{ min}$), 50 mM aq. EDTA solution pH = 8 ($5 \times 4 \text{ mL} \times 1 \text{ min}$), *N,N*-dimethylformamide ($5 \times 4 \text{ mL} \times 1 \text{ min}$) and dichloromethane ($5 \times 4 \text{ mL} \times 1 \text{ min}$), the resin was cleaved using a mixture of TFA (3.30 mL, 82.5 %), *m*-Cresol (200 mL, 5 %), thioanisol (200 mL, 5 %), $\text{mq-H}_2\text{O}$ (200 mL, 5 %) and TIPS (100 mL, 2.5 %) for 2 h at room temperature and then washed with TFA ($1 \times 1 \text{ mL} \times 1 \text{ min}$). The combined cleavage and washing solutions were added dropwise to ice cold diethyl ether (20 mL), leading to precipitate formation that was collected by centrifugation, washed with ice cold diethyl ether ($3 \times 20 \text{ mL} \times 2 \text{ min}$, 2000 rpm), dried, re-dissolved in mqH_2O :DMSO and treated with Tris(2-carboxyethyl)phosphine hydrochloride (2 equiv.). The solution was injected and purified over a RP-HPLC (Synergi RP Polar, 5% MeCN in 0.1% aq. TFA to 80% over 14 min), the fractions containing the product identified by mass spectrometry collected and then lyophilized to give the title compound as a white solid.

HRMS (ES) calculated for $[\text{M}+\text{H}]^+$ (m/z): 1048.3980, found 1048.3822.



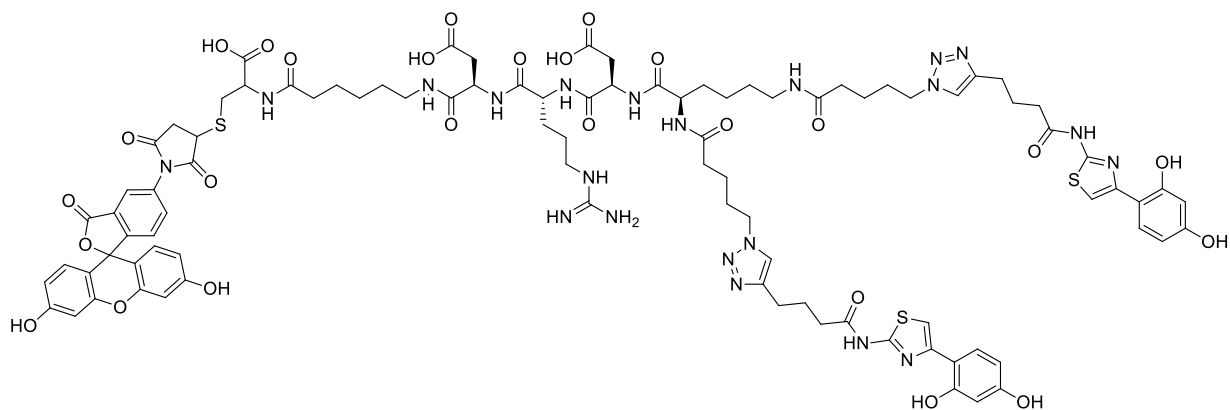
FI-Monomer: to a solution of C-C6-DRD-monomer-Thiamidol (2.0 mg, 1 equiv.) in dimethyl sulfoxide (100 μL) was added a 0.1 M solution of commercially available fluorescein-5-maleimide (0.8 mg, 1.0 equiv.) in dimethyl sulfoxide (19.1 μL). After stirring for 30 min in the dark, the reaction was quenched with the proper volume of DMSO:mqH₂O, injected and purified over a reversed-phase HPLC (Synergi RP Polar, 5% MeCN in 0.1% aq. TFA to 70% over 14 min). The fractions containing the product were identified by mass spectrometry, collected and lyophilized to give the title compound as a yellow solid.

HRMS (ES) calculated for $[\text{M}+2\text{H}]^+$ (m/z): 1476.4753, found 1476.4056.



Medium_Dimer: after removing the Fmoc-group, 0.2 mmol of the resin was reacted with a solution of Fmoc-Lys(Fmoc)-OH (4 equiv., 0.8 mmol), DIPEA (8 equiv., 1.6 mmol) and HATU (4.0 equiv., 0.8 mmol) in *N,N*-dimethylformamide (8 mL) for 2 h. After washing with *N,N*-dimethylformamide ($5 \times 8 \text{ mL} \times 1 \text{ min}$). The peptide was capped to the 5-azido pentanoic acid fixing the coupling conditions (5-azido pentanoic acid and HATU 6 equiv., DIPEA 12 equiv.) and using the same washing step reported before. After this last coupling step, the Cu-catalysed alkyne-azide cycloaddition was performed. A solution of sodium ascorbate (1.5 equiv.), 2,6-lutidine (15 equiv.) and DIPEA (15 equiv.) in degassed mqH_2O as added to a solution of CuI (1.5 equiv.) in *N,N*-dimethylformamide. The resulting solution and the alkyne (3 equiv.) were added to the resin and allowed to react for 16 h. After washing with *N,N*-dimethylformamide ($5 \times 8 \text{ mL} \times 1 \text{ min}$), 50 mM aq. EDTA solution pH = 8 ($5 \times 8 \text{ mL} \times 1 \text{ min}$), *N,N*-dimethylformamide ($5 \times 8 \text{ mL} \times 1 \text{ min}$) and dichloromethane ($5 \times 8 \text{ mL} \times 1 \text{ min}$), the resin was cleaved using a mixture of TFA (6.6 mL, 82.5 %), *m*-Cresol (400 mL, 5 %), thioanisol (400 mL, 5 %), $\text{mq-H}_2\text{O}$ (400 mL, 5 %) and TIPS (200 mL, 2.5 %) for 2 h at room temperature and then washed with TFA ($1 \times 4 \text{ mL} \times 1 \text{ min}$). The combined cleavage and washing solutions were added drop-wise to ice cold diethyl ether (40 mL) leading to precipitate formation that was collected by centrifugation, washed again with ice cold diethyl ether ($3 \times 40 \text{ mL} \times 2 \text{ min}$, 2000 rpm), dried, redissolved in mqH_2O :DMSO and treated with Tris(2-carboxyethyl)phosphine hydrochloride (2 equiv.). This solution was injected and purified over a reversed-phase HPLC HPLC (Synergi RP Polar, 5% MeCN in 0.1% aq. TFA to 80% over 14 min), the fractions containing the product identified by mass spectrometry, collected and lyophilized to give the title compound as a white solid.

HRMS (ES) calculated for $[\text{M}+\text{H}]^+$ (m/z): 1603.6244, found 1603.5746.

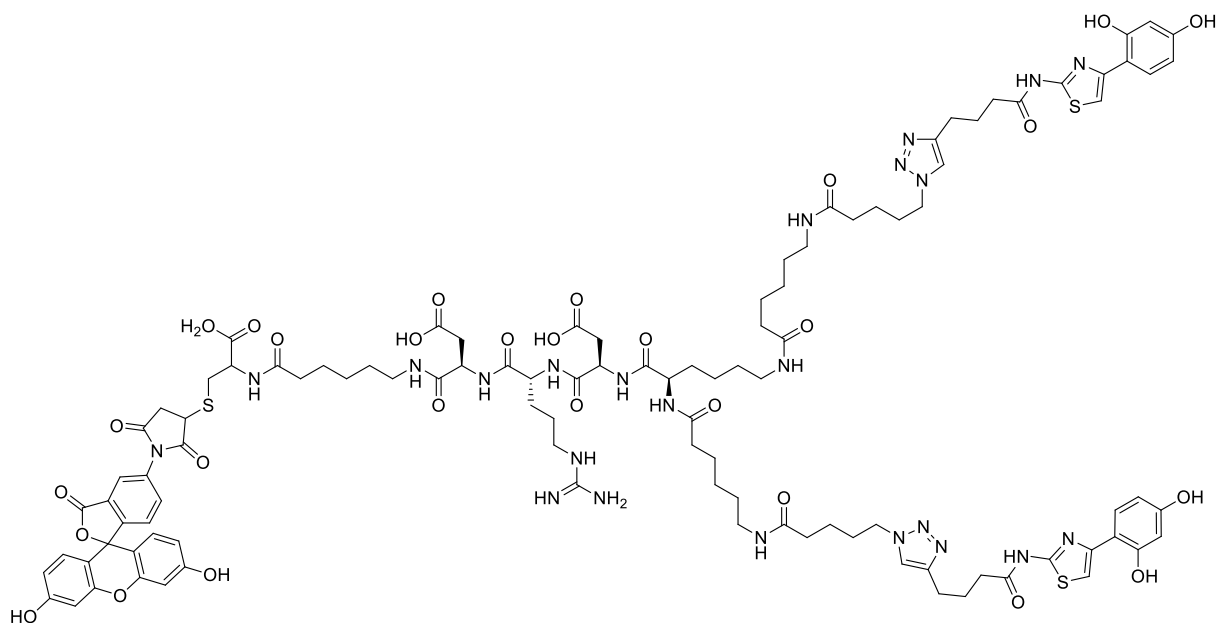


FI-medium_Dimer: to a solution of the so-obtained compound (3.2 mg, 1 equiv.) in dimethyl sulfoxide (100 μL) was added a 0.1 M solution of commercially available fluorescein-5-maleimide (0.8 mg, 1.0 equiv.) in dimethyl sulfoxide (20 μL). After stirring for 30 min in the dark, the reaction was quenched with the proper volume of DMSO:mqH₂O, injected and purified over a reversed-phase HPLC (Synergi RP Polar, 5% MeCN in 0.1% aq. TFA to 80% over 14 min). The fractions containing the product were identified by mass spectrometry, collected and lyophilized to give the title compound as a yellow solid.

HRMS (ES) calculated for [M+H]⁺ (m/z): 2031.6970, found 2031.6736.

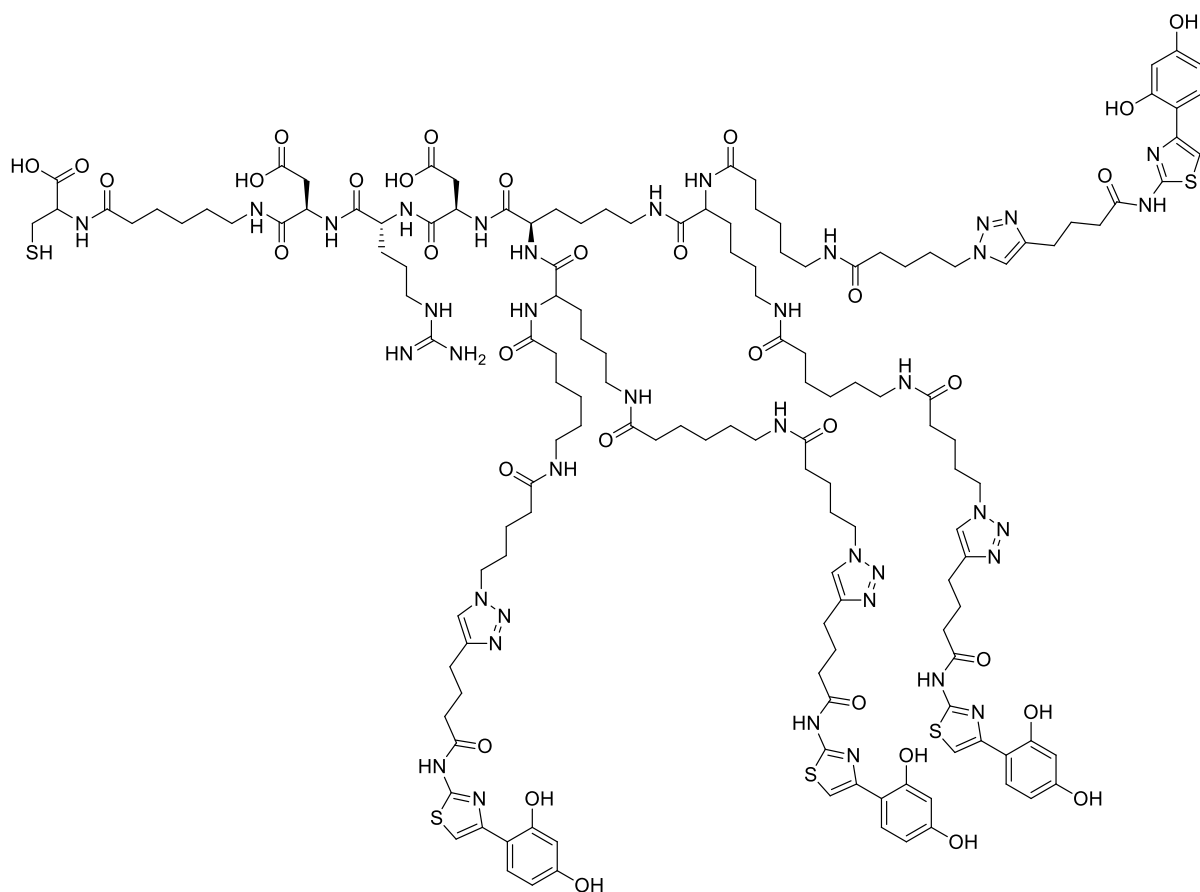
over a RP HPLC (Synergi RP Polar, 5% MeCN in 0.1% aq. TFA to 80% over 14 min), the fractions containing the product identified by mass spectrometry, collected and lyophilized to give the title compound as a white solid.

HRMS (ES) calculated for $[M+2H]^+$ (m/z): 1830.8004, found 1830.7086.



FI-long_Dimer: To a solution of the so-obtained compound (3.2 mg, 1 equiv.) in dimethyl sulfoxide (100 μ L) was added a 0.1 M solution of commercially available fluorescein-5-maleimide (0.8 mg, 1.0 equiv.) in dimethyl sulfoxide (20 μ L). After stirring for 30 min in the dark, the reaction was quenched with the proper volume of DMSO:mqH₂O, injected and purified over a reversed-phase HPLC (Synergi RP Polar, 5% MeCN in 0.1% aq. TFA to 80% over 14 min). The fractions containing the product were identified by mass spectrometry, collected and lyophilized to give the title compound as a yellow solid.

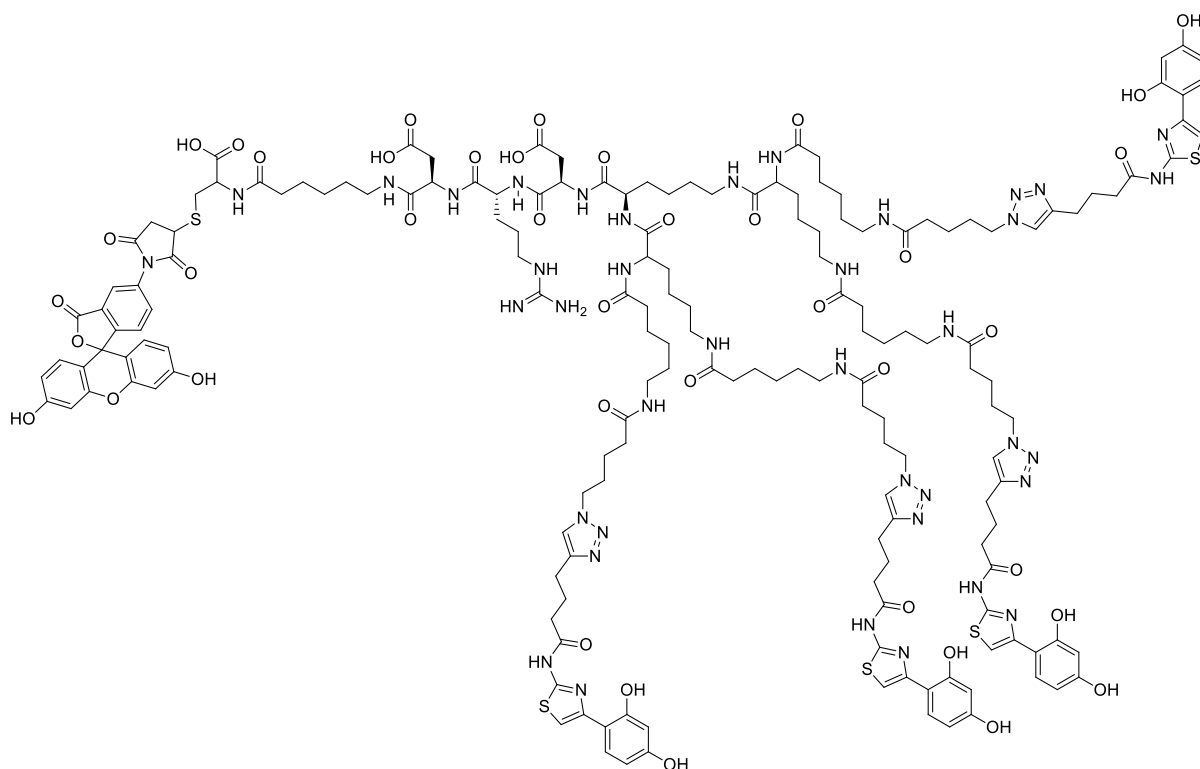
HRMS (ES) calculated for $[M+H]^+$ (m/z): 2257.8651, found 2258.0203.



Tetramer: after removing the Fmoc-group, 0.2 mmol of the resin was reacted with a solution of Fmoc-Lys(Fmoc)-OH (4 equiv., 0.8 mmol), DIPEA (8 equiv., 1.6 mmol) and HATU (4.0 equiv, 0.8 mmol) in *N,N*-dimethylformamide (8 mL) for 2 h. After washing with *N,N*-dimethylformamide ($5 \times 8 \text{ mL} \times 1 \text{ min}$) the peptide was extended with Fmoc-Lys(Fmoc)-OH, Fmoc-6-aminocaproic acid and then capped with 5-azido pentanoic acid fixing the coupling conditions (Fmoc-Lys(Fmoc)-OH and HATU 6 equiv., DIPEA 12 equiv., Fmoc-6-aminocaproic or 5-azido pentanoic and HATU 12 equiv., DIPEA 24 equiv.), using the same Fmoc deprotection conditions (20 % piperidine in DMF) and washing step mentioned before. After the last coupling step, the Cu-catalysed alkyne-azide cycloaddition was performed. A solution of sodium ascorbate (3 equiv.), 2,6-lutidine (30 equiv.) and DIPEA (30 equiv.) in degassed $\text{m}^{\text{q}}\text{H}_2\text{O}$ was added to a solution of CuI (3 equiv.) in *N,N*-dimethylformamide. The resulting solution and the alkyne (6 equiv.) were added to the resin and allowed to react for 16 h. After washing with *N,N*-dimethylformamide ($5 \times 8 \text{ mL} \times 1 \text{ min}$), 50 mM aq. EDTA solution pH = 8 ($5 \times 8 \text{ mL} \times 1 \text{ min}$), *N,N*-dimethylformamide ($5 \times 8 \text{ mL} \times 1 \text{ min}$) and dichloromethane ($5 \times 4 \text{ mL} \times 1 \text{ min}$), the resin was cleaved using a mixture of TFA (6.60 mL, 82.5 %), *m*-Cresol (400 mL, 5 %), thioanisol (400 mL, 5 %), $\text{m}^{\text{q}}\text{-H}_2\text{O}$ (400 mL, 5 %) and TIPS (200 mL, 2.5 %) for 2 h at room temperature and washed with TFA ($1 \times 4 \text{ mL} \times 1 \text{ min}$). The combined cleavage

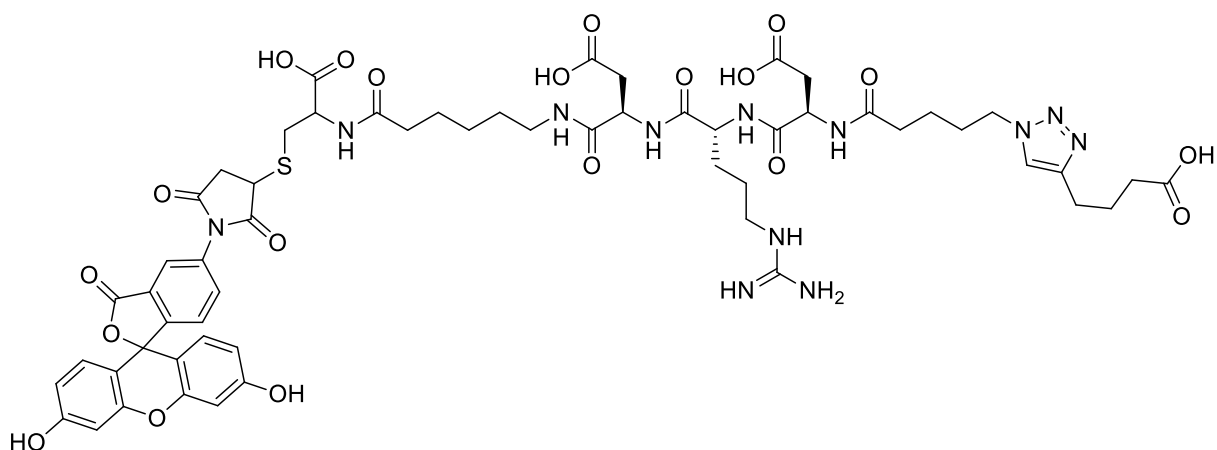
and washing solutions were added dropwise to ice cold diethyl ether (40 mL) leading to precipitate formation that was collected by centrifugation, washed again with ice cold diethyl ether ($3 \times 40 \text{ mL} \times 2 \text{ min}$, 2000 rpm), dried, re-dissolved in $\text{mqH}_2\text{O}:\text{DMSO}$ and treated with Tris(2-carboxyethyl)phosphine hydrochloride (2 equiv.). The solution was injected and purified over a RP HPLC (Synergi RP Polar, 5% MeCN in 0.1% aq. TFA to 80% over 14 min), the fractions containing the product identified by mass spectrometry, collected and lyophilized to give the title compound as a white solid.

HRMS (ES) calculated for $[\text{M}+2\text{H}]^+$ (m/z): 1584.2132, found 1584.2404.



FI-Tetramer: To a solution of the so-obtained compound (4.9 mg, 1 equiv.) in dimethyl sulfoxide (100 μL) was added a 0.1 M solution of commercially available fluorescein-5-maleimide (0.6 mg, 1.0 equiv.) in dimethyl sulfoxide (15.5 μL). After stirring for 30 min in the dark, the reaction was quenched with the proper volume of $\text{DMSO}:\text{mqH}_2\text{O}$, injected and purified over a reversed-phase HPLC (Synergi RP Polar, 5% MeCN in 0.1% aq. TFA to 80% over 14 min). The fractions containing the product were identified by mass spectrometry, collected and lyophilized to give the title compound as a yellow solid.

HRMS (ES) calculated for $[\text{M}+2\text{H}]^+$ (m/z):, 1797.7523 found 1798. 15.



negative control: after removing the Fmoc-group, 0.1 mmol of the obtained resin was reacted with a solution of 5-azido pentanoic acid (4 equiv., 0.4 mmol), DIPEA (8.0 equiv., 0.4 mmol) and HATU (4.0 equiv., 0.4 mmol) in *N,N*-dimethylformamide (4 mL) for 2 h. After washing with *N,N*-dimethylformamide ($5 \times 4 \text{ mL} \times 1 \text{ min}$) the Cu-catalysed alkyne-azide cycloaddition was performed. A solution of sodium ascorbate (1 equiv.), 2,6-lutidine (10 equiv.) and DIPEA (10 equiv.) in degassed mqH₂O was added to a solution of CuI (1.0 equiv.) in *N,N*-dimethylformamide. The resulting solution and the 5-hexynoic acid (2.0 equiv.) were added to the resin and allowed to react for 16 h. After washing with *N,N*-dimethylformamide ($5 \times 4 \text{ mL} \times 1 \text{ min}$), 50 mM aq. EDTA solution pH = 8 ($5 \times 4 \text{ mL} \times 1 \text{ min}$), *N,N*-dimethylformamide ($5 \times 4 \text{ mL} \times 1 \text{ min}$) and dichloromethane ($5 \times 4 \text{ mL} \times 1 \text{ min}$), the resin was cleaved using a mixture of TFA (3.30 mL, 82.5 %), *m*-Cresol (200 mL, 5 %), thioanisol (200 mL, 5 %), mq-H₂O (200 mL, 5 %) and TIPS (100 mL, 2.5 %) for 2 h at room temperature and then washed with TFA ($1 \times 1 \text{ mL} \times 1 \text{ min}$). The combined cleavage and washing solutions were added dropwise to ice cold diethyl ether (20 mL). The obtained precipitate was centrifuged, washed with ice cold diethyl ether ($3 \times 20 \text{ mL} \times 2 \text{ min}$, 2000 rpm), dried, re-dissolved in mqH₂O:DMSO and treated with Tris(2-carboxyethyl)phosphine hydrochloride (2 equiv.). This solution was injected and purified over a reversed-phase HPLC (Synergi RP Polar, 5% MeCN in 0.1% aq. TFA to 80% over 14 min), the fractions containing the product were identified by mass spectrometry collected and then lyophilized to give the title compound as a white solid.

To a solution of the so-obtained compound (2.0 mg, 1 equiv.) in dimethyl sulfoxide (100 μL) was added a 0.1 M solution of commercially available fluorescein-5-maleimide (1.0 mg, 1.0 equiv.) in DMSO (19.1 μL). After stirring for 30 min in the dark, the reaction was quenched with the proper volume of DMSO:mqH₂O, injected and purified over a reversed-phase HPLC (Synergi RP Polar, 5% MeCN in 0.1% aq. TFA to 80% over 14 min). The fractions containing

the product were identified by mass spectrometry, collected and lyophilized to give the title compound as a yellow solid.

HRMS (ES) calculated for $[M+H]^+$ (m/z): 1285.4472, found 1285.3888.

3.6.3. Biological evaluation

Enzymatic assay

The enzymatic activity of Tyrosinase was measured at 25 °C following already described procedures using L-DOPA as substrate [224,225]. In 384-well microtiter clear plates (Greiner non-binding), a mixture of 1 mM L-DOPA, 4 mM MBTH, 200 nM human Tyrosinase and the inhibitor was prepared (final volume 30 μ L in PBS 1% DMSO, pH=6.8). The increase of the absorption at 490-510 nm, due to the formation of the L-dopaquinone-MBTH complex, was recorded using a Spectra Max Paradigm multimode plate reader (Molecular Devices) over 10 minutes. Experiments were performed in duplicates and the values were fitted using Graphpad Prism software. The obtained OD values were plotted as a function of time. Linear regression of the plotted points was performed. IC₅₀ values were calculated fitting the obtained slope as function of the inhibitor concentration.

Fluorescence polarization

The dilution series were done in a non-binding black 384-well microplate (Greiner Bio On.). In a final volume of 30 μ L, 50 nM of the fluorescein-conjugated ligand was incubated with a 1:1 dilution series of TYRP1 in PBS pH 7.4. The fluorescence anisotropy was measured on a Spectra Max Paradigm multimode plate reader (Molecular Devices). Experiments were performed in triplicate and the anisotropy values fitted using Graphpad Prism software.

ELISA

The Enzyme-Linked ImmunoSorbent Assay (ELISA) was performed following already described procedures.[237] Nunc MaxiSorp™ ELISA stripes (ThermoFisher) were incubated over night at 4 °C with 100 μ L of 100 nM solution in PBS of protein (i.e., TYR and TYRP1). The supernatant was removed and 200 μ L of a 4% solution of Milk powder in PBS (M-PBS) was used as blocking agent for 30-45 minutes. Wells were then washed three times with 200 μ L PBS and dried. 50 μ L of a pre-made serial dilution of the fluorescein-ligand conjugate was added and incubated for 45 minutes in the dark. Carefully, the supernatant was removed and the wells were quickly washed twice with 200 μ L PBS. 100 μ L of anti-fluorescein IgG (200

nM) in 2% M-PBS were added and incubated for 45 minutes. The supernatant was removed and wells washed three times with 200 μ L PBS. 100 μ L of a solution of 1:1000 diluted enzyme-linked protein (i.e., proteinA-HRP) in 2% M-PBS was added and incubated for 45 minutes in the dark. The supernatant was removed and wells washed three times with 200 μ L of a 0.1% solution of Tween 20 in PBS and three times with PBS. Finally, 60 μ L of 3,3',5,5'-tetramethylbenzidine (TMB) was added to each well and left for 10 to 50 seconds at room temperature developing in the dark until formation of a visible intense blue. The reaction was then quenched upon addition of 30 μ L of 1 M $H_2SO_{4(aq)}$. Absorbance at 450 nm and 620 nm were measured with Spectra Max Paradigm multimode plate reader (Molecular Devices) and values were fitted using Graphpad Prism software.

Flow Cytometry

Adherent B16F10 cells cultured in T-150 flasks were detached with 2 mM EDTA. Resuspended cells are counted, centrifuged, and resuspended in FACS buffer (2 mM EDTA + 0.5% BSA in PBS, filtered solution) to reach a concentration of 2.5 Mio/mL. In 96-well plate (Greiner Bio On.), 500.000 cells were incubated with 10 μ M solutions of fluorescein linked ligands in FACS buffer. After 60 minutes, 1x wash was performed and then cells were incubated with Cy5-conjugated anti-Fluorescein IgG (100 nM) for 60 minutes. Cells were 2x washed and sorted by FACS (CytoFLEX, BeckmanCoulter, Brea, CA) and analyzed using FlowJo software (FlowJo,Ashland, OR).

Bibliography

- [1] C.T. Supuran, Exploring the multiple binding modes of inhibitors to carbonic anhydrases for novel drug discovery, *Expert Opin. Drug Discov.* 15 (2020) 671–686.
- [2] X. Wang, W. Conway, R. Burns, N. McCann, M. Maeder, Comprehensive study of the hydration and dehydration reactions of carbon dioxide in aqueous solution, *J. Phys. Chem. A.* 114 (2010) 1734–1740.
- [3] K.M. Gilmour, Perspectives on carbonic anhydrase, *Comp. Biochem. Physiol. Part A Mol. Integr. Physiol.* 157 (2010) 193–197.
- [4] C.T. Supuran, Carbonic anhydrases: From biomedical applications of the inhibitors and activators to biotechnological use for CO₂ capture, *J. Enzyme Inhib. Med. Chem.* 28 (2013) 229–230.
- [5] C.T. Supuran, Structure and function of carbonic anhydrases, *Biochem. J.* 473 (2016) 2023–2032.
- [6] S. Zimmerman, J. Ferry, The β and γ Classes of Carbonic Anhydrase, *Curr. Pharm. Des.* 14 (2008) 716–721.
- [7] C. Capasso, C.T. Supuran, An overview of the alpha-, beta- and gamma-carbonic anhydrases from Bacteria: Can bacterial carbonic anhydrases shed new light on evolution of bacteria?, *J. Enzyme Inhib. Med. Chem.* 30 (2015) 325–332.
- [8] J.G. Ferry, The γ class of carbonic anhydrases, *Biochim. Biophys. Acta - Proteins Proteomics.* 1804 (2010) 374–381.
- [9] S. Kikutani, K. Nakajima, C. Nagasato, Y. Tsuji, A. Miyatake, Y. Matsuda, Thylakoid luminal Θ -carbonic anhydrase critical for growth and photosynthesis in the marine diatom *Phaeodactylum tricornutum*, *Proc. Natl. Acad. Sci. U. S. A.* 113 (2016) 9828–9833.
- [10] S. Del Prete, D. Vullo, V. De Luca, C.T. Supuran, C. Capasso, Biochemical characterization of the δ -carbonic anhydrase from the marine diatom *Thalassiosira weissflogii*, *J. Enzyme Inhib. Med. Chem.* 29 (2014) 906–911.
- [11] S. Del Prete, D. Vullo, G.M. Fisher, K.T. Andrews, S.A. Poulsen, C. Capasso, C.T. Supuran, Discovery of a new family of carbonic anhydrases in the malaria pathogen

- Plasmodium falciparum - The η -carbonic anhydrases, *Bioorganic Med. Chem. Lett.* 24 (2014) 4389–4396.
- [12] C.T. Supuran, C. Capasso, The η -class carbonic anhydrases as drug targets for antimalarial agents, *Expert Opin. Ther. Targets.* 19 (2015) 551–563.
- [13] S. Del Prete, A. Nocentini, C.T. Supuran, C. Capasso, Bacterial ι -carbonic anhydrase: a new active class of carbonic anhydrase identified in the genome of the Gram-negative bacterium *Burkholderia territorii*, *J. Enzyme Inhib. Med. Chem.* 35 (2020) 1060–1068.
- [14] Y. Xu, L. Feng, P.D. Jeffrey, Y. Shi, F.M.M. Morel, Structure and metal exchange in the cadmium carbonic anhydrase of marine diatoms, *Nature.* 452 (2008) 56–61.
- [15] B.C. Tripp, C.B. Bell, F. Cruz, C. Krebs, J.G. Ferry, A Role for Iron in an Ancient Carbonic Anhydrase, *J. Biol. Chem.* 279 (2004) 6683–6687.
- [16] S.R. MacAuley, S.A. Zimmerman, E.E. Apolinario, C. Evilia, Y.M. Hou, J.G. Ferry, K.R. Sowers, The archetype γ -class carbonic anhydrase (cam) contains iron when synthesized in vivo, *Biochemistry.* 48 (2009) 817–819.
- [17] J.B. Hunt, M.J. Rhee, C.B. Storm, A rapid and convenient preparation of apocarbonic anhydrase, *Anal. Biochem.* 79 (1977) 614–617.
- [18] C.T. Supuran, Structure-based drug discovery of carbonic anhydrase inhibitors Structure-based drug discovery of carbonic anhydrase inhibitors, 6366 (2012).
- [19] C.T. Supuran, A. Scozzafava, Carbonic-anhydrase inhibitors and their therapeutic potential, *Expert Opin. Ther. Pat.* 10 (2000) 575–600.
- [20] J.E. Coleman, Zinc enzymes, *Curr. Opin. Chem. Biol.* 2 (1998) 222–234.
- [21] S. Lindskog, Structure and mechanism of carbonic anhydrase, *Pharmacol. Ther.* 74 (1997) 1–20.
- [22] D.A. Whittington, A. Waheed, B. Ulmasov, G.N. Shah, J.H. Grubb, W.S. Sly, D.W. Christianson, Crystal structure of the dimeric extracellular domain of human carbonic anhydrase XII, a bitopic membrane protein overexpressed in certain cancer tumor cells, *Proc. Natl. Acad. Sci. U. S. A.* 98 (2001) 9545–9550.
- [23] C.T. Supuran, Carbonic anhydrases: Novel therapeutic applications for inhibitors and activators, *Nat. Rev. Drug Discov.* 7 (2008) 168–181.

- [24] J.F. Domsic, B.S. Avvaru, U.K. Chae, S.M. Gruner, M. Agbandje-McKenna, D.N. Silverman, R. McKenna, Entrapment of carbon dioxide in the active site of carbonic anhydrase II, *J. Biol. Chem.* 283 (2008) 30766–30771.
- [25] B. Sjöblom, M. Polentarutti, K. Djinović-Carugo, Structural study of X-ray induced activation of carbonic anhydrase, *Proc. Natl. Acad. Sci. U. S. A.* 106 (2009) 10609–10613.
- [26] V. Alterio, A. Di Fiore, K. D’Ambrosio, C.T. Supuran, G. De Simone, Multiple binding modes of inhibitors to carbonic anhydrases: How to design specific drugs targeting 15 different isoforms?, *Chem. Rev.* 112 (2012) 4421–4468.
- [27] C. Lomelino, R. McKenna, Carbonic anhydrase inhibitors: a review on the progress of patent literature (2011–2016), *Expert Opin. Ther. Pat.* 26 (2016) 947–956.
- [28] B.S. Avvaru, C.U. Kim, K.H. Sippel, S.M. Gruner, M. Agbandje-McKenna, D.N. Silverman, R. McKenna, A Short, Strong Hydrogen Bond in the Active Site of Human Carbonic Anhydrase II, *Biochemistry.* 49 (2010) 249–251.
- [29] C.M. Maupin, N. Castillo, S. Taraphder, C. Tu, R. McKenna, D.N. Silverman, G.A. Voth, Chemical rescue of enzymes: Proton transfer in mutants of human carbonic anhydrase II, *J. Am. Chem. Soc.* 133 (2011) 6223–6234.
- [30] C. Forsman, B. Jonsson, S. Lindskog, Role of Histidine 64 in the Catalytic Mechanism of Human Carbonic Anhydrase II Studied with a Site-Specific Mutant?, 28 (1989) 7913–7918.
- [31] J. Vidgren, A. Liljas, N.P.C. Walker, Refined structure of the acetazolamide complex of human carbonic anhydrase II at 1.9 Å, *Int. J. Biol. Macromol.* 12 (1990) 342–344.
- [32] H. An, C. Tu, K. Ren, P.J. Laipis, D.N. Silverman, Proton transfer within the active-site cavity of carbonic anhydrase III, *Biochim. Biophys. Acta - Proteins Proteomics.* 1599 (2002) 21–27.
- [33] V. De Luca, D. Vullo, A. Scozzafava, V. Carginale, M. Rossi, C.T. Supuran, C. Capasso, An α -carbonic anhydrase from the thermophilic bacterium *Sulphurihydrogenibium azorense* is the fastest enzyme known for the CO₂ hydration reaction, *Bioorganic Med. Chem.* 21 (2013) 1465–1469.
- [34] M. Aggarwal, C.D. Boone, B. Kondeti, R. McKenna, Structural annotation of human

- carbonic anhydrases, *J. Enzyme Inhib. Med. Chem.* 28 (2012) 267–277.
- [35] I. Nishimori, D. Vullo, T. Minakuchi, A. Scozzafava, C. Capasso, C.T. Supuran, Restoring catalytic activity to the human carbonic anhydrase (CA) related proteins VIII, X and XI affords isoforms with high catalytic efficiency and susceptibility to anion inhibition, *Bioorganic Med. Chem. Lett.* 23 (2013) 256–260.
- [36] V. Alterio, M. Hilvo, A. Di Fiore, C.T. Supuran, P. Pan, S. Parkkila, A. Scaloni, J. Pastorek, S. Pastorekova, C. Pedone, A. Scozzafava, S.M. Monti, G. De Simone, Crystal structure of the catalytic domain of the tumor-associated human carbonic anhydrase IX, *Proc. Natl. Acad. Sci. U. S. A.* 106 (2009) 16233–16238.
- [37] S. Zamanova, A.M. Shabana, U.K. Mondal, M.A. Ilies, Carbonic anhydrases as disease markers, *Expert Opin. Ther. Pat.* 29 (2019) 509–533.
- [38] N. Robertson, C. Potter, A.L. Harris, Role of carbonic anhydrase IX in human tumor cell growth, survival, and invasion, *Cancer Res.* 64 (2004) 6160–6165.
- [39] S. Pastorekova, J. Kopacek, J. Pastorek, Carbonic Anhydrase Inhibitors and the Management of Cancer, *Curr. Top. Med. Chem.* 7 (2007) 865–878.
- [40] S. Durdagi, D. Vullo, P. Pan, N. Kähkönen, J.A. Määttä, V.P. Hytönen, A. Scozzafava, S. Parkkila, C.T. Supuran, Protein-protein interactions: Inhibition of mammalian carbonic anhydrases I-XV by the murine inhibitor of carbonic anhydrase and other members of the transferrin family, *J. Med. Chem.* 55 (2012) 5529–5535.
- [41] M. Imtaiyaz Hassan, B. Shajee, A. Waheed, F. Ahmad, W.S. Sly, Structure, function and applications of carbonic anhydrase isozymes, *Bioorganic Med. Chem.* 21 (2013) 1570–1582.
- [42] H.M. Becker, M. Klier, J.W. Deitmer, *Carbonic Anhydrase: Mechanism, Regulation, Links to Disease, and Industrial Applications*, 2014.
- [43] Y.C. Chai, C.H. Jung, C.K. Lii, S.S. Ashraf, S. Hendrich, B. Wolf, H. Sies, J.A. Thomas, Identification of an abundant S-thiolated rat liver protein as carbonic anhydrase III; characterization of S-thiolation and dethiolation reactions, *Arch. Biochem. Biophys.* 284 (1991) 270–278.
- [44] C.K. Lii, Y.C. Chai, W. Zhao, J.A. Thomas, S. Hendrich, S-Thiolation and Irreversible Oxidation of Sulfhydryls on Carbonic Anhydrase III during Oxidative Stress: A Method

- for Studying Protein Modification in Intact Cells and Tissues, *Arch. Biochem. Biophys.* 308 (1994) 231–239.
- [45] A. Waheed, W.S. Sly, Membrane Associated Carbonic Anhydrase IV (CA IV): A Personal and Historical Perspective, in: *Subcell. Biochem.*, 2014: pp. 157–179.
- [46] C.T. Supuran, Carbonic anhydrase inhibitors in the treatment and prophylaxis of obesity, *Expert Opin. Ther. Pat.* 13 (2003) 1545–1550.
- [47] F. Frassetto, T.M. Parisotto, R.C.R. Peres, M.R. Marques, S.R.P. Line, M. Nobre Dos Santos, Relationship among salivary carbonic anhydrase VI activity and flow rate, biofilm pH and caries in primary dentition, *Caries Res.* 46 (2012) 194–200.
- [48] A. Thiry, J.-M. Dogne, C. Supuran, B. Masereel, Carbonic Anhydrase Inhibitors as Anticonvulsant Agents, *Curr. Top. Med. Chem.* 7 (2007) 855–864.
- [49] A. Aspatwar, M. E.E. Tolvanen, C. Ortutay, S. Parkkila, Carbonic Anhydrase Related Protein VIII and its Role in Neurodegeneration and Cancer, *Curr. Pharm. Des.* 16 (2010) 3264–3276.
- [50] A. Di Fiore, S.M. Monti, M. Hilvo, S. Parkkila, V. Romano, A. Scaloni, C. Pedone, A. Scozzafava, C.T. Supuran, G. De Simone, Crystal structure of human carbonic anhydrase XIII and its complex with the inhibitor acetazolamide, *Proteins Struct. Funct. Bioinforma.* 74 (2009) 164–175.
- [51] C. T. Supuran, A. Di Fiore, V. Alterio, S. Maria Montib, G. De Simone, Recent Advances in Structural Studies of the Carbonic Anhydrase Family: The Crystal Structure of Human CA IX and CA XIII, *Curr. Pharm. Des.* 16 (2010) 3246–3254.
- [52] J. Pastorek, S. Pastorekova, M. Zatovicova, Cancer-Associated Carbonic Anhydrases and Their Inhibition, *Curr. Pharm. Des.* 14 (2008) 685–698.
- [53] A. Innocenti, S. Pastorekova, J. Pastorek, A. Scozzafava, G. De Simone, C.T. Supuran, The proteoglycan region of the tumor-associated carbonic anhydrase isoform IX acts as an intrinsic buffer optimizing CO₂ hydration at acidic pH values characteristic of solid tumors, *Bioorganic Med. Chem. Lett.* 19 (2009) 5825–5828.
- [54] G. De Simone, C.T. Supuran, Carbonic anhydrase IX: Biochemical and crystallographic characterization of a novel antitumor target, *Biochim. Biophys. Acta - Proteins Proteomics.* 1804 (2010) 404–409.

- [55] S. Pastorekova, S. Parkkila, A.K. Parkkila, R. Opavsky, V. Zelnik, J. Saarnio, J. Pastorek, Carbonic anhydrase IX, MN/CA IX: Analysis of stomach complementary DNA sequence and expression in human and rat alimentary tracts, *Gastroenterology*. 112 (1997) 398–408.
- [56] J. Tostain, G. Li, A. Gentil-Perret, M. Gigante, Carbonic anhydrase 9 in clear cell renal cell carcinoma: A marker for diagnosis, prognosis and treatment, *Eur. J. Cancer*. 46 (2010) 3141–3148.
- [57] C.T. Supuran, V. Alterio, A. Di Fiore, K. D' Ambrosio, F. Carta, S.M. Monti, G. De Simone, Inhibition of carbonic anhydrase IX targets primary tumors, metastases, and cancer stem cells: Three for the price of one, *Med. Res. Rev.* 38 (2018) 1799–1836.
- [58] C.C. Wykoff, N.J.P. Beasley, P.H. Watson, K.J. Turner, J. Pastorek, A. Sibtain, G.D. Wilson, H. Turley, K.L. Talks, P.H. Maxwell, C.W. Pugh, P.J. Ratcliffe, A.L. Harris, Hypoxia-inducible expression of tumor-associated carbonic anhydrases, *Cancer Res.* 60 (2000) 7075–7083.
- [59] J.R. Gnarra, K. Tory, Y. Weng, L. Schmidt, M. H. Wei, H. Li, F. Laifti, S. Liu, F. Chen, F. M. Duh, I Lubensky, D. R. Duan, C. Florence, R. Pozzatti, M.M. Walther, N.H. Banders, H.B. Grossman, H. Brauch, S. Pomer, J.D. Brooks, W.B. Isaacs, M.I. Lerman, B. Zbar, W.M. Linehan, Mutations of the VHL tumour suppressor gene in renal carcinoma, *Nature* 7 (1994) 85–90.
- [60] F. Cianchi, M.C. Vinci, C.T. Supuran, B. Peruzzi, P. De Giuli, G. Fasolis, G. Perigli, S. Pastorekova, L. Papucci, A. Pini, E. Masini, L. Puccetti, Selective inhibition of carbonic anhydrase IX decreases cell proliferation and induces ceramide-mediated apoptosis in human cancer cells, *J. Pharmacol. Exp. Ther.* 334 (2010) 710–719.
- [61] A.B. Stillebroer, P.F.A. Mulders, O.C. Boerman, W.J.G. Oyen, E. Oosterwijk, Carbonic Anhydrase IX in Renal Cell Carcinoma: Implications for Prognosis, Diagnosis, and Therapy, *Eur. Urol.* 58 (2010) 75–83.
- [62] B.P. Mahon, M.A. Pinard, R. McKenna, Targeting carbonic anhydrase IX activity and expression, *Molecules*. 20 (2015) 2323–2348.
- [63] J. Kazokaitė, A. Aspatwar, S. Parkkila, D. Matulis, An update on anticancer drug development and delivery targeting carbonic anhydrase IX, *PeerJ*. 2017 (2017) 1–31.

- [64] Y. Li, H. Wang, E. Oosterwijk, C. Tu, K.T. Shiverick, D.N. Silverman, S.C. Frost, Expression and activity of carbonic anhydrase IX is associated with metabolic dysfunction in MDA-MB-231 breast cancer cells, *Cancer Invest.* 27 (2009) 613–623.
- [65] J. Pastorek, S. Pastorekova, Hypoxia-induced carbonic anhydrase IX as a target for cancer therapy: From biology to clinical use, *Semin. Cancer Biol.* 31 (2015) 52–64
- [66] S.J.A. Van Kuijk, A. Yaromina, R. Houben, R. Niemans, P. Lambin, L.J. Dubois, Prognostic significance of carbonic anhydrase IX expression in cancer patients: A meta-analysis, *Front. Oncol.* 6 (2016) 1–16.
- [67] M. Takacova, M. Barathova, M. Zatovicova, T. Golias, I. Kajanova, L. Jelenska, O. Sedlakova, E. Svastova, J. Kopacek, S. Pastorekova, Carbonic anhydrase IX—mouse versus human, *Int. J. Mol. Sci.* 21 (2020) 1–21.
- [68] S. Singh, C.L. Lomelino, M.Y. Mboge, S.C. Frost, R. McKenna, Cancer drug development of carbonic anhydrase inhibitors beyond the active site, *Molecules.* 23 (2018).
- [69] A. Nocentini, C.T. Supuran, Carbonic anhydrase inhibitors as antitumor/antimetastatic agents: a patent review (2008–2018), *Expert Opin. Ther. Pat.* 28 (2018) 729–740.
- [70] Ö. Türeci, U. Sahin, E. Vollmar, S. Siemer, E. Göttert, G. Seitz, A.K. Parkkila, G.N. Shah, J.H. Grubb, M. Pfreundschuh, W.S. Sly, Human carbonic anhydrase XII: cDNA cloning, expression, and chromosomal localization of a carbonic anhydrase gene that is overexpressed in some renal cell cancers, *Proc. Natl. Acad. Sci. U. S. A.* 95 (1998) 7608–7613.
- [71] A. Waheed, W.S. Sly, Carbonic anhydrase XII functions in health and disease, *Gene.* 623 (2017) 33–40.
- [72] S.M. Monti, C.T. Supuran, G. De Simone, Anticancer carbonic anhydrase inhibitors: A patent review (2008-2013), *Expert Opin. Ther. Pat.* 23 (2013) 737–749.
- [73] J. Chiche, K. Ilc, J. Laferrière, E. Trottier, F. Dayan, N.M. Mazure, M.C. Brahimi-Horn, J. Pouyssegur, Hypoxia-inducible carbonic anhydrase IX and XII promote tumor cell growth by counteracting acidosis through the regulation of the intracellular pH, *Cancer Res.* 69 (2009) 358–368.
- [74] N.C. Denko, Metabolism in the Solid Tumour, *Nat. Rev. Cancer.* 8 (2008) 705–713.

- [75] J. Li, G. Zhang, X. Wang, X.F. Li, Is carbonic anhydrase IX a validated target for molecular imaging of cancer and hypoxia?, *Futur. Oncol.* 11 (2015) 1531–1541.
- [76] J. Welte, S. Loges, S. Dimmeler, P. Carmeliet, Recent molecular discoveries in angiogenesis and antiangiogenic therapies in cancer, *J. Clin. Invest.* 123 (2013) 3190.
- [77] S.K. Parks, J. Chiche, J. Pouyssegur, Disrupting proton dynamics and energy metabolism for cancer therapy, *Nat. Rev. Cancer.* 13 (2013) 611–623.
- [78] C.T. Supuran, Carbonic anhydrase inhibition and the management of hypoxic tumors, *Metabolites.* 7 (2017).
- [79] S. Weinhouse, O. Warburg, D. Burk, A.L. Schade, On Respiratory Impairment in Cancer Cells, *Science* 124 (1956) 267–272.
- [80] B.P. Mahon, A. Bhatt, L. Socorro, J.M. Driscoll, C. Okoh, C.L. Lomelino, M.Y. Mboge, J.J. Kurian, C. Tu, M. Agbandje-Mckenna, S.C. Frost, R. McKenna, The Structure of Carbonic Anhydrase IX Is Adapted for Low-pH Catalysis, *Biochemistry.* 55 (2016) 4642–4653.
- [81] M.G. Vander Heiden, L.C. Cantley, C.B. Thompson, Understanding the Warburg Effect: The Metabolic Requirements of Cell Proliferation, *Science* 324 (2009) 1029–1033.
- [82] D. Neri, C.T. Supuran, Interfering with pH regulation in tumours as a therapeutic strategy, *Nat. Rev. Drug Discov.* 10 (2011) 767–777.
- [83] O. Sedlakova, Carbonic anhydrase IX, a hypoxia-induced catalytic component of the pH regulating machinery in tumors, *Front. Physiol.* 4 (2014) 1–14.
- [84] H.M. Becker, Carbonic anhydrase IX and acid transport in cancer, *Br. J. Cancer.* 122 (2020) 157–167.
- [85] H.M. Becker, J.W. Deitmer, Transport metabolons and acid/base balance in tumor cells, *Cancers (Basel).* 12 (2020) 1–18.
- [86] P. Swietach, R.D. Vaughan-Jones, A.L. Harris, Regulation of tumor pH and the role of carbonic anhydrase 9, *Cancer Metastasis Rev.* 26 (2007) 299–310.
- [87] S.H. Lee, D. McIntyre, D. Honess, A. Hulikova, J. Pacheco-Torres, S. Cerdán, P. Swietach, A.L. Harris, J.R. Griffiths, Carbonic anhydrase IX is a pH-stat that sets an acidic tumour extracellular pH in vivo, *Br. J. Cancer.* 119 (2018) 622–630.

- [88] C. Corbet, O. Feron, Tumour acidosis: From the passenger to the driver's seat, *Nat. Rev. Cancer*. 17 (2017) 577–593.
- [89] M. Mboge, B. Mahon, R. McKenna, S. Frost, Carbonic Anhydrases: Role in pH Control and Cancer, *Metabolites*. 8 (2018) 19.
- [90] M. Stubbs, P.M.J. McSheehy, J.R. Griffiths, C.L. Bashford, Causes and consequences of tumour acidity and implications for treatment, *Mol. Med. Today*. 6 (2000) 15–19.
- [91] J.W. Wojtkowiak, D. Verduzco, K.J. Schramm, R.J. Gillies, Drug resistance and cellular adaptation to tumor acidic pH microenvironment, *Mol. Pharm.* 8 (2011) 2032–2038.
- [92] C. Daniel, C. Bell, C. Burton, S. Harguindey, S.J. Reshkin, C. Rauch, The role of proton dynamics in the development and maintenance of multidrug resistance in cancer, *Biochim. Biophys. Acta - Mol. Basis Dis.* 1832 (2013) 606–617.
- [93] P.C. McDonald, J.Y. Winum, C.T. Supuran, S. Dedhar, Recent developments in targeting carbonic anhydrase IX for cancer therapeutics, *Oncotarget*. 3 (2012) 84–97.
- [94] S.K. Parks, J. Chiche, J. Pouyssegur, pH control mechanisms of tumor survival and growth, *J. Cell. Physiol.* 226 (2011) 299–308.
- [95] M.K. Sun, D.L. Alkon, Carbonic anhydrase gating of attention: Memory therapy and enhancement, *Trends Pharmacol. Sci.* 23 (2002) 83–89.
- [96] C.T. Supuran, Carbonic anhydrase activators, *Future Med. Chem.* 10 (2018) 561–573.
- [97] F. Carta, C.T. Supuran, Diuretics with carbonic anhydrase inhibitory action: A patent and literature review (2005-2013), *Expert Opin. Ther. Pat.* 23 (2013) 681–691.
- [98] E. Masini, F. Carta, A. Scozzafava, C.T. Supuran, Antiglaucoma carbonic anhydrase inhibitors: A patent review, *Expert Opin. Ther. Pat.* 23 (2013) 705–716.
- [99] C.T. Supuran, How many carbonic anhydrase inhibition mechanisms exist?, *J. Enzyme Inhib. Med. Chem.* 31 (2016) 345–360.
- [100] J.Y. Winum, J.L. Montero, A. Scozzafava, C.T. Supuran, Zinc Binding Functions in the Design of Carbonic Anhydrase Inhibitors, *Drug Des. Zinc-Enzyme Inhib. Funct. Struct. Dis. Appl.* (2009) 39–72.
- [101] C. Temperini, A. Scozzafava, C.T. Supuran, Carbonic anhydrase inhibitors. X-ray crystal studies of the carbonic anhydrase II–trithiocarbonate adduct—An inhibitor

- mimicking the sulfonamide and urea binding to the enzyme, *Bioorg. Med. Chem. Lett.* 20 (2010) 474–478.
- [102] F. Carta, M. Aggarwal, A. Maresca, A. Scozzafava, R. McKenna, C.T. Supuran, Dithiocarbamates: A new class of carbonic anhydrase inhibitors. Crystallographic and kinetic investigations, *Chem. Commun.* 48 (2012) 1868–1870.
- [103] F. Carta, A. Akdemir, A. Scozzafava, E. Masini, C.T. Supuran, Xanthates and trithiocarbonates strongly inhibit carbonic anhydrases and show antiglaucoma effects in vivo, *J. Med. Chem.* 56 (2013) 4691–4700.
- [104] A. Scozzafava, C.T. Supuran, Hydroxyurea is a carbonic anhydrase inhibitor, *Bioorganic Med. Chem.* 11 (2003) 2241–2246.
- [105] A. Di Fiore, A. Maresca, C.T. Supuran, G. De Simone, Hydroxamate represents a versatile zinc binding group for the development of new carbonic anhydrase inhibitors, *Chem. Commun.* 48 (2012) 8838–8840.
- [106] F. Carta, A. Scozzafava, C.T. Supuran, Sulfonamides: a patent review (2008 – 2012), *Expert Opin. Ther. Pat.* 22 (2012) 747–758.
- [107] S.K. Nair, P.A. Ludwig, D.W. Christianson, Two-Site Binding of Phenol in the Active Site of Human Carbonic Anhydrase II: Structural Implications for Substrate Association, *J. Am. Chem. Soc.* 116 (1994) 3659–3660.
- [108] F. Carta, C. Temperini, A. Innocenti, A. Scozzafava, K. Kaila, C.T. Supuran, Polyamines Inhibit Carbonic Anhydrases by Anchoring to the Zinc-Coordinated Water Molecule, *J. Med. Chem.* 53 (2010) 5511–5522.
- [109] A. Maresca, C. Temperini, H. Vu, N.B. Pham, S.A. Poulsen, A. Scozzafava, R.J. Quinn, C.T. Supuran, Non-zinc mediated inhibition of carbonic anhydrases: Coumarins are a new class of suicide inhibitors, *J. Am. Chem. Soc.* 131 (2009) 3057–3062.
- [110] A. Maresca, C. Temperini, L. Pochet, B. Masereel, A. Scozzafava, C.T. Supuran, Deciphering the mechanism of carbonic anhydrase inhibition with coumarins and thiocoumarins, *J. Med. Chem.* 53 (2010) 335–344.
- [111] K. D'Ambrosio, S. Carradori, S.M. Monti, M. Buonanno, D. Secci, D. Vullo, C.T. Supuran, G. De Simone, Out of the active site binding pocket for carbonic anhydrase inhibitors, *Chem. Commun.* 51 (2015) 302–305.

- [112] M. D'Ascenzio, S. Carradori, C. De Monte, D. Secci, M. Ceruso, C.T. Supuran, Design, synthesis and evaluation of N-substituted saccharin derivatives as selective inhibitors of tumor-associated carbonic anhydrase XII, *Bioorganic Med. Chem.* 22 (2014) 1821–1831.
- [113] C. De Monte, S. Carradori, D. Secci, M. D'Ascenzio, D. Vullo, M. Ceruso, C.T. Supuran, Cyclic tertiary sulfamates: Selective inhibition of the tumor-associated carbonic anhydrases IX and XII by N- and O-substituted acesulfame derivatives, *Eur. J. Med. Chem.* 84 (2014) 240–246.
- [114] S. Carradori, D. Secci, C. De Monte, A. Mollica, M. Ceruso, A. Akdemir, A.P. Sobolev, R. Codispoti, F. De Cosmi, P. Guglielmi, C.T. Supuran, A novel library of saccharin and acesulfame derivatives as potent and selective inhibitors of carbonic anhydrase IX and XII isoforms, *Bioorg. Med. Chem.* 24 (2016) 1095–1105.
- [115] M. D'Ascenzio, D. Secci, S. Carradori, S. Zara, P. Guglielmi, R. Cirilli, M. Pierini, G. Poli, T. Tuccinardi, A. Angeli, C.T. Supuran, 1,3-Dipolar Cycloaddition, HPLC Enantioseparation, and Docking Studies of Saccharin/Isoxazole and Saccharin/Isoxazoline Derivatives as Selective Carbonic Anhydrase IX and XII Inhibitors, *J. Med. Chem.* 63 (2020) 2470–2488.
- [116] F. Pacchiano, F. Carta, P.C. McDonald, Y. Lou, D. Vullo, A. Scozzafava, S. Dedhar, C.T. Supuran, Ureido-substituted benzenesulfonamides potently inhibit carbonic anhydrase IX and show antimetastatic activity in a model of breast cancer metastasis, *J. Med. Chem.* 54 (2011) 1896–1902.
- [117] C.T. Supuran, Carbonic anhydrase inhibitors as emerging agents for the treatment and imaging of hypoxic tumors, *Expert Opin. Investig. Drugs.* 27 (2018) 963–970.
- [118] A. Nocentini, C.T. Supuran, Advances in the structural annotation of human carbonic anhydrases and impact on future drug discovery, *Expert Opin. Drug Discov.* 14 (2019) 1175–1197.
- [119] F. Abbate, A. Casini, T. Owa, A. Scozzafava, C.T. Supuran, Carbonic anhydrase inhibitors: E7070, a sulfonamide anticancer agent, potently inhibits cytosolic isozymes I and II, and transmembrane, tumor-associated isozyme IX, *Bioorganic Med. Chem. Lett.* 14 (2004) 217–223.
- [120] B.P. Mahon, A.M. Hendon, J.M. Driscoll, G.M. Rankin, S.A. Poulsen, C.T. Supuran, R.

- McKenna, Saccharin: A lead compound for structure-based drug design of carbonic anhydrase IX inhibitors, *Bioorganic Med. Chem.* 23 (2015) 849–854.
- [121] K. Köhler, A. Hillebrecht, J. Schulze Wischeler, A. Innocenti, A. Heine, C.T. Supuran, G. Klebe, Saccharin inhibits carbonic anhydrases: Possible explanation for its unpleasant metallic aftertaste, *Angew. Chemie - Int. Ed.* 46 (2007) 7697–7699.
- [122] A.B. Murray, C.L. Lomelino, C.T. Supuran, R. McKenna, “seriously Sweet”: Acesulfame K Exhibits Selective Inhibition Using Alternative Binding Modes in Carbonic Anhydrase Isoforms, *J. Med. Chem.* 61 (2018) 1176–1181.
- [123] G. Rotondi, P. Guglielmi, S. Carradori, D. Secci, C. De Monte, B. De Filippis, C. Maccallini, R. Amoroso, R. Cirilli, A. Akdemir, A. Angeli, C.T. Supuran, Design, synthesis and biological activity of selective hCAs inhibitors based on 2-(benzylsulfinyl)benzoic acid scaffold, *J. Enzyme Inhib. Med. Chem.* 34 (2019) 1400–1413.
- [124] F.M.F. Chen, N.L. Benoiton, The preparation and reactions of mixed anhydrides of N-alkoxycarbonylamino acids, *Can. J. Chem.* 65 (1987) 619–625.
- [125] T. Soeta, S. Matsuzaki, Y. Ukaji, A one-pot O -sulfinate passerini/oxidation reaction: Synthesis of α -(sulfonyloxy)amide derivatives, *J. Org. Chem.* 80 (2015) 3688–3694.
- [126] R.G. Khalifah, The Carbon Dioxide Hydration Activity of Carbonic Anhydrase., *J. Biol. Chem.* 246 (1971) 2561–2573.
- [127] H.C. Cheng, The power issue: Determination of KB or Ki from IC50 - A closer look at the Cheng-Prusoff equation, the Schild plot and related power equations, *J. Pharmacol. Toxicol. Methods.* 46 (2001) 61–71.
- [128] R.G. Gieling, M. Babur, L. Mamnani, N. Burrows, B.A. Telfer, F. Carta, J.Y. Winum, A. Scozzafava, C.T. Supuran, K.J. Williams, Antimetastatic effect of sulfamate carbonic anhydrase IX inhibitors in breast carcinoma xenografts, *J. Med. Chem.* 55 (2012) 5591–5600.
- [129] S. Carradori, A. Mollica, M. Ceruso, M. D’Ascenzio, C. De Monte, P. Chimenti, R. Sabia, A. Akdemir, C.T. Supuran, New amide derivatives of Probenecid as selective inhibitors of carbonic anhydrase IX and XII: Biological evaluation and molecular modelling studies, *Bioorganic Med. Chem.* 23 (2015) 2975–2981.

- [130] P. Guglielmi, G. Rotondi, D. Secci, A. Angeli, P. Chimenti, A. Nocentini, A. Bonardi, P. Gratteri, S. Carradori, C.T. Supuran, Novel insights on saccharin- and acesulfame-based carbonic anhydrase inhibitors: design, synthesis, modelling investigations and biological activity evaluation, *J. Enzyme Inhib. Med. Chem.* 35 (2020) 1891–1905.
- [131] S. Carradori, P. Guglielmi, Mechanisms of action of carbonic anhydrase inhibitors: Compounds that bind “out of the binding site” and compounds with an unknown mechanism of action, Elsevier Inc., 2019.
- [132] A. Scozzafava, F. Carta, C.T. Supuran, Secondary and tertiary sulfonamides: a patent, *Expert Opin Ther Patents.* 23 (2013) 203–213.
- [133] V. Coviello, B. Marchi, S. Sartini, L. Quattrini, A.M. Marini, F. Simorini, S. Taliani, S. Salerno, P. Orlandi, A. Fioravanti, T. Di Desidero, D. Vullo, F. Da Settimo, C.T. Supuran, G. Bocci, C. La Motta, 1,2-Benzisothiazole Derivatives Bearing 4-, 5-, or 6-Alkyl/arylcarboxamide Moieties Inhibit Carbonic Anhydrase Isoform IX (CAIX) and Cell Proliferation under Hypoxic Conditions, *J. Med. Chem.* 59 (2016) 6547–6552.
- [134] A. Zubriene, E. Čapkauskaitė, J. Gylyte, M. Kišonaite, S. Tumkevičius, D. Matulis, Benzenesulfonamides with benzimidazole moieties as inhibitors of carbonic anhydrases I, II, VII, XII and XIII, *J. Enzyme Inhib. Med. Chem.* 29 (2014) 124–131.
- [135] J. Ivanova, J. Leitans, M. Tanc, A. Kazaks, R. Zalubovskis, C.T. Supuran, K. Tars, X-ray crystallography-promoted drug design of carbonic anhydrase inhibitors, *Chem. Commun.* 51 (2015) 7108–7111.
- [136] V. Alterio, M. Tanc, J. Ivanova, R. Zalubovskis, I. Vozny, S.M. Monti, A. Di Fiore, G. De Simone, C.T. Supuran, X-ray crystallographic and kinetic investigations of 6-sulfamoyl-saccharin as a carbonic anhydrase inhibitor, *Org. Biomol. Chem.* 13 (2015) 4064–4069.
- [137] J. Ivanova, F. Carta, D. Vullo, J. Leitans, A. Kazaks, K. Tars, R. Žalubovskis, C.T. Supuran, N-Substituted and ring opened saccharin derivatives selectively inhibit transmembrane, tumor-associated carbonic anhydrases IX and XII, *Bioorganic Med. Chem.* 25 (2017) 3583–3589.
- [138] M. D’ascenzio, P. Guglielmi, S. Carradori, D. Secci, R. Florio, A. Mollica, M. Ceruso, A. Akdemir, A.P. Sobolev, C.T. Supuran, Open saccharin-based secondary sulfonamides as potent and selective inhibitors of cancer-related carbonic anhydrase IX and XII

- isoforms, *J. Enzyme Inhib. Med. Chem.* 32 (2017) 51–59.
- [139] N.R. Uda, V. Seibert, F. Stenner-Liewen, P. Müller, P. Herzig, G. Gondi, R. Zeidler, M. Van Dijk, A. Zippelius, C. Renner, Esterase activity of carbonic anhydrases serves as surrogate for selecting antibodies blocking hydratase activity, *J. Enzyme Inhib. Med. Chem.* 30 (2015) 955–960.
- [140] A. Nocentini, M. Ferraroni, F. Carta, M. Ceruso, P. Gratteri, C. Lanzi, E. Masini, C.T. Supuran, Benzenesulfonamides Incorporating Flexible Triazole Moieties Are Highly Effective Carbonic Anhydrase Inhibitors: Synthesis and Kinetic, Crystallographic, Computational, and Intraocular Pressure Lowering Investigations, *J. Med. Chem.* 59 (2016) 10692–10704.
- [141] M.G. El-Gazzar, N.H. Nafie, A. Nocentini, M.M. Ghorab, H.I. Heiba, C.T. Supuran, Carbonic anhydrase inhibition with a series of novel benzenesulfonamide-triazole conjugates, *J. Enzyme Inhib. Med. Chem.* 33 (2018) 1565–1574.
- [142] R. Kumar, L. Vats, S. Bua, C.T. Supuran, P.K. Sharma, Design and synthesis of novel benzenesulfonamide containing 1,2,3-triazoles as potent human carbonic anhydrase isoforms I, II, IV and IX inhibitors, *Eur. J. Med. Chem.* 155 (2018) 545–551.
- [143] L. Vats, V. Sharma, A. Angeli, R. Kumar, C.T. Supuran, P.K. Sharma, Synthesis of novel 4-functionalized 1,5-diaryl-1,2,3-triazoles containing benzenesulfonamide moiety as carbonic anhydrase I, II, IV and IX inhibitors, *Eur. J. Med. Chem.* 150 (2018) 678–686.
- [144] F.M.F. Chen, N.L. Benoiton, The preparation and reactions of mixed anhydrides of N-alkoxycarbonylamino acids, *Can. J. Chem.* 65 (1987) 619–625.
- [145] C. Shao, X. Wang, Q. Zhang, S. Luo, J. Zhao, Y. Hu, Acid-base jointly promoted copper(I)-catalyzed azide-alkyne cycloaddition, *J. Org. Chem.* 76 (2011) 6832–6836.
- [146] K. V. Kutonova, M.E. Trusova, P. Postnikov, V.D. Filimonov, J. Parello, A simple and effective synthesis of aryl azides via arenediazonium tosylates, *Synth.* 45 (2013) 2706–2710.
- [147] C. Shao, X. Wang, Q. Zhang, S. Luo, J. Zhao, Y. Hu, Acid–Base Jointly Promoted Copper(I)-Catalyzed Azide–Alkyne Cycloaddition, *J. Org. Chem.* 76 (2011) 6832–6836.
- [148] E. Bruno, M.R. Buemi, A. Di Fiore, L. De Luca, S. Ferro, A. Angeli, R. Cirilli, D. Sadutto, V. Alterio, S.M. Monti, C.T. Supuran, G. De Simone, R. Gitto, Probing

- Molecular Interactions between Human Carbonic Anhydrases (hCAs) and a Novel Class of Benzenesulfonamides, *J. Med. Chem.* 60 (2017) 4316–4326.
- [149] A. Angeli, F. Vaiano, F. Mari, E. Bertol, C.T. Supuran, Psychoactive substances belonging to the amphetamine class potently activate brain carbonic anhydrase isoforms VA, VB, VII, and XII, *J. Enzyme Inhib. Med. Chem.* 32 (2017) 1253–1259.
- [150] A. Angeli, D. Tanini, A. Capperucci, G. Malevolti, F. Turco, M. Ferraroni, C.T. Supuran, Synthesis of different thio-scaffolds bearing sulfonamide with subnanomolar carbonic anhydrase II and IX inhibitory properties and X-ray investigations for their inhibitory mechanism, *Bioorg. Chem.* 81 (2018) 642–648.
- [151] A. Nocentini, M. Ferraroni, F. Carta, M. Ceruso, P. Gratteri, C. Lanzi, E. Masini, C.T. Supuran, Benzenesulfonamides Incorporating Flexible Triazole Moieties Are Highly Effective Carbonic Anhydrase Inhibitors: Synthesis and Kinetic, Crystallographic, Computational, and Intraocular Pressure Lowering Investigations, *J. Med. Chem.* 59 (2016) 10692–10704.
- [152] X. Lai, H.J. Wichers, M. Soler-Lopez, B.W. Dijkstra, Structure and Function of Human Tyrosinase and Tyrosinase-Related Proteins, *Chem. - A Eur. J.* 24 (2018) 47–55.
- [153] C. Olivares, F. Solano, New insights into the active site structure and catalytic mechanism of tyrosinase and its related proteins, *Pigment Cell Melanoma Res.* 22 (2009) 750–760.
- [154] M. Kanteev, M. Goldfeder, A. Fishman, Structure-function correlations in tyrosinases, *Protein Sci.* 24 (2015) 1360–1369.
- [155] H.S. Raper, The aerobic oxidases, *Physiol. Rev.* 8 (1928) 245–282.
- [156] C.A. Ramsden, P.A. Riley, Tyrosinase: The four oxidation states of the active site and their relevance to enzymatic activation, oxidation and inactivation, *Bioorganic Med. Chem.* 22 (2014) 2388–2395.
- [157] S. Ito, K. Wakamatsu, Chemistry of mixed melanogenesis - Pivotal roles of dopaquinone, *Photochem. Photobiol.* 84 (2008) 582–592.
- [158] I.J. Jackson, P. Budd, J.M. Horn, R. Johnson, S. Raymond, K. Steel Genetics and Molecular Biology of Mouse Pigmentation, *Pigment Cell Res.* 7 (1994) 73–80.

- [159] F. Solano, On the metal cofactor in the tyrosinase family, *Int. J. Mol. Sci.* 19 (2018).
- [160] E. Solomon, M.D. Lowery, *Electronic Structure Contributions to Function in Bioinorganic Chemistry*, 259 (1993).
- [161] N.J. Kus, M.B. Dolinska, K.L. Young, E.K. Dimitriadis, P.T. Wingfield, Y. V. Sergeev, Membrane-associated human tyrosinase is an enzymatically active monomeric glycoprotein, *PLoS One*. 13 (2018) 1–11.
- [162] A. Bunsen Lerner, T.B. Fitzpatrick, E. Calkins, W. Summerson, Mammalian tyrosinase: the relationship of copper to enzymatic activity, *J. Biol. Chem* (1950)
- [163] F. Solano, C. Jiménez-Cervantes, J.H. Martínez-Liarte, J.C. García-Borrón, J.R. Jara, J.A. Lozano, Molecular mechanism for catalysis by a new zinc-enzyme, dopachrome tautomerase, *Biochem. J.* 313 (1996) 447–453.
- [164] X. Lai, H.J. Wichers, M. Soler-Lopez, B.W. Dijkstra, Structure of Human Tyrosinase Related Protein 1 Reveals a Binuclear Zinc Active Site Important for Melanogenesis, *Angew. Chemie - Int. Ed.* 56 (2017) 9812–9815.
- [165] H. Decker, T. Schweikardt, F. Tuczek, The first crystal structure of tyrosinase: All questions answered?, *Angew. Chemie - Int. Ed.* 45 (2006) 4546–4550.
- [166] P. Aroca, J.C. Garcia-Borrón, F. Solano, J.A. Lozano, Regulation of mammalian melanogenesis I: partial purification and characterization of a dopachrome converting factor: dopachrome tautomerase, *BBA - Gen. Subj.* 1035 (1990) 266–275.
- [167] P. Aroca, F. Solano, J.C. Garcia-Borrón, J.A. Lozano, Specificity of dopachrome tautomerase and inhibition by carboxylated indoles. Considerations on the enzyme active site, *Biochem. J.* 277 (1991) 393–397.
- [168] R.E. Boissy, C. Sakai, H. Zhao, T. Kobayashi, V.J. Hearing, Human tyrosinase related protein-1 (TRP-1) does not function as a DHICA oxidase activity in contrast to murine TRP-1, *Exp. Dermatol.* 7 (1998) 198–204.
- [169] X. Lai, M. Soler-Lopez, W.T. Ismaya, H.J. Wichers, B.W. Dijkstra, Crystal structure of recombinant tyrosinase-binding protein MtaL at 1.35% resolution, *Acta Crystallogr. Sect. Struct. Biol. Commun.* 72 (2016) 244–250.
- [170] G. Ghanem, J. Fabrice, Tyrosinase related protein 1 (TYRP1/gp75) in human cutaneous

- melanoma, *Mol. Oncol.* 5 (2011) 150–155.
- [171] A. Körner, J. Pawelek, Mammalian tyrosinase catalyzes three reactions in the biosynthesis of melanin, *Science* (80-.). 217 (1982) 1163–1165.
- [172] X. Lai, M. Soler-Lopez, H.J. Wichers, B.W. Dijkstra, Large-scale recombinant expression and purification of human tyrosinase suitable for structural studies, *PLoS One*. 11 (2016) 1–16.
- [173] Á. Sánchez-Ferrer, J. Neptuno Rodríguez-López, F. García-Cánovas, F. García-Carmona, Tyrosinase: a comprehensive review of its mechanism, *Biochim. Biophys. Acta - Protein Struct. Mol. Enzymol.* 1247 (1995) 1–11.
- [174] C.A. Ramsden, M.R.L. Stratford, P.A. Riley, The influence of catechol structure on the suicide-inactivation of tyrosinase, *Org. Biomol. Chem.* 7 (2009) 3388–3390.
- [175] C. Citek, C.T. Lyons, E.C. Wasinger, T.D.P. Stack, Self-assembly of the oxy-tyrosinase core and the fundamental components of phenolic hydroxylation, *Nat. Chem.* 4 (2012) 317–322.
- [176] N. Fujieda, S. Yabuta, T. Ikeda, T. Oyama, N. Muraki, G. Kurisu, S. Itoh, Crystal structures of copper-depleted and copper-bound fungal pro-tyrosinase: Insights into endogenous cysteine-dependent copper incorporation, *J. Biol. Chem.* 288 (2013) 22128–22140.
- [177] E. Buitrago, R. Hardré, R. Haudecoeur, H. Jamet, C. Belle, A. Boumendjel, L. Bubacco, M. Réglie, Are Human Tyrosinase and Related Proteins Suitable Targets for Melanoma Therapy?, *Curr. Top. Med. Chem.* 16 (2016) 3033–3047.
- [178] S. Ito, IFPCS presidential lecture: A chemist's view of melanogenesis, *Pigment Cell Res.* 16 (2003) 230–236.
- [179] F. Solano, S. Briganti, M. Picardo, G. Ghanem, Hypopigmenting agents: An updated review on biological, chemical and clinical aspects, *Pigment Cell Res.* 19 (2006) 550–571.
- [180] S.Y. Lee, N. Baek, T.G. Nam, Natural, semisynthetic and synthetic tyrosinase inhibitors, *J. Enzyme Inhib. Med. Chem.* 31 (2016) 1–13.
- [181] R. Speeckaert, N. van Geel, Vitiligo: An Update on Pathophysiology and Treatment

- Options, *Am. J. Clin. Dermatol.* 18 (2017) 733–744.
- [182] S. Zolghadri, A. Bahrami, M.T. Hassan Khan, J. Munoz-Munoz, F. Garcia-Molina, F. Garcia-Canovas, A.A. Saboury, A comprehensive review on tyrosinase inhibitors, *J. Enzyme Inhib. Med. Chem.* 34 (2019) 279–309.
- [183] T. Mann, W. Gerwat, J. Batzer, K. Eggers, C. Scherner, H. Wenck, F. Stäb, V.J. Hearing, K.H. Röhm, L. Kolbe, Inhibition of Human Tyrosinase Requires Molecular Motifs Distinctively Different from Mushroom Tyrosinase, *J. Invest. Dermatol.* 138 (2018) 1601–1608.
- [184] T. Mann, C. Scherner, K.H. Röhm, L. Kolbe, Structure-activity relationships of thiazolyl resorcinols, potent and selective inhibitors of human tyrosinase, *Int. J. Mol. Sci.* 19 (2018).
- [185] L. Kolbe, T. Mann, W. Gerwat, J. Batzer, S. Ahlheit, C. Scherner, H. Wenck, F. Stäb, 4-N-Butylresorcinol, a Highly Effective Tyrosinase Inhibitor for the Topical Treatment of Hyperpigmentation, *J. Eur. Acad. Dermatology Venereol.* 27 (2013) 19–23.
- [186] S.H. Jeon, K.H. Kim, J.U. Koh, K.H. Kong, Inhibitory effects on L-dopa oxidation of tyrosinase by skin-whitening agents, *Bull. Korean Chem. Soc.* 26 (2005) 1135–1137.
- [187] T. Pillaiyar, M. Manickam, V. Namasivayam, Skin whitening agents: Medicinal chemistry perspective of tyrosinase inhibitors, *J. Enzyme Inhib. Med. Chem.* 32 (2017) 403–425.
- [188] V.J. Hearing, K. Tsukamoto, Enzymatic control of pigmentation in mammals, *FASEB J.* 5 (1991) 2902–2909.
- [189] M. Pretzler, A. Bijelic, A. Rompel, Heterologous expression and characterization of functional mushroom tyrosinase (AbPPO4), *Sci. Rep.* 7 (2017) 1–10.
- [190] T. Pillaiyar, V. Namasivayam, M. Manickam, S.H. Jung, Inhibitors of Melanogenesis: An Updated Review, *J. Med. Chem.* 61 (2018) 7395–7418.
- [191] A. Yoshimori, T. Oyama, S. Takahashi, H. Abe, T. Kamiya, T. Abe, S.I. Tanuma, Structure-activity relationships of the thujaplicins for inhibition of human tyrosinase, *Bioorganic Med. Chem.* 22 (2014) 6193–6200.
- [192] H.M. Wang, C.Y. Chen, Z.H. Wen, Identifying melanogenesis inhibitors from

- Cinnamomum subavenium with in vitro and in vivo screening systems by targeting the human tyrosinase, *Exp. Dermatol.* 20 (2011) 242–248.
- [193] S.Y. Huh, J.W. Shin, J.I. Na, C.H. Huh, S.W. Youn, K.C. Park, The efficacy and safety of 4-n-butylresorcinol 0.1% cream for the treatment of melasma: A randomized controlled split-face trial, *Ann. Dermatol.* 22 (2010) 21–25.
- [194] P. Cordes, W. Sun, R. Wolber, L. Kolbe, G. Klebe, K.H. Röhm, Expression in non-melanogenic systems and purification of soluble variants of human tyrosinase, *Biol. Chem.* 394 (2013) 685–693.
- [195] S. Khatib, O. Nerya, R. Musa, M. Shmuel, S. Tamir, J. Vaya, Chalcones as potent tyrosinase inhibitors: The importance of a 2,4-substituted resorcinol moiety, *Bioorganic Med. Chem.* 13 (2005) 433–441.
- [196] C. Arrowitz, A.M. Schoelermann, T. Mann, L.I. Jiang, T. Weber, L. Kolbe, Effective Tyrosinase Inhibition by Thiamidol Results in Significant Improvement of Mild to Moderate Melasma, *J. Invest. Dermatol.* 139 (2019) 1691–1698.
- [197] W.G. Philipp-Dormston, A. Vila Echagüe, S.H. Pérez Damonte, J. Riedel, A. Filbry, K. Warnke, C. Lofrano, D. Roggenkamp, G. Nippel, Thiamidol containing treatment regimens in facial hyperpigmentation: An international multi-centre approach consisting of a double-blind, controlled, split-face study and of an open-label, real-world study, *Int. J. Cosmet. Sci.* 42 (2020) 377–387.
- [198] A.N. Houghton, M. Eisinger, A.P. Albino, J.G. Cairncross, L.J. Old, Surface antigens of melanocytes and melanomas. Markers of melanocyte differentiation and melanoma subsets., *J. Exp. Med.* 156 (1982) 1755–1766.
- [199] A.J. Vargas, S. Sittadjody, T. Thangasamy, E.E. Mendoza, K.H. Limesand, R. Burd, Exploiting tyrosinase expression and activity in melanocytic tumors: Quercetin and the central role of p53, *Integr. Cancer Ther.* 10 (2011) 328–340.
- [200] J.L. Boyle, H.M. Haupt, J.B. Sterne, H.A.B. Mulhaupt, Tyrosinase expression in malignant melanoma, desmoplastic melanoma and peripheral nerve tumours, *Arch Patol Lab Med* 126 (2002).
- [201] C. Zhan, J. Cheng, B. Li, S. Huang, F. Zeng, S. Wu, A Fluorescent Probe for Early Detection of Melanoma and Its Metastasis by Specifically Imaging Tyrosinase Activity

- in a Mouse Model, *Anal. Chem.* 90 (2018) 8807–8815.
- [202] A.M. Jordan, T.H. Khan, H. Malkin, H.M.I. Osborn, Synthesis and analysis of urea and carbamate prodrugs as candidates for melanocyte-directed enzyme prodrug therapy (MDEPT), *Bioorganic Med. Chem.* 10 (2002) 2625–2633.
- [203] P.A. Riley, C.J. Cooksey, C.I. Johnson, E.J. Land, A.M. Latter, C.A. Ramsden, Original Paper Development : Effect of Side-chain Variations on the Cytotoxicity of Tyrosinase-generated Ortho-quinones in a Model Screening System *, 33 (1997) 135–143.
- [204] B. Bandarchi, L. Ma, R. Navab, A. Seth, G. Rasty, From melanocyte to metastatic malignant melanoma, *Dermatol. Res. Pract.* 2010 (2010).
- [205] I. Drexler, E. Antunes, M. Schmitz, T. Wölfel, C. Huber, V. Erfle, P. Rieber, M. Theobald, G. Sutter, Modified vaccinia virus ankara for delivery of human tyrosinase as melanoma-associated antigen: Induction of tyrosinase- and melanoma-specific human leukocyte antigen A*0201-restricted cytotoxic T cells in vitro and in vivo, *Cancer Res.* 59 (1999) 4955–4963.
- [206] R.G. Meyer, C.M. Britten, U. Siepmann, B. Petzold, T.A. Sagban, H.A. Lehr, B. Weigle, M. Schmitz, L. Mateo, B. Schmidt, H. Bernhard, T. Jakob, R. Hein, G. Schuler, B. Schuler-Thurner, S.N. Wagner, I. Drexler, G. Sutter, N. Arndtz, P. Chaplin, J. Metz, A. Enk, C. Huber, T. Wölfel, A phase I vaccination study with tyrosinase in patients with stage II melanoma using recombinant modified vaccinia virus Ankara (MVA-hTyr), *Cancer Immunol. Immunother.* 54 (2005) 453–467.
- [207] T. Tai, M. Eisinger, S.I. Ogata, K.O. Lloyd, Glycoproteins as Differentiation Markers in Human Malignant Melanoma and Melanocytes, *Cancer Res.* 43 (1983) 2773–2779.
- [208] F. Journe, H.I. Boufker, L. Van Kempen, M.D. Galibert, M. Wiedig, F. Salès, A. Theunis, D. Nonclercq, A. Frau, G. Laurent, A. Awada, G. Ghanem, TYRP1 mRNA expression in melanoma metastases correlates with clinical outcome, *Br. J. Cancer.* 105 (2011) 1726–1732.
- [209] S. Welt, M.J. Mattes, R. Grando, T.M. Thomson, R.W. Leonard, P.B. Zanzonico, R.E. Bigler, S. Yeh, H.F. Oettgen, L.J. Old, Monoclonal antibody to an intracellular antigen images human melanoma transplants in nu/nu mice, *Proc. Natl. Acad. Sci. U. S. A.* 84 (1987) 4200–4204.

- [210] Y.M. Saenger, Y. Li, K.C. Chiou, B. Chan, G. Rizzuto, S.L. Terzulli, T. Merghoub, A.N. Houghton, J.D. Wolchok, Improved tumor immunity using anti-tyrosinase related protein-1 monoclonal antibody combined with DNA vaccines in murine melanoma, *Cancer Res.* 68 (2008) 9884–9891.
- [211] D.N. Khalil, M.A. Postow, N. Ibrahim, D.L. Ludwig, J. Cosaert, S.R.P. Kambhampati, S. Tang, D. Grebennik, J.S.W. Kauh, H.J. Lenz, K.T. Flaherty, F.S. Hodi, D.P. Lawrence, J.D. Wolchok, An open-label, dose-escalation phase I study of anti-TYRP1 monoclonal antibody IMC-20D7S for patients with relapsed or refractory melanoma, *Clin. Cancer Res.* 22 (2016) 5204–5210.
- [212] M. Srinivasarao, C. V. Galliford, P.S. Low, Principles in the design of ligand-targeted cancer therapeutics and imaging agents, *Nat. Rev. Drug Discov.* 14 (2015) 203–219.
- [213] M. Srinivasarao, P.S. Low, Ligand-Targeted Drug Delivery, *Chem. Rev.* 117 (2017) 12133–12164.
- [214] N. Krall, J. Scheuermann, D. Neri, Small targeted cytotoxics: Current state and promises from DNA-encoded chemical libraries, *Angew. Chemie - Int. Ed.* 52 (2013) 1384–1402.
- [215] S. Cazzamalli, A. Dal Corso, F. Widmayer, D. Neri, Chemically defined antibody- and small molecule-drug conjugates for in vivo tumor targeting applications: A comparative analysis, *J. Am. Chem. Soc.* 140 (2018) 1617–1621.
- [216] G. Bassi, N. Favalli, M. Vuk, M. Catalano, A. Martinelli, A. Trenner, A. Porro, S. Yang, C.L. Tham, M. Moroglu, W.W. Yue, S.J. Conway, P.K. Vogt, A.A. Sartori, J. Scheuermann, D. Neri, A single-stranded DNA-encoded chemical library based on a stereoisomeric scaffold enables ligand discovery by modular assembly of building blocks, *Adv. Sci.* 2001970 (2020) 1–10.
- [217] D. Neri, R.A. Lerner, DNA-Encoded Chemical Libraries: A Selection System Based on Endowing Organic Compounds with Amplifiable Information, *Annu. Rev. Biochem.* 87 (2018) 479–502.
- [218] S. Brenner, R.A. Lerner, Encoded combinatorial chemistry, *Proc. Natl. Acad. Sci. U. S. A.* 89 (1992) 5381–5383.
- [219] N. Favalli, G. Bassi, J. Scheuermann, D. Neri, DNA-encoded chemical libraries – achievements and remaining challenges, *FEBS Lett.* 592 (2018) 2168–2180.

- [220] M.A. Clark, R.A. Acharya, C.C. Arico-Muendel, S.L. Belyanskaya, D.R. Benjamin, N.R. Carlson, P.A. Centrella, C.H. Chiu, S.P. Creaser, J.W. Cuzzo, C.P. Davie, Y. Ding, G.J. Franklin, K.D. Franzen, M.L. Gefter, S.P. Hale, N.J.V. Hansen, D.I. Israel, J. Jiang, M.J. Kavarana, M.S. Kelley, C.S. Kollmann, F. Li, K. Lind, S. Mataruse, P.F. Medeiros, J.A. Messer, P. Myers, H. O'Keefe, M.C. Oliff, C.E. Rise, A.L. Satz, S.R. Skinner, J.L. Svendsen, L. Tang, K. Van Vloten, R.W. Wagner, G. Yao, B. Zhao, B.A. Morgan, Design, synthesis and selection of DNA-encoded small-molecule libraries, *Nat. Chem. Biol.* 5 (2009) 647–654.
- [221] W. Decurtins, M. Wichert, R.M. Franzini, F. Buller, M.A. Stravs, Y. Zhang, D. Neri, J. Scheuermann, Automated screening for small organic ligands using DNA-encoded chemical libraries, *Nat. Protoc.* 11 (2016) 764–780.
- [222] N.J. Moerke, Fluorescence Polarization (FP) Assays for Monitoring Peptide-Protein or Nucleic Acid – Protein Binding, 1 (2009) 1–15.
- [223] W.A. Lea, A. Simeonov, Fluorescence Polarization Assay, *Expert Opin Drug Discov.* 6 (2012) 17–32.
- [224] A.J. Winder, H. Harris, New assays for the tyrosine hydroxylase and dopa oxidase activities of tyrosinase, *Eur. J. Biochem.* 198 (1991) 317–326.
- [225] J.C. Espín, M. Morales, P.A. García-Ruiz, J. Tudela, F. García-Cánovas, Improvement of a Continuous Spectrophotometric Method for Determining the Monophenolase and Diphenolase Activities of Mushroom Polyphenol Oxidase, *J. Agric. Food Chem.* 45 (1997) 1084–1090.
- [226] V.M. Krishnamurthy, L.A. Estroff, G.M. Whitesides, Multivalency in Ligand Design, 2006.
- [227] M. Mammen, S.K. Choi, G.M. Whitesides, Polyvalent interactions in biological systems: Implications for design and use of multivalent ligands and inhibitors, *Angew. Chemie - Int. Ed.* 37 (1998) 2754–2794.
- [228] J. Shi, Y.S. Kim, S. Zhai, Z. Liu, X. Chen, S. Liu, Improving tumor uptake and pharmacokinetics of ⁶⁴Cu-labeled cyclic RGD peptide dimers with Gly 3 and PEG 4 linkers, *Bioconjug. Chem.* 20 (2009) 750–759.
- [229] S.R. Banerjee, M. Pullambhatla, H. Shallal, A. Lisok, R.C. Mease, M.G. Pomper, A

- modular strategy to prepare multivalent inhibitors of prostate-specific membrane antigen (PSMA), *Oncotarget*. 2 (2011) 1244–1253.
- [230] S. Lindner, C. Michler, B. Wängler, P. Bartenstein, G. Fischer, R. Schirrmacher, C. Wängler, PESIN multimerization improves receptor avidities and in vivo tumor targeting properties to GRPR-overexpressing tumors, *Bioconjug. Chem.* 25 (2014) 489–500.
- [231] N. Krall, F. Preto, W. Decurtins, G.J.L. Bernardes, C.T. Supuran, D. Neri, A small-molecule drug conjugate for the treatment of carbonic anhydrase IX expressing tumors, *Angew. Chemie - Int. Ed.* 53 (2014) 4231–4235.
- [232] A. Pina, M. Kadri, D. Arosio, A. Dal Corso, J.L. Coll, C. Gennari, D. Boturyn, Multimeric Presentation of RGD Peptidomimetics Enhances Integrin Binding and Tumor Cell Uptake, *Chem. - A Eur. J.* 26 (2020) 7492–7496.
- [233] A. Borbély, F. Thoreau, E. Figueras, M. Kadri, J.L. Coll, D. Boturyn, N. Sewald, Synthesis and Biological Characterization of Monomeric and Tetrameric RGD-Cryptophycin Conjugates, *Chem. - A Eur. J.* 26 (2020) 2602–2605.
- [234] I.R. Vlahov, C.P. Leamon, Engineering folate-drug conjugates to target cancer: From chemistry to clinic, *Bioconjug. Chem.* 23 (2012) 1357–1369.
- [235] S. Cazzamalli, A.D. Corso, D. Neri, Targeted delivery of cytotoxic drugs: Challenges, opportunities and new developments, *Chimia (Aarau)*. 71 (2017) 712–715.
- [236] S. Ingale, P.E. Dawson, On resin side-chain cyclization of complex peptides using CuAAC, *Org. Lett.* 13 (2011) 2822–2825.
- [237] M. Catalano, S. Oehler, L. Prati, N. Favalli, G. Bassi, J. Scheuermann, D. Neri, Complexation with a Cognate Antibody Fragment Facilitates Affinity Measurements of Fluorescein-Linked Small Molecule Ligands, *Anal. Chem.* 92 (2020) 10822–10829.
- [238] S. Vijayasaradhi, B. Bouchard, A.N. Houghton, The melanoma antigen gp75 is the human homologue of the mouse b (brown) locus gene product, *J. Exp. Med.* 171 (1990)

List of publications

1. M. Catalano, G. Bassi, G. **Rotondi**, L. Khettabi, M. Dichiara, P. Murer, J. Scheuermann, M. Soler-Lopez, D. Neri, Discovery, affinity maturation and multimerization of small molecule ligands against human Tyrosinase and Tyrosinase related protein 1. Submitted and accepted by RSC Medicinal Chemistry.
2. P. Guglielmi, **G. Rotondi**, D. Secci, A. Angeli, P. Chimenti, A. Nocentini, A. Bonardi, P. Gratteri, S. Carradori, C. T. Supuran, Novel insights on saccharin- and acesulfame based carbonic anhydrase inhibitors: design, synthesis, modelling investigations and biological activity evaluation, *J. Enzyme Inhib. Med. Chem.* 34 (2020) 1891-1905.
3. P. Guglielmi, **G. Rotondi**, D. Secci, S. Carradori, An update on Eg5 kinesin inhibitors for the treatment of cancer in *Advances in Medicinal Chemistry Research*.
4. P. Guglielmi, D. Secci, A. Petzer; D. Bagetta, P. Chimenti, **G. Rotondi**, C. Ferrante, L. Recinella, S. Leone, S. Alcaro, G. Zengin, J. P. Petzer, F. Ortuso, S. Carradori, Benzo[b]tiophen-3-ol derivatives as effective inhibitors of human monoamine oxidase: design, synthesis, and biological activity, *J. Enzyme Inhib. Med. Chem.* 34 (2019) 1511-1525.
5. **G. Rotondi**, P. Guglielmi, S. Carradori, D. Secci, C. De Monte, B. De Filippis, C. Maccallini, R. Amoroso, R. Cirilli, A. Akdemir, A. Angeli, C.T. Supuran, Design, synthesis and biological activity of selective hCAs inhibitors based on 2-(benzylsulfinyl)benzoic acid scaffold, *J. Enzyme Inhib. Med. Chem.* 34 (2019) 1400-1413.
6. P. Guglielmi, S. Carradori, G. Poli, D. Secci, R. Cirilli, **G. Rotondi**, P. Chimenti, A. Petzer, J. P. Petzer, Design, Synthesis, Docking Studies and Monoamine Oxidase Inhibition of a Small Library of 1-Acetyl- and 1-Thiocarbamoyl-3,5-Diphenyl-4,5-Dihydro-(1*H*)-Pyrazoles, *Molecules* 24 (2019).

Compliance with the protection of copyrights

Material provided solely for study and research purposes and for personal use. Any subsequent reproduction or publication for commercial use is strictly prohibited (Law No. 633/1941, Law No. 159/1993).